CR 73133

Spectrolab

12484 GLADSTONE AVENUE, SYLMAR, CALIFORNIA
EMPIRE 5-4623 TWX: 213-764-5923

Final Report FR 6002

Analytical, Experimental & Developmental Work

for a

Radiative Heating System

Volume II of III

Contract No.: NAS2-1620

Prepared by

Spectrolab, Div. of Textron Electronics, Inc.
12484 Gladstone Avenue
Sylmar, California

for

National Aeronautics and Space Administration

Ames Research Center

Moffett Field, California

FR 6002

Final Report

Analytical, Experimental & Developmental Work

for a

Radiative Heating System

Volume II of III

Contract No.: NAS2-1620

Prepared by

Spectrolab, Div. of Textron Electronics, Inc.
12484 Gladstone Avenue
Sylmar, California

for

National Aeronautics and Space Administration
Ames Research Center
Moffett Field, California

This report has been divided into three volumes.

Volume I entitled "System Development" covers the work performed in the optical system concept study, optical and thermal design, and the fabrication and evaluation of the prototype optical system.

Volume II entitled "Source Development" describes the development program on the radiation source, including the work performed under subcontract and covers all test runs in the operation of the final prototype radiation source.

Volume III entitled "Facility Design" covers the detailed design of the radiative heating system facility.

TABLE OF CONTENTS

Continued

TABLE OF CONTENTS
(Continued)

Continued

TABLE OF CONTENTS
(Continued)

LIST OF ILLUSTRATIONS

Continued

LIST OF ILLUSTRATIONS
(Continued)

APPENDICES

Number	Description
	Data Summary Sheet - Model L-60 Light Source
DM 272-1	Brazing Test Results
DM 272-2	Energy Absorption in the Envelope of a Plasma Radiation Source
DM 272-3	Determination of the Heat Transfer Coefficient from the Envelope to the Cooling Medium
DM 272-4	Radial Temperature Distribution in the Envelope of a Plasma Radiation Source
DM 272-5	Simplified Stress Analysis of a Radiation Source Envelope
DM 272-6	Transient Heat Transfer in the Envelope of a Plasma Radiation Source
DM 272-7	Heat Transfer in a Composite Diffuser
DM 272-8	Recirculator Testing
DM 272-10	DC Electrical System Calibration
DM 272-11	Recirculator Testing
DM 272-14	Radiation Source Evaluation Testing (Runs 1-4)
DM 272-16	Radiation Source Performance During Prototype Testing
DM 272-17	Documentation of Source Performance in Test Run 10
DM 272-22	Polar Distribution and Total Energy Runs 13.1, 13.2 and 13.3
DM 272-23	Documentation of Source Performance in Test Runs 11, 12 and 13
DM 272-24	Radiation Source Life Tests (Runs 14 Through 19 and 22)
DM 272-25	Documentation of Source Operation During Spectral Tests (Runs 20 and 21)

Continued

APPENDICES
(Continued)

Number	Description
DM 272-27	Spectral Distribution of 150 KW Radiation Source
DM 272-28	Spectral Distribution of 150 KW Vortex Stabilized Argon Plasma Arc Source
DM 272-29	Micro-radiance Distribution in Final Radiation Source
DM 272-30	Source Documentation - Runs 23 through 30
DM 272-34	Recalibration of Prototype DC Electrical System
DM 272-36	Documentation of Source Performance in Test Runs 33, 34 and 35
DM 272-37	Source Documentation in Test Runs 36 through 39, Including $2\frac{1}{2}$ Hour Continuous Run
DM 272-38	Documentation of Source Performance in Runs 40 and 41, Including Failure of Outer Envelope
DM 272-43	Source Documentation - Test Runs 42 through 49
DM 272-48	Micro-radiance Plot Calibration
DM 272-52	Recirculator Evaluation
DM 272-61	Heat Transfer in the Cathode
DM 272-62	Total Reflection in the Plasma Radiation Source
DM 272-63	Radial Heat Flux and Thermal Stresses in a Sleeve

1. SUMMARY

The development of a high power plasma radiation source including analytical studies and experimental results is described. This development was performed initially at Giannini Scientific Corporation (Plasmadyne) under subcontract from Spectrolab. The latter portions of the work were performed at Spectrolab after termination of the subcontract.

Initially a 60 KW rated lamp was developed as a prototype for the final 150 KW lamp and to ~~enable~~ test~~ing of~~ a prototype optical system. This lamp used a double concentric envelope design with a tungsten cathode and a hollow bore anode. The lamp was cantilevered from the anode end with the cathode portion being supported by three tierods placed 120° apart. The major effort in the 60 KW lamp development was devoted to anode design. The final anode was made of copper with a tungsten sleeve press fit into the inside diameter of the bore. The tungsten protruded from the copper body into the arc chamber. It was found necessary to fully anneal the outer quartz envelope and to water-cool the tierods in order to achieve required life times at the designed operating parameters.

An experimental radiation source unit was constructed in order to permit an orderly upgrading of the 60 KW prototype source to the specified 150 KW power input level. This experimental unit was designed to accommodate three different size inner quartz envelopes and four different size electrode pairs. The initial work with this source was devoted to the bore type anodes. During the course of this development, the solid anode configuration was conceived and tested and proved to be superior to the bore type anode previously employed. The limiting power level for different size inner quartz envelopes was determined and operation at 150 KW with an efficiency of approximately 30% was achieved with this experimental unit.

With the data obtained from the testing of the experimental unit as well as the several analyses which were performed, the final radiation source design was conceived and detailed. This design contained a solid anode and employed a cantilevered self-supporting outer quartz envelope. The final manufacture, assembly and testing of the final radiation source was performed at Spectrolab after termination of the subcontract. The radiation source was operated at current levels up to 1600 amps and satisfactory performance was obtained for a period of two hours continuous operation as well as approximately 25 intermittant test

runs of 15 minutes duration. The final source was operated with input gas pressures as high as 290 psig and no difficulties were experienced with the operation of the self-supporting envelope. The source was then incorporated into the prototype optical system for evaluation testing of the complete prototype system.

The design of the anode in the final radiation source deserves particular mention since it is considered a novel design. The details of the design are presented in the body of the report. The anode employs a refractory metal diffuser to provide constriction of the arc by influencing the vortex flow of the gas; and the anode footpoint of the arc is diffused by fluid dynamic forces after passing through the diffuser in order to reduce the specific heat input to the anode.

Very little difficulties were experienced in the operation of the anode and no failure of the radiation source was caused by failure of the anode design. Some problems were encountered with the expulsion of material from the cathode tip in the final radiation source. There were tungsten particles deposited on the inner quartz envelope necessitating replacement of the inner envelope. Development work on the radiation source was stopped by directive from NASA before these problems could be solved. It appears very likely that the performance of the radiation source can be upgraded by minor modifications to the electrodes.

2. INTRODUCTION

The original work statement of the contract required the procurement of a large radiation source and system for initial evaluation. The final radiation source was specified to be operated at a minimum power level of 150 KW. In addition, the source had to be suitable for operation in the prototype optical system and was to be complete with gas recirculator, cooling system, power supply, and controls. The performance and operating characteristics of the final radiation source were specified as follows:

a. Spectral distribution of emitted flux closely matching the desired spectral distribution.

b. Conversion efficiency (output radiant power/input electrical power) of at least 30%.

c. Output solid angle of approximately 10 steradians.

d. Average brightness in excess of 7000 watts/cm^2-str.

e. Minimum operating time of one hour at maximum rated power level with a maximum of one-half hour between runs.

This portion of the original contract was amplified and made the Statement of Work in Spectrolab's subcontract to Plasmadyne Corporation. (Plasmadyne Corporation was later renamed Giannini Scientific Corporation.)

The radiation source for initial testing was specified as having an input power level of 60 KW. Also included in the Giannini Scientific subcontract was the development of a gas recirculator system and the maintenance of the radiation source system for prototype integration and demonstration to NASA/Ames.

Giannini Scientific completed the delivery of the 60 KW source and the design of the final 150 KW radiation source. Before the fabrication of the final radiation source was completed, the subcontract was terminated due to the complete expenditure of authorized funds by Giannini Scientific. Full details of the termination of the subcontract are contained in memoranda and letters from Spectrolab to the NASA Contracting Officer. The testing of the final radiation source was performed at Spectrolab. The final source did not fulfill the spectral distribution and radiance specifications. In addition, the output solid angle from the final source was limited to approximately 8 steradians.

3. 60 KW PROTOTYPE RADIATION SOURCE

3.1 DESCRIPTION OF THE SOURCE DESIGN - A cross-section of the 60 KW prototype source developed and tested at Giannini Scientific and employed in the first prototype optical system at Spectrolab is shown in Figure 1. This source incorporated two concentric quartz envelopes with the source assembly supported at the anode housing and the cathode end cantilevered from this mounting surface. Three rods placed 120° apart were used to connect the anode and cathode ends of the radiation source. The forces exerted on the electrode assemblies by the gas pressure were supported by these rods. The cathode had a conical shape with a thoriated tungsten tip while the anode had a hollow bore in the center in which the arc was terminated. The gas and cooling water entries for the anode and heat exchanger were located on the anode end while only the cathode cooling entry and exit were located on the cathode end of the source. The gas was guided through the annular channel created by the concentric envelopes from the anode to the cathode end of the source. The gas was then introduced into the arc chamber through a series of near tangential injector nozzles on the periphery of the cathode housing to produce the proper vortex motion of the gas for arc stabilization. The gas exited through the bore in the anode and through a heat exchanger integral with the radiation source. Upon leaving the heat exchanger, the gas was exhausted to the atmosphere through a valve to enable independent control of pressure and flow.

3.2 TEST FACILITY - The auxiliary equipment used to operate the radiation source consisted of an arc starter, power supplies, control console and test enclosure.

3.2.1 Starter - The starter used to ignite the radiation source generated a voltage of approximately 20,000 volts at a frequency in the area of 1,000 KC. This starter was of the Tessler design and was sufficient to ignite the radiation source in argon at an electrode spacing of 10 millimeters and a gas pressure less than 100 psi.

3.2.2 Power Supply - The 60 KW radiation source was operated with two Plasmadyne PS 62 power supplies connected in parallel. Each power supply has a rated output power of 40 KW at an open circuit voltage of 320 volts. The power supplies were variable in output with control exerted by an external variac. These supplies are essentially identical to the Miller rectifier Model SR 1000-C. The control circuit is slightly different from the standard Miller unit and was specially designed for Plasmadyne.

3.2.3 Control Console - The control console contained the equipment necessary to start and control the arc power as well as gas flow instrumentation and electrical instrumentation.

3.2.4 Enclosure - The 60 KW radiation source was tested in a wooden enclosure during development and evaluation testing at Giannini Scientific. An exhaust fan and ducting were connected to the enclosure to remove ozone. The enclosure had ports in the walls for viewing the radiation source during operation and for monitoring the source operation.

3.3 INSTRUMENTATION - The instrumentation employed in the evaluation of the 60 KW radiation source consisted of the instruments necessary to measure the input power, the gas flow and pressure, the water flow and temperature as well as the image of the arc.

3.3.1 Electrical Instrumentation - Current and voltage were measured by standard meters mounted on the panel of the control console. The voltage which was measured in the tests was essentially the voltage produced by the power supply and included the voltage drop across the starter coil and in the water-cooled cables as well as the voltage of the arc. Amperage readings were obtained by using a shunt as is standard practice for high DC currents.

3.3.2 Gas Flow and Pressure - Gas flow was measured by a Brooks rotameter mounted in the console panel. Gas pressure was monitored both at the input to the source and after exit from the source heat exchanger. A mercury thermometer was employed to monitor the exit gas temperature.

3.3.3 Water Flow and Temperature - Each water path contained a Brooks rotameter to monitor the water flow as well as thermometers to measure both the input and output water temperatures. A water pump was employed to maintain water pressure at 120 psig. Initially dial type bimetal thermometers were used for water temperature measurement. These were later replaced by alcohol thermometers.

3.3.4 Arc Image - The arc was projected onto a screen by a lens which magnified the image of the arc in order to enable monitoring of the performance of the electrodes and measurement of the arc parameters. Since the electrode spacing was preset and known, the relative dimensions of the image could be reduced to actual size for evaluation of the performance of the source.

3.4 MAJOR DEVELOPMENT EFFORT ON COMPONENTS

3.4.1 Electrode Development - The major developmental effort in the evaluation of the 60 KW radiation source was in the design of a bore type anode configuration which could be operated at a current level of 600 amps for several hours. The first anode tested was similar to the one shown in Figure 1 but without the sleeve inserted. The bore diameter in the front portion was 5 mm. The material was 2% thoriated sintered tungsten. This anode worked satisfactorily at high power from the arc standpoint; however, it failed because of corrosion. The cooling mechanism involved was nucleate and film boiling. At elevated temperatures, the water vapor decomposed into oxygen molecules which progressively formed tungsten oxide through the anode wall. The corrosion rate was about 0.1 mm per minute. Finally, the arc burned a hole through the wall with a subsequent destruction of the anode.

The next step in the anode development was the application of corrosion preventive coatings to the tungsten surface exposed to water. Silver plating flaked off at relatively low temperatures. A combination of rhenium and rhodium where the rhodium was applied as a second coat on top of the rhenium did not solve the problem either, although it was temperature resistant. The reason was found in the microstructure of tungsten. Sintered tungsten does not have a solid surface since it is composed of many crystals. The plating would bridge a gap and then, under expansion, crack. As soon as oxygen molecules could pass a pin hole, it was only a question of time until total corrosion occurred.

Pure copper electrodes were tested as a substitute for tungsten. The first one having a 7 mm bore melted at 40 KW. The seond,

with a 9 mm hole, retained its integrity at 60 KW and 250 psi, but imploded at 300 psi gas pressure since the pressure differential between the gas and water passage was more than 200 psi. Finally, best operation was achieved with a copper anode having a tungsten sleeve pressed into the bore as shown in Figure 1. The heat was transferred from the sleeve to the copper and subsequently to the coolant. With an inside diameter of 7 mm and a slight protrusion of the sleeve over the copper, this anode assembly operated at 50 and 60 KW power levels and 300 psi gas pressure for a total of 172 minutes. However, some problems were encountered with the tungsten-copper anode assembly. The tungsten sleeve separated from the copper periodically due to differential thermal expansion - copper expands four times more than tungsten - and cracks in the tungsten sleeve occurred occasionally because of the high thermal stresses induced due to the alternating temperature gradient. Radial cracks were not harmful. However, tangential cracks presented a heat barrier to the radial heat flux resulting in immediate destruction of the sleeve. Experiments showed that about two anodes out of three could be used, hence it was found that the 60 KW radiation source could meet the requirements for preliminary system studies.

3.4.2 Envelopes - The use of two concentric envelopes had a dual purpose. First, all impurities in the gas including metallic particles deposited on the inner envelope. Second, the quartz utilized was opaque to radiation below 0.18 microns, hence, the energy below 0.18 microns was absorbed by the inner tube, thus the inner tube acted as a heat shield for the outer envelope. Since the pressure differential between the annulus and the arc chamber was small, the inner tube could operate at much higher temperatures due to the absence of mechanical stresses. Special attention was paid to the design of the outer envelope since it supported the entire gas pressure. The 60 KW source was equipped with tierods, hence, the outer tube was primarily subjected to tangential stresses. The ends of both tubes were shaped in order to fit the bearings. The OD tolerance of a standard size quartz tube was $\pm$ 3%, that represented for the outer tube a total variation of $\overline{3}$ mm with respect to the diameter. Early pressure tests of the tubes indicated that fire annealing of the quartz was insufficient to avoid internal stresses. Only the annealing procedure recommended for fused silica by General Electric solved the problem. Satisfactory operation at pressure levels up to 300 psig at 60 KW was achieved.

3.4.3 Tierods - The uncooled rods in the original source design were observed to fail by plastic deformation at a power level of 55 KW. The portions of the rods nearest to the arc heated up

to a red hot condition. The ultimate stress limit at that temperature was greatly reduced, too low to support 300 pounds per rod. This failure dictated the necessity of a different rod mechanism. Ceramic (Al_2O_3) coated rods were tried in an effort to improve the reflectivity. The coating discolored after a few minutes of operation and subsequently flaked off. The next approach was water-cooled rods. The tube around the rod containing the coolant had an elliptical shape with the small axis facing the arc for minimum obstruction of radiation. These rods were found to work satisfactorily and no problems were encountered under long term operation at 60 KW.

3.5 TESTS PERFORMED

3.5.1 Evaluation Tests Performed at Giannini Scientific Corporation -

Ten test runs were made on the 60 KW radiation source before shipment of the source to Spectrolab. The anode configuration employed and the test results are summarized in the data summary sheets for each test which are included as an appendix to this report.

The spectral distribution of the radiation source was measured using a Bausch and Lomb monochromator. These data were obtained during several test runs and at different power and pressure levels. The spectral distribution from .25 to 1.0 microns is shown in Figures 2 and 3. Figure 2 shows the relative intensity of each .05 micron bandwidth for 21.4 KW input power and 16.2 atmospheres input pressure. Figure 3 shows the relative spectral intensity at a power level of 60.3 KW and a pressure of 19.7 atmospheres. All data were obtained at 90° to the arc axis. Figure 4 shows a plot of the relative intensity in the .40 to .45 micron band against the input power to the radiation source with the lamp pressure as a parameter. The tests shown on this figure can be related to the summary test results given in the Appendix.

Data obtained at two different power levels are summarized in the following table. The efficiency η_{cal} was obtained by subtracting the power dissipated in the cooling water as obtained by calorimetric measurements from the input power to give the output power of the source. This output power was then divided by the input electrical power to give the efficiency.

Electrode Spacing 9.5 mm

Anode Bore 7 mm

Input Power	50 KW	60 KW
Test Time	60 min.	122 min.
Gas Pressure	300 psig	300 psig
Arc Diameter	3 mm	3.5 mm
Current	350 A	360 A
Voltage	143 V	167 V
Argon Flow	20 SCFM	20 SCFM
Average Efficiency η_{cal}	31%	-

3.5.2 Tests Performed at Spectrolab - For the proper collector design with a maximum efficiency, the micro-radiance distribution, polar distribution and spectral distribution were measured as a reference for the high power unit.

a. Micro-radiance Distribution: Figure 5 presents the micro-radiance plot. The plot was made by imaging the arc with a lens of approximately 14 in. focal length. The sensor size is shown on the graph. The rounding of the contour lines at the anode was artificial in that the arc extended into the anode bore and should have displayed a sharp cut-off. This rounding of contours was caused by the finite size of the sensor in addition to vignetting at the lens by the anode itself.

b. Polar Distribution: The polar distribution of the 60 KW source is shown in Figure 6. The energy, total intensity and the intensity of the UV portion (Corning 2404 filter) are plotted. The Eppley thermopile was calibrated at 0.00547 mv/mw/cm^2. The signal was amplified by a Dymec amplifier with a gain setting of 5.31. For conversion to absolute intensities, zonal constants were applied as a substitute for unit sphere. Furthermore, a correction factor was used for reduction of the actual radius to unit sphere. The evaluation was made as follows:

$$\text{Absolute intensity} = \frac{\text{Scale Reading}}{5.31 \times 0.00547} = \text{mw/cm}^2$$

Total energy = (Intensity) x (Zonal Constant) x $(\text{Radius})^2$

Applying this method, the radiant output of the source was 6.25 KW at 45.6 KW input power. Hence, the radiant efficiency was $\eta_{rad} = 13.8\%$.

c. Spectral Distribution: The spectral characteristics shown in Figure 7 were measured with a Spectrolab Model P-10 spectroradiometer which had a prism monochromator. The P-10 response was calibrated with a National Bureau of Standards quartz iodine lamp through the spectral range from 0.25 to 2.6 microns. In measuring the spectral distribution, the arc was viewed at a 90° angle with respect to the lamp axis. The arc was 44 inches from the P-10 and shielded from stray energy by a 30 inch long tube.

3.6 DATA EVALUATION - From the tests, it became evident that the arc diameter and accordingly the arc area changed with certain parameters. As current was increased, the arc diameter increased and as gas pressure increased, the arc was constricted. When the pressure and current were increased simultaneously, the parameters compensated each other to some extent. With this in mind, the arc area was considered constant for the radiance calculations as shown below.

The following table shows the average radiance with the source operating at various power levels. The arc area was assumed as 0.261 cm^2, the electrode spacing was 8.17 mm.

Power (KW)	Gas Pressure (PSI)	Current (AMP)	Radiance (W/cm^2/STER)
32.5	200	260	1077
45.6	250	300	2335
57.5	302	340	2996

Concerning the efficiency, a distinction was made between the efficiency calculated from the energy balance derived from calorimetric readings η_{cal} and the efficiency calculated from radiance measurements designated as η_{rad}. These two numbers should be equal. However, a rather large discrepancy was noticed. The calorimetric efficiency η_{cal} was much higher than the radiant

efficiency η_{rad}. One reason was the insufficient thermal insulation of the source components, thus, a fair amount of energy was not included in the calorimetric readings.

Looking at the spectral distribution, the spectral output shifts toward the ultraviolet region when the pressure and power are increased as readily can be deduced from Figure 2 and Figure 3.

The result shown in Figure 3 as measured by Giannini was duplicated by Spectrolab and presented in Figure 7. The operating parameters of the source were about the same. The characteristics of the two curves are in agreement, that is, a first intensity peak occurs at 0.4 micron and a second peak at 0.8 micron. However, the magnitude of the relative intensity differs considerably. One cause may be traced to the narrow resolution bandwidth of 0.010 micron employed by Spectrolab which allowed the sensing of many fine spectral lines.

Figure 4 is a graph showing the relationship between the input power, gas pressure and intensity. The intensity increases with increasing power and pressure.

The polar distribution as shown in Figure 6 shows a peak when looking into the anode bore. The increased optical depth of the arc at that angle as well as reflections from the anode face account for this increase.

3.7 CONCLUSIONS - As far as the source reliability was concerned, the critical components were the outer envelope and the anode. For satisfactory operation, the quartz had to be annealed according to the manufacturer's specifications. In regard to the 150 KW source, more work was necessary to solve the anode problem, and more particularly, the anode cooling problem. For current levels above 400 amps, tungsten inserts as employed in the prototype source were not found practical.

3.8 RECIRCULATOR DEVELOPMENT - Concurrent with the development of the 60 KW radiation source, investigations were undertaken to develop a recirculator system which would be capable of providing gas flow for the final 150 KW source. This development was culminated by the purchase of a duplex diaphragm compressor manufactured by Lapp Insulator Company, LeRoy, New York.

The initial work on recirculators was performed using a Sears Roebuck paint spray compressor with a modified cam. This compressor

has a rubber diaphragm which is moved mechanically by an electric motor. The modified pump had a displacement of 1 cu. in. and was driven by a 1/4 hp motor at 1750 rpm. A pressure differential up to 35 psi was obtained with this pump. Pumps of this type were operated in series in order to provide the required differential pressure and were used successfully in the operation of a Giannini Scientific 25 KW radiation source. Fairly severe problems were encountered with filtration and specially designed filters were made in order to produce the necessary operating life.

Based on the operation of these pumps a survey was made of the manufacturers of diaphragm compressors. Based on this survey, a pump was ordered from Lapp Insulator Company. This pump was specified to be capable of delivering 50 scfm of argon gas with an inlet pressure of 200 psig and an outlet pressure of 300 psig. Two compressor heads connected in parallel and 180° apart discharged into the same line. These two compressor heads were driven by a common motor operating at 380 rpm thus giving an effective pump rate of 760 strokes per minute. The pump employed a Type 316 stainless steel diaphragm which was guaranteed by the manufacturer for 2500 hours continuous operation.

The 60 KW radiation source was operated only on an open loop basis. The preliminary paint spray compressors were used only to operate the Giannini Scientific 25 KW radiation source. The final Lapp compressor was not used until close to the last test with the experimental unit. More will be said about this Lapp compressor in the description of the final radiation source.

4. EXPERIMENTAL RADIATION SOURCE

4.1 SCOPE - Since the major problems which were expected in the design of the final 150 KW radiation source related to the development of suitable electrodes and to the dimensions and shapes of the envelopes, and since these problems are not readily solvable by analytical methods, an empirical study program was undertaken to provide answers for the development of these items. A program to evaluate the various parameters associated with the anode design and envelope design in order to achieve sufficient operating life at high power levels was devised. Different anode shapes, anode sizes, and anode cooling mechanisms were studied as well as the minimum quartz envelope diameter. In order to accomplish this empirical design program in the most efficient manner, a versatile experimental radiation source was designed. This experimental unit enabled the use of a large number of anode and envelope sizes without major modifications of the basic source hardware.

4.2 SOURCE DESIGN - The basic source design is shown in Figures 8 and 9. The design concept was similar to the 60 KW prototype source described in paragraph 3.1. Water-cooled tierods were utilized with the only difference being that the water jacket was brazed to one end of the rod and the other end of the jacket was sealed by O-rings to allow thermal expansion of the jacket without distortion of the rod. Components were fabricated to assemble three different sizes of the lamp. The differences of these three sizes were primarily in the area immediately surrounding the arc. The inner quartz envelope, anode, cathode, cathode housing, and anode housing were the main items which differed among the three units. Provision was incorporated to use thermocouples to measure the anode temperature during source operation.

4.3 TEST FACILITY - Since the 60 KW radiation source had been shipped to Spectrolab along with associated equipment including the starter, power supplies, and control console, it was necessary to build a new facility for testing the experimental radiation source. The wooden enclosure which was employed for the 60 KW source was observed to ignite and burn during operation at 60 KW. Therefore, it became necessary to design and fabricate a new test enclosure. This test facility consisted of the following main items.

4.3.1 Starter - A new starter was developed for the experimental unit which produced an output voltage of 50 KV. This was a bread-board type starter and was of essentially similar design to the one used on the 60 KW source. A major change was in the secondary transformer where the transforming ratio was changed from 2:1 to 5:1. In addition, larger diameter copper tubing was used to wire the secondary of the secondary transformer in order to provide for the increased current carrying capacity.

4.3.2 Power Supplies - Five Plasmadyne Model PS 62 power supplies were used for the experimental source. These supplies were connected in parallel. Initially, the output voltage was set at 320 volts open circuit for each machine. This setting was changed to 160 volts open circuit for the high current runs with the solid anode.

4.3.3 Control Console - A console essentially identical to the one used for the 60 KW radiation source was constructed. A major change was the incorporation of the larger variac in order to control the five power supplies simultaneously.

4.3.4 Enclosure - Because of the problem with the 60 KW testing, a water-cooled enclosure was designed and constructed for the testing of the experimental unit. This enclosure consisted of a vertical

cylindrical housing of double walled construction whereby water-cooling was used between the two walls. This housing was clamped to a water-cooled aluminum base which was supported by a tripod. The inside of the enclosure and the top of the base were coated with black paint to reduce reflections and to indicate the emitted radiation by monitoring the water flow and temperature to the enclosure. The enclosure was a welded aluminum structure and was troubled by water leaks which delayed testing for several weeks. These leaks were finally sealed by a layer of epoxy which was applied with a plasma spray gun.

4.4 INSTRUMENTATION - One additional instrument was added to the ones described in paragraph 3.3 consisting of a thermocouple meter for recording the axial temperature distribution in the anode. The platinum-rhodium thermocouples were installed on the outside of the anodes in regular spacings. The sensing tips of the thermocouples were silver soldered to the anode to obtain good thermal conduction. The recording meter was disconnected during starting of the source by the use of knife switches in the thermocouple leads to protect the meter from damage by the high voltage spark used to start the arc. The knife switches were enclosed in a housing to keep the contacts at a uniform temperature. In addition, an isolation transformer was built into the circuit to eliminate disturbances from the input power.

4.5 DEVELOPMENT EFFORT

4.5.1 Bore Type Anode - In the first phase of the high power source development, bore type anodes were investigated. The influence of different bore diameters at various power levels on the radiancy was subject of investigation. In addition to that, the anode temperatures were measured. The test results are discussed in paragraph 4.8. It was believed that there was an optimum relationship between the bore and arc diameters at a given power level to produce optimum life, arc stability and efficiency. The arc diameter could be controlled by the gas flow and vortex strength. For all experimental anodes used in the first phase, copper was selected as the anode material. Copper was not the optimum anode material but was chosen for experimental testing because of the relatively low price and its ease of machining.

The requirements of a high performing anode material are high melting temperature, resistance to thermal shock as well as high thermal and electric conductivity. The thermal properties of different anode materials may be compared in the following manner.

The heat conducted through an element is

$$q = kA \frac{\Delta T}{\Delta x}$$

where q = heat transfer rate

k = thermal conductivity

ΔT = temperature differential through the element

Δx = thickness of the element

A = Area

The above equation may be expressed as follows:

$$q = \frac{A\ (k\ \Delta T)}{\Delta x}$$

The product in the parenthesis on the right side of the equation exhibits the criterion on which the suitability of different materials can be compared. The maximum amount ΔT can assume is the melting temperature of the material, thus, ΔT is substituted by the melting temperature T_{melt}. For a comparison, it is convenient to use copper as a reference and set the product $(k \times T_{melt})_{Cu}$ equal to unity. Some materials under consideration are listed in the following table:

Material	T_{melt} (°F)	k (BTU/hr.ft.°F)	El. Resistance (micro-ohm)	$\frac{k \times T_{melt}}{(k \times T_{melt})_{Cu}}$
Copper	1981	200	2.03	1.000
Chromium Copper	2147	187	-	0.998
Silver	1761	242	1.59	1.100
Gold	1945	172	2.35	0.847
Tungsten	6170	90	5.48	1.222
Molybdenum	4750	70	5.17	0.746
Platinum	3224	42	14.9	0.316
Tantalum	5425	31	12.4	0.373
Rhodium	3571	50	4.51	0.412

This evaluation shows that only tungsten is considerably better than copper since it allows a greater heat transfer rate. Thus, the replacement of the copper anodes by tungsten anodes would allow a current increase of approximately 20%.

A second, third and fourth phase in this development program was devoted to the anode cooling mechanism, arc constriction and predetermined location of the arc foot respectively; in other words, the upgrading of the best suitable anode in regard to life established during the first phase.

For the systematic investigation of the bore size on the arc performance, four bore diameters had been chosen: 8 mm, 12 mm, 16 mm and 20 mm. Every one of these anodes were accommodated in the best suited version of the experimental source. The technical data are summarized in the following table.

Anode Bore DIA (mm)	INNER QUARTZ TUBE		OUTER QUARTZ TUBE	
	ID (mm)	OD (mm)	ID (mm)	OD (mm)
8	40	43	95	104
12	40	43	95	104
16	60	64	95	104
20	80	84	95	104

The investigation program of the bore type anode was completed as far as the first phase was concerned. The program was then discontinued because of the progress made with a new type anode, the so called solid anode, which was based on an entirely different concept.

4.5.2 Solid Anode - The new anode design was derived from the conventional solid electrode configuration. The solid anode is generally constructed with a blunt cone or a flat plate for electron impingement. The solid anode is superior to the bore type anode in terms of efficiency of radiation output. The increased efficiency is obtained due to the shorter arc than in the bore type anode, thus producing a lower voltage. In addition, the arc does not have to penetrate the cold boundary layer of gas to reach the anode surface, thus reducing the potential drop in the anode fall region. Solid anodes have been widely used in industry. An advanced design of a nonconsumable solid electrode was published by Busz - Peuchert and Finkelnburg[1] in 1954.

The major problems encountered with solid anodes were the attainment of long life at elevated current levels. Life is governed by the current density at the anode which is in direct relationship to the heat input and consequently to the anode

1) Z. Physik, Vol. 139, p. 212, 1954

surface temperature. When the bore type anode is compared to the solid anode, the latter one is characterized by the attachment of the arc foot to the anode at the same spot and the absence of convective gas cooling in the interface of plasma and anode surface. In the bore type anode, a lower surface temperature is obtained for the following reasons: the vortex action of the gas forces the arc column to rotate, as a result the arc foot executes a translating motion on the bore surface with respect to the anode axis. Furthermore, the breakdown and build-up of the electric field causes the arc foot to oscillate axially along the bore. The combination of these motions results in an elliptical flat pattern development distributing the heat over a large surface. In addition, only the core of the arc is at an elevated temperature, the gas layer near the bore surface is relatively cool due to the axial gas flow.

In order to maintain a high current density in the arc column and a low current density at the anode, a new technique was proposed causing the arc foot to diffuse over a large anode surface, thus reducing significantly the current density. The diffusion of the arc foot was accomplished by aerodynamic effects and geometrical design. A ring was inserted between the anode arcing surface and the cathode to produce the aerodynamic diffusion. This ring is referred to simply as the "diffuser."

Discussing the aerodynamic effects first, the diffusion was essentially achieved by reversing the parameters which act to aerodynamically constrict the arc. The vortex generates a radial pressure drop toward the axis. Since the mass of the plasma is extremely small, the pressure forces exceed the centrifugal forces acting on a fluid element thus concentrating the plasma around the axis. The flow passage inside the ring near the anode arcing surface was chosen in a manner that a radial pressure drop toward the outside was established accompanied by increasing flow velocity thus producing a dispersed anode foot.

The geometrical diffusion was accomplished by providing a counter sink to the face of the anode in order to reduce the specific heat input to the anode surface by increasing the area of arc attachment. Because of this concave anode contour, the shortest path to the anode of a charged particle in the anode region was not along the arc axis but at some inclination to this axis. The optimum counter sink was a half angle of 45°. Greater half angles were tried experimentally but were found to be inferior.

Since the diffuser ring was at the same potential as the anode arcing surface and was closer to the cathode, a potential difficulty of arc attachment to the diffuser ring existed. No problems were experienced, however. The reason may be found in

the fact that both sides of the diffuser, the one facing the arc and the one facing the anode, were shielded by a cold layer of gas. Since the penetration of electrons through this cold boundary layer required a higher potential drop than the impingement on the anode arcing surface where no such cold gas layer existed, the arc chose the latter surface as its termination point.

Summarizing, the diffuser ring caused a diffusing action of the arc by aerodynamic means. The bore in the diffuser was slightly greater than the arc diameter while the arc attachment area on the anode was at least an order of magnitude greater than the cross-sectional area of the arc. A photograph of the diffused arc foot is shown in Figure 21.

A fair amount of difficulty was experienced in selecting the proper diffuser material. Sintered tungsten which was used first survived the intense radiation from the arc. However, the tungsten proved to be sensitive to thermal shocks. Cracks occurred in the radial and azimuth directions. Radial cracks did not interfere with the cooling mechanism but the cracks in the azimuth direction constituted a heat barrier and those portions of the diffuser melted in a short period of time. Molybdenum showed a greater thermal shock resistance and, therefore, was used for most of the tests.

An attempt was made to employ a water-cooled diffuser design. The diffuser was a hollow copper ring with a water separator between the walls. The coolant flowed from the periphery toward the center on the arc side and was guided in a radial direction back to the anode body on the anode side. This design was tested but was not successful. Difficulties were encountered in providing the proper geometry for the gas passage behind the diffuser since the water-cooled diffuser required a larger cross section in order to accommodate the cooling passages. This unit had the larger half angle counter sink which also contributed to the failure. The anode failed at a current level less than 1000 amps. The water-cooled diffuser concept was not pursued since it appeared that the radiation cooled diffuser could meet the requirements.

4.5.3 Envelopes - A major objective of the experimental program was to find the required size of the quartz tubes in terms of inside diameter and wall thickness. The inner quartz tube was subjected to high specific heat inputs which could lead to failures (devitrification, melting, cracking). For a given tube size, the

failure was dependent on the power level and operating time. Analytical studies indicated that thermal equilibrium was established in the quartz after approximately one hour of continuous operation. All three envelope sizes as described in paragraph 4.5.1 were tested to their limits. A maximum allowable power level at equilibrium conditions is shown in the following table:

Tube Size (inner envelope)	ID/OD mm	Max. Power (kw)
Small	40/43	65
Medium	60/64	100
Large	80/84	150

During testing, the large tube was operated in a two hour continuous test and also for a total elapsed time of ten hours. Since operation was at the required power level of 150 KW, it was concluded that the large tube size was proper for the final source design.

4.6 ANALYTICAL WORK - In order to provide guidance in the source design, four analyses were conducted, namely:

a. Total Reflection in the Plasma Radiation Source (Appendix DM 272-62).

b. Radial Heat Flux Through a Sleeve (Appendix DM 272-63).

c. Heat Transfer in the Cathode (Appendix DM 272-61).

d. Determination of the Heat Transfer Coefficient from the Envelope to the Cooling Medium (Appendix DM 272-3).

During the experimental source design, considerable effort was expended in the design of a self-supporting envelope for the final radiation source. All analytical work performed in relation to the final source is described in paragraph 5.3.

4.7 TESTS PERFORMED - The tests performed during the development program of the experimental unit included performance testing and temperature measurements in the bore type anode. The range of activity is outlined in the following paragraphs.

4.7.1 Performance Testing - Discussing the bore type anode first, a test program was devised to establish the parametric relationship between the bore diameter, current, radiation output, gas flow, gas pressure and efficiency. Useful data were obtained with the 8 mm and 16 mm bore anode. The 12 mm anode was destroyed as a result of a tube failure. Tests with the 20 mm anode were discontinued in favor of the solid anode. The reduced data are presented in Figures 11, 12 and 13. The results are discussed in paragraph 4.8.

Similar tests as described above were conducted for evaluation of the solid anode. The data are plotted in Figures 17 and 18. The purpose of these tests was to achieve operation at an input power of 150 KW with a minimum efficiency of 30%. A molybdenum diffuser with a 0.600 inch bore was used exclusively in relation to the data reported. Above a power level of 130 KW, the 0.600 inch diameter orifice started to deteriorate. At a power level of 150 KW, the erosion of the orifice stopped at 0.670 inch. With that diameter, a molybdenum diffuser was operated at 150 KW during two hours of continuous operation. The evaluation of the data is presented in paragraph 4.8.

4.7.2 Temperature Measurements in the Bore Type Anode - The installation of thermocouples in the anode served a dual purpose. The first purpose of the thermocouples was to allow the unit to be extinguished before the destruction point of the anode was reached. Secondly, the knowledge of the axial temperature profile in the anode was mandatory to find the temperature peaks.

Figure 14 indicates the axial temperature profile in the 16 mm bore type anode at currents of 600 and 700 amps with the gas flow rate as a parameter. Since previous tests showed evidence that the arc foot path inside the bore was an ellipse rather than a circle, these measured profiles were indicative of the specific locations of the thermocouples which were arranged in one plane containing the anode axis. A different tangential distribution of the thermocouples would probably have led to a somewhat different temperature curve. However, the essential result would not have been changed.

The data show the highest temperature to be at the front face in all cases. A second maximum occurred between 3/4" and $1\frac{1}{2}$" downstream from the entrance. This second peak can only be interpreted as the arc foot region since it is known from visual observation that the arc does not strike near the front face of the anode. It is surprising that the arc foot region is at a lower temperature than the front face of the anode. These temperature curves are in agreement with the observations

that all copper anodes which failed melted near the front face and then imploded since the gas pressure in the arc chamber was higher than the water pressure in the cooling passage inside the anode.

The temperature profile can be explained by studying the anode heat input in conjunction with the cooling mechanism. Figure 15 is useful to explain the temperature distribution. From the entrance to the arc foot region, the arc generates an equal amount of radiated heat which is absorbed by the anode. This is expressed as # 1 in Figure 15. In the arc foot region, the heat created by the impact of the electrons adds to the radiated heat as shown by # 4 in Figure 15. In the front face of the anode, the anode head absorbs heat from the arc as shown by # 2, in addition, the conical outer section of the anode receives additional heat input due to the absorption of a portion of the radiation reflected by the quartz tubes as shown by # 3 in Figure 15. Since the heat input at a specific location is additive, there is a concentration of heat input in front of the anode and also in the arc foot region.

The temperature in the anode is not only a function of the amount of heat input, but it also depends on the heat transfer coefficient to the coolant, or in other words, how well that portion of the anode is cooled. In the arc foot region, the heat is conducted axially and radially away from the hot spot and transferred to the cooling medium over a much larger surface than that in the anode head. The arc foot region is cooled quite well whereas the anode head with the largest heat input is lacking an efficient cooling, thus, the principles of ideal cooling are violated. For any future application of bore type anodes, this deficiency would have to be overcome by an adequate cooling mechanism.

Figure 16 plots the temperature near the anode entrance against the cooling water flow rate. The purpose of this test was to gain more insight as to the minimum required water flow rate. One point was recorded at maximum water flow of 11 gallons per minute. The corresponding equilibrium temperature was 700°F. Then the cooling flow was reduced. The anode temperature changed very little as the flow was reduced from 11 to 5 gallons per minute. Below 5 gallons per minute, a rapid increase in anode temperature was noticed and the failure occurred near 1200°F, that is, the anode approached the melting temperature of 1980°F on the arc side.

4.8 DATA EVALUATION - All data of importance have been reduced and are plotted in Figures 11, 12 and 13 for the bore type anode, and Figures 17 and 18 for the solid anode. The evaluation of the data is presented in the following sections.

4.8.1 Bore Type Anode - Figure 11 shows the luminous efficiency in lumens per watt as a function of the current with the gas flow, gas pressure, and bore diameter as parameters. The luminous efficiency increased as the current increased at constant gas flow rate and, generally, also increased with decreasing gas flow rate at constant current. As was found in earlier tests and predicted, the luminous efficiency increased approximately in proportion to the pressure level.

Figure 12 is a plot of the arc voltage versus the volume flow rate of the gas for the 16 mm diameter bore anode at a current of 650 amps. As the gas flow rate was increased, the arc voltage increased due to the higher gas velocities in the anode bore and the consequent elongation of the actual arc length as the arc was carried further downstream in the bore. The data indicate that for low flows (10 scfm to 15 scfm), the voltage change was considerable whereas above 15 scfm only a marginal increase in voltage was noticed. This indicates that the elongation of the arc by increased gas flow rates reaches a limit before extinction of the arc occurs.

Figure 13 presents a plot of the total efficiency (measured calorimetrically) versus the arc current with the argon flow rate as a parameter. The general tendency is for an increase in efficiency as the current is increased at constant gas flow rate and an increase in efficiency by reducing the gas flow rate at a constant current. During the evaluation, some inconsistencies of the data were noticed. The discrepancies may be explained by difficulties in achieving equilibrium conditions because of the variation of the input power due to the operation of other equipment in the test site utilizing the same power supply net. Another effect influencing the luminous efficiency might have been a slight change in polar distribution from the use of different anodes. Since the foot candle meter was always located at the same position relative to the source, a change in polar distribution would have influenced the measured luminous efficiency without changing the total amount of light output necessarily.

4.8.2 Solid Anode - The performance curves are shown in Figures 17 and 18 for orifice diameters of 0.5" and 0.67" respectively. The radiated power was derived from the calorimetric efficiency and the input power. The radiated power increases with increased current as expected. However, the 0.5" orifice anode shows a

falling efficiency with increased current, hence the increase in radiant power is marginal. The arc diameter increases with increasing current which is a well known phenomenon when the gas flow rate and the gas pressure are kept constant. For both orifices, the brightness was approximately constant throughout testing and it was higher for the smaller orifice. This implies that the brightness "B" is related to the current density of the arc. Based on the arc cross-section, the current density "j" for the 0.5" orifice anode was approximately 28 Amp/mm^2 and for the 0.67" orifice anode approximately 22 Amp/mm^2. There is

$$\frac{B\ (0.5"\ \text{orifice})}{B\ (0.67"\ \text{orifice})} = \frac{23}{19} \simeq 1.2$$

and

$$\frac{j\ (0.5"\ \text{orifice})}{j\ (0.67"\ \text{orifice})} = \frac{28}{22} \simeq 1.2$$

The solid anode development culminated in a two hour endurance run at 150 KW without failure. The result of this test is presented in the table below which is also an instructive summary between the performance of the bore type and solid anode.

Parameter	Bore Type Anode		Solid Anode
	8 mm	16 mm	Orifice DIA=0.67"
Current (Amp)	700	900	1480
Voltage (V)	120	130	102
Power (KW)	84	117	150
Luminous Efficiency (Lm/Watt)	14	10	18
Efficiency η_{cal} (%)	32	28	30
Relative UV Rad.	0.41	0.42	0.44
Arc DIA (mm)	3	8	10
Electrode Spacing (mm)	10	10	15
Gas Flow (SCFM)	20	20	34
Gas Pressure (psig)	250	300	300

4.9 SYSTEM DEVELOPMENT - The experimental unit was operated almost exclusively with an open loop argon system. One of the last tests performed on the experimental radiation source employed the duplex metal diaphragm compressor purchased from Lapp Insulator Company. Great difficulty was encountered in obtaining proper operation of this pump and the one test where the pump was employed caused serious damage to the outer envelope of the source due to rupture of the diaphragm allowing oil to enter the argon system. The oil adhered to the outer envelope and caused failure of the lamp.

The 50 KV starter employed with the experimental radiation source had sufficient capability to ignite the source only at a pressure level of approximately 50 psig with a 15 mm arc gap. In order to evaluate the possibility of starting the lamp at design pressure of approximately 250 to 300 psig, an experimental 500 KV starter was manufactured. This starter was successfully bench tested and the 500 KV output was proven by the creation of an arc in air of approximately 7". When the 500 KV starter was assembled to the experimental radiation source, the arc could not be started since the extremely high voltage spark found innumerable paths to ground. Since it was felt that it would be impossible to eliminate all of these extraneous paths, further testing of this 500 KV starter was discarded.

4.10 CONCLUSIONS - From the tests performed with the 150 KW experimental source, the following conclusions may be made:

a. A bore type anode can be built for a power level of 150 KW. However, the performance in terms of efficiency is inferior to the solid anode. Thus, the bore type anode is not recommended for radiation source applications.

b. It is possible to build a solid anode for operation at 150 KW with conventional water-cooling. A two-hour endurance run has been demonstrated.

c. The large size inner envelope (84 mm OD/80 mm ID) is required for a power level of 150 KW when regular gas cooling is applied.

d. It is feasible to build a 150 KW radiation source suitable for incorporation in a simulator.

5. FINAL 150 KW RADIATION SOURCE

The final radiation source was derived from the experimental unit. A layout of the final source was submitted to the contract monitor for approval. Two changes were incorporated into the design layout as requested by Spectrolab. The cathode half angle was adjusted to provide a shorter outer tube by making the included angle of the cathode body larger. An adjustable cathode was also included to allow a variation of the electrode spacing.

5.1 DESIGN CONCEPT - During the development period, a number of requirements in regard to the final source design became obligatory in order to achieve best mating conditions between

the source and the optical system. Least obstruction of the emitted energy and maximum collection of radiation were essential factors for the design concept. A study was made of various mounting possibilities of the source with respect to the collector. A cantilevered arrangement was found most practical with the anode housing mounted in the vertex of the collector. The supporting mechanism of the source was designed to make all necessary adjustment operations. A self-supporting envelope was pursued to minimize the cutout of the collector. There was another reason to abandon tierods, namely, the radiation output could be improved because of the absence of shadows. The anode housing could be greatly reduced in weight by dimensioning the heat exchanger for the minimum required capacity necessary to cool the gas down to 200°F so that the gas could be ducted to a secondary heat exchanger in the system with standard hoses. The directives for the final source design are summarized as follows:

a. Solid anode configuration.

b. Radiation cooled diffuser.

c. Two concentric envelopes.

d. Outer envelope self-supporting.

e. Envelopes cooled by convective gas cooling.

f. Cathode opening angle 70°.

g. Adjustable electrode spacing from 10 to 20 mm.

h. Two heat exchangers for the gas where the primary heat exchanger is an integral part of the anode housing.

A cross-section of the final source is shown in Figure 19. The only part which differed significantly from the experimental source and had to be developed for the final source was the self-supporting envelope. During the development of the 60 KW prototype source, it became apparent that the envelope exhibited one of the major problems. The envelope suffers high mechanical and thermal stresses during operation of the source. The tensile strength of clear fused quartz is 7000 psi as specified by the manufacturer. But this figure is to be considered as an ideal number and no manufacturer would guarantee it. Because of the uncertainty of the maximum allowable tensile strength,

it is a standard practice to use a safety factor of 10 whenever quartz is utilized. Since radiation is involved, the problem cannot necessarily be solved simply by adding material. Deeper penetration of radiation causes more energy absorption with a subsequent increase in thermal stresses. The balance of thermal and mechanical stresses leads ultimately to the optimum envelope design. Preliminary studies indicated that for radiation source applications an industrial safety factor of 10 cannot be maintained if the source is expected to operate with a high radiant output. Much effort was expended to improve the fabrication of the tubes including the thermal treatment of the quartz in order to approach the ideal tensile strength of 7000 psi. Special checking procedures were devised to detect impurities in the quartz and to find residual stresses with polaroids. Impurities in the quartz are especially detrimental for two reasons. First, they cause a local stress concentration and, second, they absorb more energy resulting in local melting of the quartz. Some envelope failures on the experimental source were traced to this phenomenon. In order to concentrate the design effort on high power electrodes, the 60 KW prototype unit and the experimental 150 KW source were equipped with tie-rods which supported all axial forces, thus no major problems were encountered. For the final source, a self-supporting envelope was desirable. From the mechanical and fabricational viewpoint, a self-supporting envelope appeared feasible.

The crucial points of a self-supporting envelope are the regions where the forces are transmitted to the supporting structure, that is, the quartz to metal coupling. This quartz to metal coupling deserves special attention that no stresses are imposed on the envelope when the source is being assembled and that the load is evenly distributed during operation. An envelope design was chosen consisting of an outside flange on one end and an inward flange on the other end. The outside flange was connected to the anode housing whereas the cantilevered end with the inward flange supported the cathode. This particular design required a minimum diameter hole in the collector and also produced a maximum solid angle of radiation from the source. The problem encountered with an inward flange was the generation of tensile stresses as a result of the forces acting on the flange in the axial direction. An outside flange is subjected to compression rather than tension and since the ultimate compression strength of quartz is 27 times higher than the tensile strength, the outside flange exhibits a superior design from the viewpoint of stresses. However, other advantages of the inward flange on the cathode side of the envelope as mentioned above were in favor of the "inward-outward-flange" configuration.

A considerable amount of effort was expended in devising a method to shape the quartz tubes. The first experiments to mold flanges to a tube with a wall thickness of 4 mm failed because the hydrogen flame used generated an insufficient amount of heat. Additional heat input was accomplished by using a plasma torch on the outside and a hydrogen torch on the inside of the tube. Special water-cooled molybdenum tools were manufactured in order to shape the quartz. Graphite tools did not serve the purpose because of deposition of small graphite particles on the quartz and because of the high decomposition rate of graphite in the temperature environment present. The combined use of a hydrogen and a plasma torch was partially successful. The flanges could be molded on both ends but the required wall thickness of the tube could not be maintained. The molding technique was not further developed because the machining of the tube out of a quartz ingot promised a more practical approach to the problem. The technique of grinding and polishing with several intermediate annealing processes was successful. A photograph of the first manufactured envelope applying the grinding technique is shown in the lower half of Figure 20. The tube was pressure checked at 200 psig. During operation at full power, the tube survived pressures as high as 290 psig.

5.2 COMPLETION OF THE FINAL SOURCE - The detailed drawings of the final radiation source and approximately two-thirds of the fabrication of the source components were completed under the subcontract from Spectrolab to Giannini Scientific Corporation. At this point in the program, the subcontract was terminated by Spectrolab because all funds had been expended by Giannini. The decision was made to complete the fabrication of the source and to assemble and test it at Spectrolab.

The manufacture of the source components indicated a problem area with the anode heat exchanger and this portion was redesigned at Spectrolab and successfully fabricated using furnace brazing techniques. All equipment including the recirculating compressor was delivered by Giannini Scientific to Spectrolab and incorporated into Spectrolab's R&D Lab. The radiation source was placed inside the test enclosure with the control console, recirculator, etc., located in the main portion of the test lab. Outside of the enclosure, the test facility and instrumentation were essentially the same as described for the experimental unit in paragraphs 4.3 and 4.4.

5.3 ANALYTICAL WORK - Concurrent with the testing of the experimental source, analytical work was performed toward the design of the

self-supporting envelope. A number of investigations were required to estimate the stresses in the envelope. These investigations were summarized as development memorandums and are included in the Appendix. They include:

a. Energy Absorption in the Envelope of a Plasma Radiation Source (Appendix DM 272-2).

b. Radial Temperature Distribution on the Envelope of a Plasma Radiation Source (Appendix DM 272-4).

c. Simplified Stress Analysis of a Radiation Source Envelope (Appendix DM 272-5).

d. Transient Heat Transfer in the Envelope of a Plasma Radiation Source (Appendix DM 272-6).

While these investigations do not represent a complete analysis of the self-supporting envelope, they represent the division of the one problem into relatively simple problems in order to enable easy analytical treatment with straightforward solutions. The more detailed analysis could not be finished because of the directive from NASA/Ames to stop all source development work. In addition to the self-supporting envelope, problems were encountered in the manufacture of the diffuser for the anode.

An analysis was made of the heat transfer in a composite diffuser (Appendix DM 272-7) which indicated that a composite of a refractory inner ring and an outer copper ring could give increased performance over a pure refractory or pure copper diffuser. A secondary reason for the incorporation of the composite diffuser into the final radiation source design was the difficulty in achieving a good brazed joint with a single refractory diffuser. Brazing tests were conducted with the assistance of our furnace brazing supplier and the results of these tests are documented in DM 272-1, which is included in the Appendix to this report. The composite diffuser design enabled easy inspection of the difficult brazed joint between the refractory metal portion of the diffuser and the copper outer ring. No difficulties were expected or encountered in the brazing of this outer copper ring to the copper anode body.

5.4 TESTING - The final radiation source was operated successfully both by itself and integrated with the prototype optical system. All tests performed with the final radiation source have been

documented in detail in the development memoranda which are included as appendices to this report. No additional development work on the radiation source was conducted after integration with the prototype system under direction from NASA/Ames.

Test runs 1 through 4 which were performed to evaluate the radiation source are documented in DM 272-14. During these tests, the source was operated with a copper diffuser in the anode. Each test run represented a parametric variation of the arc current at constant gas pressure levels of 200, 225, 250 and 275 psig. A polar plot of the radiation source was also obtained during Run 1. Complete data for these four test runs and information regarding the test setup and data acquisition methods are contained in DM 272-14.

Test runs 5 through 9 were performed with the radiation source integrated with the prototype optical system. These tests were performed to obtain data relating to intensity in the target plane. DM 272-16 gives the performance of the radiation source during these tests. The optical data obtained are presented in Volume I of this report. Test runs 5 and 6 were performed with the copper diffuser; and beginning with Test run 7, all further testing was performed with a molybdenum diffuser.

Test runs 10 through 13 were performed without the prototype optical system in order to obtain a relative calibration of various intensity sensors. In addition, during test run 13, a polar plot and micro-radiance data were obtained. The performance of the radiation source during these tests is documented in Development Memoranda 272-17 and 272-23.

The polar distribution and total energy calculations with the radiation source operated at three different current levels are described in DM 272-22. The micro-radiance distribution including the test setup and the micro-radiance plot at different currents and pressure levels is presented in DM 272-29.

Test runs 14 through 19 and 22 were performed as life tests of the radiation source and are described in detail in DM 272-24. Because of the intermittent nature of the planned operational conditions for the radiation source, the life tests were performed as a series of relatively short test runs with a maximum of five minutes duration at the rated power level. A total of 25 complete cycles of the radiation source was obtained in this test series. After the 25th cycle during Run 22, a quantity of oil was noted on the inner quartz envelope of the

radiation source due to a failure of the diaphragm in the recirculator pump. This failure of the pump caused discontinuance of the test series since the inner quartz envelope had to be changed. During this test series, the radiation source was operated at a current level as high as 1620 amps.

Test runs 20 and 21 were performed to enable measurement of the spectral distribution of the energy coming from the radiation source. The source operation during these test runs is documented in DM 272-25. The spectral distribution of the final radiation source at three different test conditions and the method of data reduction is described in DM 272-27. A description of the method of measuring the spectral distribution and the calibration factors is given in DM 272-28.

Test runs 23 through 30 were performed with the radiation source integrated with the prototype optical system in order to obtain data relating to the performance of the optical system. A description of the source operational characteristics and of the individual tests is presented in DM 272-30. Test runs 33 through 35 were also performed with the radiation source integrated into the prototype optical system and these tests are documented in DM 272-36.

Test runs 36 through 39 were performed with the radiation source integrated with the prototype optical system and these tests were used to evaluate several parameters relating to the radiation source operation. In Test run 36, the flow rate of the argon gas was varied in order to evaluate the effect of gas flow on target intensity. Both arc voltage and target intensity were observed to increase as the gas flow was reduced while maintaining arc current constant. During test run 37, gas pressure data were obtained at five different locations in the argon system in order to provide inputs for the design of the final radiative heating system. Test run 38 was a continuous life test of the radiation source which resulted in a continuous operating time at current levels in excess of 1550 amps for a total of 145.4 minutes. The current was increased several times to 1600 amps and no indication of any degradation of the radiation source was encountered. The test was voluntarily terminated and at the completion of the test, some degradation of the O-ring seals was noted. The radiation source was reignited and a total of 60 minutes of continuous operation in Test run 39 was obtained before a failure of the inner quartz envelope was anticipated due to a deformation of the quartz. These tests are documented in DM 272-37.

Test runs 40 and 41 were performed with the radiation source integrated with the collector with the purpose of obtaining

target intensity data. Failure of the recirculator pump due to rupture of the diaphragm allowing oil to enter the argon system caused a termination of Test run 41. After the argon system had been cleaned, the source was reassembled and on repressurization, a failure of the outer quartz envelope occurred. This failure occurred during static gas pressure test of the reassembled source at a gas pressure of 250 psi. Complete details, including photographs, relating to this failure are presented in DM 272-38.

Test runs 42 through 49 were performed in order to obtain further data on the prototype optical system. The operation of the radiation source during these tests was documented in DM 272-43.

Several additional tests were performed to aid in the design of the final radiative heating system. One additional test was performed with the radiation source not integrated with the collector in order to obtain absolute values for the micro-radiance contours previously obtained. This test run and the calibration of the micro-radiance are presented in DM 272-48. The peak radiance obtained for this radiation source was 6215 watts/cm^2-str. as described in the referenced development memorandum.

In addition to the operational tests of the radiation source, work was performed relating to the system. Development Memoranda 272-10 and 272-34 present a calibration of the DC system used with the radiation source in order to allow measurement of the actual voltage drop across the source. These reports give data and curves for the voltage drop through the DC system with a shorting bar used in place of the radiation source.

Significant problems were encountered with the argon recirculator pump throughout the testing of the final radiation source and these problems are summarized in Development Memoranda 272-8, 272-11 and 272-52. A fair amount of work was expended by Spectrolab personnel in the rework of the recirculator pump in order to make it a more useable instrument for its purpose. This rework included changes to the oil makeup pump, additional plumbing in the oil system, the addition of filters to the oil system and the argon system and the manufacture of precision gaskets and diaphragms. In addition, an analysis was performed of the diaphragm indicating that the material specified by the manufacturer was excessively thick. At the end of the testing period, the recirculator was operated with diaphragms made from .010" stainless steel stock and appeared to operate in a satisfactory manner.

5.5 CONCLUSIONS - The final radiation source developed under this program operated successfully at currents up to 1600 amps and at pressure levels as high as 290 psi. The major problem area with the radiation source lies in the cathode tip and in the prevention of the expulsion of molten material from this tip during operation of the source.

The output of the final radiation source, while satisfactory, can be improved by minor modifications to the design.

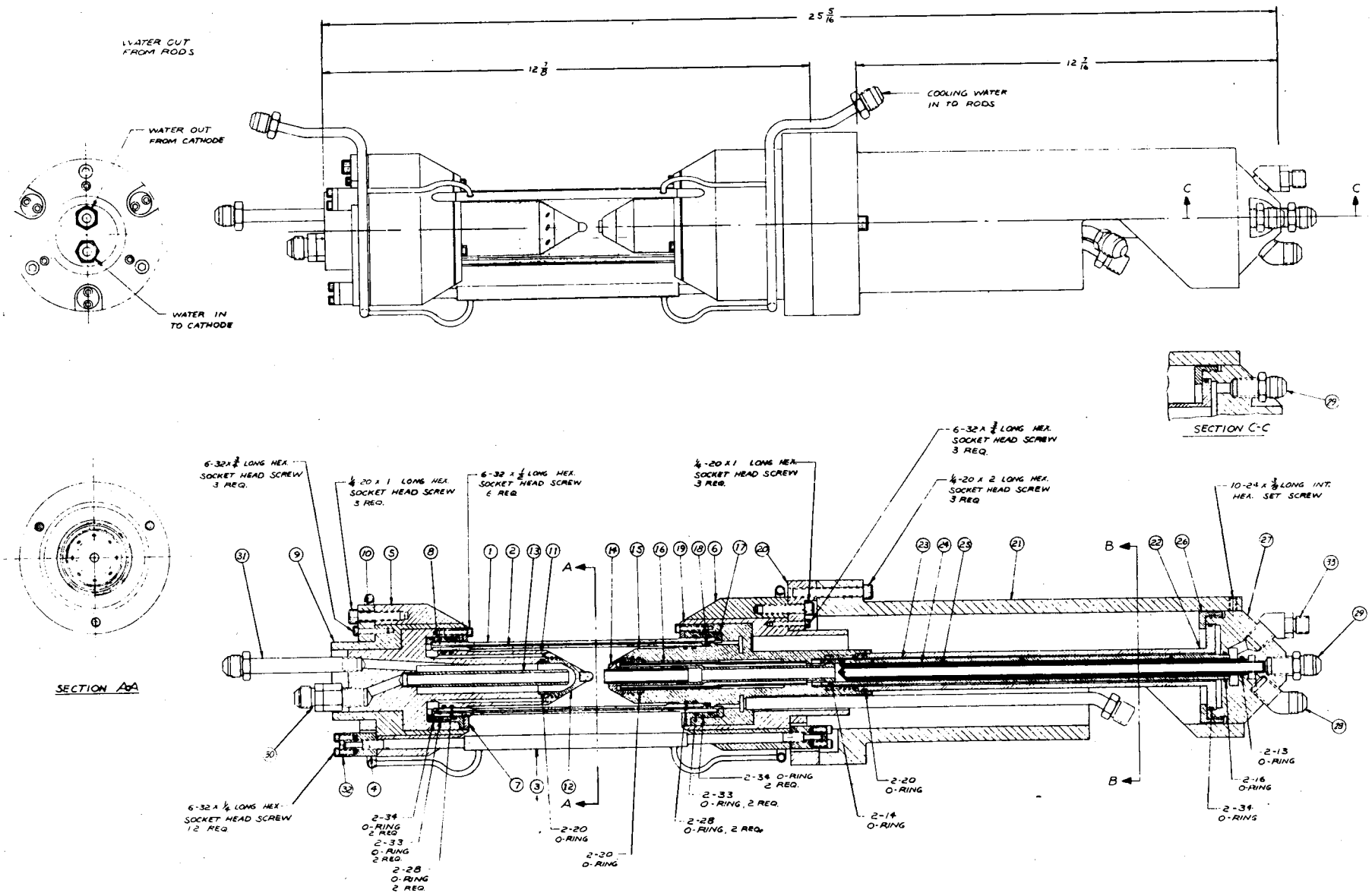

60 KW PROTOTYPE RADIATION SOURCE

FIG. 1

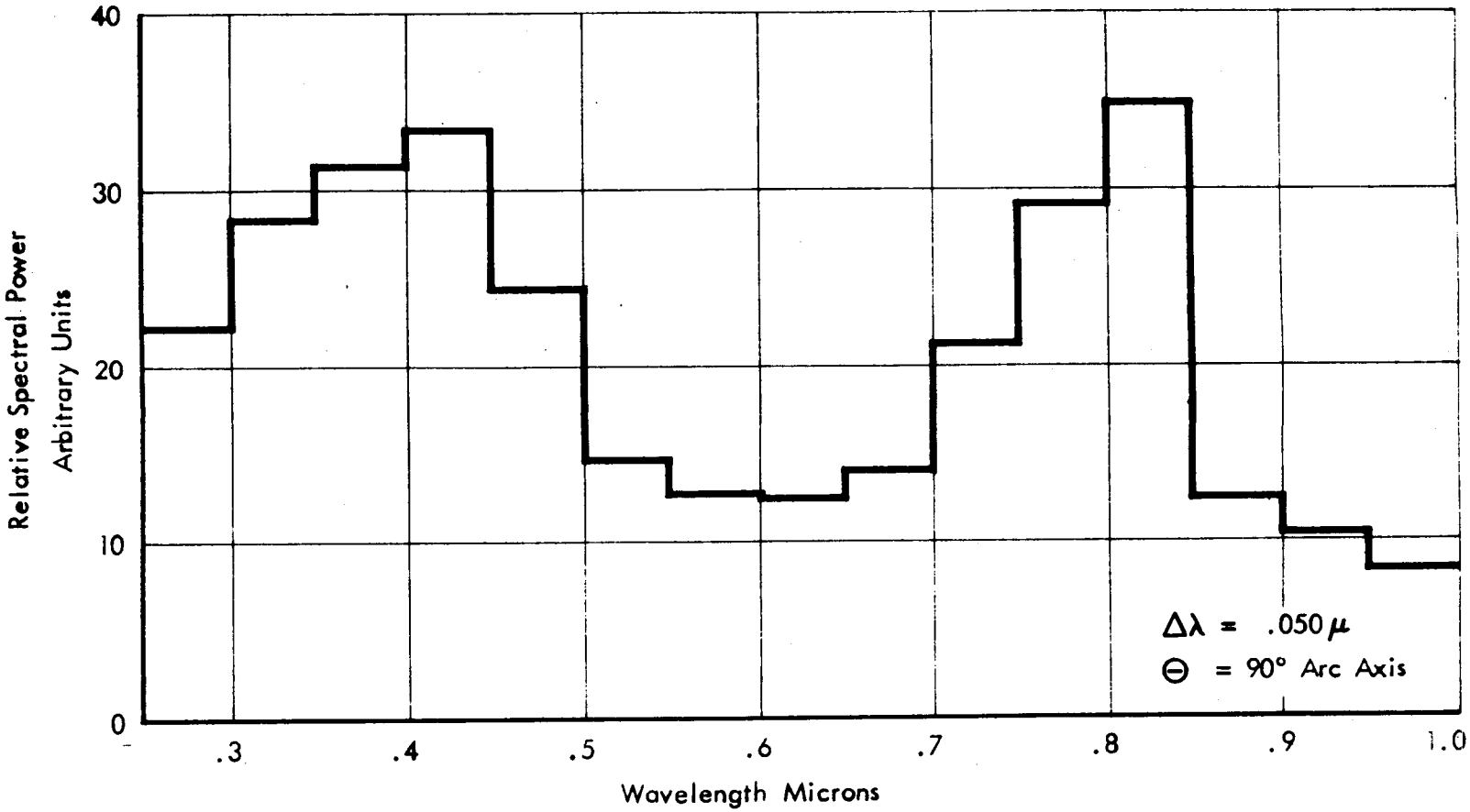

Figure 2 RELATIVE SPECTRAL POWER 21.4 KW ARGON VSRS 16.2 ATM
60 KW Prototype Source

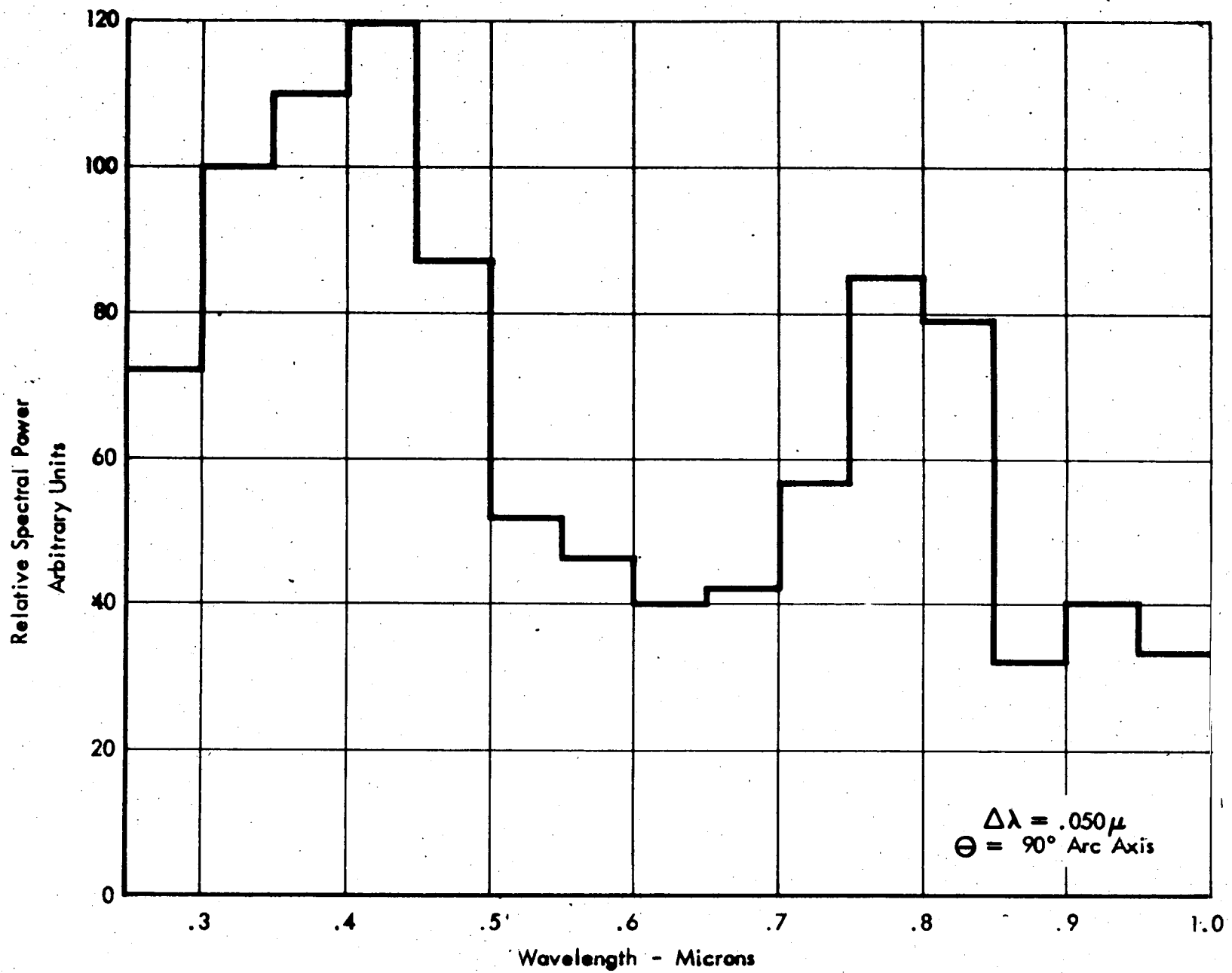

Figure 3 RELATIVE SPECTRAL POWER 60.3 KW ARGON VSRS 19.7 ATM
60 KW Prototype Source

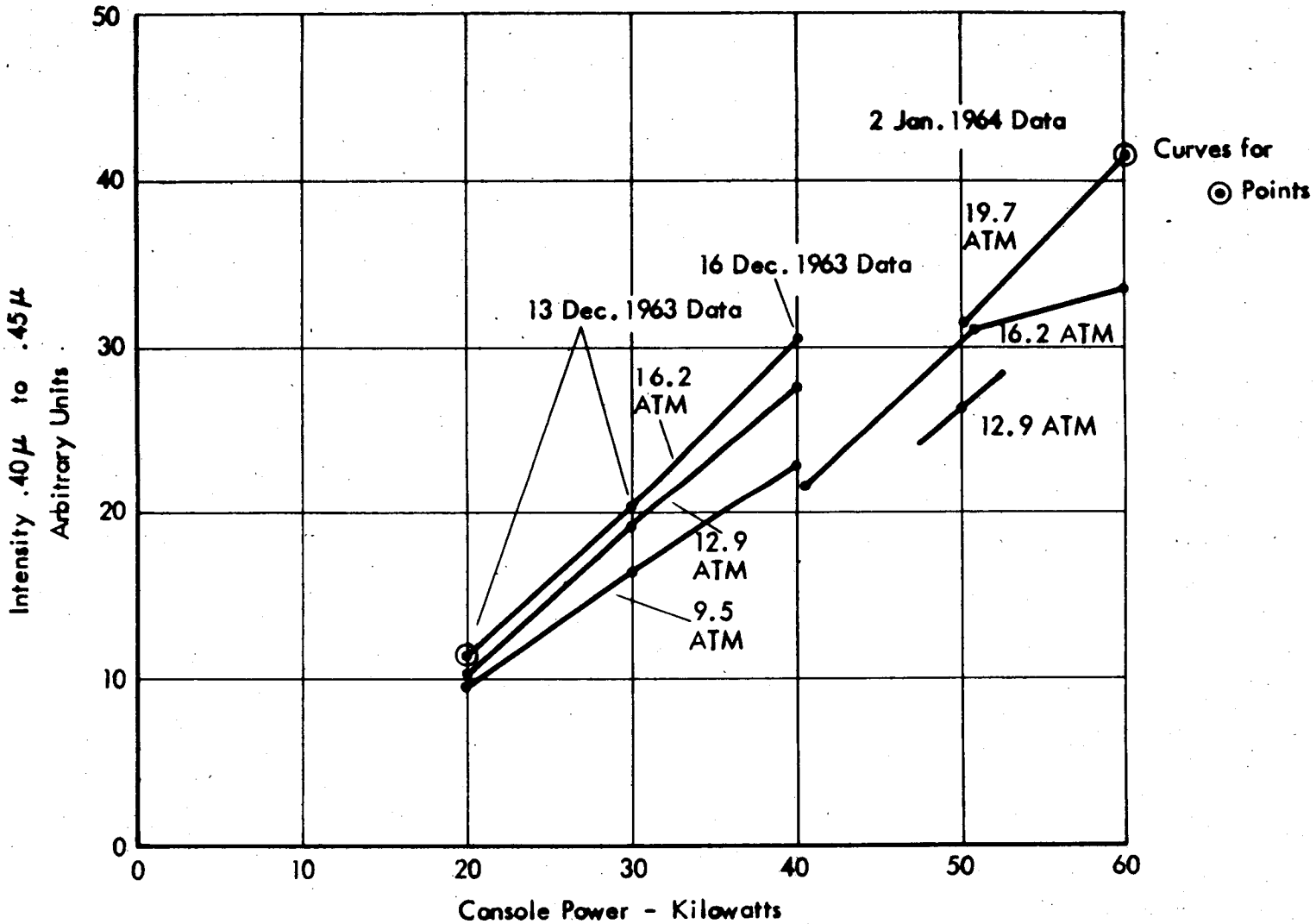

Figure 4 .425 μ INTENSITY VS. POWER AND PRESSURE
60 KW Prototype Source

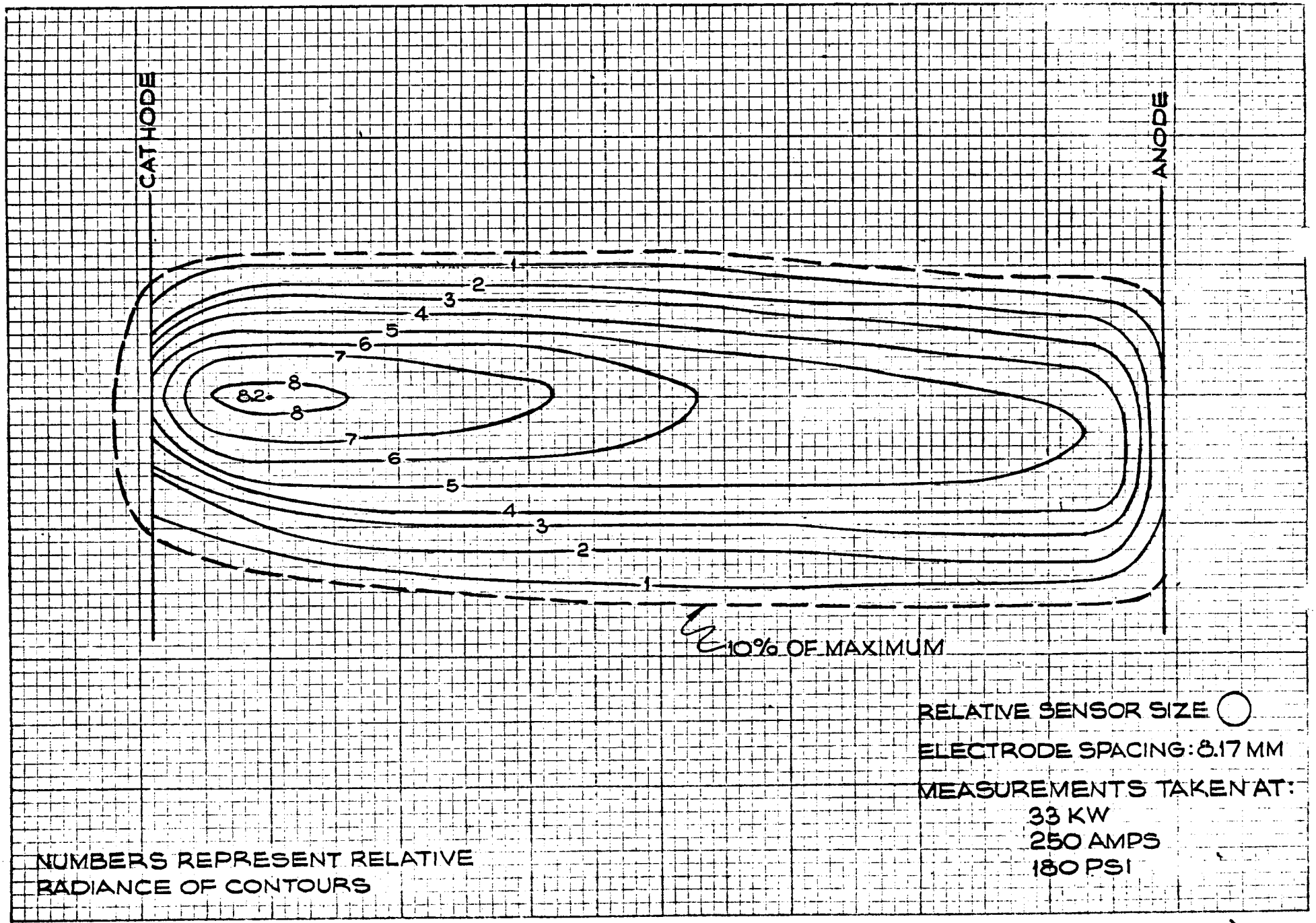

ARC IMAGE MICRO-RADIANCE CONTOURS (60 KW RADIATION SOURCE)

FIGURE 5.

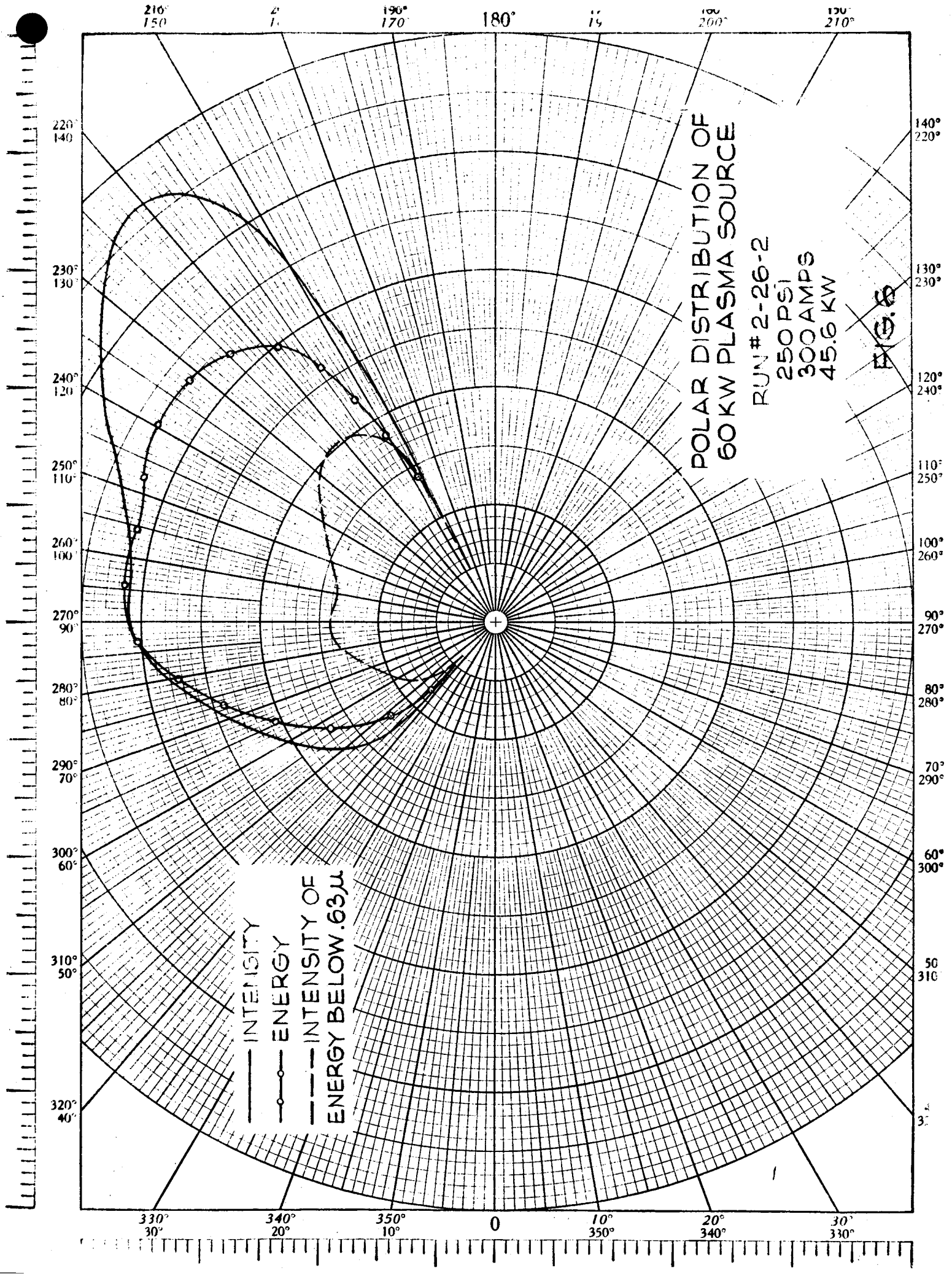
POLAR DISTRIBUTION OF
60 KW PLASMA SOURCE
RUN # 2-26-2
250 PSI
300 AMPS
45.6 KW
FIG. 10
INTENSITY
ENERGY
INTENSITY OF
ENERGY BELOW .63μ
180°
0
210°
150°
190°
170°
200°
220°
140°
230°
130°
240°
120°
250°
110°
260°
100°
270°
90°
280°
80°
290°
70°
300°
60°
310°
50°
320°
40°
330°
30°
340°
20°
350°
10°
10°
350°
20°
340°
30°
330°

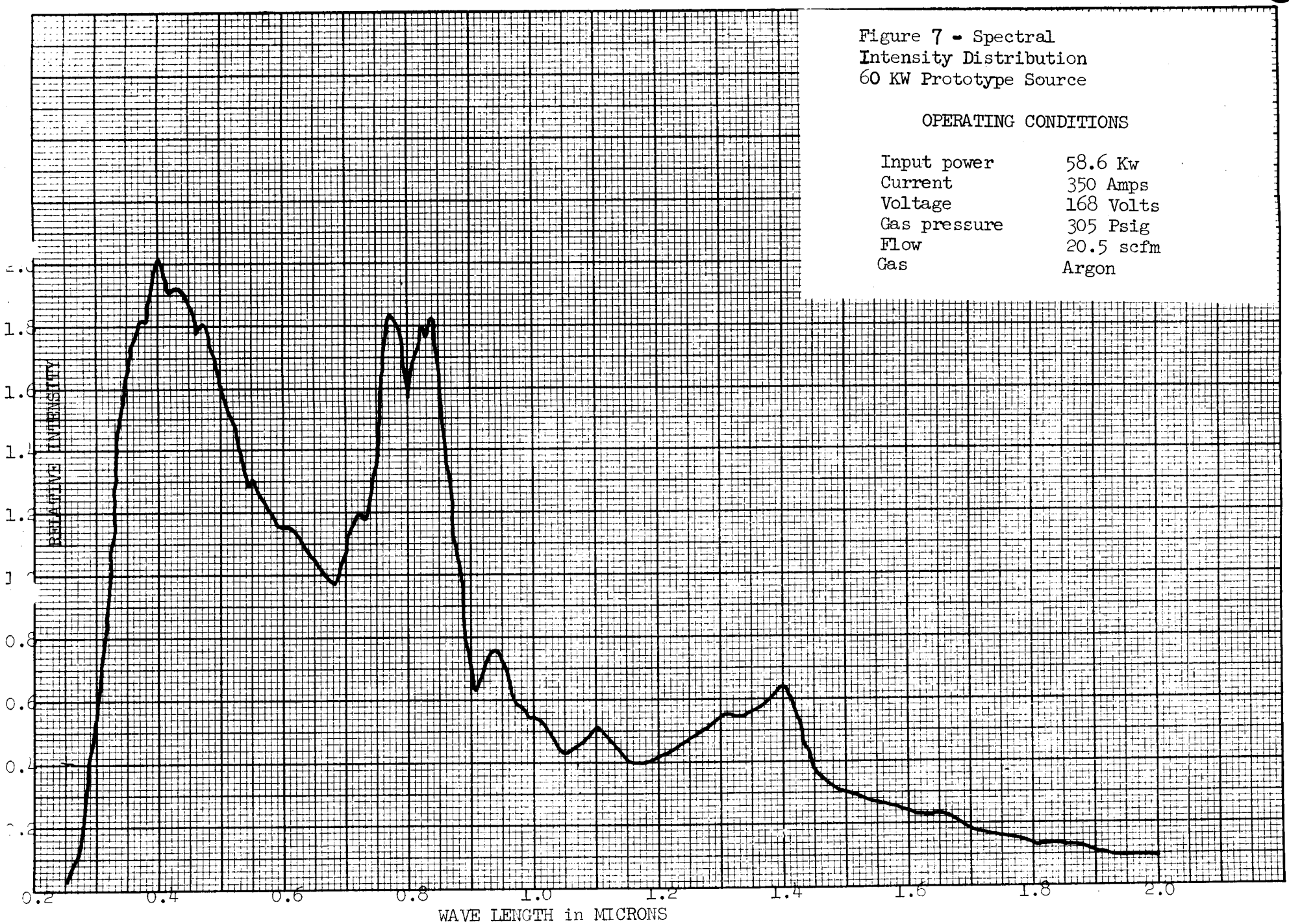

Figure 7 - Spectral Intensity Distribution 60 KW Prototype Source

OPERATING CONDITIONS

Input power	58.6 Kw
Current	350 Amps
Voltage	168 Volts
Gas pressure	305 Psig
Flow	20.5 scfm
Gas	Argon

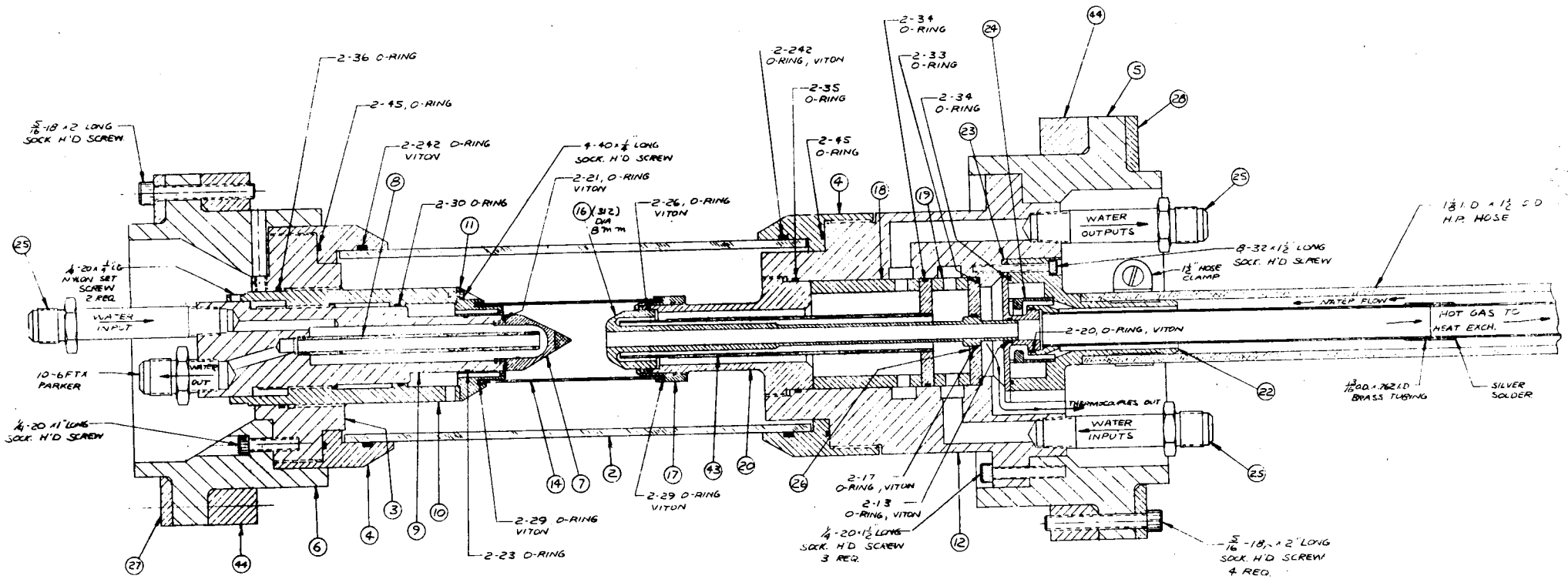

150 KW EXPERIMENTAL RADIATION SOURCE

43 MM O.D. INNER TUBE ASSEMBLY

8 MM BORE TYPE ANODE

FIG. 8

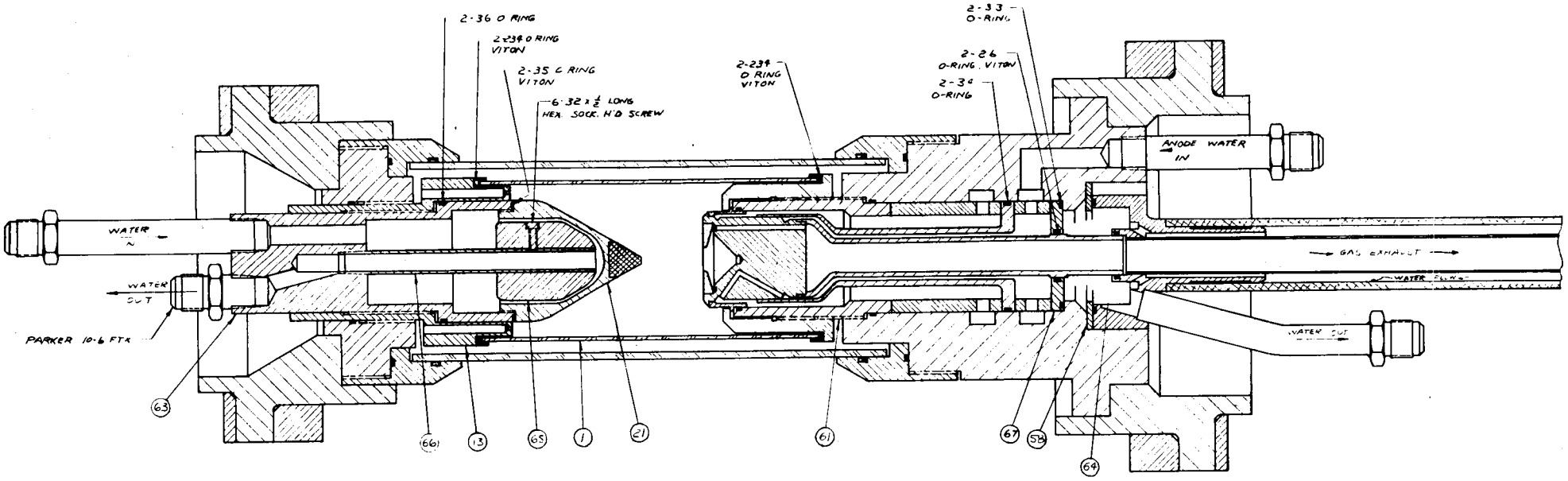

150 KW EXPERIMENTAL RADIATION SOURCE

84 MM O.D. INNER TUBE ASSEMBLY
SOLID ANODE ASSEMBLY

FIG. 9

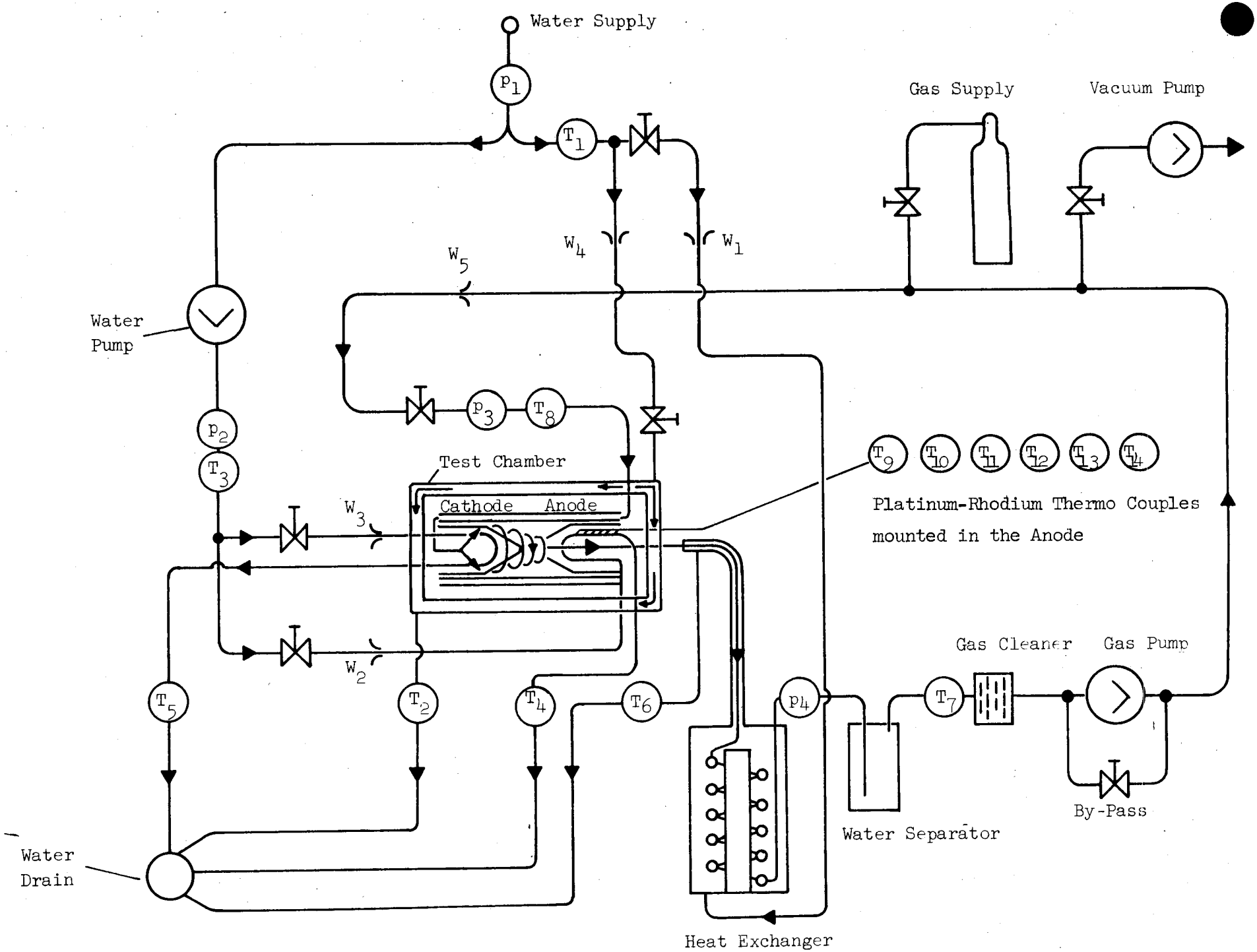

Figure 10a - Instrumentation - Schematic - 150 KW Experimental Unit

Temperature - pressure - and flow gauges

T_1	Temperature, low pressure cooling water to test chamber and heat exchanger
T_2	Temperature, test chamber out
T_3	Temperature, high pressure cooling water to the electrodes
T_4	Temperature, anode cooling water out
T_5	Temperature, cathode cooling water out
T_6	Temperature, heat exchanger cooling water out
T_7	Temperature, gas before gas cleaner
T_8	Temperature, gas before light source
T_9	Temperature in anode body
T_{10}	Temperature in anode body
T_{11}	Temperature in anode body
T_{12}	Temperature in anode body
T_{13}	Temperature in anode body
T_{14}	Temperature in anode body
P_1	Pressure, low pressure cooling water
P_2	Pressure, high pressure cooling water
P_3	Pressure, gas to the light source
P_4	Pressure, gas after the light source
W_1	Flow, cooling water to the heat exchanger
W_2	Flow, cooling water to the anode
W_3	Flow, cooling water to the cathode
W_4	Flow, cooling water to the test chamber

Figure 10b - Instrumentation - Listing of the Instruments
150 KW Experimental Unit

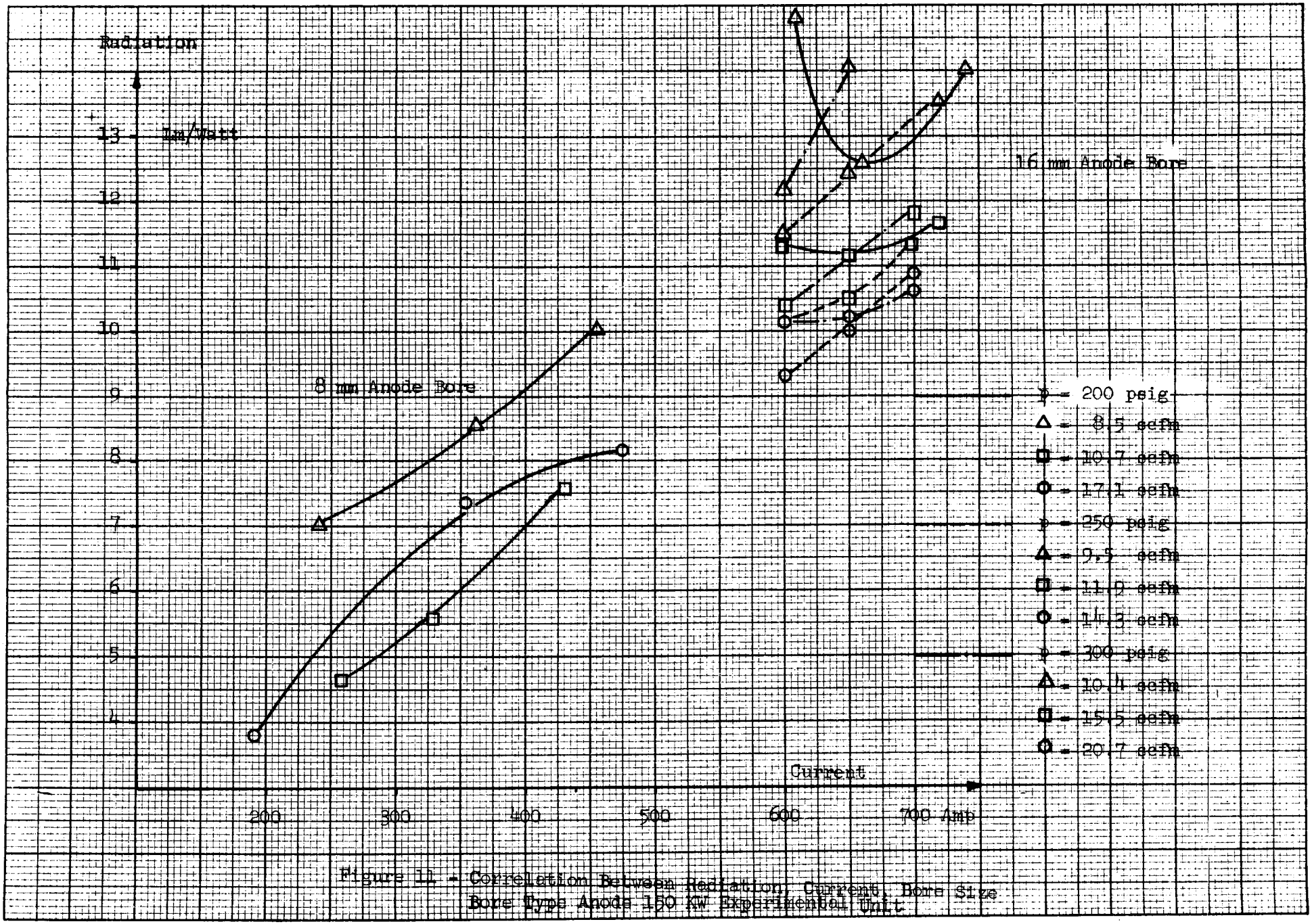

Figure 11 - Correlation Between Radiation, Current, Bore Size
Bore Type Anode 150 KW Experimental Unit

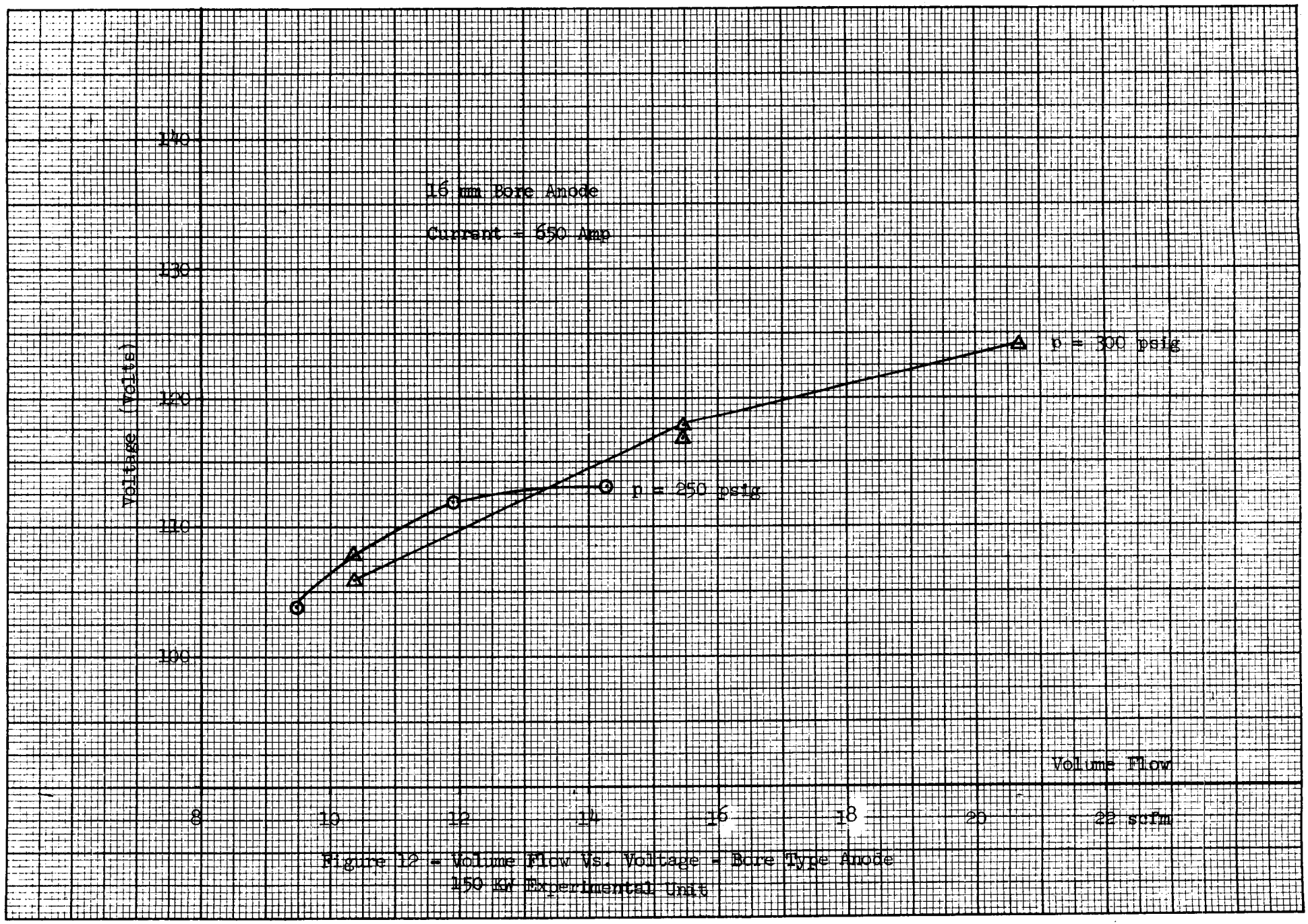

Figure 12 - Volume Flow Vs. Voltage - Bore Type Anode
150 KW Experimental Units

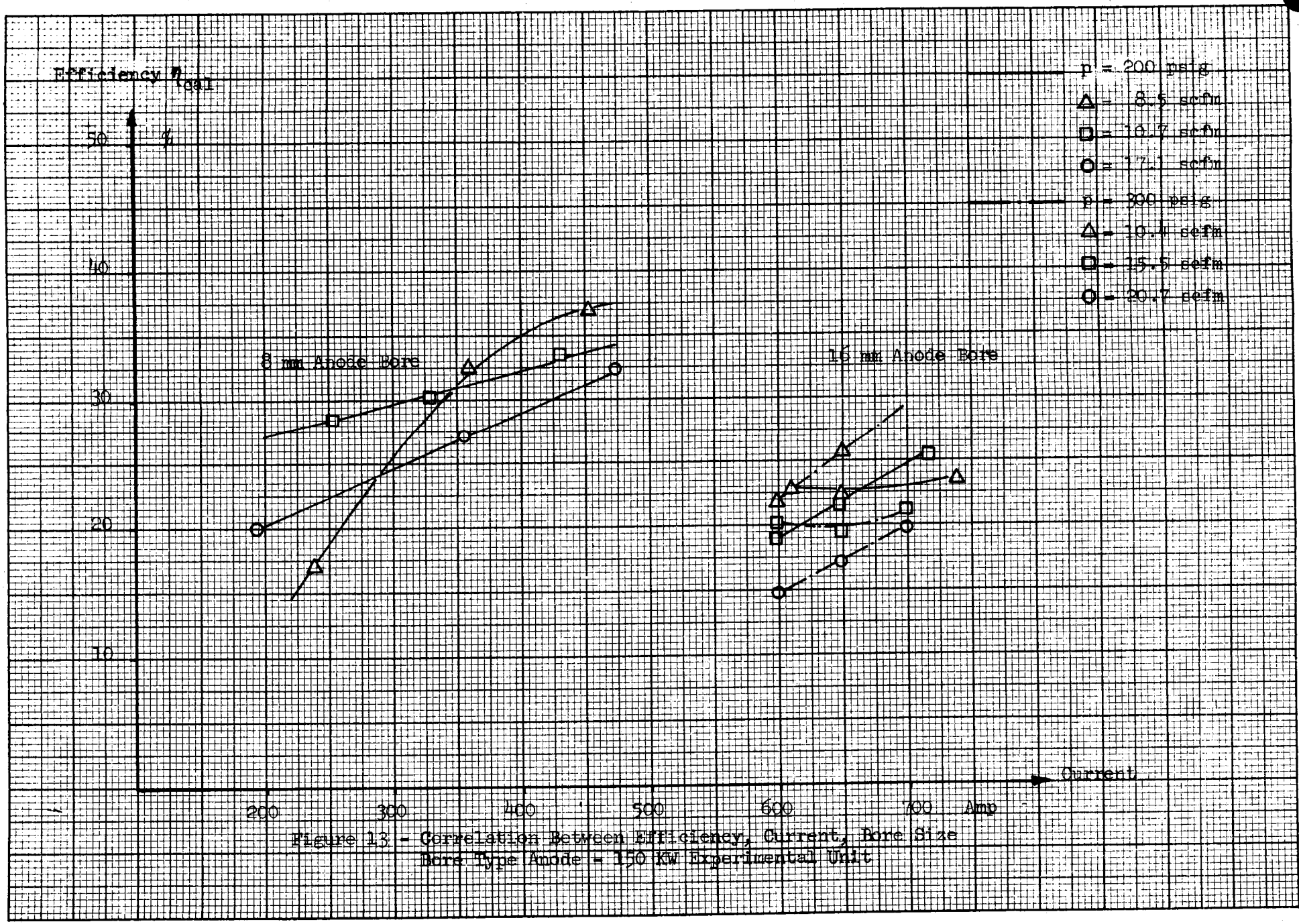

Figure 13 - Correlation Between Efficiency, Current, Bore Size
Bore Type Anode - 150 KW Experimental Unit

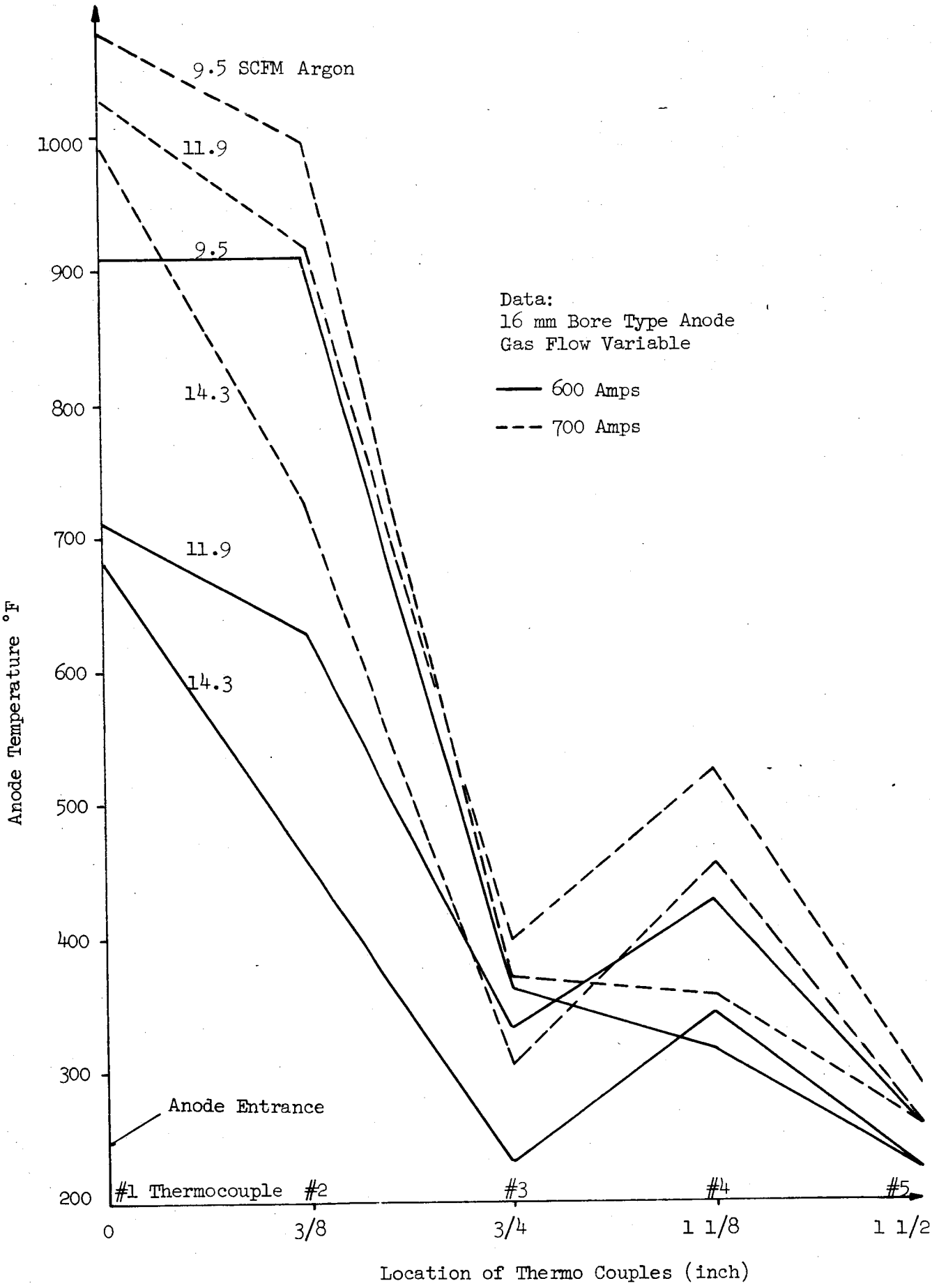

Figure 14 - Axial Temperature Distribution in the Anode
150 KW Experimental Unit

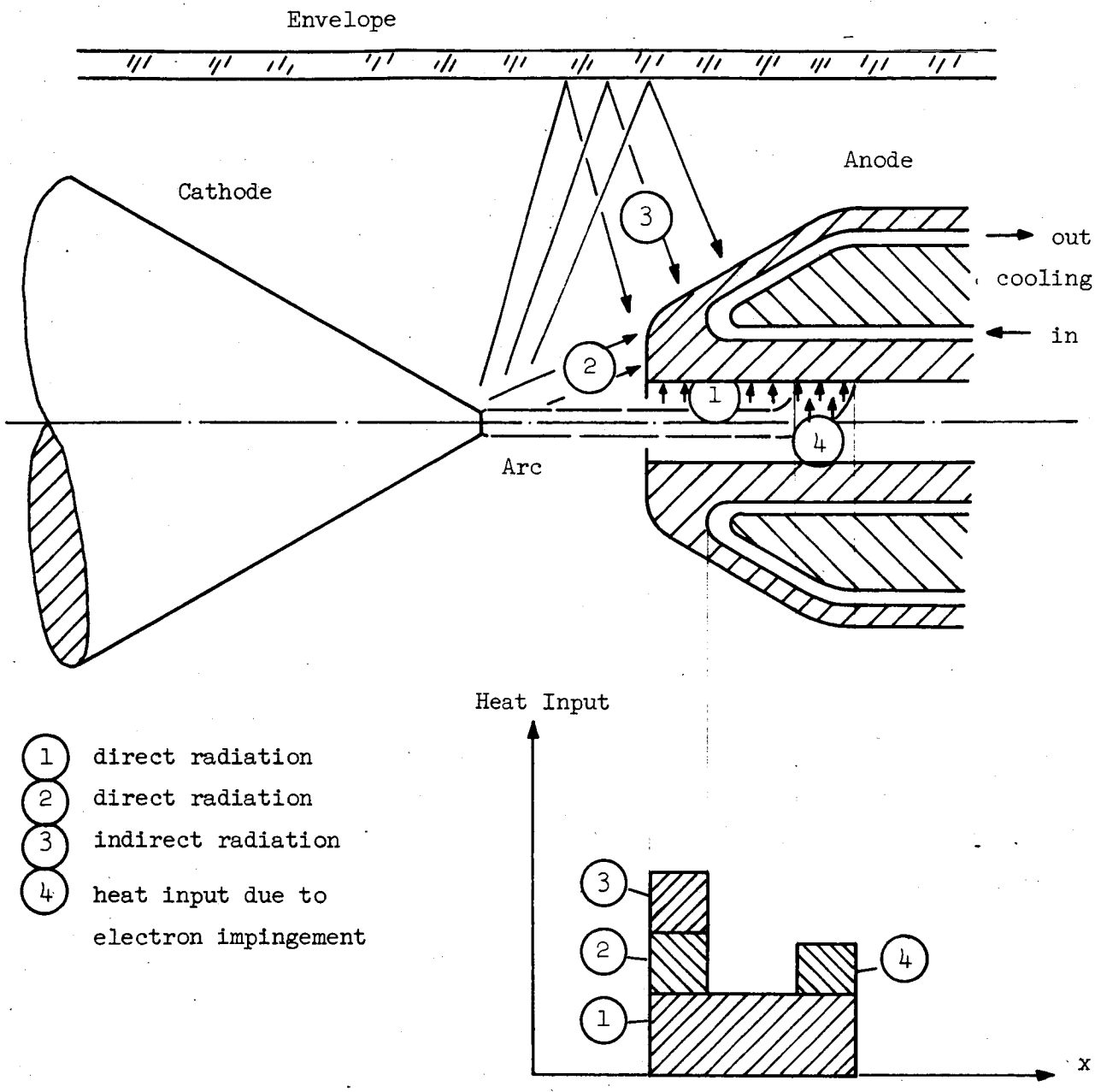

Figure 15 - Heat Input to the Anode - Bore Type Anode
150 KW Experimental Unit

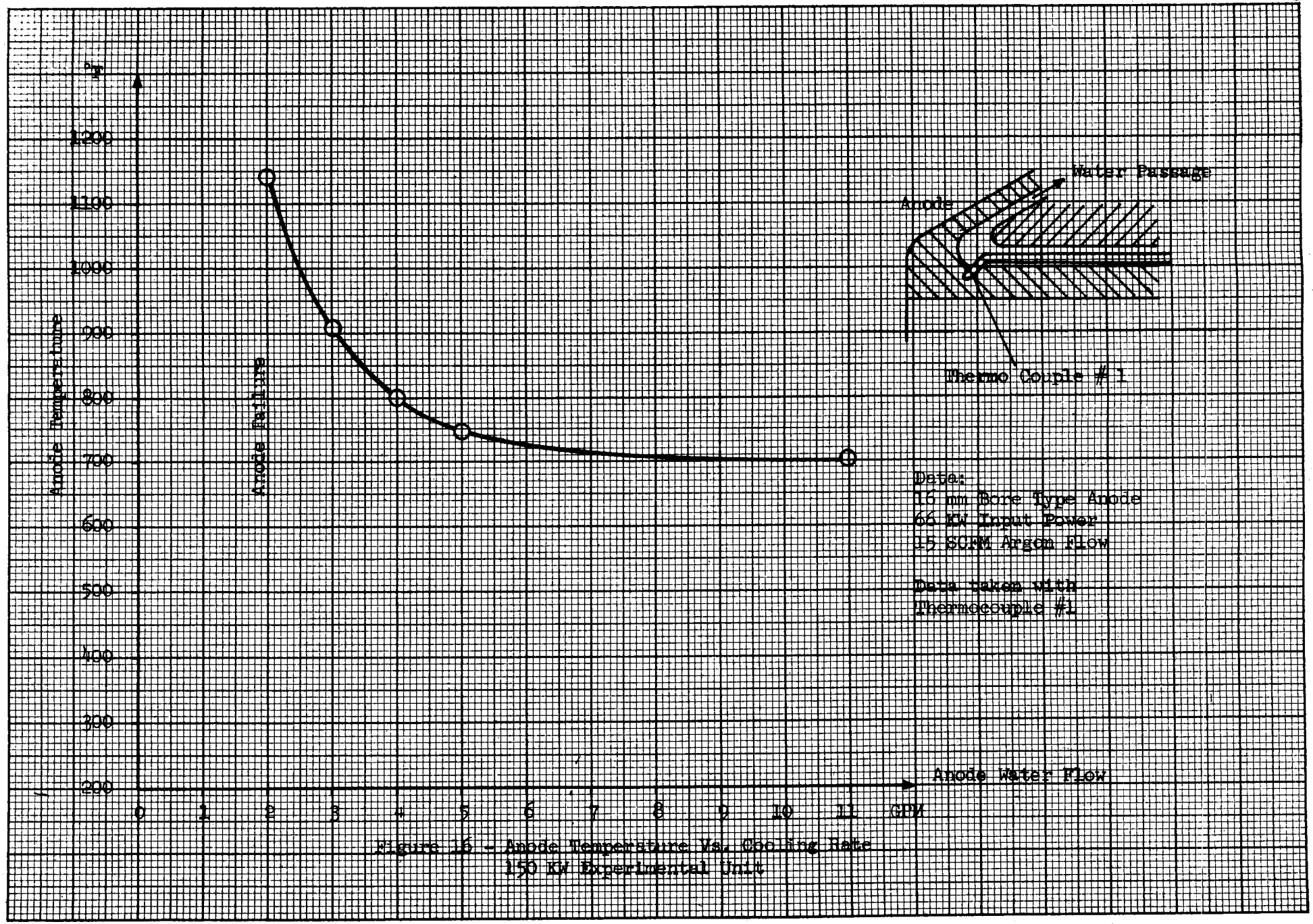

Figure 16 - Anode Temperature Vs. Cooling Rate
150 KW Experimental Unit

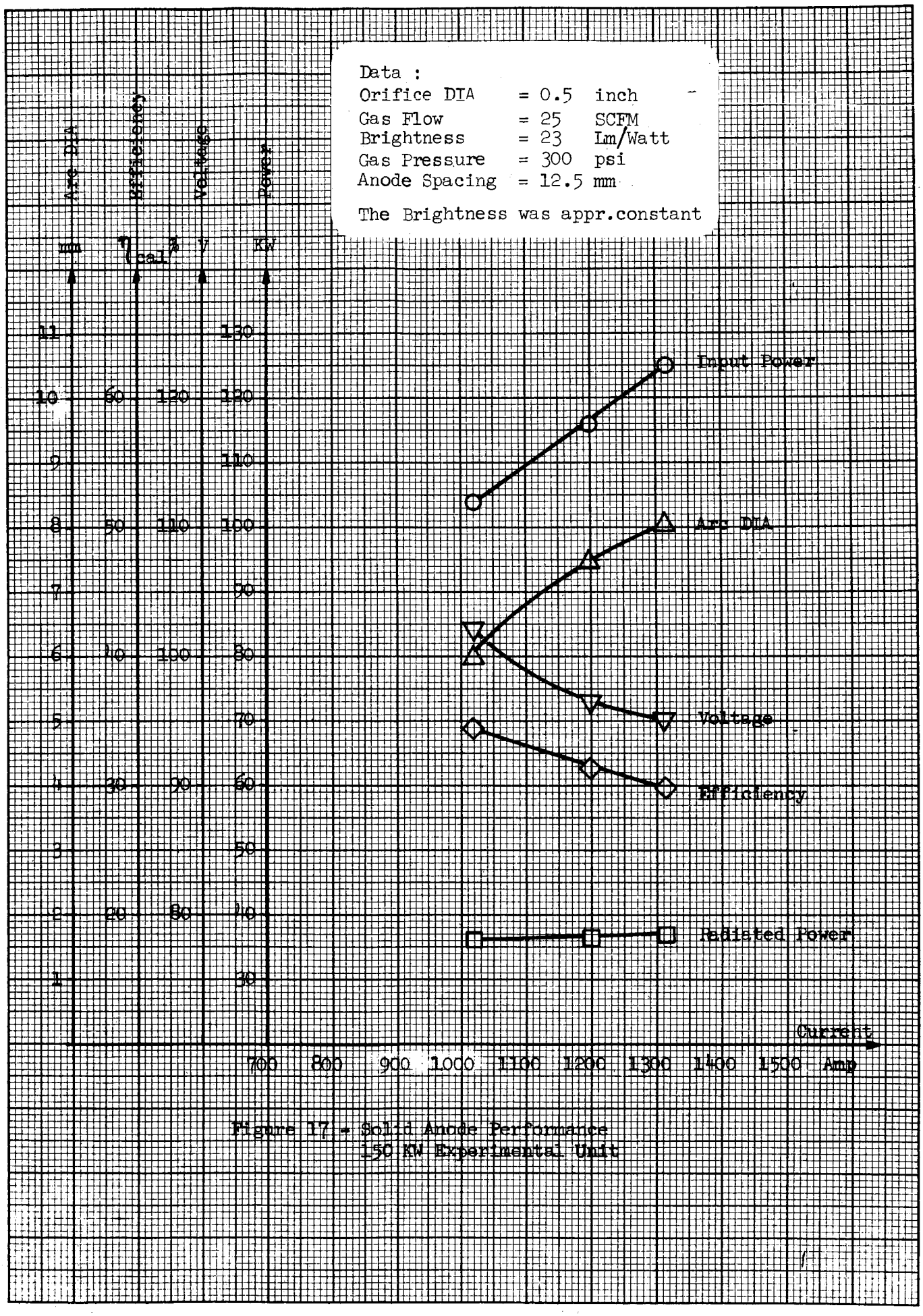

Figure 17 - Solid Anode Performance
150 KW Experimental Unit

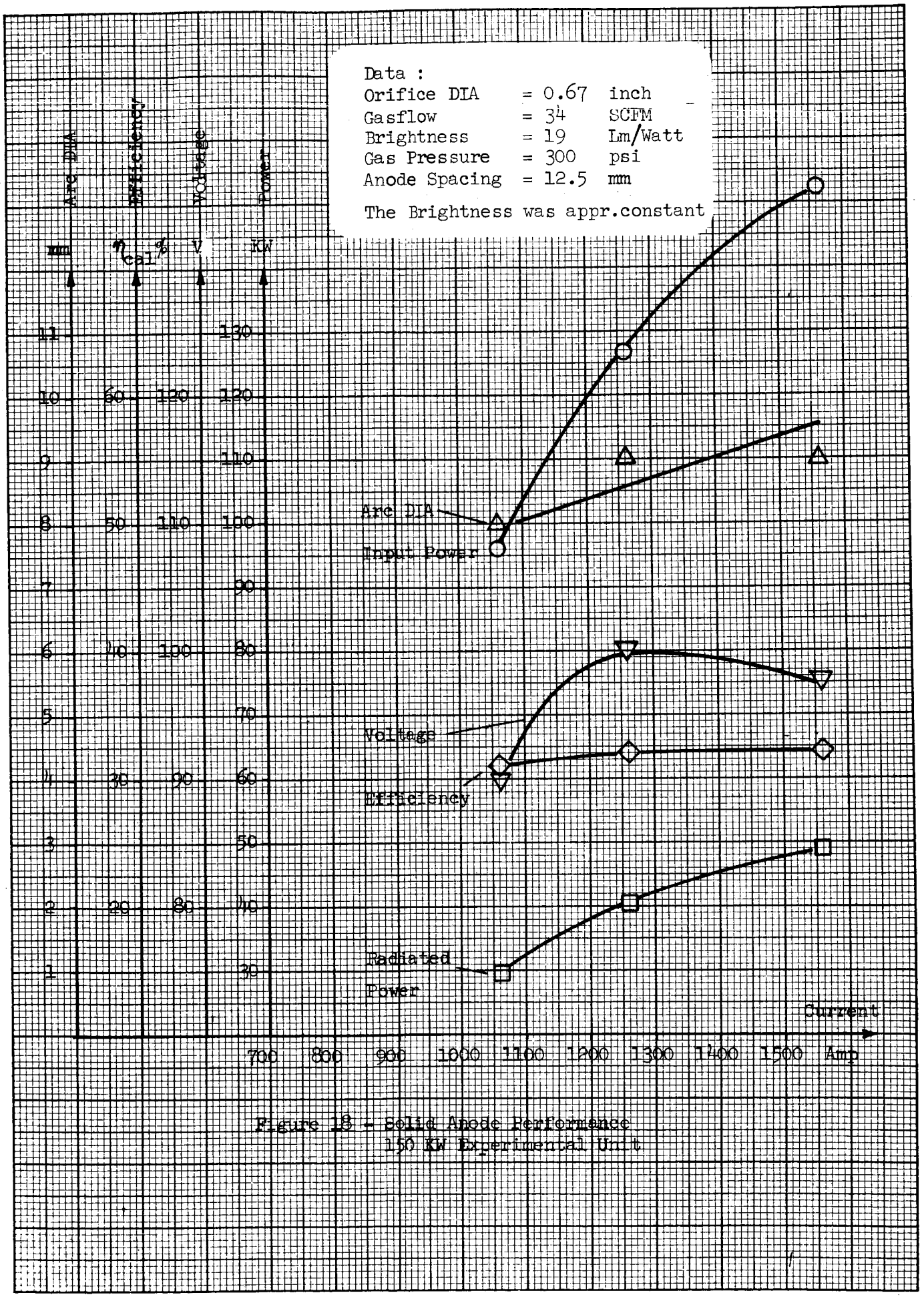

Figure 18 - Solid Anode Performance
150 KW Experimental Unit

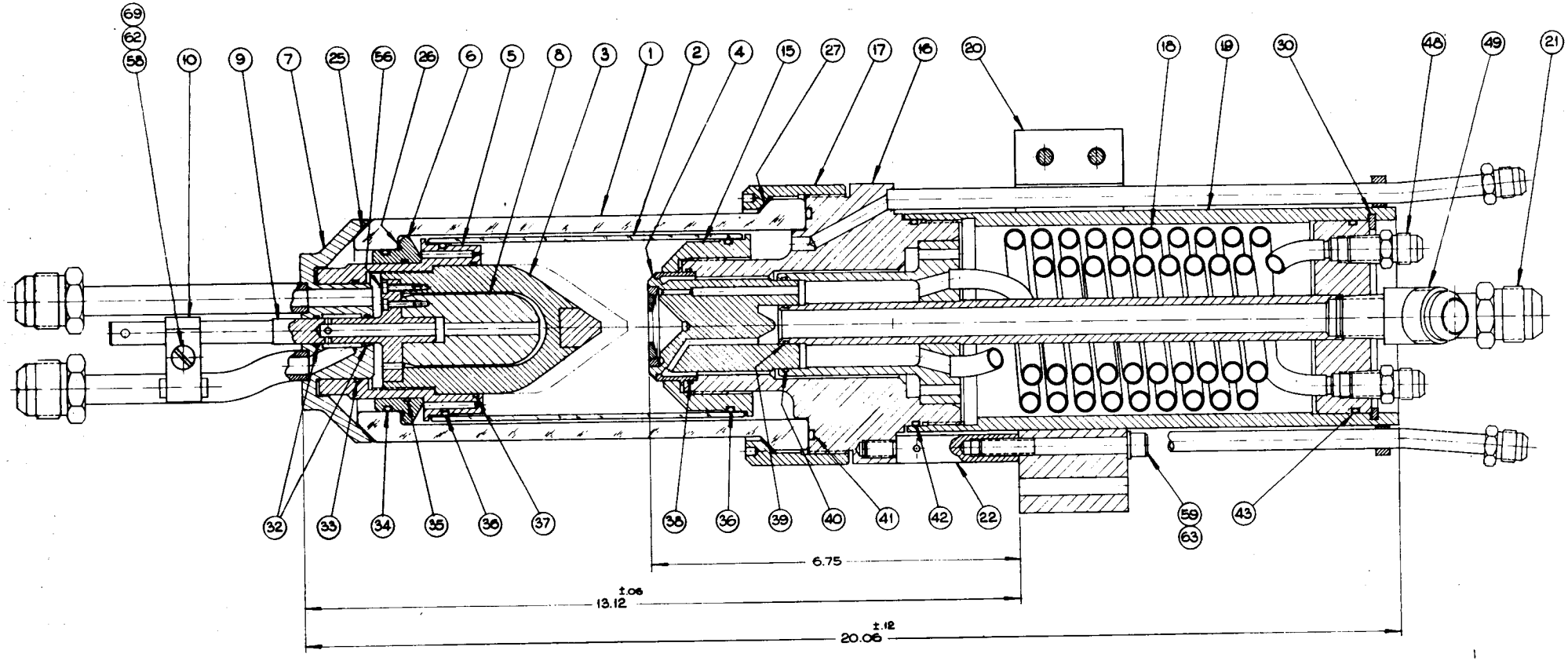

150 KW FINAL RADIATION SOURCE

FIG. 19

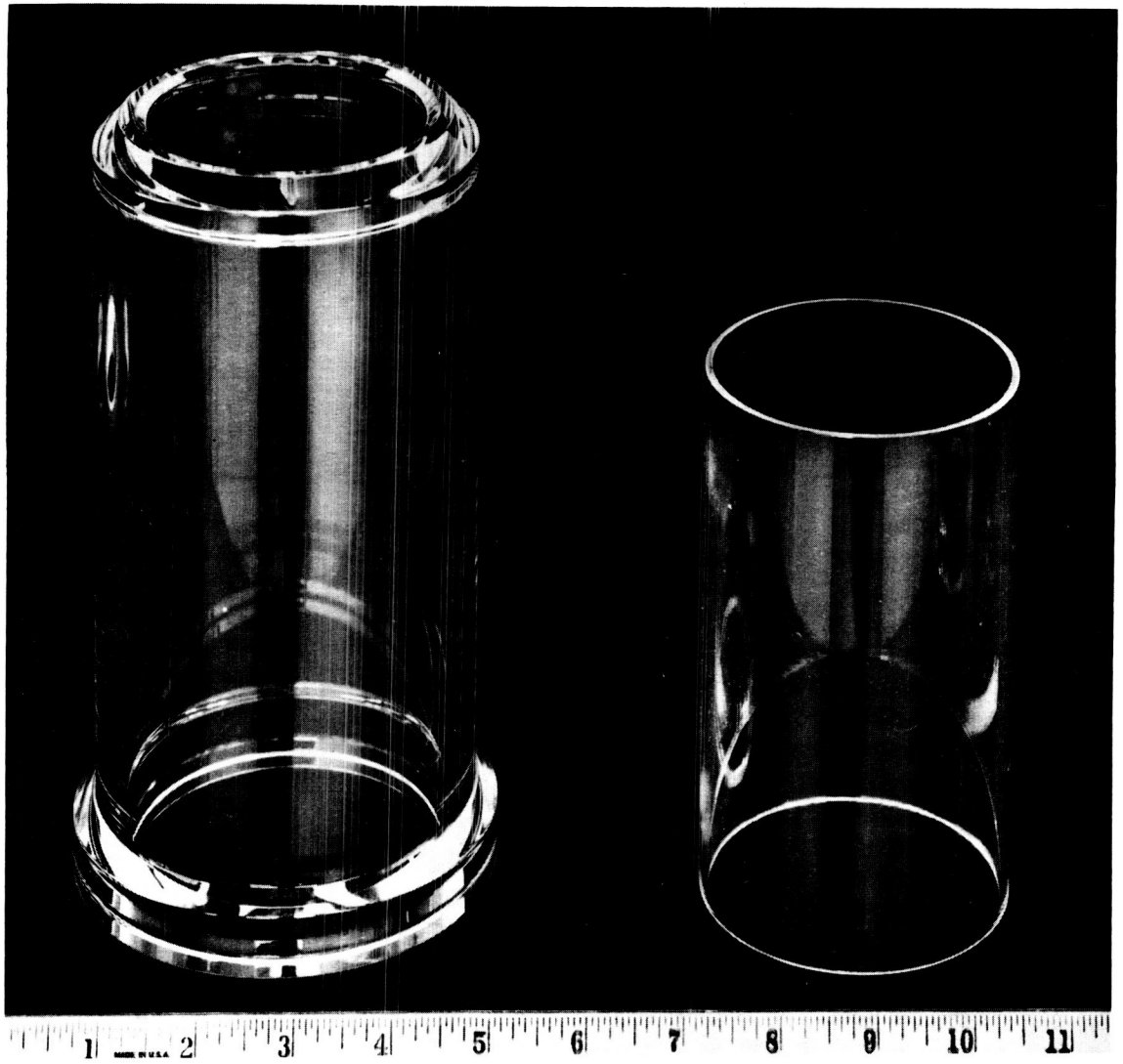

Figure 20 - Quartz Envelope in Final Radiation Source

Upper Picture - Inner Envelope
Lower Picture - Outer Envelope (Self-supporting)

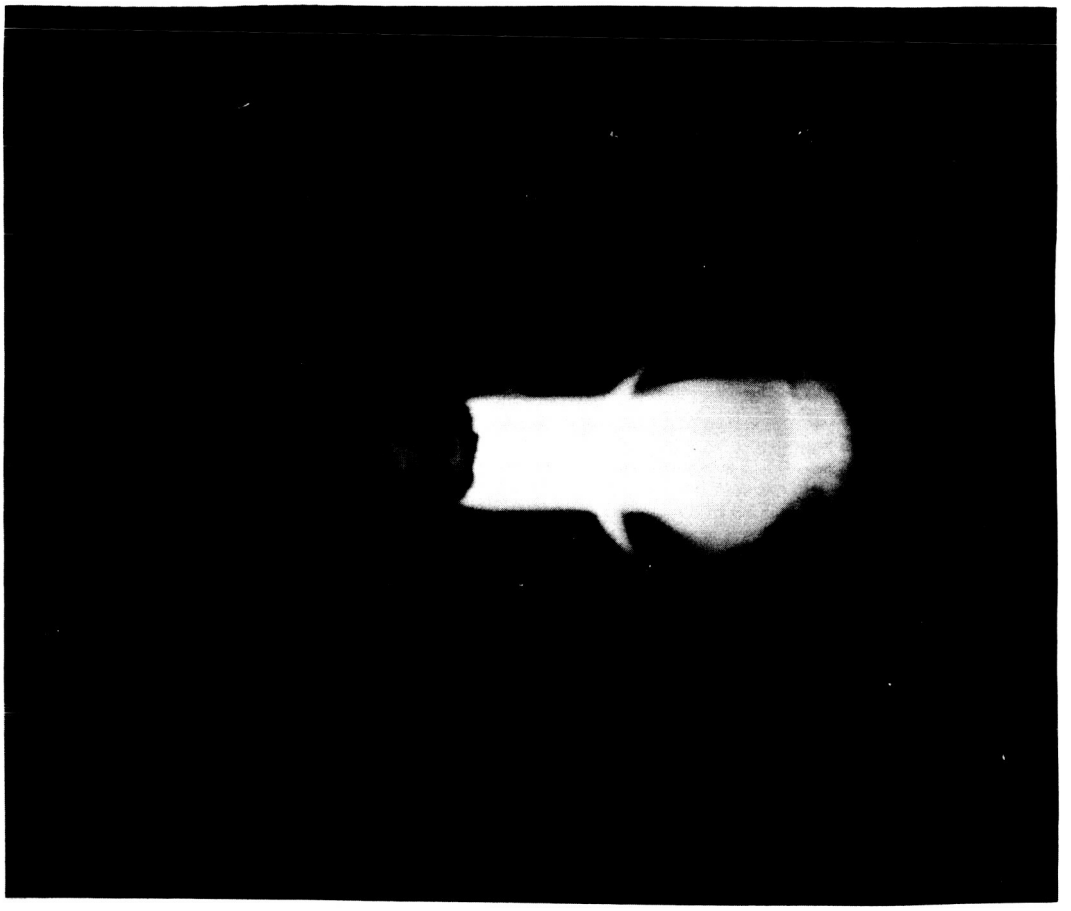

Figure 21 - Diffusion of the Arc Foot

This photograph was taken under an inclination of 45° with respect to the arc axis looking into the diffuser bore. The exposure presents the diffusion of the arc foot at the anode of a 1500 amp arc. The distinct bright spot on the left side of the arc is due to reflection on the diffuser front face. On the right side of the picture, the contour of the cathode tip is visible.

DATA SUMMARY SHEET

MODEL L-60 LIGHT SOURCE

TEST NO. 1 - 12-9-63

Anode configuration:

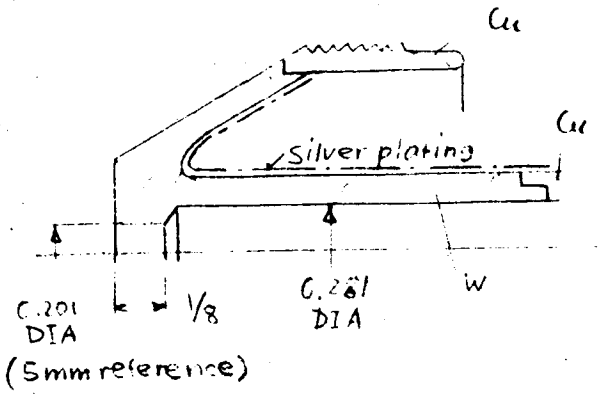

The anode consisted of a solid tungsten housing (2% thoriated). The surface exposed to the cooling water was silver plated (3 mills) to prevent oxidation of the tungsten. The anode was coated with silver after the copper parts had been gold soldered to the tungsten body.

Gap between anode and cathode: 8mm

Testing: Because the quartz tubes had not been annealed the gas pressure was limited at 100 psig. The maximum power was 42KW with an efficiency of 18.2%.

Failure: The tungsten housing cracked on the front end causing a water leak. The failure occurred at 42KW.

Observations: The throat of the anode was clean after 30 min. of running time. No signs of arc erosion were noticed. The silver plating peeled off partly on the back side of the hot spot region.

DATA SUMMARY SHEET

MODEL L-60 LIGHT SOURCE

TEST NO. 2 - 12-12-63

Anode configuration:

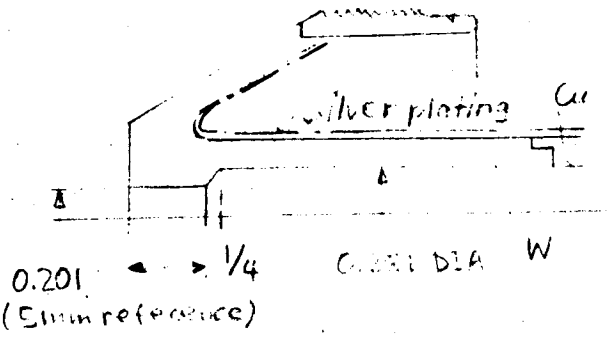

The geometry and make of the anode in Test No.2 differs from Test No. 1 only by the throat length. The purpose of a longer throat (1/4" instead of 1/8") was to force the arc foot farther downstream in order to obtain a cooler front end (reduction of thermal stresses).

Gap between anode and cathode: 8mm

Testing: The quartz tubes were not annealed. It was not advisable to raise the gas pressure above 200 psig. The highest power was 28KW with an efficiency of 42.4% (thermal equilibrium of the calorimetric measurement was questionable).

Failure: The anode leaked at the solder joint between the tungsten and the outer, threaded copper sleeve.

Observations: No erosion marks on the arc side were noticed after an operation time of 25 minutes. Again the silver coating wrinkled and split off in certain locations.

Remarks: The anode was resoldered with silver solder, but it still was not leak proof.

DATA SUMMARY SHEET

MODEL L-60 LIGHT SOURCE

TEST NO. 3 - 12-13-63

Anode Configuration:

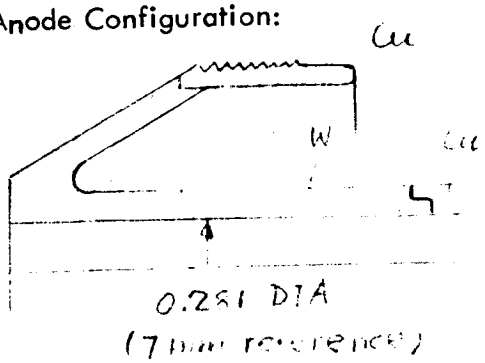

The anode had a straight bore of 0.281" diameter. No silver plating was applied. It was the purpose of this test to investigate if sintered tungsten (2% thoriated) can be water-cooled directly without a protective coating and if it was leak proof.

Gap between anode and cathode:

8mm

Testing:

Unannealed quartz tubes were used, therefore, the gas pressure was limited to approximately 200 psig The maximum power was 30.7KW with an efficiency of 33.6%.

Failure:

After 20 minutes operation time the anode broke because of erosion from the water side.

Observations:

Near the hot spot region which was approximately 3/8" downstream of the anode entrance, the tungsten corroded into tungsten oxide along the whole circumference leaving only a few mills of tungsten of the original wall thickness of 0.057" before it broke.

DATA SUMMARY SHEET

MODEL L-60 LIGHT SOURCE

TEST NO. 4 - 12-16-63

Anode configuration:

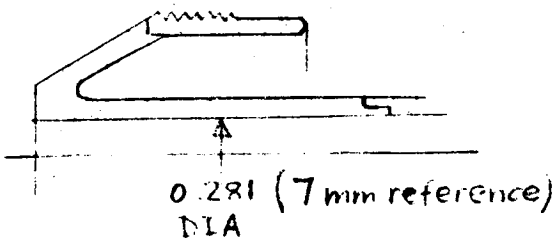

The same anode geometry as in Test No. 3 was used. The complete anode was made out of copper. The purpose of this test was to establish the power limitation for this configuration using copper.

Gap between anode and cathode: 8mm

Testing: Because of the unannealed quartz tubes, the gas pressure was kept near 200 psig. The maximum measured power was 40KW with an efficiency of 33.8%.

Failure: The copper anode melted from the inside at 40KW. The melting zone was between 1/8" and 3/8" downstream of the anode entrance.

The total running time accumulated during this test was 20 minutes.

Observations: The failure occurred as an explosion. The arc went through the water passage and damaged the wate divider.

DATA SUMMARY SHEET

MODEL L-60 LIGHT SOURCE

TEST NO. 5, a, b,
12-20-63

Anode configuration:

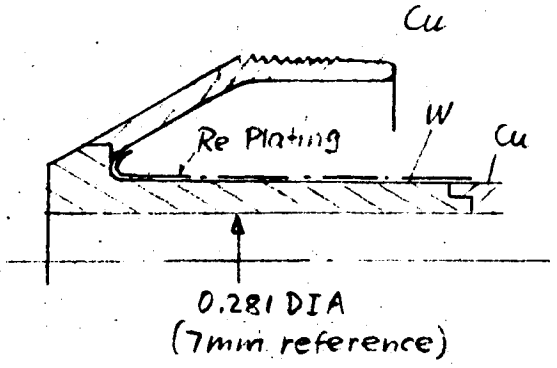

In Test No. 5,a. the anode was rhenium plated in assembled condition, i.e., after the threaded copper sleeve was soldered to the tungsten housing. The plating was poor because of the obstruction of the copper sleeve. This anode oxidized completely before any measurements were made. In Test No. 5, b. the anode was redesigned as shown in the Figure above. The conical section was part of the copper sleeve, thus the tungsten tube could be recoated (1/2 mil) without any obstruction.

Gap between anode and cathode: 8mm

Testing: Unannealed quartz tubes limited the gas pressure to 200 psig. The maximum measured power was 51 KW and 34.4% efficiency.

Failure: The anode broke at 55KW because of water corrosion.

Observations: The recoating was imperfect at two locations. Small pin holes caused a subsequent oxidation of the tungsten. Total elapsed running time - 75 minutes.

DATA SUMMARY SHEET

MODEL L-60 LIGHT SOURCE

TEST NO. 6 - 12-27-63

Anode Configuration:

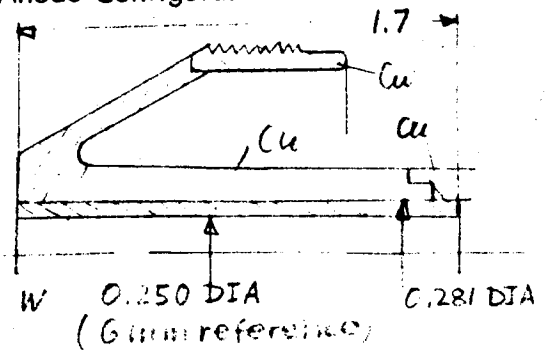

A tungsten tube (0.250 ID x 0.281 O.D. x 1.7" long) was pressed into the copper anode (shrink fit). The tungsten tube was flush with the copper housing.

Gap between anode and cathode: 8mm

Testing: Unannealed quartz tubes limited the pressure to 200 psig. At 55.4KW the efficiency was measured with 26.7%.

Failure: After 20 minutes of operation the supporting rods suffered an elongation due to overheating. The cathode sagged a few degrees causing the arc to strike the copper housing which was completely destroyed.

Observation: At 55KW the rods were red hot in the plane perpendicular to the arc. In that section the rods started to yield. Coating the rods with alumina oxide did not solve the problem.

DATA SUMMARY SHEET

MODEL L-60 LIGHT SOURCE

TEST NO. 7 - 12-28-63

Anode configuration:

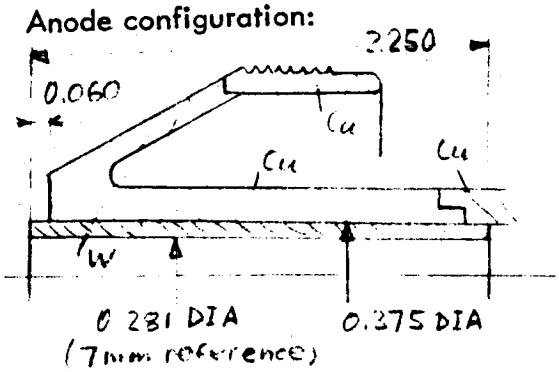

Gap between anode and cathode:

Testing:

Failure:

Observations:

Rod cooling:

The anode was redesigned to accomodate a tungsten insert with a bore of 7 mm. The tungsten tube protruded the copper housing by 0.060" to prevent arcing to the copper. The tungsten sleeve was held in position by a shrink fit, furthermore, the downstream end of the tungsten insert was silver plated to improve electric contact. 9.5mm, the new gap width was caused by a shorter piece of tungsten protruding the copper (0.060" instead of the original 0.125"). Annealed quartz tubes were installed. The maximum pressure (gas) measured was 250 psig. During a period of 30 minutes, 60KW was maintained with an average efficiency of 26%.

No failure occurred during this test.

The front end of the tungsten insert was eroded for about 1/8".

The supporting rods were water cooled. The rod temperature did not exceed 100°F during operation.

DATA SUMMARY SHEET

MODEL L-60 LIGHT SOURCE

TEST NO. 8 - 12-30-63

Anode configuration:

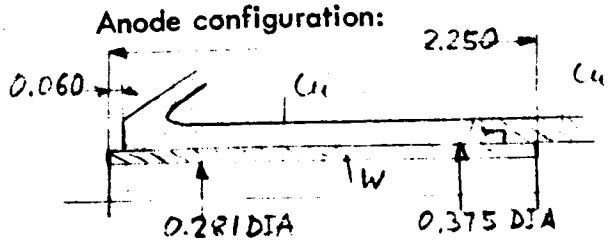

Gap between anode and cathode:

The same geometry was applied as in Test No. 7. The tungsten insert was shrunk into the copper housing and the downstream end of the tungsten tube was silver plated to improve electric contact.

9.5mm

Testing:

Annealed quartz tubes were used, the maximum gas pressure measured was 302 psig. The light source operated at 50KW during 50 minutes and at 60KW for 122 minutes. The average efficiency was around 31%.

Failure:

No failure occurred during this test.

Observations:

The front end of the tungsten insert was eroded for about 1/4" clear to the copper housing.

It was noticed that the portion of the tungsten protruding out of the copper changed its color (from dark red to a bright white in a frequency of about 1 cycle/second). This phenomenon was due to the unsteady heat transfer mechanism caused by different expansion coefficients of tungsten and copper.

DATA SUMMARY SHEET

MODEL L-60 LIGHT SOURCE

TEST NO. 9 - 12-31-63

Anode configuration:

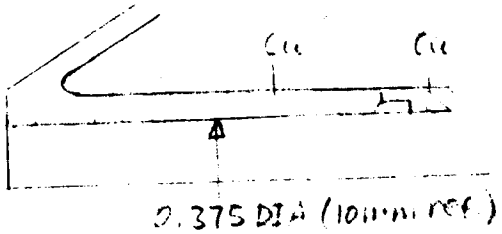

A pure copper anode was used with a straight bore of 10mm. Because of the enlarged bore diameter the specific heat loading was reduced to some extent and it was the purpose of this test to find the power limitation for that hole size.

Gap between anode and cathode:

11mm

Testing:

Annealed quartz tubes were used. The maximum measured gas pressure was 250 psig. A power of 60KW with an efficiency of 28% were maintained during a period of 15 minutes.

Failure:

By increasing the gas pressure from 250 psig to 300 psig the copper anode imploded. The complete front end was melted.

Observations:

The temperature of the anode was too high at 60KW to withstand a differential pressure of 200 psig between the vortex chamber and the cooling passage.

DATA SUMMARY SHEET

MODEL L-60 LIGHT SOURCE

TEST NO. 10 - 1-2-64

Anode configuration:

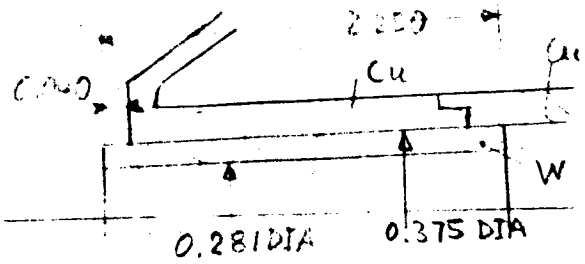

The anode used in Test No. 9 was rebuilt and tested in Test No. 10. The tungsten protruded above the copper housing by 0.040".

Gap between anode and cathode:

10mm

Testing:

Annealed quartz tubes were used. The maximum gas pressure was 290 psig. The power was varied between 40 and 60KW for spectrographic measurements. After one hour of testing, no failure occurred.

Failure:

Some erosion on the tungsten insert was noticed. The test was terminated voluntarily.

Observations:

The design described above was found to last for a few hours at 60KW.

Rod Cooling:

The water cooled rods worked satisfactorily since their installation.

SPECTROLAB

DEVELOPMENT MEMORANDUM NO. 272- 1

SUBJECT: Brazing Test Results

WRITTEN BY: W. Geideman
DATE: September 29, 1964
JOB NUMBER: 6002-56

BRAZING TEST RESULTS

INTRODUCTION

A serious reliability consideration is present in the manufacture of the anode for the high power radiation source. This reliability problem is manifested in the quality of the joint between the diffuser and the anode body. Therefore, a study of various techniques of joining molybdenum to copper was undertaken. This study involved analytical and experimental effort.

This joint had previously been assembled using gold solder with an oxy-acetylene torch providing the necessary heat. Since this gold soldering was performed in the atmosphere, it was necessary to use a flux to prevent oxidation of the mating parts during the soldering operation. Experience with this fabrication method at Giannini Scientific Corporation indicated an anode reliability of approximately 50% with failure occurring at the brazed joint.

These failures were due to an incomplete joining of the molybdenum to the copper. A portion of the joint did not contain solder material and was filled only with the flux. This inconsistency could not be determined by visual observation and was discovered only on operation of the radiation source. The symptom was a premature failure of the diffuser due to a lack of heat conduction across the joint into the water cooled copper.

In addition to the reliability element, the necessity of using flux in this fabrication technique produced a heat barrier which reduced the thermal conduction from the molybdenum to the copper and, consequently, produced a diffuser which failed at lower heat inputs than would have been the case if a flux free joint were employed.

The large difference in coefficient of thermal expansion between molybdenum and copper precluded the use of a shrink fit joint between these metals.

Therefore, it was decided to attempt to furnace braze the molybdenum to the copper using a high temperature brazing alloy.

PURPOSE

The purpose of these brazing tests was to determine the reliability of a furnace brazed joint between molybdenum and copper and also to arrive at the optimum joint design.

TEST RESULTS

A preliminary test was performed at Superweld Company. For this test a molybdenum ring of approximately the same size as the diffuser for the high power radiation source was manufactured along with a mating copper shell. Discussions were held with metallurgists at Superweld to determine the proper location of the brazing material and also the composition of the brazing alloy.

This test was performed with the molybdenum ring being slightly thicker than the counterbore in the copper housing. The brazing alloy was placed inside the housing and the parts were brazed with the molybdenum sitting on a ceramic plate. The intention was to cast the brazing alloy between the molybdenum and the copper using a gravitational flow technique. The brazing alloy used was Nioro which contains 82% gold and 18% nickel. The brazing temperature for this alloy is approximately 1850°F.

The normal furnace brazing technique of using capillary action in the flow of the brazing alloy between the mating parts could not be employed in this case because, at the brazing temperature, the calculated gap between the molybdenum and the copper was .007" and capillary action will not work with a gap larger than .002". The molybdenum and copper were assembled with an interference fit in their room temperature condition.

The results of this brazing test were inconclusive since the exact composition of the copper alloy was unknown. The parts were brazed

in a hydrogen atmosphere. All of the brazing alloy went to one side of the part in the first test. This was believed to have been caused by the part slipping off the ceramic block so that gravity drew the alloy metal to one side of the part. Superweld attempted to rebraze the part in an X-O atmosphere which is a composite of hydrogen, CO and CO_2. This attempt was unsuccessful and the brazing metal was not remelted. A subsequent rerun of the test sample in a hydrogen atmosphere also failed to correct the original error. Superweld advised us that much better results could possibly have been obtained if we had used oxygen free high conductivity copper.

The oxygen free high conductivity copper was purchased and two additional test samples were prepared. During the lead time in procuring the material and preparing the test samples, another company, Vac-Hyd, was contacted and it was decided to have these latter test samples brazed at Vac-Hyd since they agreed to perform the test work on a no cost basis.

For this second test series, two different joint designs were employed. The first was identical to the one which had been previously tried at Superweld. The second employed a taper on the outside of the molybdenum ring with a matching taper on the inside of the copper housing. The intention of the tapered design was to allow the molybdenum to "sink" into the copper housing as the parts were brought to temperature. It was felt that this design would produce a gap which was compatible with that required for capillary action of the brazing material. The only fear in using the tapered design was the possibility of the molybdenum part "sinking" unevenly into the copper housing and producing a tilted joint where complete brazing could not be accomplished.

These two test samples were run in a hydrogen atmosphere using a 50% copper-50% gold brazing alloy. The straight ring design produced a joint where the brazing material filled the gap for approximately 75% of the circumference. The remainder was joined only in a narrow area. This joint was completely unsatisfactory since the heat conduction

would be severely restricted over that portion of the molybdenum diffuser which did not have a complete bond to the copper.

The joint with the tapered design looked promising on first inspection. However, it was impossible to determine if the brazing material had completely filled the joint. Therefore, the test sample was returned to the machine shop and faced off so that the joint might be inspected. After several thousandths had been removed from the face, the piece was sawed in half and the faces along the cut were polished to allow inspection of the brazed joint.

Inspection of this joint indicated that a good bond had been obtained and no gaps were observed.

CONCLUSION

1. Because of the differential coefficient of thermal expansion between copper and molybdenum, it is not feasible to join these materials using furnace brazing with a cylindrical joint design.

2. A tapered joint design where the dimensions are properly figured to account for the differential thermal expansion can be successfully employed in fabricating a molybdenum to copper joint.

3. It is necessary to use oxygen free high conductivity copper for furnace brazing because of the requirements of using a hydrogen atmosphere and a high melting point brazing alloy.

4. A 50% copper-50% gold brazing alloy will wet molybdenum and copper and produce a good high conductivity brazed joint.

SPECTROLAB

DEVELOPMENT MEMORANDUM NO. 272-2

SUBJECT : Energy Absorption in the Envelope of a Plasma Radiation Source
WRITTEN BY: Kurt Muller
DATE : September 25, 1964
JOB NUMBER: 6002-21

INTRODUCTION

The parameters governing the absorption of radiant energy in the envelopes are the transmission characteristics of the envelope material and the spectral distribution of the radiated energy. While transmission curves for quartz have been established with a fair accuracy, some guesswork has to be done in regard to the spectral distribution. To date, the spectral distribution of the plasma radiation source has been measured only within the transmission range of commercial optical grade quartz, that is, between 0.2 and 3.5 microns. For all radiated energy below 0.2 microns, the quartz is opaque, and the energy is, therefore, fully absorbed and converted into heat. It is believed that a considerable percentage of the heat input to the envelope is produced by radiation in the regions where quartz is opaque. A special research program to establish the short wave radiation of a plasma source would be most beneficial to the envelope design. Until reliable data are available, some assumptions are inevitable.

In the two envelope system as employed in the high power source, the radiation below 0.2 microns is absorbed by the inner envelope. Thus, the inner envelope acts as a heat shield to the outer envelope which supports the gas pressure. Therefore, the spectrally averaged absorption coefficients of the two envelopes are not identical, the one for the inner tube will have a higher value.

METHOD OF ANALYSIS

For a parallel beam traversing a quartz plate, the decrease in energy per unit area dE is proportional to the thickness dx and the incident energy E, or

$$dE = -\alpha E\, dx \tag{1}$$

where α is a factor of proportionality called the absorption coefficient. The absorption coefficient represents the energy removed from the beam per unit length of the path. Eq. 1 becomes upon integration

$$E_2 = E_1 e^{-\alpha s} \tag{2}$$

E_1 is the initial intensity of the beam and E_2 is the intensity after it has traversed the thickness s.

The absorbed energy becomes

$$E_1 - E_2 = E_1 (1 - e^{-\alpha s}) \tag{3}$$

For nonparallel radiation penetrating a cylindrical envelope, the intensity, as well as the area of penetration, become functions of the radius. However, for a large tube radius r and a thin wall s, that is $s/r \ll 1$, eq. 3 may be applied to calculate the energy absorbed with a reasonable accuracy.

The absorption coefficient is calculated from the spectral distribution of the radiated energy and the transmissivity of the envelope material under consideration. Fig. 1 presents a typical spectral distribution measured on a 60 KW source operated with argon. The same figure indicates the transmission curve for 1 cm thickness of GE 204 quartz excluding reflection.

$E_1(\lambda)$ and $E_2(\lambda)$ denote the average energies in the spectral band width $d\lambda$ entering and leaving the quartz tube respectively. Since $E_2(\lambda)$ is the measured value, it is convenient to express the absorbed energy by the following equation

$$E_1(\lambda) - E_2(\lambda) = E_2(\lambda)\left[\frac{1}{\tau(\lambda)} - 1\right] \tag{4}$$

The total energy absorbed over the whole spectral range is

$$E_1 - E_2 = \int_{\lambda_1}^{\lambda_2} E_2(\lambda)\left[\frac{1}{\tau(\lambda)} - 1\right] d\lambda \tag{5}$$

The combination of eqs. 2 and 5 then yields

$$\alpha = \frac{\ln\left\{\left[\frac{1}{E_2}\int_{\lambda_1}^{\lambda_2} E_2(\lambda)\left(\frac{1}{\tau(\lambda)} - 1\right)d\lambda\right] + 1\right\}}{s} \tag{6}$$

Table I lists the relative power transmitted and absorbed as a function of the wave length. Both curves are plotted in Fig. 1. The energy absorbed by the inner tube between 0.1 and 0.2 microns was extrapolated. This method is highly artificial because of the large contribution of this spectral region to the total absorbed energy, hence, a wrong assumption can introduce a large error. Nevertheless, the assumed energy below 0.2 microns as shown in Fig. 1 appears to be a realistic value and the following calculations are based on this assumption. The maximum radiated energy of the high power source is 50 KW. Assuming 10 steradians of free radiation the radiated power per steradian becomes

$$J = 5000 \text{ watt/steradian}$$

Since the transmission curve, as shown in Fig. 1, applies for a 1 cm thick wall, the same wall thickness must also be used in eq. 6 to calculate α. The result is presented in Table II.

Parameter	Inner Envelope	Outer Envelope
Relative Absorbed Energy per 1 cm	17.20 %	5.20 %
Inside Radius of Envelope r_1 (cm)	4.0 cm	4.4 cm
Theoretical Coefficient of Absorption $\alpha_{theo.}$ (cm^{-1})	0.157	0.050
Effective Coefficient of Absorption $\alpha_{eff.}$ (cm^{-1})	0.314	0.075

TABLE II Coefficient of Absorption for the Inner and Outer Envelope

The absorption coefficient derived from the transmission curve must be considered a theoretical value since the transmissivity was established under ideal conditions, that is, using quartz free of contaminations, and more particularly, with a clean surface. In a plasma radiation source, it is difficult to prevent deposition of microscopic particles on the envelopes. This contamination might originate from electrode evaporation or dust accumulated in the system. The inner envelope is naturally more subjected to dirt accumulation than the outer tube. In view of these circumstances, the theoretical absorptivities have been increased. For the inner tube α was increased by 100%, and for the outer tube α was increased by 50%. The amount of the increase was arbitrary. However, the effective absorption coefficients may represent actual running conditions more realistically than the theoretical values after a few hours of operation.

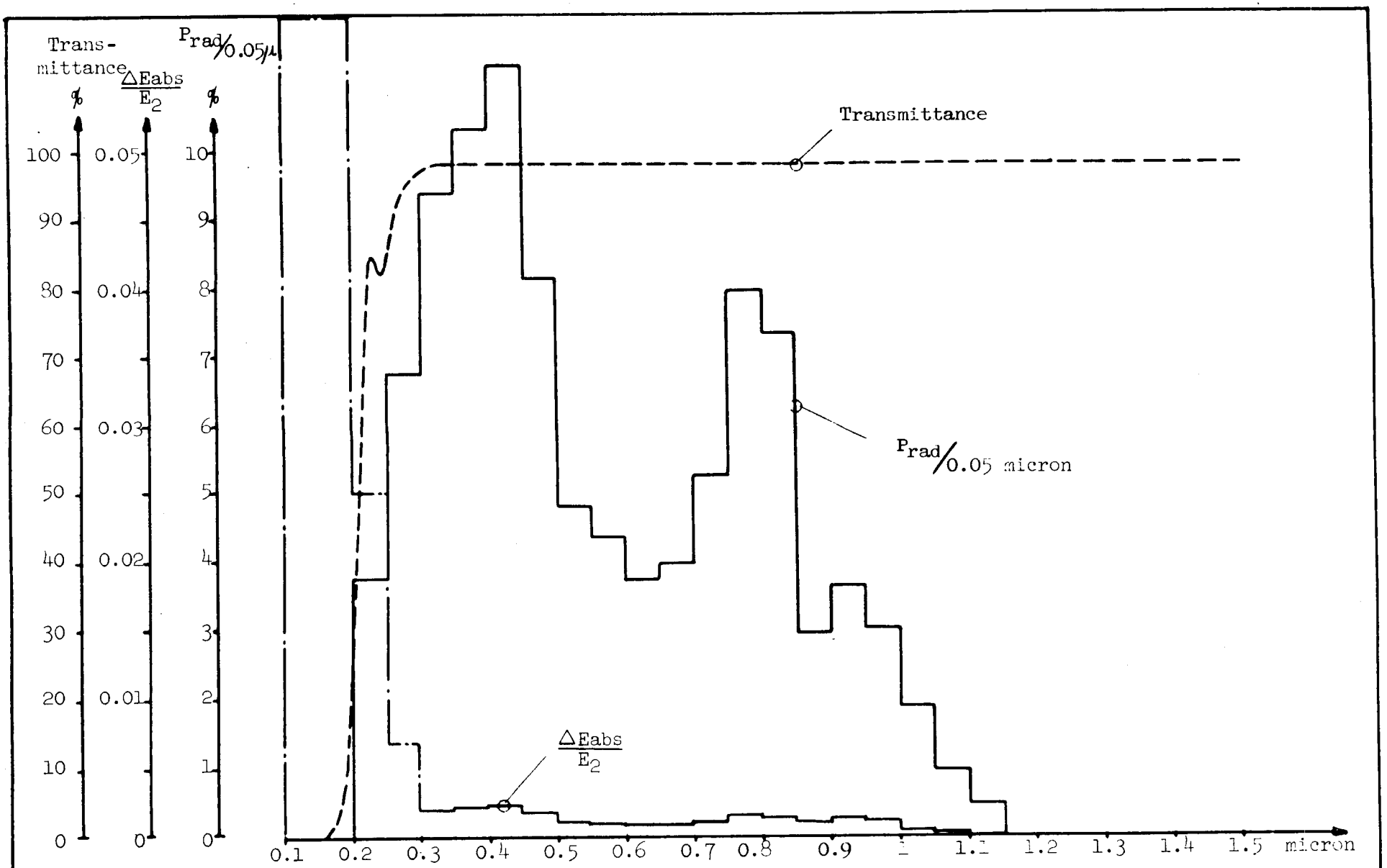

Fig. 1 Transmittance Characteristic (GE 204 Quartz, 1 cm, reflectivity excluded)
Spectrum of the radiated power (band width 0.05 microns)
Absorbed energy with respect to the transmitted energy E_2

Wave length Increment	Power Transmitted	Relative Power Transmitted	Average Transmission Coefficient (1 cm) (reflection excluded)	Reciprocal value of Transmittance	Relative Absorption	Relative Power Absorbed by the Envelope
Microns $\Delta\lambda$	rel.units per 0.05μ	$\frac{E_2(\lambda)}{E_2}\Delta\lambda$	τ	$\frac{1}{\tau(\lambda)}$	$\frac{1}{\tau(\lambda)} - 1$	$\frac{\Delta E(\lambda)}{E_2}$
0.10-0.15	0	0	0			(0.0600)
0.15-0.20	0	0	0			(0.0600)
0.20-0.25	40	0.0376	0.600	1.666	0.666	0.0250
0.25-0.30	72	0.0677	0.908	1.101	0.101	0.0068
0.30-0.35	100	0.0940	0.980	1.020	0.020	0.0019
0.35-0.40	110	0.1034	0.980	1.020	0.020	0.0021
0.40-0.45	120	0.1127	0.980	1.020	0.020	0.0023
0.45-0.50	87	0.0817	0.980	1.020	0.020	0.0017
0.50-0.55	51	0.0479	0.980	1.020	0.020	0.0010
0.55-0.60	46	0.0433	0.980	1.020	0.020	0.0009
0.60-0.65	40	0.0375	0.980	1.020	0.020	0.0008
0.65-0.70	42	0.0395	0.980	1.020	0.020	0.0008
0.70-0.75	56	0.0526	0.980	1.020	0.020	0.0010
0.75-0.80	85	0.0799	0.980	1.020	0.020	0.0016
0.80-0.85	78	0.0733	0.980	1.020	0.020	0.0015
0.85-0.90	31	0.0292	0.980	1.020	0.020	0.0006
0.90-0.95	39	0.0367	0.980	1.020	0.020	0.0008
0.95-1.00	32	0.0301	0.980	1.020	0.020	0.0007
1.00-1.05	20	0.0188	0.980	1.020	0.020	0.0004
1.05-1.10	10	0.0034	0.980	1.020	0.020	0.0002
1.10-1.15	5	0.0047	0.980	1.020	0.020	0.0001
1.15-1.20	0	0	0.980	1.020	0.020	0
Total =		1.0000			Outer Envelope =	0.0520
					Inner Envelope =	0.1720

Table I - Relative Spectral Transmission and Absorption

SPECTROLAB

DEVELOPMENT MEMORANDUM NO. 272-3

SUBJECT: Determination of the Heat Transfer Coefficient from the Envelope to the Cooling Medium

WRITTEN BY: Kurt Muller

DATE: September 25, 1964

JOB NUMBER: 6002-21

INTRODUCTION

In an earlier report (Giannini 8th Monthly Progress Report, 26 May 1964), it was attempted to devise a model describing the heat transfer mechanism from the envelopes to the cooling medium. Since the validity of the temperature field in the envelopes depends very much on the accuracy of the heat transfer coefficients, the assumptions have been thoroughly reviewed.

In the following paragraphs, the pertinent equations, as well as the changes and corrections, are summarized. For explanation of the symbols, please refer to the report mentioned above.

FLOW PATTERN IN THE VORTEX CHAMBER

$$c = r_3 \sqrt{2(i_o - c_p T_3) - \left(\frac{\dot{m}}{2\pi r_3 L \rho_3}\right)^2}$$

T_o = 350°K

p_o = 22 at absolute

ρ_o = 29.7 kg/m^3

R = 208 Joule/kg°C

$\dot{m}$ = 33 gr/s

c_p = 523 Joule/kg°C

L = 0.030 m

r_3 = 0.009 m

r_2 = 0.040 m

$p_o - p_3$ = 1.0 at

The constant "c" is calculated as

$c = 0.712\ m^2/s$

The tangential velocity components become

$u_2 = 17.8\ m/s$

$u_3 = 79.0\ m/s$

Assuming again a kinetic conversion efficiency of 50%, the effective tangential velocity component near the inside of the inner envelope becomes

$$U^{**} = \sqrt{2 \times 0.5 \times \frac{(17.8 \times \cos 30°)^2}{2}} = 11.0\ m/s$$

in which the angle of 30° denotes the inclination of the injector hole with respect to a plane perpendicular to the arc axis.

DETERMINATION OF THE HEAT TRANSFER COEFFICIENT h_{11}

For flat plates and moderately curved surfaces and for turbulent flow (Re_{crit}=300,000), the Nusselt number may be expressed by

$$Nu = 0.0325\ Re_L^{0.8}\ Pr^{1/3}$$

The physical properties are referred to the average temperature T_m, that is,

$$T_m = \frac{T_\infty + T_{wall}}{2} = 700°K$$

Data:

$\dot{V}$	=	40 scfm	(Argon)
u	=	11 m/s	Velocity near the envelope surface
L	=	0.25 m	Circumference of the tube
p	=	22 at	Absolute gas pressure
T	=	350° K	Intake temperature of the gas
R	=	208 Joule/kg°C	Gas constant

c_p	=	523 Joule/kg°C	Specific heat at constant pressure
k	=	0.0346 watt/m°C	Thermal conductivity of Argon at 700°K
μ	=	40×10^{-6} kg/ms	Absolute viscosity

The calculation of the Reynolds number gives

$$Re_L = \frac{u \times L}{\nu} = 1.02 \times 10^6$$

And the Prandtl number becomes

$$Pr = \frac{\mu c_p}{k} = 0.605$$

The Nusselt number is

$$Nu = 0.0325\, Re_L^{0.8} Pr^{1/3} = 1730$$

Finally, the heat transfer coefficient is calculated as

$$h_{11} = 240 \text{ watt/m}^2\text{°C}$$

DETERMINATION OF THE HEAT TRANSFER COEFFICIENTS IN THE ANNULUS h_{12}, h_{21}

A. Cooling Medium, Gas

For turbulent flow in concentric annuli (Re_{crit} = 2300), the following relation is recommended

$$\frac{h_g}{c_p G}\left(\frac{c_p \mu_b}{k}\right)_L^{2/3}\left(\frac{\mu_w}{\mu_b}\right)^{0.14} = \frac{0.023}{\left(\frac{D_e G}{\mu_b}\right)^{0.2}}$$

Subscript w refers to "wall"

Subscript b refers to "bulk" (e.g. bulk temperature of the gas)

Data:

D_{12}	=	0.084 m	O. D. of the inner tube
D_{21}	=	0.096 m	I. D. of the outer tube
D_e	=	0.012 m	equivalent diameter
A	=	$17 \times 10^{-4} m^2$	cross section of the passage
ρ	=	$29.6 kg/m^3$	density of the gas
c_p	=	523 Joule/kg°C	specific heat
k	=	0.021 watt/m°C	thermal conductivity of the gas
μ_b	=	25×10^{-6} kg/ms	absolute viscosity (bulk temperature 350°K)
μ_w	=	50×10^{-6} kg/ms	absolute viscosity (wall temperature 800°K)
$\dot{m}$	=	33.5×10^{-3} kg/s	mass flow
u	=	0.667 m/s	axial velocity in the annulus
G	=	$19.7 kg/sm^2$	specific flow rate

The Reynolds number is calculated as Re = 9500

The heat transfer coefficient becomes:

for the experimental source $h_{12} = 47$ watt/m^2°C

for the self-supporting version $h_{12} = 140$ watt/m^2°C

In the latter case, the following data were used:

D_{12}	=	0.084 m
D_{21}	=	0.088 m
D_e	=	0.004 m
A	=	$5.4 \times 10^{-4} m^2$
u	=	2.1 m/s
G	=	$62 kg/sm^2$

The wall temperature has a secondary influence on the heat transfer coefficient, thus,

$$h_{12} \cong h_{21}$$

B. Cooling Medium, Water

For water flow in the annular passage in the laminar range ($Re_{crit} = 2300$), the heat transfer coefficient may be deduced from the following relation:

$$\frac{h\,De}{k} = 1.02\ Re_m^{0.45}\ Pr_m^{0.5}\ Gr_m^{0.05} \left(\frac{D_{21}}{D_{12}}\right)^{0.8} \left(\frac{De}{L}\right)^{0.4} \left(\frac{\mu_m}{\mu_w}\right)^{0.14}$$

All physical properties are referred to $T_m = \frac{T_\infty + T_{wall}}{2} = 325°K$

Subscript: m = mean (condition at T_m)

w = wall (condition at T_w)

The flow rate of water was arbitrarily assumed with 2 GPM. If the surface temperature of the envelope is higher than 212°F, nucleate boiling heat transfer takes place. For nucleate boiling, the heat transfer coefficient may be higher or lower than the one calculated from the equation above, depending on the surface temperature of the envelope. Therefore, the actual heat transfer coefficient has to be determined by an iteration process.

For a first approximation, the following data were used:

Data:

$\dot{m}$	=	0.13 kg/s	water flow (2 GPM arbitrarily assumed)
u	=	0.241 m/s	axial flow velocity
μ	=	0.6×10^{-3} kg/sm	absolute viscosity
ν	=	0.6×10^{-6} m^2/s	dynamic viscosity
c	=	4186 Joule/kg°C	specific heat of water
k	=	0.64 watt/m°C	thermal conductivity
L	=	0.200 m	length of the passage
β	=	$0.207 \times 10^{-3} °C^{-1}$	volumetric expansion coefficient
D_e	=	0.004 m	equivalent diameter
ρ	=	1000 kg/m^3	density of water
g	=	9.81 m/s^2	gravitational constant
ΔT	=	100°C	temperature differential
D_{12}	=	0.084 m	
D_{21}	=	0.088 m	

$$Gr_m = \frac{\beta \Delta T D_e^3 \rho g}{\mu^2} = 35$$

$$Re_m = \frac{u D_e}{\nu} = 1600$$

$$Pr_m = \frac{\mu c}{k} = 3.92$$

The corresponding Nusselt number becomes

Nu = 14.3

The heat transfer coefficient follows from the Nusselt number

$$h_{12} = \frac{Nu\ k}{D_e} = 2280 \text{ watt/m}^2\text{°C}$$

and again

$h_{12} \cong h_{21}$

DETERMINATION OF THE HEAT TRANSFER COEFFICIENT h_{20} FROM THE OUTER ENVELOPE TO THE ENVIRONMENT

The surrounding medium is air in atmospheric condition. The equation which describes free convective heat transfer from a horizontal cylinder is:

$$\frac{h\, D_{20}}{k_f} = 0.53 \left[\frac{D_{20}^3\, \rho_f^2\, g\, \beta_f\, \Delta T}{\mu_f^2} \left(\frac{C_p\, \mu}{k} \right)_f \right]^{0.25}$$

"f" refers to the mean temperature defined as

$$T_f = \frac{T_\infty + T_{wall}}{2}$$

Data:

ΔT	=	600°C	Temperature difference (estimated)
D_{20}	=	0.104	O. D. of the outer envelope
k	=	3.18×10^{-2} w/m°C	thermal conductivity of air
ρ	=	1.2 kg/m^3	density of air
β	=	1/273°k^{-1}	coefficient of volumetric expansion
g	=	9.81 m/s^2	gravitational constant
μ	=	25×10^{-6} kg/sm	absolute viscosity of air
c_p	=	1000 Joule/kg°C	specific heat

$$Gr = \frac{D_{20}^3\, \rho^2\, g\, \beta\, \Delta T}{\mu^2} = 5.6 \times 10^7$$

$$Pr = \frac{C_p\, \mu}{k} = 0.785$$

h_{20} = 13.0 watt/m^2°C

SUMMARY

	Heat Transfer Coefficient	Cooling Medium		
		Water (2 GPM)	Argon (40 scfm)	Air (free conv.)
Experimental Source	h_{11}	--	240 w/m^2°C	--
	h_{12}	--	47 w/m^2°C	--
	h_{21}	--	47 w/m^2°C	--
	h_{20}	--	--	13 w/m^2°C
Self-Supporting Envelope	h_{11}	--	240 w/m^2°C	--
	h_{12}	2280 w/m^2°C	140 w/m^2°C	--
	h_{21}	2280 w/m^2°C	140 w/m^2°C	--
	h_{20}	--	--	13 w/m^2°C

h_{20} = 13.0 watt/m^2°C

SUMMARY

	Heat Transfer Coefficient	Cooling Medium		
		Water (2 GPM)	Argon (40 scfm)	Air (free conv.)
Experimental Source	h_{11}	--	240 w/m^2°C	--
	h_{12}	--	47 w/m^2°C	--
	h_{21}	--	47 w/m^2°C	--
	h_{20}	--	--	13 w/m^2°C
Self-Supporting Envelope	h_{11}	--	240 w/m^2°C	--
	h_{12}	2280 w/m^2°C	140 w/m^2°C	--
	h_{21}	2280 w/m^2°C	140 w/m^2°C	--
	h_{20}	--	--	13 w/m^2°C

SPECTROLAB

DEVELOPMENT MEMORANDUM NO. 272-4

SUBJECT : Radial Temperature Distribution in the Envelope of a Plasma Radiation Source
WRITTEN BY: Kurt Muller
DATE : September 25, 1964
JOB NUMBER: 6002-21

INTRODUCTION

Exact knowledge of the temperature distribution in a radiation source envelope is mandatory because of two major problems: divitrification of the quartz and thermal stresses. The detailed analysis of the radial and axial temperature field is a complex problem because there is no analytical solution which satisfies the differential equations of heat transfer and the boundary conditions at the same time. The problem has been simplified by disregarding axial heat conduction. This assumption may be justified by the fact that quartz is a poor thermal conductor. Most of the heat is dissipated from the envelope surface by convection and reradiation and only a small amount is conducted in the axial direction toward the water cooled housings. The highest temperature in the envelope occurs in a zone lying in the plane passing through the arc center normal to the arc axis. This zone is the subject of investigation in the following paragraphs.

CALCULATIONS

Since the envelope thickness is relatively small compared to the radius, that is, $s/r_1 \ll 1$, where s denotes the wall thickness and r_1 the inside diameter of the tube, a section of the envelope may be substituted by a flat plate. This simplification was made primarily to facilitate the transient heat transfer analysis where the treatment of the envelope as a cylinder results is a time consuming calculation. For small values of s/r_1, the flat plate approximation gives realistic results without serious departure from actual facts.

The heat transferred per unit area, q, for the linear steady state case is

$$q = - k \frac{dT}{dx} \tag{1}$$

k = thermal conductivity of the material

T = temperature

dx = length

The heat generated in the envelope by the incident energy E, within the depth x is calculated by

$$q_{abs} = E_1(1 - e^{-\alpha x}) \tag{2}$$

Equation 2 differentiated with respect to x gives

$$dq_{abs} = \alpha E_1 e^{-\alpha x} dx \tag{3}$$

From eq. 1 follows

$$dq = - k \frac{d^2T}{dx^2} dx \tag{4}$$

The combination of eqs. 3 and 4 then yields

$$\frac{d^2T}{dx^2} = - \frac{\alpha E_1}{k} e^{-\alpha x} \tag{5}$$

The general solution of eq. 5 is

$$T = - \frac{E_1}{\alpha k} e^{-\alpha x} + Ax + B \tag{6}$$

Boundary condition:

For x = 0 $\quad T = T_1$

For x = s $\quad T = T_2$

Thus,

$$T_1 = -\frac{E_1}{\alpha k} + B$$

and

$$B = T_1 + \frac{E}{\alpha k} \tag{7}$$

Furthermore,

$$T_2 = -\frac{E_1}{\alpha k} e^{-\alpha s} + As + B$$

hence,

$$B = T_2 + \frac{E_1}{\alpha k} e^{-\alpha s} - As \tag{8}$$

For reasons of compatibility, the integration constant A follows from eqs. 7 and 8

$$A = \frac{E_1}{\alpha k s}\left(e^{-\alpha s} - 1\right) + \frac{1}{s}\left(T_2 - T_1\right) \tag{9}$$

Substituting eqs. 8 and 9 into eq. 6

$$T = \frac{E_1}{\alpha k} e^{-\alpha x} + \frac{1}{s}\left[\frac{E_1}{\alpha k}\left(e^{-\alpha s} - 1\right) + \left(T_2 - T_1\right)\right] x + \left(\frac{E_1}{\alpha k} + T_1\right) \tag{10}$$

Rearranging the equation above gives the following expression:

$$T = T_1 + \frac{E}{\alpha k}\left(1 - e^{-\alpha x}\right) - \frac{1}{s}\left[\frac{E_1}{\alpha k}\left(1 - e^{-\alpha s}\right) + T_1 - T_2\right] x \tag{11}$$

The maximum temperature is derived from

$$\frac{dT}{dx}\left[T(x)\right] = 0$$

or

$$\frac{E_1}{k} e^{-\alpha x} - \frac{1}{s}\left[\frac{E_1}{\alpha k}\left(1-e^{-\alpha s}\right) + T_1 - T_2\right] = 0 \qquad (12)$$

substituting

$$U = \frac{E_1}{k}$$

and

$$V = \frac{1}{s}\left[\frac{E_1}{\alpha k}\left(1-e^{-\alpha s}\right) + T_1 - T_2\right]$$

then, the location at which the maximum temperature occurs may be written as

$$x = \frac{1}{\alpha} \ln \frac{U}{V} \qquad (13)$$

The envelope surface temperatures T_1 (inner) and T_2 (outer) are established by the equilibrium condition of heat generation and heat dissipation in and from the envelope respectively. The cooling mechanism includes radiation and convection (conduction may be disregarded for a first approximation).

The heat transfer mechanism is illustrated schematically in Fig. 1.

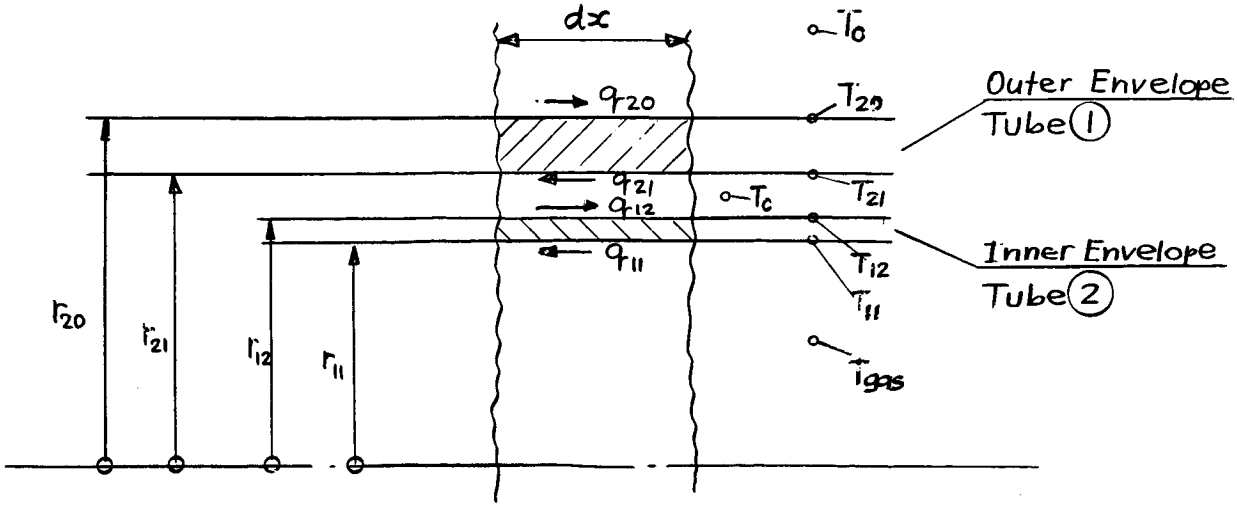

Fig. 1 Heat Transfer Mechanism in the Envelope

For the subsequent calculations, the distinction between the inner and outer envelopes is made by using the following notations:

Subscript: 11 inner surface of the inner envelope

12 outer surface of the inner envelope

21 inner surface of the outer envelope

20 outer surface of the outer envelope

0 condition of the environment

HEAT TRANSFER IN THE INNER ENVELOPE

On the inside no appreciable heat transfer takes place by radiation since the opposite wall of the inner envelope is at the same temperature. However, the axial temperature distribution is a bell shaped curve, hence, some heat is radiated to the lateral sections from the hot spot region. Since the angle of incidence is shallow, the amount of the radiated power is negligible due to the shape factor.

The inside of the inner envelope is primarily cooled by forced convection induced by the vortex action.

If h denotes the heat transfer coefficient, the heat dissipated per unit area by convection becomes

$$q_{11} = h_{11} \left(T_{11} - T_{gas} \right) \tag{14}$$

From the inner envelope, heat is radiated to the outer envelope which has a lower temperature. Furthermore, heat is dissipated by forced convection of the cooling medium in the annular passage. The total heat dissipated from the outside of the inner envelope becomes

$$q_{12} = h_{12} \left(T_{12} - T_c \right) + \frac{6}{\frac{1}{\varepsilon_1} + \frac{r_{12}}{r_{21}} \left(\frac{1}{\varepsilon_2} - 1 \right)} \left[\left(\frac{T_{12}}{100} \right)^4 - \left(\frac{T_{21}}{100} \right)^4 \right] \tag{15}$$

T_c = Temperature of the cooling medium

σ = Stefan - Boltzmann constant

ε = Emissivity

HEAT TRANSFER IN THE OUTER ENVELOPE

Beside the heat generated inside the envelope, an additional amount is absorbed by radiation from the inner envelope, namely,

$$q = \frac{\sigma}{\frac{1}{\varepsilon_1} + \frac{r_{12}}{r_{21}}\left(\frac{1}{\varepsilon_2} - 1\right)} \left[\left(\frac{T_{12}}{100}\right)^4 - \left(\frac{T_{21}}{100}\right)^4 \right] \tag{16}$$

The heat loss by forced convection is

$$q_{21} = h_{21} \left(T_{21} - T_c \right) \tag{17}$$

On the outside of the outer envelope heat is dissipated by free convection and radiation to the environment. The sum of the energy transferred becomes

$$q_{20} = h_{20} \left(T_{20} - T_0 \right) + \sigma \varepsilon_2 \left[\left(\frac{T_{20}}{100}\right)^4 - \left(\frac{T_0}{100}\right)^4 \right] \tag{18}$$

The energy exchange at the boundary demands the following requirements:

For the inner tube

$$\frac{dT}{dx}\left[T(x) \right]_{x=0} = \frac{1}{k} q_{11}(T_{11}) \tag{19}$$

$$\frac{dT}{dx}\left[T(x) \right]_{x=s_1} = -\frac{1}{k} q_{12}\left(T_{12}, T_{21}\right) \tag{20}$$

Equation 11 written in the notation used for the inner envelope is

$$T = T_{11} + \frac{E_{11}}{\alpha_1 k}\left(1 - e^{-\alpha_1 x}\right) - \frac{1}{s_1}\left[\frac{E_{11}}{\alpha_1 k}\left(1 - e^{-\alpha_1 s_1}\right) + T_{11} - T_{12} \right] x \tag{21}$$

$$\frac{dT}{dx} = \frac{E_{11}}{k} e^{-\alpha_1 x} - \frac{1}{s_1}\left[\frac{E_{11}}{\alpha_1 k}\left(1 - e^{-\alpha_1 s_1}\right) + T_{11} - T_{12} \right] \tag{22}$$

From eqs. 19 and 22 follows for x = 0

$$\frac{E_{11}}{\alpha_1 k}\left(1-e^{-\alpha_1 s_1}\right)+T_{11}-T_{12} = s_1\left[\frac{E_{11}}{k}-\frac{h_{11}}{k}\left(T_{11}-T_{gas}\right)\right] \tag{23}$$

With the substitution

$$\vartheta_1 = T_{11}-T_{12}$$

equation 23 resolved for ϑ_1 becomes

$$\vartheta_1 = \frac{s_1}{k}\left[E_{11}-h_{11}\left(T_{11}-T_{gas}\right)\right]-\frac{E_{11}}{\alpha_1 k}\left(1-e^{-\alpha_1 s_1}\right) \tag{24}$$

From eqs. 20 and 22 follows for x = s

$$E_{11}\,e^{-\alpha_1 s_1}-\frac{k}{s_1}\left[\frac{E_{11}}{\alpha_1 k}\left(1-e^{-\alpha_1 s_1}\right)+\vartheta_1\right] = -h_{12}\left(T_{11}-\vartheta_1-T_c\right)-\frac{\sigma}{\frac{1}{\varepsilon_1}+\frac{r_{12}}{r_{21}}\left(\frac{1}{\varepsilon_2}-1\right)}\left[\left(\frac{T_{11}-\vartheta_1}{100}\right)^4-\left(\frac{T_{21}}{100}\right)^4\right] \tag{25}$$

or

$$T_{11} = \frac{1}{h_{12}}\left\{\frac{k}{s_1}\left[\frac{E_{11}}{\alpha k}\left(1-e^{-\alpha_1 s_1}\right)+\vartheta_1\right]-E_{11}e^{-\alpha_1 s_1}-\frac{\sigma}{\frac{1}{\varepsilon_1}+\frac{r_{12}}{r_{21}}\left(\frac{1}{\varepsilon_2}-1\right)}\left[\left(\frac{T_{11}-\vartheta_1}{100}\right)^4-\left(\frac{T_{21}}{100}\right)^4\right]+h_{12}\left(\vartheta_1+T_c\right)\right\} \tag{26}$$

From eqs. 24 and 26, T_{11} and may be deduced. Since T_{11} in eq. 26 cannot be expressed explicitly, this system of nonlinear equations was solved by iteration with T_{21} as a parameter.

The temperature T_{21} and the temperature differential $\vartheta_2 = T_{21}-T_{20}$ are calculated accordingly

$$E_2 = E_{21}+\frac{\sigma}{\frac{1}{\varepsilon_1}+\frac{r_{12}}{r_{21}}\left(\frac{1}{\varepsilon_2}-1\right)}\left[\left(\frac{T_{12}}{100}\right)^4-\left(\frac{T_{21}}{100}\right)^4\right] \tag{27}$$

$$\vartheta_2 = \frac{s_2}{k}\left[E_2-h_{21}\left(T_{21}-T_c\right)\right]-\frac{E_2}{\alpha_2 k}\left(1-e^{-\alpha_2 s_2}\right) \tag{28}$$

$$T_{21} = \frac{1}{h_{20}} \left\{ \frac{k}{s_2} \left[\frac{E_2}{\alpha_2 k} \left(1 - e^{-\alpha_2 s_2} \right) + \vartheta_2 \right] - E_2 e^{-\alpha_2 s_2} - 6 \varepsilon_2 \left[\left(\frac{T_{21} - \vartheta_2}{100} \right)^4 - \left(\frac{T_0}{100} \right)^4 \right] + h_{20} \left(\vartheta_2 + T_0 \right) \right\} \quad (29)$$

In eq. 27, the temperature T_{12} was considered a parameter.

The temperature distribution in the inner and outer envelope may now be calculated as a function of the variables T_{12} and T_{21}. Finally, the temperature curves of both envelopes may be found by matching T_{12} to T_{21}.

Some complication is introduced by a large variation of some of the physical properties of quartz with temperature. One of the physical parameters influenced by temperature is the emissivity. Disregarding the secondary influence of the wall thickness, see Fig. 2, the emissivity may be linearly approximated by the following expression

$$\varepsilon = 0.167 \left(6.350 - \frac{T}{T_0} \right) \quad (30)$$

in which

T = temperature °K

T_o = reference Temperature (300°K)

Equation 30 is applicable for the temperature range

$$300°K \leq T \leq 1200°K$$

All physical data except the emissivity have been considered to be invariant. The values were selected at an estimated average temperature. The temperature distributions of three different cases have been calculated. The result is shown in Figs. 3, 4, 5.

Fig. 3 presents the radial temperature curves existing in the envelopes of the experimental radiation source. The outer envelope has a wall thickness $s = 4$ mm.

Fig. 4 illustrates the temperature distributions of the final source which incorporates a self-supporting envelope with a wall thickness s = 8 mm.

Fig. 5 shows the result of the same design as described in Fig. 4 but with water cooling instead of gas cooling in the annular passage between the inner and outer envelopes.

The pertinent parameters and constants utilized in the analysis are listed in Table II.

DISCUSSION OF THE RESULTS

Looking at the experimental radiation source, the highest temperature was found in the inner envelope T_{1max} = 1142°K (Fig. 3). According to the quartz manufacturer (Engelhard), the critical temperature at which divitrification of quartz occurs is near 1300°K. Above this temperature, divitrification takes place at a rate of 0.2 mm/minute.

The self-supporting envelope assembly (Fig. 4) shows a higher temperature in the outer tube because more heat is absorbed due to the increased wall thickness. The peak temperature in the inner tube (Fig. 4) is about 60°C lower than the corresponding peak temperature in the inner tube (Fig. 3). The reason for this phenomenon is simply the smaller gap between the inner and outer envelope in the final assembly, causing the flow velocity of the cooling medium and, subsequently, the heat transfer coefficient to be higher.

Applying water cooling instead of gas cooling in the annular passage (Fig. 5), the temperatures in the inner, as well as in the outer, envelope are greatly reduced. However, a higher temperature gradient in the outer tube and thus, higher thermal stresses are the consequence. In order to reduce the thermal stresses in the outer envelope, the latter one should also be water cooled on the outside. Double cooling of the outer envelope could be accomplished by means of a third envelope which provides an annular passage for water flow between the second and third tube.

Parameter		Fig. 3	Fig. 4	Fig. 5
Wall thickness inner envelope	s_1 cm	0.2	0.2	0.2
Wall thickness outer envelope	s_2 cm	0.4	0.8	0.8
Inside radius inner envelope	r_{11} cm	3.95	3.95	3.95
Outside radius inner envelope	r_{12} cm	4.20	4.20	4.20
Inside radius outer envelope	r_{21} cm	4.80	4.40	4.40
Outside radius outer envelope	r_{20} cm	5.20	5.20	5.20
Heat transfer coefficient inner envelope	h_{11} w/cm^2°C	0.0240	0.0240	0.0240
Heat transfer coefficient inner envelope	h_{12} w/cm^2°C	0.0057	0.0117	0.2000
Heat transfer coefficient outer envelope	h_{21} w/cm^2°C	0.0057	0.0117	0.2000
Heat transfer coefficient outer envelope	h_{20} w/cm^2°C	0.0013	0.0013	0.0013
Incident energy inner envelope	E_{11} w/cm^2	310	310	310
Incident energy outer envelope	E_{21} w/cm^2	220	220	220
Coefficient of absorption inner envelope	α_1 cm^{-1}	0.314	0.314	0.314
Coefficient of absorption outer envelope	α_2 cm^{-1}	0.073	0.073	0.073
Radiated Power	P Kw	50	50	50
Thermal Conductivity	k w/cm°C	0.0184	0.0184	0.0184
Temperature of Environment	T_o °K	350	350	350
Temperature of the Gas	T_{gas} °K	350	350	350
Temperature of the Cooling Medium	T_c °K	350	350	350
Gas flow Argon	$\dot{V}$ scfm	40	40	40
Water flow	$\dot{V}$ GPM	--	--	2
Cooling medium inside inner envelope		Argon	Argon	Argon
Cooling medium in annulus		Argon	Argon	Water
Cooling medium outside outer envelope		Air	Air	Air

Table II Data for the Heat Transfer Calculation

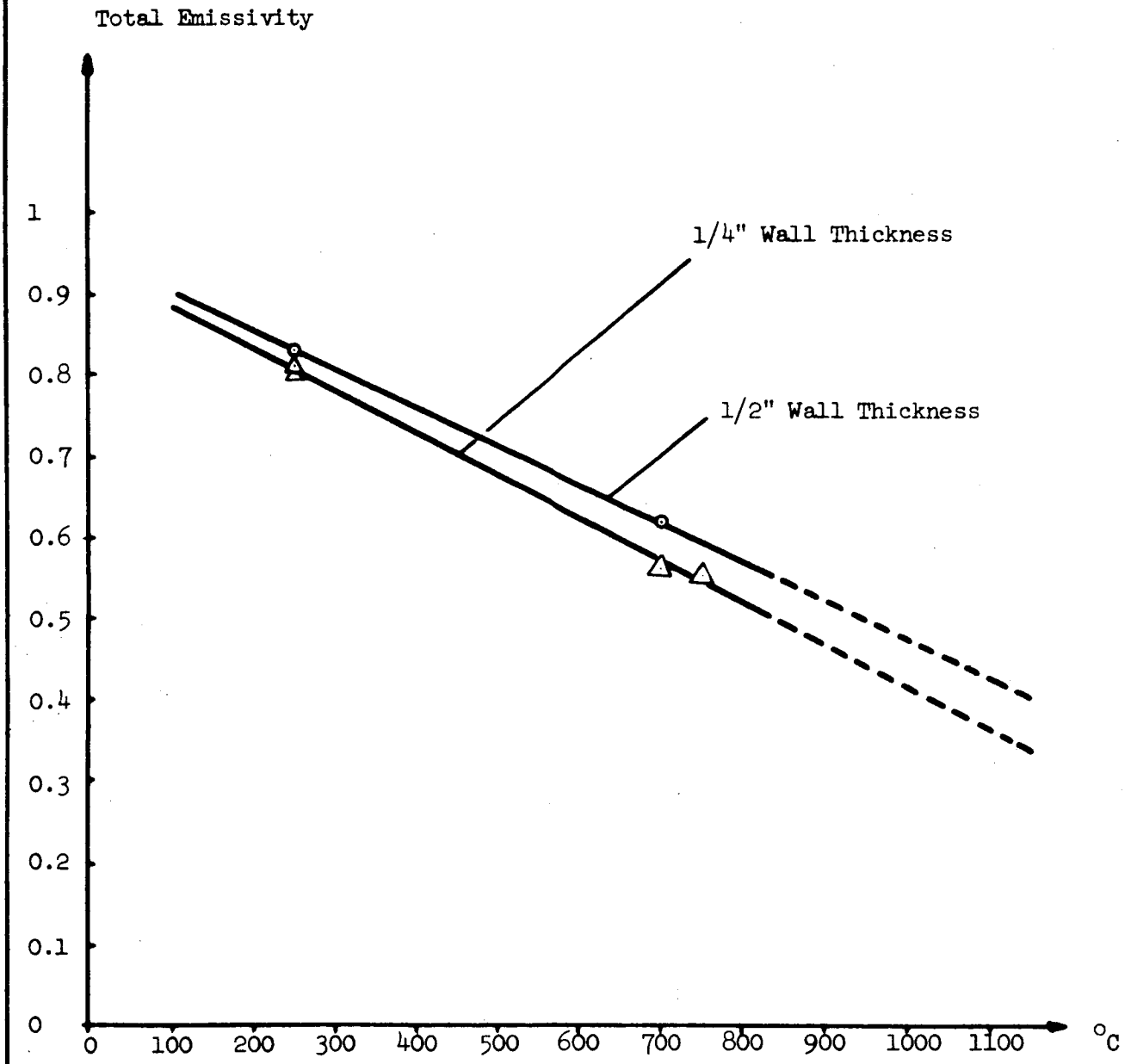

Fig. 2 Emissivity of Clear Fused Quartz
(Information from: Glass Engineering Handbook, E.Shand)

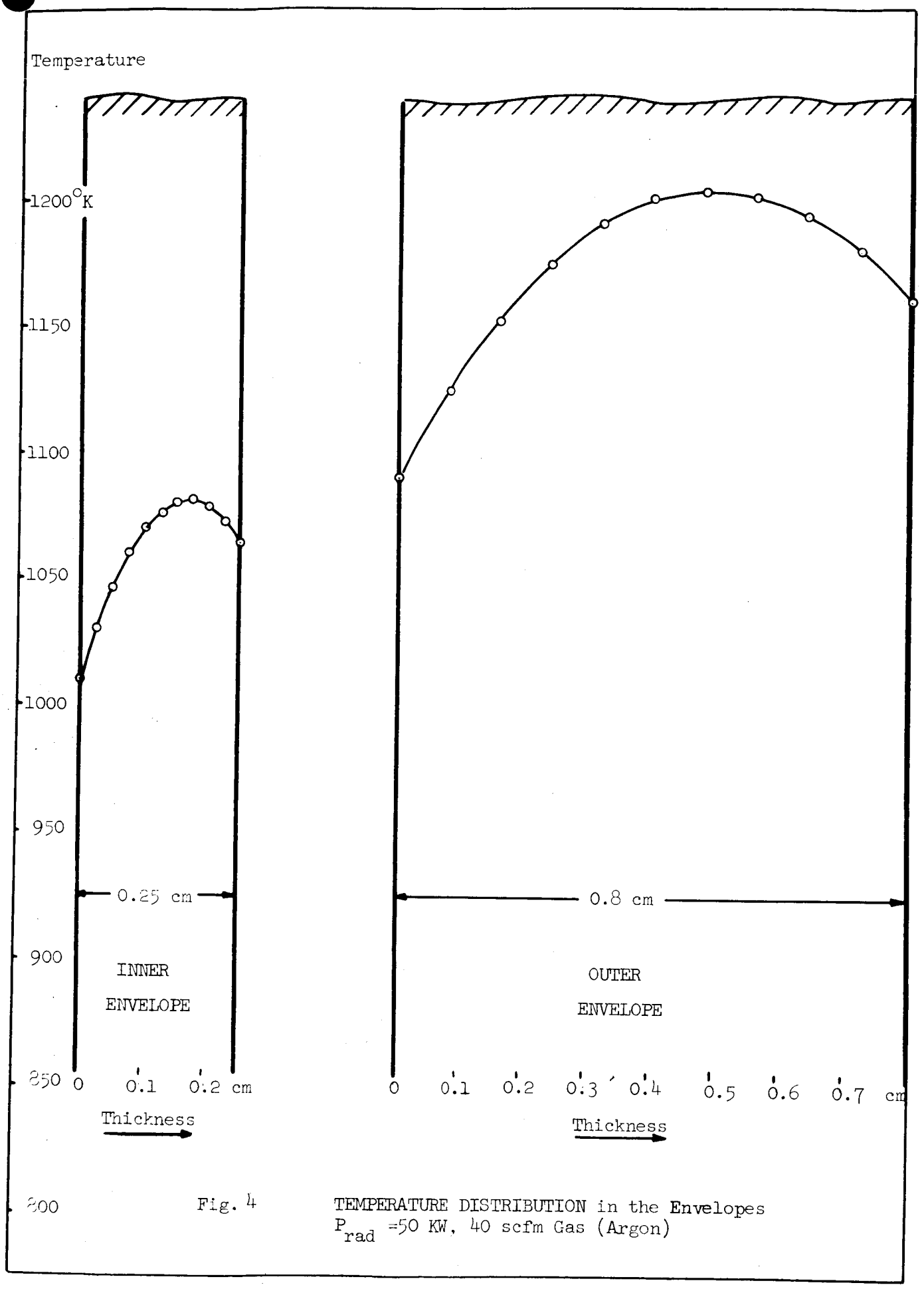

Fig. 4 TEMPERATURE DISTRIBUTION in the Envelopes
P_{rad} =50 KW, 40 scfm Gas (Argon)

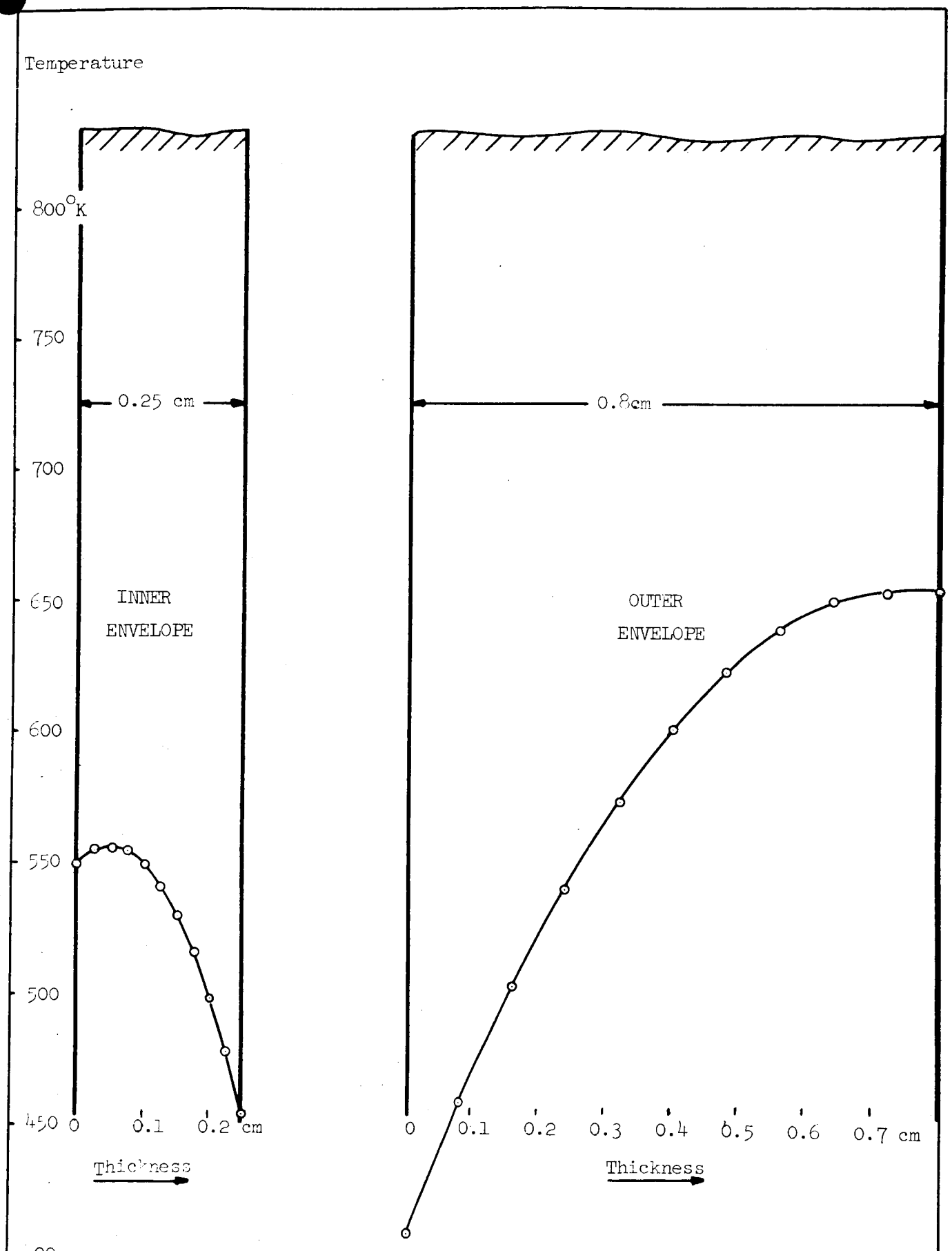

Fig. 5 TEMPERATURE DISTRIBUTION in the Envelopes
P_{rad} =50 KW, 40 scfm Gas (Argon) 2 GPM water in annular passage

SPECTROLAB

DEVELOPMENT MEMORANDUM NO. 272-5

SUBJECT: Simplified Stress Analysis of a Radiation Source Envelope
WRITTEN BY: Kurt Muller
DATE: September 25, 1964
JOB NUMBER: 6002-21

INTRODUCTION

The major problem areas in the development of plasma radiation sources are the electrode design and the envelope design. The envelope suffers high mechanical and thermal stresses during operation of the source. Clear fused silica, which is used as the envelope material, has a relatively low tensile strength compared to steel. For metals, the maximum allowable tensile strength varies little and will be guaranteed by the manufacturer within certain limits; however, no such guaranty exists for quartz. In regard to radiation sources where thermal stresses are encountered, the problem may not be solved by adding material because a thicker wall absorbs more energy with a subsequent increase in thermal stresses.

During the past years, methods have been devised to calculate mechanical and thermal stresses in straight tubes (or with flanges attached) and with nonuniform radial and axial temperature fields. However, the analysis is time consuming. Therefore, an attempt has been made to estimate the stresses in the envelope by reducing the problem to simple calculations. A simplification is only valuable if the degree of accuracy is known. Hence, the formulation of the problem deserves special attention in order to avoid unrealistic results. From the viewpoint of stresses, much effort was expended in reducing the problems to the worst possible cases, hence, the result of this analysis must be considered as an approach from the pessimistic side.

DETERMINATION OF MECHANICAL STRESSES

Symbols

σ	=	psi	stress
F	=	lb	force
A	=	in^2	Area
s	=	in	wall thickness
l	=	in	length
r_1	=	in	inside radius of the tube
D	=	in	O.D. of tube
d	=	in	I.D. of tube
p	=	psi	gas pressure
M	=	in-lb	Bending moment
W	=	in^3	section modulus
a	=	in	distance
L	=	in	length

Subscripts

t	=	tangential
a	=	axial
b	=	bending
G	=	gravity

For $\frac{s}{r_1} < 0.2$ the tangential stress is calculated as follows

$$\sigma_t = \frac{F_t}{A_t} \qquad (1a)$$

where

$$F_t = 2 r_i \ell p \tag{1b}$$

$$A_t = 2 \ell s \tag{1c}$$

the combination of eqs. 1a, 1b, 1c gives

$$\sigma_t = p \frac{r_i}{s} \tag{1d}$$

The axial stress is determined by

$$\sigma_a = \frac{F_a}{A_a} \tag{2a}$$

where

$$F_a = \pi r_i^2 p \tag{2b}$$

$$A_a = 2\pi s (r_i + s/2) \tag{2c}$$

thus,

$$\sigma_a = p \frac{r_i^2}{2s(r_i + s/2)} \tag{2d}$$

For the calculation of the bending stresses caused by the gas pressure, a single beam was considered whose shape corresponds to the cross section of the envelope and whose width is unity in the circumferential direction. The cross section of the beam in a plane perpendicular to the envelope axis is assumed to be rectangular. Geometry of the beam see Fig. 1.

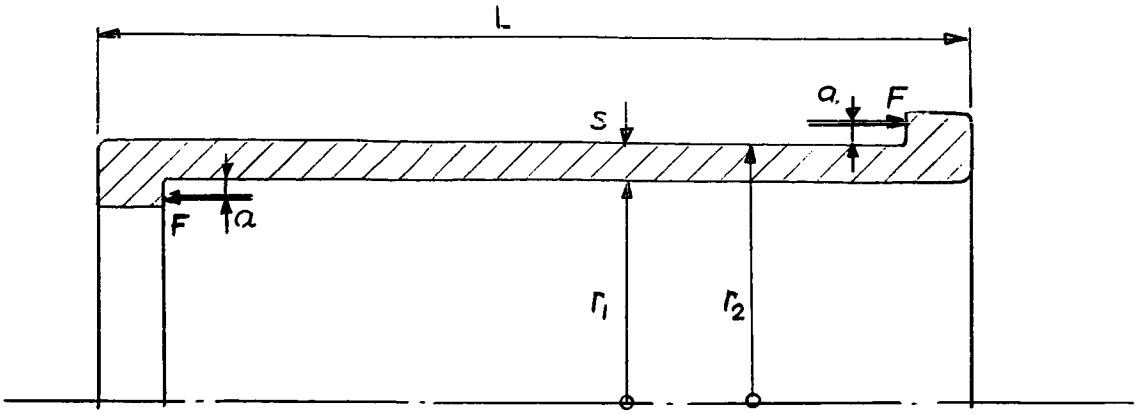

Fig. 1 Geometry of the Envelope

The moment per unit circumference is

$$M = p \frac{r_1}{2} \frac{a + s/2}{1 - a/r_1} \tag{3a}$$

the section modulus of a rectangular cross section with height s and width 1 becomes

$$W = \frac{s^2}{6} \tag{3b}$$

and the bending stresses per unit circumference are

$$\sigma_b' = 3p \frac{r_1}{s^2} \frac{(a + s/2)}{(1 - a/r_1)} \tag{3c}$$

The bending stress due to gravity of the cantilevered end is calculated by

$$\sigma_b'' = \frac{F_G L}{W_{Tube}} (r_1 + s) \tag{4a}$$

$$W_{Tube} = \frac{\pi}{64} (D^4 - d^4) \tag{4b}$$

hence,

$$\sigma_b'' = \frac{\pi}{64} \frac{F_G L}{D^4 - d^4} (r_1 + s) \tag{4c}$$

Data:

$a = 0.197$ in

$r_1 = 1.730$ in

$s = 0.315$ in

$L = 7.0$ in

$F_G = 10$ lb

$D = 4.095$ in

$d = 3.465$ in

$P = 300$ psig

On the basis of 300 psig gas pressure, the following data have been obtained

$\sigma_t = 1650$ psi

$\sigma_a = 760$ psi

$\sigma_b' = 6270$ psi

$\sigma_b'' = 22$ psi

The total stress in an element acting in the axial direction is

$$\sigma_{a\,tot} = \sigma_a + \sigma_b' + \sigma_c'' = 7052 \text{ psi}$$

The total stress in the tangential direction is

$$\sigma_{t\,tot} = \sigma_t = 1650 \text{ psi}$$

The recommended stress hypothesis for brittle materials, such as quartz, is the method of "maximum principal stress", that is, the failure occurs when the maximum stress approaches the ultimate strength of the material. Other theories, e.g., "maximum shear stress" concept appear to be more suitable to ductile materials.

CONCLUSION

The maximum mechanical stress in the self-supporting envelope occurs in axial direction in a plane perpendicular to the envelope axis and it's total amount is 7052 psi. The approximate tensile strength of clear fused quartz is 7000 psi. Thus, the self-supporting envelope will fail near 300 psi gas pressure.

As a comparison, the maximum mechanical stress in a straight envelope (8 mm wall), utilizing tie rods, is 1650 psi at 300 psi gas pressure.

THERMAL STRESSES

The pertinent equations describing the thermal stresses in a long hollow cylinder in the axial, radial and tangential directions are:

$$\varepsilon_a = \frac{dw}{da} = \frac{\sigma_a}{E} - \frac{\mu}{E}(\sigma_r + \sigma_t) + \alpha\vartheta \tag{5a}$$

$$\varepsilon_r = \frac{du}{dr} = \frac{\sigma_r}{E} - \frac{\mu}{E}(\sigma_a + \sigma_t) + \alpha\vartheta \tag{5b}$$

$$\varepsilon_t = \frac{u}{r} = \frac{\sigma_t}{E} - \frac{\mu}{E}(\sigma_a + \sigma_r) + \alpha\vartheta \tag{5c}$$

where ε represents the elongation, w and u the displacement in the axial and radial directions respectively, α denotes the thermal expansion coefficient and ϑ the temperature increase (ϑ = T-Tambient). The Poisson's ratio is given by μ and the modulus of elasticity by E.

From the equilibrium condition of an envelope ring element, the following differential equation for the elongation u is obtained:

$$\frac{d^2u}{dr^2} + \frac{1}{r}\frac{du}{dr} - \frac{u}{r^2} = \frac{1+\mu}{1-\mu}\alpha\frac{d\vartheta}{dr} \tag{6}$$

Integration with respect to r gives

$$u = \frac{1}{r}\frac{1+\mu}{1-\mu}\int_{r_1}^{r}\alpha\vartheta r\,dr + C_1 r + \frac{C_2}{r} \tag{7}$$

With the boundary conditions $(\sigma_r)_{r=r_1} = 0$ and $(\sigma_r)_{r=r_2} = 0$, the integration constants are determined as

$$C_1 = \frac{(1+\mu)(1-2\mu)}{1-\mu} \frac{1}{r_2^2 - r_1^2} \int_{r_1}^{r_2} \alpha \vartheta r \, dr - \mu \varepsilon_a \tag{8a}$$

$$C_2 = \frac{1+\mu}{1-\mu} \frac{r_1^2}{r_2^2 - r_1^2} \int_{r_1}^{r_2} \alpha \vartheta r \, dr \tag{8b}$$

In reality, $(\sigma_r)_{r=r_1}$ corresponds to the internal gas pressure which might be as much as 300 psi. However, this amount is small compared to the axial and tangential stresses and was, therefore, neglected. The general equations for the tangential stresses and axial stresses due to the tangential stresses become

$$\sigma_t = \frac{E}{1-\mu}\left[\frac{1}{r^2} \int_{r_1}^{r} \alpha \vartheta r \, dr + \frac{r^2 + r_1^2}{r^2(r_2^2 - r_1^2)} \int_{r_1}^{r_2} \alpha \vartheta r \, dr - \alpha \vartheta \right] \tag{9a}$$

$$\sigma_a = \frac{E}{1+\mu}\left[\varepsilon_a + \frac{\mu}{1-2\mu}\left(\varepsilon_a + \varepsilon_r + \sigma_t \right) \right] - \frac{\alpha \vartheta E}{1-2\mu} \tag{9b}$$

The temperature distribution in the 8 mm thick envelope established at 50 KW radiated power is shown in Fig. 2. Using a parabolic approximation, the temperature ϑ may be expressed as a function of the radius

$$\vartheta = a + br + cr^2 \tag{10}$$

The constants a, b, c are determined by three points defining the curve

ϑ_1 = 1990°F at r_1 = 1.732 in (inside radius)

ϑ_2 = 2122°F at r_2 = 2.047 in (outside radius)

ϑ_3 = 2202°F at r_3 = 1.921 in (radius at peak temperature)

$$a = \frac{\begin{vmatrix} \vartheta_1 & r_1 & r_1^2 \\ \vartheta_2 & r_2 & r_2^2 \\ \vartheta_3 & r_3 & r_3^2 \end{vmatrix}}{\begin{vmatrix} 1 & r_1 & r_1^2 \\ 1 & r_2 & r_2^2 \\ 1 & r_3 & r_3^2 \end{vmatrix}}$$

$$b = \frac{\begin{vmatrix} 1 & \vartheta_1 & r_1^2 \\ 1 & \vartheta_2 & r_2^2 \\ 1 & \vartheta_3 & r_3^2 \end{vmatrix}}{\begin{vmatrix} 1 & r_1 & r_1^2 \\ 1 & r_2 & r_2^2 \\ 1 & r_3 & r_3^2 \end{vmatrix}}$$

$$C = \frac{\begin{vmatrix} 1 & r_1 & \vartheta_1 \\ 1 & r_2 & \vartheta_2 \\ 1 & r_3 & \vartheta_3 \end{vmatrix}}{\begin{vmatrix} 1 & r_1 & r_1^2 \\ 1 & r_2 & r_2^2 \\ 1 & r_3 & r_3^2 \end{vmatrix}}$$

The constants are calculated as

$$a = -18385°F$$

$$b = 21378°F/in$$

$$c = -5550°F/in^2$$

Thus,

$$\vartheta = -18385 + 21378\,r - 5550\,r^2 \qquad [\,1.732 \leq r \leq 2.047\,]$$

The integral in eq. 9 becomes

$$\int_{r_1}^{r_2} \alpha \vartheta r\, dr = \alpha \int_{r_1}^{r_2} (a + br + cr^2)\, r\, dr$$

$$\int_{r_1}^{r_2} \alpha \vartheta r\,dr = \alpha \left(\frac{a}{2} r^2 + \frac{b}{3} r^3 + \frac{c}{4} r^4 \right) \Bigg|_{r_1}^{r_2}$$

$$\int_{r_1}^{r_2} \alpha \vartheta r\,dr = \alpha \left[\frac{a}{2} \left(r_2^2 - r_1^2 \right) + \frac{b}{3} \left(r_2^3 - r_1^3 \right) + \frac{c}{4} \left(r_2^4 - r_1^4 \right) \right]$$

The evaluation of eq. 9 leads to the stress distribution shown in Fig. 2. The maximum axial stress due to thermal stresses in the tangential direction was determined as approximately 200 psi. In a first approximation, the mechanical and thermal stresses may be superimposed. Thus, we arrive at the following stress pattern occurring at 300 psi gas pressure:

$$\sigma_{a\,max} = \sigma_{a\,mech} + \sigma_{a\,therm} = 7052 + 200 = 7252 \text{ psi}$$

$$\sigma_{t\,max} = \sigma_{t\,mech} + \sigma_{t\,therm} = 1650 + 594 = 2244 \text{ psi}$$

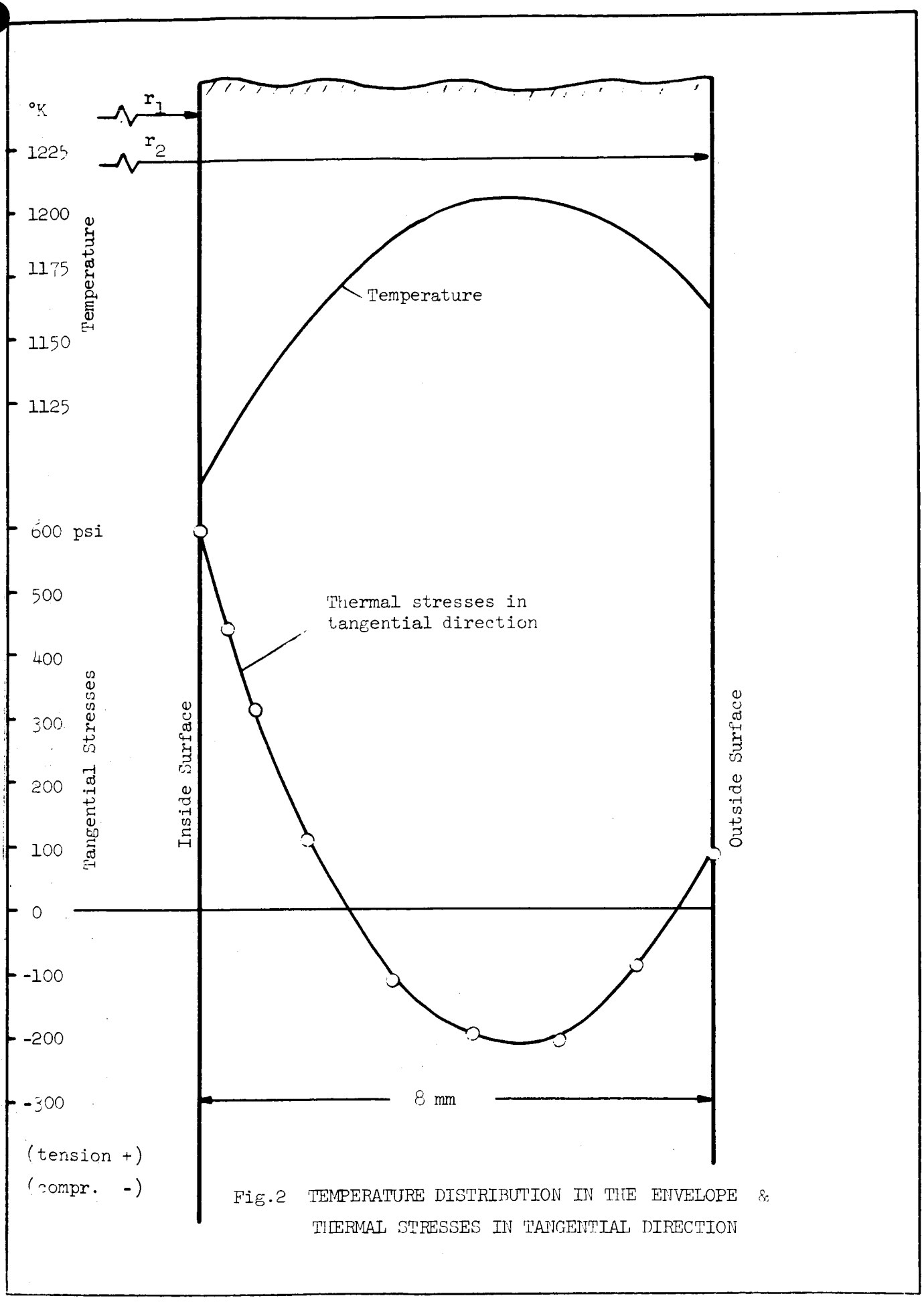

Fig.2 TEMPERATURE DISTRIBUTION IN THE ENVELOPE & THERMAL STRESSES IN TANGENTIAL DIRECTION

SPECTROLAB

DEVELOPMENT MEMORANDUM NO. 272-6

SUBJECT: Transient Heat Transfer in the Envelope of a Plasma Radiation Source

WRITTEN BY: Kurt Muller

DATE: September 24, 1964

JOB NUMBER: 6002-21

TRANSIENT HEAT TRANSFER IN THE ENVELOPE OF A PLASMA RADIATION SOURCE

INTRODUCTION

Transient heat transfer conditions in the envelope occur during power changes, especially during the starting and extinction procedures. The most severe conditions from the viewpoint of thermal stresses are the uncontrolled power changes, that is, when the radiation source is shut off instantaneously at full power because of an emergency. The latter condition is the subject of investigation in this memorandum.

The isochronal lines are presented for the cooling period of the envelope when the source is operated at 50kw output power and the arc is extinguished at time zero. The comparison between the steady state temperature distribution and the transient curves gives an indication of how much higher the transient stresses are expected to be.

METHOD OF ANALYSIS

The linear heat transfer equation is

$$\frac{\partial \vartheta}{\partial t} = a \frac{\partial^2 \vartheta}{\partial x^2} \qquad (1)$$

where

$$a = \frac{k}{\varrho c}$$

ϑ = temperature

t = time

x = radial location in the envelope where the origin of the x-axis coincides with the inner surface of the envelope, that is x=0 for $r=r_1$

k = thermal conductivity

ϱ = density

c = specific heat

Utilizing the method of finite differences eq. 1 may be expressed by

$$\vartheta_{n,m+1} - \vartheta_{n,m} = a \frac{\Delta t}{(\Delta x)^2} \left(\vartheta_{n+1,m} + \vartheta_{n-1,m} - 2\vartheta_{n,m} \right) \qquad (2)$$

with the substitution

$$a \frac{\Delta t}{(\Delta x)^2} = \frac{1}{2}$$

eq. 2 becomes

$$\vartheta_{n,m+1} = \frac{1}{2} \left(\vartheta_{n+1,m} + \vartheta_{n-1,m} \right) \qquad (3)$$

Eq. 3 is convenient for the graphical solution of the problem.

Physical data of quartz:

k = 0.0184 Watt/cm°C

c = 1.255×10^3 Joule/kg°C (at 800°C)

ϱ = 2.2×10^{-3} kg/cm^3

$$a = \frac{0.0184}{2.2 \times 10^{-3} \times 1.255 \times 10^3} = 6.66 \times 10^{-3} \text{ cm}^2/\text{s}$$

Δx = 0.1 cm

Δt = 0.75 seconds

Boundary conditions:

$$k \left(\frac{\partial \vartheta}{\partial x} \right)_{x=0} = h_1 \left(\vartheta_{x=0} - \vartheta_{gas} \right)$$

$$k \left(\frac{\partial \vartheta}{\partial x} \right)_{x=s} = -h_2 \left(\vartheta_{x=s} - \vartheta_{gas} \right)$$

Subscript 1 denotes the inside surface of the envelope . Subscript 2 denotes the outside surface of the envelope.

The heat transfer coefficient h includes convection as well as radiation, hence, it is a function of the surface temperature of the envelope (compare with the Development Memorandums 272-3 and 272-4).

DISCUSSION OF THE RESULTS

The transient temperature distribution in the envelope, as it occurs when the arc is extinguished instantaneously at 50kw radiated power, is shown in Fig. 1. At the time zero seconds, equilibrium conditions are established, that is, the heat generated in the envelope equals the heat transferred to the cooling medium. After extinction of the arc, the heat input to the envelope is zero. The heat stored in the quartz is conducted to the surface and dissipated to the surroundings. Fig. 1 shows the temperature distribution in increments of 3 seconds up to one minute. It is remarkable that during the transient condition the temperature gradient is not higher than at equilibrium condition and, consequently, the stresses are not greater than those established during steady state operation.

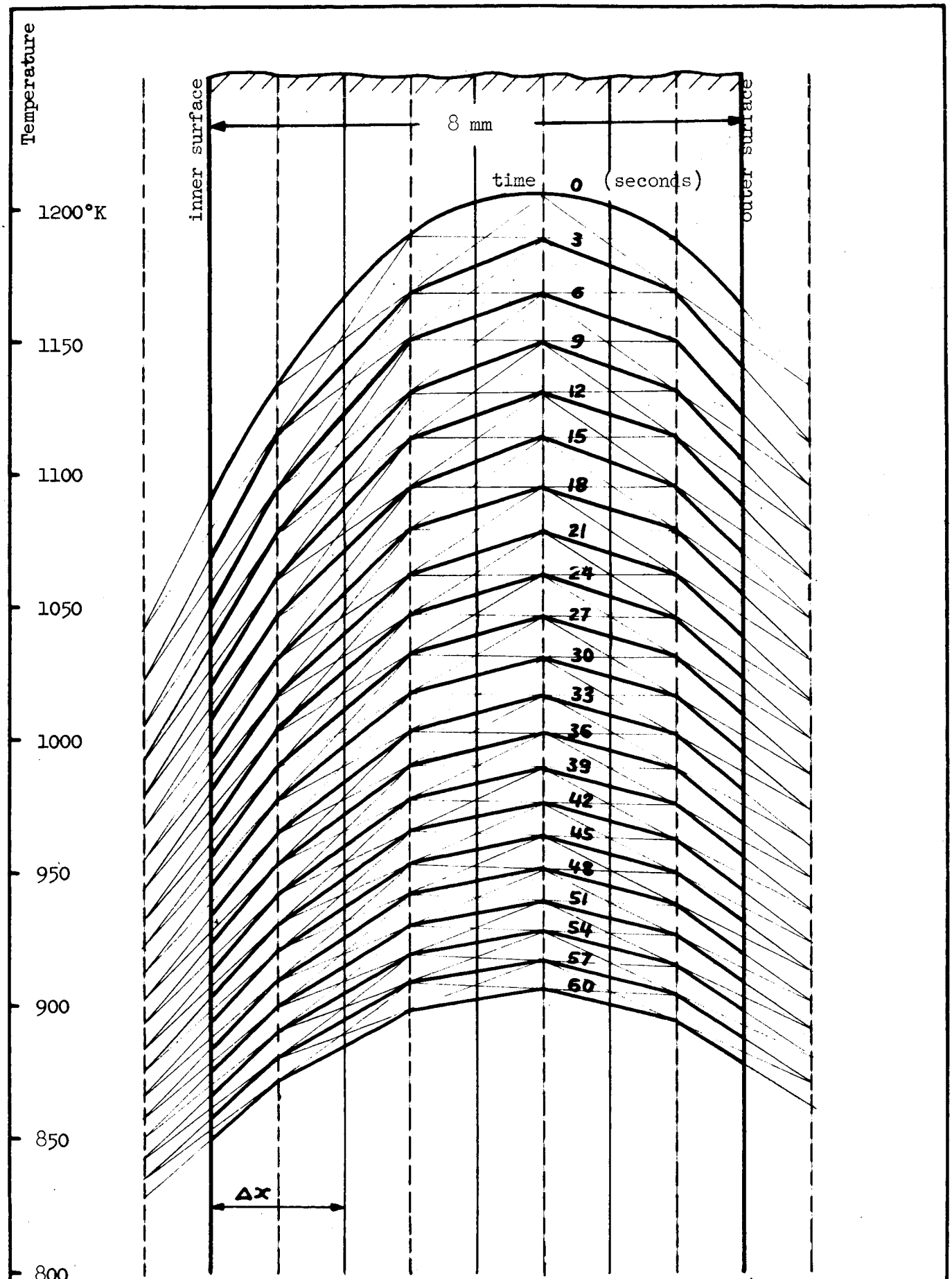

Fig.1 Transient temperature distribution in the envelope (50 KW radiated power, arc extinguished at time zero)

SPECTROLAB

DEVELOPMENT MEMORANDUM NO. 272-7

SUBJECT: Heat Transfer in a Composite Diffuser
WRITTEN BY: Kurt Muller
DATE: September 25, 1964
JOB NUMBER: 6002-21

INTRODUCTION

The requirements for the diffuser material are high melting temperature, excellent thermal conductivity, and low absorptivity in the spectral range in which the plasma radiates. Looking at the first two requirements, the tungsten-molybdenum-rhenium family appears most suitable to survive a high temperature environment; unfortunately, refractory metals are relatively poor thermal conductors. In view of these circumstances, a composite diffuser utilizing a high temperature material in the center portion and a high thermal conductive metal in the peripheral, low temperature range, looks promising on the basis of maximum radial heat transfer.

Some calculations have been performed to establish the quantity of heat transferred in the radial direction per unit diffuser width for various ring thicknesses of the composite metals.

CALCULATIONS

For a qualitative comparison, it was sufficient to substitute the trapezoidal cross section of the diffuser by a rectangular shape. The heat input to the diffuser is assumed to take place on the inside surface of the bore. The heat input to the lateral sides has been disregarded. Furthermore, the problem was simplified by using the heat transfer equations for an infinitely long cylinder.

The geometry of the composite diffuser is shown in Fig. 1

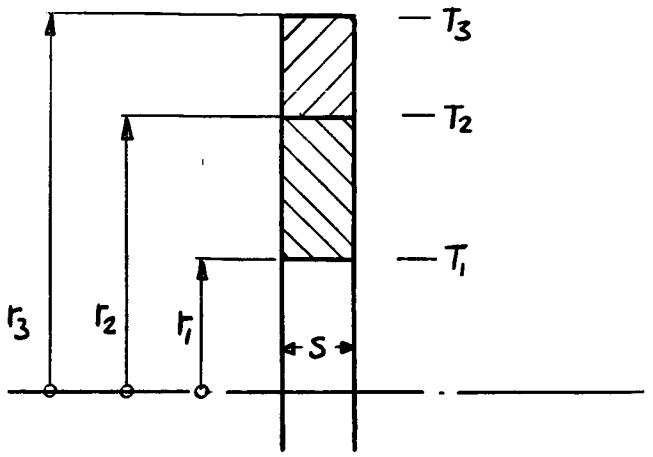

Fig. 1 Diffuser - Geometry

The radial heat flux in a cylinder is calculated by

$$q = 2\pi k_I S \frac{T_1 - T_2}{\ln \frac{r_2}{r_1}} \tag{1a}$$

and

$$q = 2\pi k_{II} S \frac{T_2 - T_3}{\ln \frac{r_3}{r_2}} \tag{1b}$$

for the inner and outer portion respectively. The combination of eqs. 1a and 1b then yields

$$\frac{q}{2\pi S} = \frac{k_I k_{II}}{k_{II} \ln \frac{r_2}{r_1} + k_I \ln \frac{r_3}{r_2}} (T_1 - T_2) \tag{2}$$

The equivalent expression for the inner part becomes

$$\frac{q}{2\pi S} = \frac{k_I}{\ln \frac{r_2}{r_1}} (T_1 - T_2) \tag{3}$$

The radius of the interface r_2 becomes

$$r_2 = r_1^{\beta} \tag{4}$$

where

$$\beta = \frac{\alpha \frac{\ln r_3}{\ln r_1} + 1}{1 + \alpha}$$

and

$$\alpha = \frac{k_I}{k_{II}} \times \frac{T_1 - T_2}{T_2 - T_3}$$

In order to find the best material or material combination, five cases have been analyzed; the maximum heat transferred through a Cu, W, Mo diffuser and the maximum heat transferred through a Mo-Cu and a W-Cu compound diffuser.

The boundary conditions for the temperatures are: the inside surface is at the melting point ($T_1 = T_{melt}$); the temperature on the periphery, T_3, is assumed to be 500°C, the temperature at the interface for the compound diffuser is the melting temperature of copper.

Since the thermal conductivity is temperature dependent (Fig. 2), average values have been chosen in the temperature range under consideration.

Evaluation of the eqs. 2, 3, 4 leads to the results listed in Table I

Parameter	Material				
	Cu	Mo	W	Mo-Cu	W-Cu
r_1 (cm)	0.76	0.76	0.76	0.76	0.76
r_2 (cm)	----	----	---	1.05	1.24
r_3 (cm)	1.85	1.85	1.85	1.85	1.85
T_1 (°C)	1080	2620	3400	2620	3400
T_2 (°C)	----	----	----	1080	1080
T_3 (°C)	500	500	500	500	500
k (w/cm°k)	3.70	0.80	1.10	0.80-3.70	1.10-3.70
$\frac{q}{2\pi s}$ (w/cm)	2410	1910	3580	3900	5250
Reflectance (at 0.5 microns)	0.43	0.46	0.49	----	----

Table I, Heat Transfer Data in Diffuser

CONCLUSION

For a single metal diffuser, tungsten is the best suitable material. For the compound diffuser, the tungsten-copper combination offers the best performance.

Copper and molybdenum are comparable in regard to the maximum heat transferred. However, a Cu-diffuser brazed to a Cu-housing may result in a more solid joint than brazing molybdenum to copper. Hence, the Cu-diffuser is expected to be superior over the Mo-diffuser.

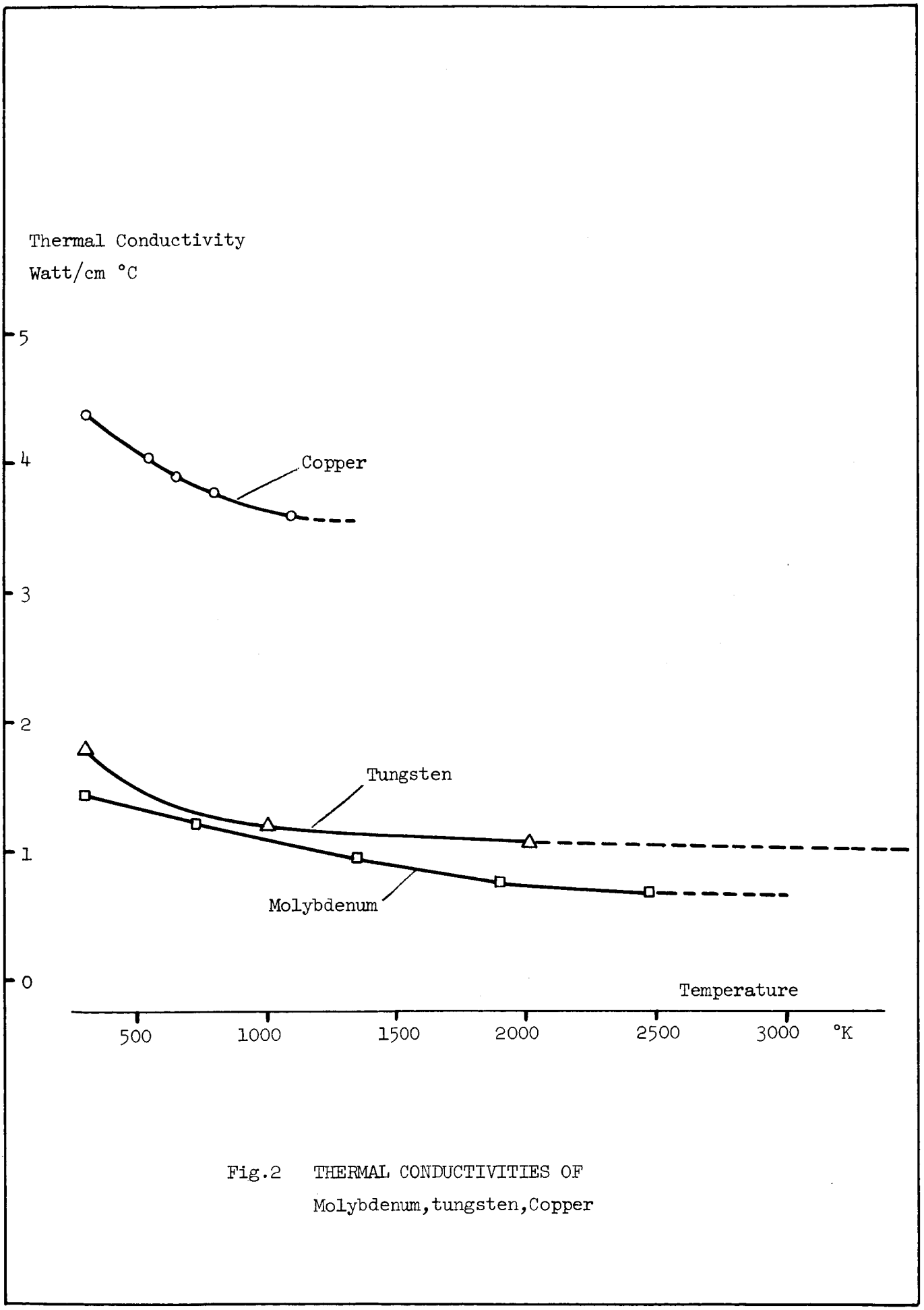

Fig.2 THERMAL CONDUCTIVITIES OF
Molybdenum, tungsten, Copper

SPECTROLAB

DEVELOPMENT MEMORANDUM NO. 272- 8

SUBJECT: Recirculator Testing

WRITTEN BY: W. Geideman
DATE: September 29, 1964
JOB NUMBER: 6002-56

INTRODUCTION

The recirculator pump which was purchased from Lapp Insulator Company by Giannini Scientific Corporation and delivered to Spectrolab was not operable because of a diaphragm failure. In addition, difficulties were encountered in operating the recirculator pump at Giannini before failure of the diaphragm occurred. These difficulties were manifested in an instability of the gas flow from the pump.

REPAIR OF DIAPHRAGM

The representatives of Lapp Insulator Company (G. D. Pribble Company) were contacted to obtain replacement diaphragms and to assist in repairing the damaged pump. The first set of diaphragms were damaged in transit. A second set of diaphragms was obtained and installed into the recirculator pump with the assistance of Mr. Pete Prentis of G. D. Pribble Company.

The damaged diaphragms were removed from the pump and inspected. Both diaphragms were observed to be "pock marked" and one diaphragm had a minute hole which allowed the oil to pass into the gas stream. All of the dents in the diaphragm were in the direction such that they appeared to have been caused by particles being present in the gas stream.

In addition to the diaphragms, two gaskets had to be replaced on each of the pump heads. It was necessary to hold these gaskets in place during assembly and a silastic compound was employed for this purpose. The diaphragms were replaced and the pump was operated with a dummy load.

INITIAL OPERATION AT SPECTROLAB

The initial operation of the pump at Spectrolab indicated that only one of the two heads was working. After approximately 30 minutes of operation, a small quantity of oil was observed in the rotometers. In addition, the head which was operating was observed to produce a very loud clacking noise at times associated with a large fluctuation in gas flow. Representatives of the pump manufacturer were again contacted to determine what was wrong with the pump and to place it in satisfactory operation. Because of the presence of oil in the gas stream, the two heads were removed to allow inspection of the diaphragms.

VISIT BY LAPP REPRESENTATIVE

Mr. Don Williams of Lapp Insulator Company visited Spectrolab to ascertain what was wrong with the pump and to put it into operation. The number 2 head was not operating at all and the cause of this was traced to the make-up oil pump. The planetary gear leading to head number 2 had become disengaged from the pump motor and, therefore, no oil was being supplied to head number 2 through the make-up system.

No indication of diaphragm failure was observed although there were about four dents in the diaphragm taken from head number 1. Mr. Williams also indicated that the heads had previously been assembled wrong since the gaskets were not properly seated. Mr. Williams advised that the silastic compound used to cement the gaskets to the heads during assembly was too thick and could possibly have produced leakage to the atmosphere. After some discussion, it was decided to use ordinary rubber cement to hold the gaskets in place during assembly. The two heads were reassembled with new diaphragms and new gaskets under Mr. Williams' direction.

The recirculator pump was then operated while Mr. Williams was present and intermittent clacking noise was observed in head number 1. Mr. Williams explained that this clacking noise was due to poor action of the oil relief valve on this head. He promised to send a replacement relief valve.

Several other things were learned during the visit of Mr. Williams. A check valve, pressure gauge and hand valve were incorporated into each of the oil lines just before the oil relief valve in order to determine the setting at which the relief valve opened and to provide a method of quickly priming the recirculator pump. Mr. Williams advised that the pump had to be reprimed every time it was turned on. In order to prime the pump, it is necessary to have a low (25 to 50 psi) pressure in the gas system. If a higher pressure is employed, the diaphragm will not move off the oil head since the oil pressure will not be sufficient to overcome the forces from the gas side. The loud clacking noise was attributed to cavitation in the oil lines behind the diaphragm. Mr. Williams also advised that it would be best to bleed the gas system to a low pressure each time the pump is shut off in order to allow easier priming of the pump on restart.

CHECKOUT OF PUMP OPERATION

Following the visit by Mr. Williams, the complete gas system being used with the final radiation source was assembled. The radiation source was not in the system. The pump was operated on September 12, 1964 with the following results. Cavitation occurred in head number 2 when the pump was operated at 300 psi gas pressure. The start up procedure for the pump was as directed by Mr. Williams. An intermittent cavitation in the number 1 head was also noticed. The total time of operation before final cavitation occurred in head number 2 was approximately fifteen minutes after full pressure had been obtained. This cavitation could only have been caused by a deficiency in the oil system. Another test run was made on September 12, using 200 psi gas pressure. The cavitation in head number 2 occurred after approximately the same operating time.

On September 14, the oil relief valves were reset to approximately 500 lbs. each and the pump was again operated. One hour operation was obtained at gas pressure of 200 psi without failure of the pump. On September 15, the recirculator pump was again operated without changing anything. This test was run with 300 psi gas pressure. After 30 minutes of operating, cavitation occurred in the number 2 head, necessitating shutdown of the pump.

After these tests, Mr. Williams was contacted to determine what was wrong with the recirculator pump. He could give no further explanation except something being wrong with the relief valves. Our analysis of the pump operation indicated that the make-up pump was not supplying sufficient oil to the heads to maintain the 300 psi gas pressure. Therefore, a new gear was purchased for the oil make-up pump. This was a 4 inch diameter gear replacing the 2-1/2 inch diameter gear supplied with the pump. After this gear was replaced, the pump was operated at 300 psi for two and one-half hours before head number 2 again cavitated. The cavitation in head number 2 was alleviated by reducing the gas pressure to 200 lbs.

The relief valve settings were again changed to provide the maximum oil pressure possible with the relief valves used. The pump was again operated and was found to work satisfactorily at 300 lbs. for approximately one hour before the number 2 head again cavitated.

It was determined during a later test that the pump would operate for a very long period of time at 200 psi gas pressure. Therefore, it was decided to employ the recirculator pump during initial tests of the high power radiation source. The pump performed satisfactorily during all radiation source tests.

CONCLUSIONS

1. It appears that the piston in the number 2 head leaks more oil than the make-up pump provides when the gas pressure is at 300 psi. However, with the new gear on the make-up oil pump, satisfactory operation can be obtained for a long enough period of time to allow the use of the recirculator pump with the radiation source.

2. Satisfactory operation of the recirculator pump was obtained for an indefinite period at a gas pressure of 200 psi.

DEVELOPMENT MEMORANDUM NO. 272-10

SUBJECT: DC Electrical System Calibration

WRITTEN BY: W. A. Geideman
DATE: October 19, 1964
JOB NUMBER: 6002-56

INTRODUCTION

The setup presently being used for both source evaluation tests and optical system prototype tests allows the DC voltage to be measured only at the console. Since previous experience has shown that there is a considerable voltage drop in the water cooled cables and in the coil of the starter, it is not possible to directly measure the voltage drop across the radiation source and thus the true input power to the radiation source cannot be measured directly. For this reason, a test was planned to measure the voltage drop in the water cooled cables and starter coil at various current levels in order to arrive at a calibration factor to transform the voltage measured at the console to the actual voltage drop across the radiation source.

TEST SETUP

A connector was employed to join the positive and negative water cooled cables where they normally enter the radiation source. This effectively shunted the radiation source and produced an electric circuit consisting only of the water cooled cables and the starter coil. The cooling water was entered through the cathode water cooled cable and exhausted through the anode water cooled cable to the drain. A water flow rate of 4.5 gpm was set in the entire system. The gas and water interlocks in the console were jumpered so that the power supplies could be operated. The power supplies were left in the same connection as was used during the source testing. The digital voltmeter employed to measure the total system voltage drop during source operation was used to measure the voltage drop in the cables and starter coil during these tests. This voltmeter is connected to the termination panels in the console. A Simpson volt-ohmeter was made available to measure the voltage drop across the starter coil during operation.

TEST RESULTS

The voltage drop across both the cables and the starter coil as measured by the digital voltmeter is plotted versus the current in Figure 1. The voltage drop in the starter coil as measured by the Simpson meter is also plotted in Figure 1 versus the total current. The minimum current which could be obtained from the five power supplies was 1165 amps with the connections employed and the load used. The actual data points formed a straight line curve of voltage versus current indicating that the system resistance is constant and is not dependent on the arc current. Therefore, the curves were extrapolated to the 900 amp level in order that they might be useful in calibrating actual source runs to show the voltage drop across the source. The data obtained in this test will be employed in reducing the data obtained from the source tests in order to allow a more representative presentation of the data.

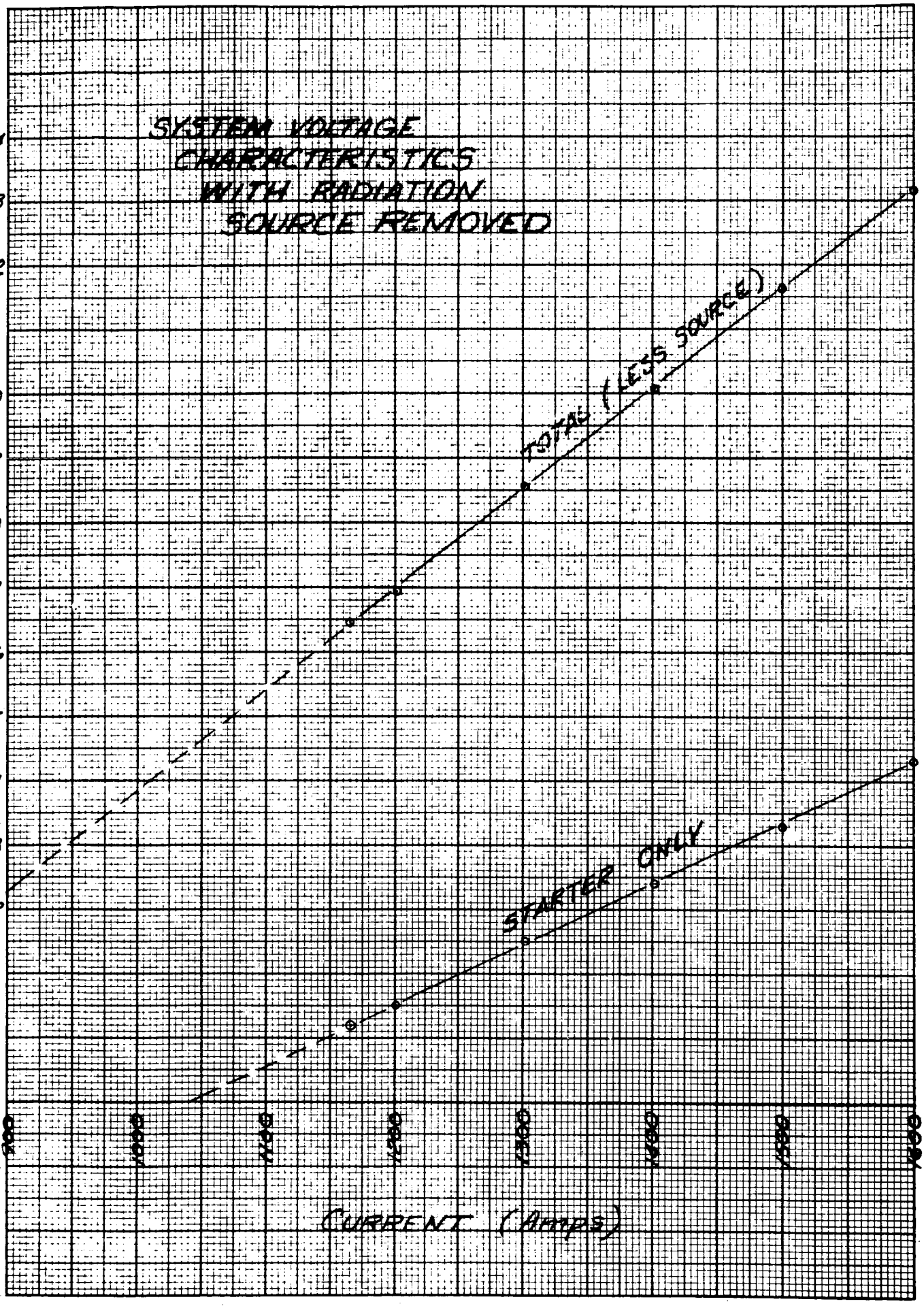
SYSTEM VOLTAGE
CHARACTERISTICS
WITH RADIATION
SOURCE REMOVED
TOTAL (LESS SOURCE)
STARTER ONLY
VOLTAGE (VOLTS)
CURRENT (AMPS)
24
23
22
21
20
19
18
17
16
15
14
13
12
11
10
9
800
1000
1200
1400
1600
1800
2000

DEVELOPMENT MEMORANDUM NO. 272-11

SUBJECT: Recirculator Testing

WRITTEN BY: W. A. Geideman
DATE: October 19, 1964
JOB NUMBER: 6002-56

INTRODUCTION

This Development Memorandum is an addendum to Development Memorandum 272-8, dated 29 September 1964. This memorandum is intended to update the record of our experiences with the Lapp pump.

RESULTS

The recirculator pump operated successfully during all source evaluation tests and no difficulty was encountered. During test run number 5 which was the initial test of the prototype optical system, the test had to be terminated because of a failure of the recirculator pump. This failure was manifested in the addition of oil to the gas lines causing oil to collect in the flow meters and necessitating source shutdown. The filter incorporated into the gas line after the flow meters to remove any oil which might be in the gas line operated satisfactorily in that the source was operated for about six minutes after oil was first observed without any serious ill effects to the source.

After the completion of this test run, the recirculator pump was disassembled to inspect the diaphragms. The diaphragms had several pock marks which started on the oil side and extended into the gas side of the diaphragm. The tops of these dents on the product side were worn off due to the action of the diaphragm hitting against the head on the product side. Although no aperture could be seen during observation of the diaphragm, it is believed that the oil leak occurred through one or more of these dents. All observed damage to the diaphragms occurred on the oil side. This fact was relayed to Don Harmon of G. D. Pribble Company on October 12, 1964.

An oil filter was placed into the line which leads from the reservoir to the make-up oil pump. The purpose of this filter is to remove any particles from the oil before it enters the make-up pump. It is hoped that this will significantly reduce the number of solid particles in the oil behind the diaphragm and, therefore, extend diaphragm life. The recirculator pump was then reassembled using new diaphragms and new diaphragm gaskets.

The presence of oil in the gas system required a complete cleaning of all gas lines and of all parts of the radiation source which are in contact with the argon.

After this repair was completed, the source was operated for a total of approximately two hours without any malfunction of the recirculator pump. However, at an operating pressure of 250 psig, a decrease in the oil pressure on head number 2 was noticed during operation. This decrease was not sufficient to cause a cavitation and, therefore, did not cause any test to be aborted.

The recirculator pump will be used for all future tests of the radiation source. New diaphragms and diaphragm gaskets have been ordered in case the diaphragm fails in any future tests.

SPECTROLAB

DEVELOPMENT MEMORANDUM NO. 272- 14

SUBJECT: Radiation Source Evaluation Testing (Runs 1 - 4)

WRITTEN BY: W. A. Geideman
DATE: October 28, 1964
JOB NUMBER: 6002-56

INTRODUCTION

The final radiation source was assembled according to Drawing 013889. The test program for evaluation of the final radiation source was outlined in an Interoffice Memorandum from Jack Castle to Fritz Benning, dated August 31, 1964. This memorandum defined the preliminary source evaluation tests which were necessary before integration of the final radiation source with the prototype optical system. The purposes of these tests were to evaluate the final radiation source as a whole, to check out the radiation source system, to obtain a polar plot of the final radiation source, and to obtain performance data at various current and pressure levels.

INSTALLATION

The final radiation source was installed in the facility using a special mounting structure. In order to reduce the stresses on the outer quartz envelope, a fixture was designed and manufactured to support the cathode end of the source to remove the gravitational forces due to the weight of the cathode structure. This fixture consisted of a spring loaded mount which was attached to the source mounting structure and which was calibrated to apply a force equal and opposite to that produced by the weight of the cathode. In addition, the water hoses to the cathode were supported by a clamp to remove the weight of the hoses from the quartz envelope.

The source was installed in a position where the existing tube into the test area was located in line with the arc and at 90° to the axis of the radiation source. The source was arranged in this manner in order that the quartz lens in the tube could be used to project an image of the arc

onto a screen for monitoring of arc operation and to enable measurement of the projected arc dimensions. An optical system was installed in the test facility to enable viewing of the anode of the radiation source during source operation. The viewing angle of this anode viewer was such as to allow monitoring of the inside diameter of the diffuser, as well as the arcing surface of the anode. A telescope was incorporated in this system to provide approximately real size of the anode to the viewer.

A view port into the testing area was provided with a mirror so as to allow the entire radiation source and the surroundings to be observed during operation. The Eppley thermopile with the quartz window was mounted on the polar scanning mechanism previously employed for the 60 KW prototype radiation source. This polar scan arm was rearranged in the test area so as not to conflict with the other apparatus. A "flapper" was designed and installed on the polar scanner to provide a mask for the sensor between readings. This "flapper" was operated by means of a flexible cable into the control room. It was spring loaded so as to cover the sensor except when readings were desired. The polar scanner was operated from the control room by means of a second flexible cable. After installation of the polar scanner, the scan arm was calibrated with the flexible cable and with the X-Y recorder to enable accuracy in measuring the location of the sensor relative to the axis of the radiation source.

The control console previously employed with the 60 KW prototype radiation source was modified for use with the final radiation source by installing new water flow interlocks, a new variac, and a new shunt. The console is shown in Figure 1. In addition, the gas lines inside the console were replumbed to put the two flow meters in parallel in order to handle the flow required for the final radiation source. The five power supplies were installed with their DC output in parallel and each supply set to give 160 volts open circuit. The recirculator system was assembled using the designed secondary heat exchanger for the source. The recirculator pump and system were checked out as described in Development Memorandum 272-8. The recirculator pump is shown in Figure 2. A small vacuum pump was provided to purge the gas system of air prior to the operation of the radiation

source. A manifold and pressure regulator for filling the closed gas loop system were installed. A filter was installed in the console between the flow meters and the radiation source to act as a protective device against oil inclusion in the gas system. The power supplies were checked for proper fan rotation and the controls of the power supplies were placed in series so that a malfunction of any one power supply would produce a shutdown of the complete system. A digital voltmeter was installed to measure the total voltage drop across the radiation source, the starter coil and the water cooled cables. A high accuracy ammeter was purchased to measure the current in the radiation source. These meters are shown in Figure 1. The voltmeter is on top of the console and the ammeter is in the rack on the right side of the console.

STATIC TEST

After the radiation source was assembled and mounted, a water flow check at full water pressure was made to check for leaks in source and system. No leaks were found. The interlocks, both gas and water, were checked for proper operation and were found to operate correctly. The arc starter was fired without the power supplies being on to check starter operation. The cable leading from the starter to the cathode of the radiation source had to be relocated due to a leak of the high frequency from this cable to the mounting structure. In addition, the operation of the starter was found to depend on the location of the starter and its position.

The radiation source was gas pressure checked to ascertain that the pressure loading was evenly distributed around the circumference of the envelope and to check the design of the envelope to find what pressure could be obtained before failure of the outer envelope under cold conditions. The gas pressure was increased to approximately 50 lbs. and the envelope was checked with polaroid film to observe the stress patterns in the quartz. No uneven distribution of stresses was discernable in this check. The source was then pressurized to a level of 200 psig and nothing happened. At the completion of this test, the source was declared ready for operation.

TEST OPERATION

The radiation source was assembled using a copper diffuser with a .650" ID and the electrode spacing was set at 15 mm. The assembled radiation source is shown in Figure 3 and a closeup of the arc area is shown in Figure 4.

The procedure for operating the radiation source was as follows:

1. Open argon cylinders in storage area. Check pressure of argon to assure adequate supply.

2. Turn on water flow to both the source and the heat exchangers. Turn on water pump.

3. Check water flow rates at the rotometers installed on the wall. The flow rate into the anode of the source should be approximately 10 gallons per minute, the flow to the cathode should be four gallons per minute, and the flow rate into the heat exchanger should be three gallons per minute. These flow rates are nominal values, and the maximum flow possible with the water system should be used in all cases.

4. Turn on master control switch in control console.

5. Purge the closed gas loop using the following procedure:
   a. Turn on vacuum pump, to a pressure of one or two inches of mercury (29 or 30 on compound gage).

   b. Fill system with argon to a pressure of 10 psig.

   c. Repeat step a.

   d. Repeat step b.

   e. Repeat step a. again.

   f. Fill system with argon to a pressure of 20 psig.

6. Check all water and gas connections for leaks. Check gas pressure for any drop caused by leakage. If there are no leaks, clear the test area

until after completion of the test. Note: No one should enter the test room while the source is under pressure.

7. Turn on recirculator pump. Check oil pressure gages until the pointer moves off the peg of the meter, bleed oil line of air. Repeat this for both pump heads until oil pressure goes above 300 psig. Pump is now primed and should be operating properly.

8. Raise gas pressure to 50 psig at entry to radiation source.

9. Turn on power supplies. Check open circuit voltage on voltmeter.

10. Ignite radiation source by pressing starter button. If source does not start, reduce gas pressure until starting is achieved. In no case should the gas pressure be below 25 psig.

11. Increase pressure and current to the operating values desired for the particular test being run. Current should not be allowed to go below 600 amps as the pressure is increased.

The first test run on the final radiation source was made on 18 September 1964. The source was ignited according to the test procedure and the gas pressure was increased to 200 psi. The current was set initially at 685 amps and data were taken at this setting. The raw data from all the source evaluation tests are presented in Table 1. After this initial test point, the current was increased in steps to 1,000 amps. At this point, a polar intensity plot was obtained using the Eppley thermopile and the polar scanner. After completion of the polar scan, the current in the arc was increased in steps of approximately 100 amps to a maximum of 1300 amps. This provided performance data from the source at a constant pressure level of 200 psig for various current settings.

Photographs were taken of the arc image as projected by the lens described previously. A grid was placed on the projection screen to provide a reference to indicate the size of the arc. Photographs were taken at each

arc setting to correlate with the raw data. The radiation source was extinguished after the 1300 amp data point to enable observation of the condition of the components of the source. The total duration of this test was 32 minutes. The arc was extinguished by reducing the current from the 1300 amp level to 600 amps while maintaining a constant gas pressure. The power supplies were then turned off to extinguish the arc.

The radiation source was ignited at a gas pressure of approximately 40 psig. The pressure was increased rapidly to the 200 psig level and no problems of any kind were encountered. The current was maintained at a minimum of 600 amps during this startup procedure. The anode was continuously viewed during this test to monitor its operation. No problems other than a slight melting of the arcing surface were encountered with the anode. After completion of this first test run, the radiation source was examined and the only degradation noted was the melting of the anode arcing surface previously observed. The intensity at 90° to the arc axis was measured for each data point using the Eppley thermopile mounted on the polar scan arm. The intensity was measured by monitoring the millivolt output of the thermopile on the X-Y recorder. At the completion of the test, it was discovered that the scan arm was not at exactly 90° for all data points after the polar plot but was displaced by about 2°. No correction was applied to the data for this slight misalignment.

A second test run was started immediately after the completion of this first test run. Test number 2 was a performance test of the radiation source at a constant gas pressure level of approximately 225 psig. Data were obtained at intervals of approximately 100 amps from 900 amps to a maximum of 1385 amps. The total duration of this test was approximately 15 minutes and the radiation source was extinguished in the same manner as on the previous test run. A slight wetting of the copper diffuser was noted at approximately 1400 amps in this test and, therefore, the maximum current was reduced to 1385 amps for the recording of data. The anode was again monitored continuously during this test and no problems were experienced in starting or operating the radiation source.

In addition to the raw data attained from the instruments in the radiation source system, intensity measurements were obtained with the Eppley thermopile and the projected arc image was recorded in two ways. The polar scan arm was readjusted prior to this test to a true 90° angle with the axis of the radiation source. The polar scan arm was not moved during this test and intensity data were obtained on the X-Y recorder at each current setting. Photographs of the projected arc image were taken in the same manner employed in test number 1. In addition, blueprint paper was positioned over the screen onto which the arc image was projected. The purpose of this was to expose the blueprint paper to the arc radiation and thus produce an arc image onto the blueprint paper. This paper was then processed through the ammonia developing solution and an image of the arc was obtained very shortly after completion of the test. The relative merits of measuring the arc dimensions by the photographic technique and the blueprint technique are discussed in detail under the heading "Data Reduction".

At the conclusion of this second test run, the parts of the radiation source were examined and no additional degradation of the electrodes or the quartz envelopes was noted. The radiation source was not disassembled but the system was completely shut down.

Test run number 3 was made on 21 September 1964. This run was a performance check at a constant gas pressure level of approximately 250 psig. The current was varied in steps of 100 amps from approximately 900 amps to a maximum of 1415 amps. At the maximum current level, a slight wetting of the inside surface of the copper diffuser was again noted. In addition, some degradation of the cathode tip occurred during this test with a consequent deposit of small particles of tungsten onto the inner envelope. The total duration of this test was 15 minutes and the source was extinguished in the same manner as described for test number 1. Again, the anode was continuously monitored during this test run and the same data taken in test run number 2 were obtained. The arc image was not photographed during this test run because the camera had been dismounted over the weekend and was not in place at the start of the test. The blueprint images of the arc were obtained. The radiant intensity was again measured by the Eppley thermopile in the same manner as employed previously.

At the conclusion of this test run, the source was examined and the degradation experienced by the electrodes was not considered sufficient to postpone further testing.

Test run number 4 was begun immediately after the examination of the source. This test was a performance check at a constant pressure level of approximately 275 psig. The current was again varied in approximately 100 amp steps from 900 amps to a maximum of 1460 amps. At this maximum current level, some melting of the copper diffuser occurred. In addition, the degradation of the cathode tip continued during the entirety of this test with consequent deposition of tungsten particles on the inner quartz envelope. The duration of this test was approximately 20 minutes. By accident, the pressure in the radiation source was increased to a maximum of slightly over 290 psig during this test.

The anode was again continuously monitored and intensity data were obtained from the Eppley thermopile. The "flapper" in front of the Eppley sensor did not operate on test points 4.5, 4.6 and 4.7. This operational failure was due to a fracture in the **flexi**ble cable connecting the "flapper" with the control room. Both photographic and blueprint methods were employed to record the image of the arc.

At the completion of this test, it was decided that no further performance data should be obtained at the present time, therefore, the source was disassembled for inspection. The arc gap had lengthened from approximately 15 mm to approximately 15.5 mm due to the erosion of the cathode tip. The condition of the cathode after removal is shown in Figure 5. The diffuser had enlarged from an original ID of .650" to a final diameter of .670". This erosion was symmetrical and the melted material froze and adhered to the inside surface of the diffuser as shown in the bottom photograph in Figure 6. The anode arcing surface showed evidence of melting but the amount of degradation was not sufficient to require replacement of the anode if this had been an operational radiation source test. The arcing surface of the anode is shown in the top photograph in Figure 6. The inner quartz envelope had a quantity of tungsten particles adhering to the inside

surface in a ring at the approximate location of the arc gap. The outer tube suffered no deterioration during these tests and no other part of the radiation source was damaged in any manner.

The total operating time on the single set of electrodes used for these tests was approximately 80 minutes. Source operation was very smooth including starting and variation in the operating parameters. The complete radiation source system was employed in these tests and no problems were encountered with any portion of the system other than a slight leakage in the closed loop gas system which was known previously. This leak occurred at some of the pipe couplings in the plumbing and was not associated with the radiation source. This preliminary operation indicated that the final radiation source is, indeed, an operational unit. The envelope, as designed, will withstand an operational pressure of at least 290 psig. No difficulty or problem area was encountered in assembling and disassembling the radiation source. The melting of the diffuser surface which was encountered can be directly attributed to running the copper diffuser at a current level in excess of the maximum for the .650" ID. The reason for the erosion of the cathode is not known at the present time. All raw data obtained in test runs 1 through 4 are presented in Table 1.

DATA REDUCTION

In order to determine the power input to the radiation source, it was necessary to measure the voltage drop in the system components at the various current levels. This test was performed and is reported in Development Memorandum No. 272-10. This voltage was subtracted from the total voltage measured at the console to provide the source input voltage which, when multiplied by the current, gives the source input power.

In order to measure the radiance of the radiation source, it is necessary to know the projected area of the arc. The projected area was to be measured by examining the photographs and blueprints taken during the test run. Assuming the electrode spacing was 15 mm, the diameter of the arc could be obtained from the reproductions of the projected arc image. A detailed and lengthy examination of both the blueprints and the

photographs was undertaken. A great deal of difficulty was encountered in defining the edge of the arc since several different people interpreted the edge in different places. In addition, the different exposure times on both the blueprint paper and the photographs resulted in the arc diameter being interpreted in such a manner that it was inconsistent with either an increase in current or an increase in pressure. Therefore, it was decided to employ a constant arc dimension of 9 mm diameter x 15 mm long in order to obtain the radiance of the arc at the various conditions.

Arc radiance values could only be determined for a view angle of 90°, i.e., normal to the arc axis, since this is the only view angle where the projected arc was displayed allowing determination of approximate arc dimensions. The sensor was located at a distance of 30.08" from the arc. This distance is sufficiently large relative to the arc size to allow utilization of the approximate intensity equation

$$E = R\omega$$

where E = radiation intensity at sensor, R the radiance of the arc, and ω is the solid angle subtended by the arc surface area A to a point on the sensor. The solid angle can be closely approximated by assuming that this observed arc area lies on the surface of a sphere of radius r where the sensor lies at the center of the sphere, therefore

$$\omega = A/r^2$$

Utilizing the above two equations, the radiance R can be expressed as

$$R = Er^2/A$$

The calibration factor utilized at Spectrolab for the Eppley thermopile #5013 is 4.80 mv/watt-cm^{-2}. Substituting the value of 30.08" for r and 9 x 15 sq mm for A and adjusting for consistent units, this equation reduces to R = 900.27E.

The output power of the radiation source was calculated using the data obtained in the polar intensity scan assuming a constant polar distribution. The method of calculating the output power in this polar scan will be described later. It was assumed that the output power was equal to 10.11 times the intensity at 90°. The source efficiency was obtained by dividing the calculated power by the source input power. The reduced data is presented in Table 2 for all four test runs.

The intensity in millivolts and the calculated radiance are plotted against arc current in Figure 7. The gas pressure is a parameter on this graph. The data for points 4.5, 4.6 and 4.7 were obtained by extrapolating the data obtained during the earlier test points in run 4. The criterion for extrapolation was that the straight line follow those of runs 1, 2 and 3.

Figure 8 is a cross plot of the data presented in Figure 7. The intensity in watt/cm^2 is plotted against pressure for constant current values. Figure 9 is a plot of the intensity in millivolts versus the source input power in KW. The different pressure levels are indicated by the different symbols on the graph.

The voltage characteristics of the radiation source are presented in Figures 10, 11 and 12. Figure 10 is a plot of the total voltage against the current for the different pressure levels. Figure 11 is a cross plot of the data presented in Figure 10 showing the total system voltage versus pressure for different current levels. Figure 12 is a plot of the source voltage versus current for the different pressure levels. This latter curve indicates the voltage characteristics of the radiation source alone.

Figure 13 relates the output power of the radiation source to the current. The pressure is used as a parameter and to clarify the graph only runs 1 and 4 are plotted. The data from runs 2 and 3 would fall between these two lines. Figure 14 is a plot of the power conversion efficiency versus current for runs 1 and 4.

The data presented in Figures 7 through 14 show some surprising results. The intensity, radiance and output power are strongly dependent on the current level but only a very small variation in these parameters with pressure was experienced. The arc diameter did not change drastically with either an increase in current or an increase in pressure indicating that the major item controlling the arc diameter is probably the inside diameter of the diffuser. These results demonstrate that the mechanical problems with the outer quartz envelope which are encountered at higher operating pressures are not justified by an increase in source output. The voltage increase associated with higher pressure accounts for the increased intensity and power output as demonstrated by Figure 9 where only a single straight line could be drawn to show the variation of intensity with source input power. The efficiency of the radiation source decreases with increasing pressure as demonstrated in Figure 14. However, the higher pressures allowed an increase in the operating current before damage to the diffuser occurred. The reason for the lack of increase in radiance and output power with increased current can only be explained by the absence of any influences of gas pressure on the arc column in this particular radiation source design. This means that the arc column can be treated as a solid body of a given diameter, which diameter is controlled only by the geometry of the radiation source. Therefore, in order to increase the radiance and the output power, it is necessary to increase the current or to change the geometry. The most influential geometrical change on the arc size is the diameter of the diffuser as this controls the gas flow in the arc region and, thus controls the diameter of the projected solid core.

The data obtained in the polar intensity scan of the radiation source at approximately 1,000 amps and 200 psig gas pressure are presented in Figure 15. The solid curve is a plot of the intensity as measured by the Eppley thermopile and the scale given for the radius lines is mv output of the thermopile. The polar power distribution was calculated from this intensity plot and normalized at 90° to enable presentation on the same graph. The calculations employed to obtain the power distribution are shown in Table 3. The zonal constant listed in Table 3 is the solid angle subtended by that particular zone of the polar distribution. The

zone area is that area of a sphere of radius 30.08" which is covered by the particular zone of radiation. This is an integration factor to enable the total power output to be calculated. The total output power is obtained by adding all figures in column 5 which represents the power incident upon each zone of the assumed sphere. For this particular setting, the total output power is 18,900 watts. The flux collection efficiency of the collector can be determined by adding those zones where the radiation produced is incident on the collector surface and dividing by the total power output of the radiation source. Assuming that the polar intensity distribution is not a function of either the current or the pressure, the total output power will be proportional to the difference in intensity at any one point on the polar intensity. Thus, the output power for each data point was calculated by using a calibration factor which was determined by dividing the 18.900 KW by the intensity recorded at 90° to the axis of the arc (1.87 mv). This produces the calibration factor of 10.11 used in Table 2.

Point No.	Current Amp	Voltage Volts	Gas Flow Meter Reading	Gas Pressure psig	Running Time min.	Intensity mv.
1.1	685	67.7	47.5	202	33.5	.96
1.2	805	69.3	46.2	193	40.7	1.40
1.3	905	73.3	46.9	204	44.4	1.63
1.4	1005	76.3	46.8	203	47.1	1.88
1.5	985	76.0	46.6	203	52.5	1.88
1.6	1105	80.2	46.6	205	56.7	2.17
1.7	1202	83.3	46.2	203	58.3	2.43
1.8	1300	87.2	45.8	205	61.7	2.78
2.1	920	75.3	47.3	224	68.8	1.66
2.2	1010	78.5	47.3	228	72.3	1.95
2.3	1105	81.5	46.7	225	74.7	2.17
2.4	1210	85.0	46.3	224	76.9	2.47
2.5	1310	88.6	46.3	225	79.4	2.78
2.6	1385	91.2	46.5	225	81.2	3.02
3.1	925	78.6	47.3	252	86.0	1.72
3.2	1005	80.2	46.2	252	89.9	1.90
3.3	1110	83.5	45.5	250	91.5	2.22
3.3a	1135	84.6	45.5	252	92.5	2.32
3.4	1205	87.1	46.5	252	93.9	2.54
3.5	1310	90.9	46.0	250	95.3	2.87
3.6	1415	94.5	45.9	250	98.2	3.22
4.1	890	78.1	46.5	278	105.3	1.67
4.2	1012	81.5	46.0	275	106.7	1.98
4.3	1100	84.6	45.5	278	109.6	2.25
4.4	1200	88.2	45.7	275	113.0	2.57
4.5	1300	92.3	45.4	278	114.3	2.90*
4.6	1410	96.2	45.5	277	116.1	3.24*
4.7	1460	97.0	45.5	277	118.2	3.40*

* Calculated from solar cell data, Eppley not working on these points due to mask remaining over sensor.

Table 1 - Raw Data from Source Evaluation Tests

		(1)	(2)	(3)	(4)	(5)	(6)	(7)	(8)	(9)
Point No.	Gas Pressure	Current	Total Voltage	Source Voltage	Total Input Power (KW)	Source Input Power (KW)	Intensity mv	(6) x 900.27 Radiance w/cm²-str	(6) x 10.11 Output Power (calculated) (KW)	Source Efficiency (%)
1.1	202	685	67.7				.96			
1.2	193	805	69.3				1.40			
1.3	204	905	73.3	60.9	66.3	55.1	1.63	1468	16.48	29.91
1.4	203	1005	76.3	62.4	76.7	62.7	1.88	1693	19.01	30.32
1.5	203	985	76.0	63.0	74.9	62.1	1.87	1684	18.91	30.45
1.6	205	1105	80.2	64.7	88.6	71.5	2.17	1955	21.94	30.69
1.7	203	1202	83.3	66.3	100.1	79.7	2.43	2189	24.57	30.83
1.8	205	1300	87.2	68.6	113.4	89.2	2.78	2504	28.11	31.51
2.1	224	920	75.3	62.7	69.3	57.7	1.66	1495	16.78	29.08
2.2	228	1010	78.5	64.5	79.3	65.1	1.95	1757	19.71	30.28
2.3	225	1105	81.5	66.0	90.1	72.9	2.17	1955	21.94	30.10
2.4	224	1210	85.0	67.8	102.9	82.0	2.47	2225	24.97	30.45
2.5	225	1310	88.6	69.9	116.1	91.6	2.78	2504	28.11	30.69
2.6	225	1385	91.2	71.3	126.3	98.8	3.02	2720	30.53	30.90
3.1	252	925	78.6	65.9	72.7	61.0	1.72	1549	17.39	28.51
3.2	252	1005	80.2	66.3	80.6	66.6	1.90	1711	19.21	28.84
3.3	250	1110	83.5	67.9	92.7	75.4	2.22	2000	22.44	29.76
3.3a	252	1135	84.6	68.6	96.0	77.9	2.32	2090	23.46	30.12
3.4	252	1205	87.1	70.0	105.0	84.4	2.54	2288	25.68	30.43
3.5	250	1310	90.9	72.2	119.1	94.6	2.87	2585	29.02	30.68
3.6	250	1415	94.5	74.2	133.7	105.0	3.22	2900	32.55	31.00
4.1	278	890	78.1	65.9	69.5	58.7	1.67	1504	16.88	28.76
4.2	275	1012	81.5	67.5	82.5	68.3	1.98	1784	20.02	29.31
4.3	278	1100	84.6	69.2	93.1	76.1	2.25	2027	22.75	29.89
4.4	275	1200	88.2	71.2	105.8	85.4	2.57	2315	25.98	30.42
4.5	278	1300	92.3	73.7	120.0	95.8	2.90	2612	29.32	30.61
4.6	277	1410	96.2	75.9	135.6	107.0	3.24	2918	32.76	30.62
4.7	277	1460	97.0	76.0	141.6	111.0	3.40	3063	34.37	30.96

Assumptions

(7) Nominal Arc Dimensions of 9 x 15 mm at 90° utilized

(7)(8)(9) Eppley Calibration Factor of 4.8 mv/w-cm^{-2} used

(8)(9) Polar Intensity Distribution Remains Constant

Table 2 - Reduced Data from Test Runs 1 - 4

(1) Angular Zone	(2) Eppley Reading mv	(3) Zonal Constant	(4) Zone Area cm^2	(5) Power in Zone Watts
45-50	0	.4041	2359	0
50-55	0.21	.4349	2539	111.1
55-60	0.51	.4623	2698	286.7
60-65	0.72	.4862	2838	425.7
65-70	0.95	.5064	2956	585.1
70-75	1.23	.5228	3052	782.1
75-80	1.45	.5352	3124	943.7
80-85	1.64	.5435	3172	1108.4
85-90	1.82	.5476	3196	1121.2
90-95	1.91	.5476	3196	1271.8
95-100	1.94	.5435	3172	1282.0
100-105	1.98	.5352	3124	1288.7
105-110	2.03	.5228	3052	1290.7
110-115	2.08	.5064	2956	1280.9
115-120	2.14	.4862	2838	1265.3
120-125	2.20	.4623	2698	1236.6
125-130	2.28	.4349	2539	1206.0
130-135	2.35	.4041	2359	1154.9
135-140	2.28	.3703	2161	1026.5
140-145	1.78	.3337	1948	722.4
145-150	1.10	.2945	1719	393.9
150-155	0.38	.2531	1477	116.9
155-160	0	.2098	1225	0
			Total	18901

(1) = Zone of Polar Plot
(2) = Actual Average Eppley Reading Over Zone
(3) = Solid Angle Subtended by Zone
(4) = $(30.08 \times 2.54)^2$ times Zonal Constant
(5) = Zone Area Times Average Reading Divided by Eppley Constant

Total Power Output = Sum of Column (5) = 18,901 watts
Total Power Collected = Sum of Column (5) up to 125° = 14,280 watts
Collection Efficiency = 75.6%

Table 3 - Raw and Reduced Data From Polar Scan (Run 1.5)

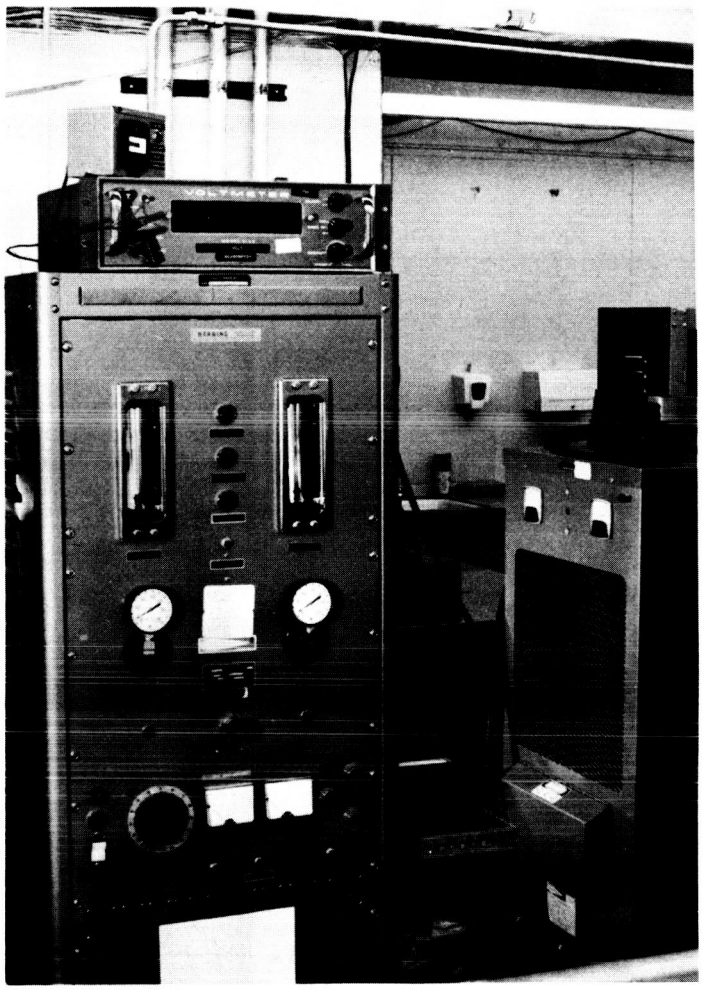

Figure 1 - Control Console and Instruments Used with Final Radiation Source

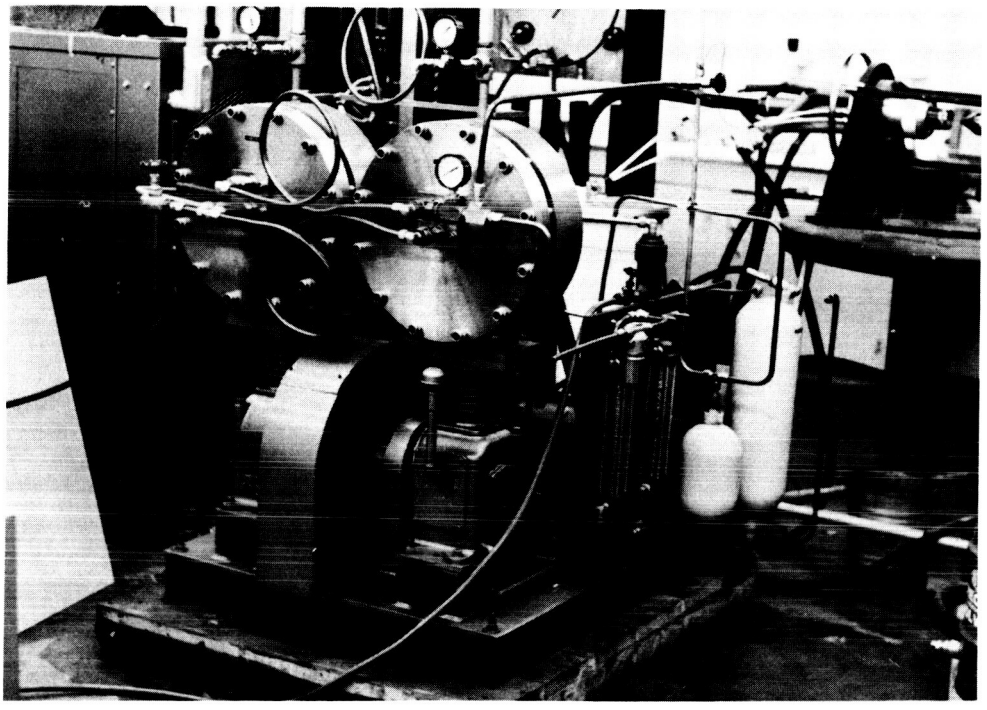

Figure 2 - Recirculator Pump as Installed in Laboratory

Figure 3 - Assembled Final Radiation Source

Figure 4 – Closeup of Arc Area in Final Radiation Source

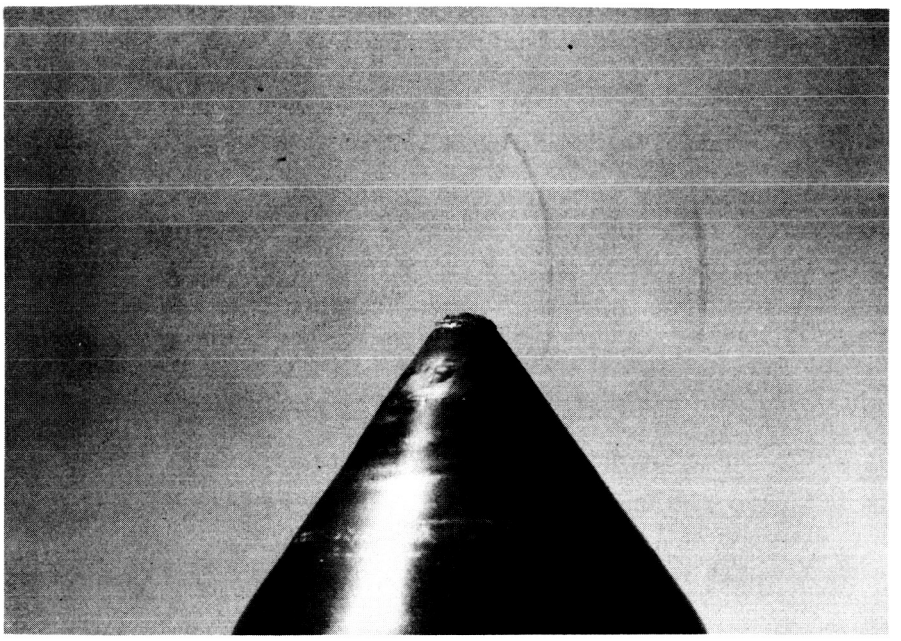

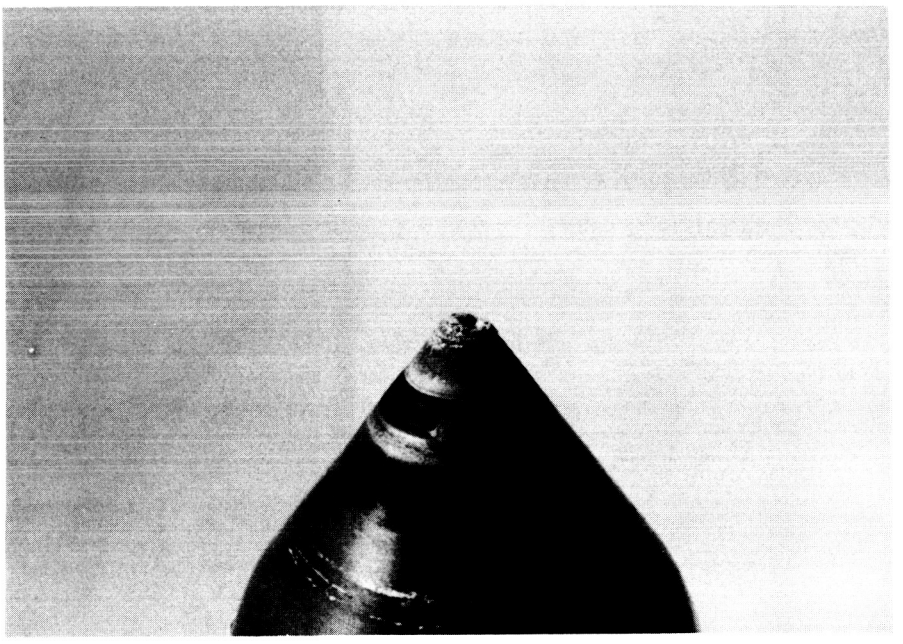

Figure 5 - Cathode After Test Run 4

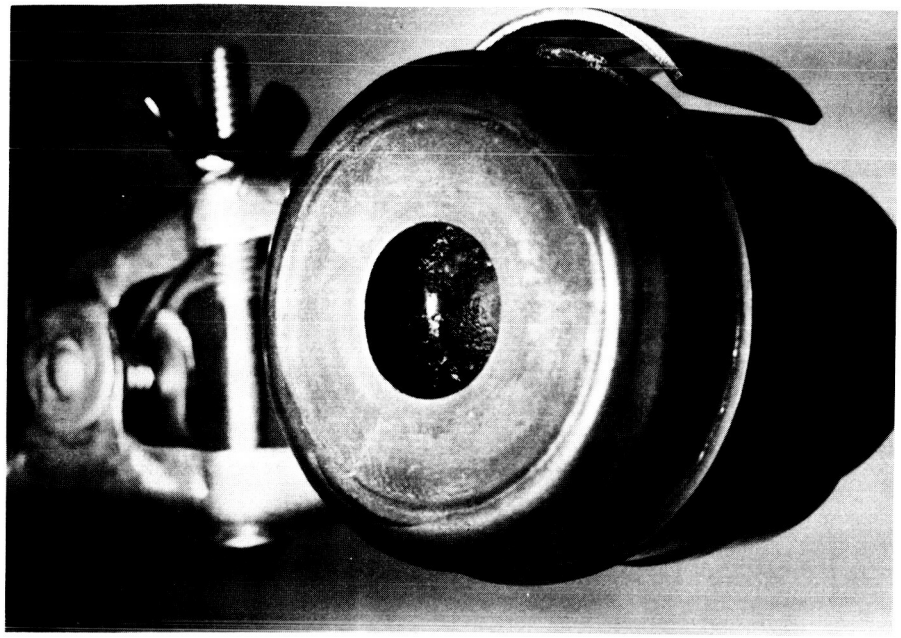

View Showing Melting of Arcing Surface

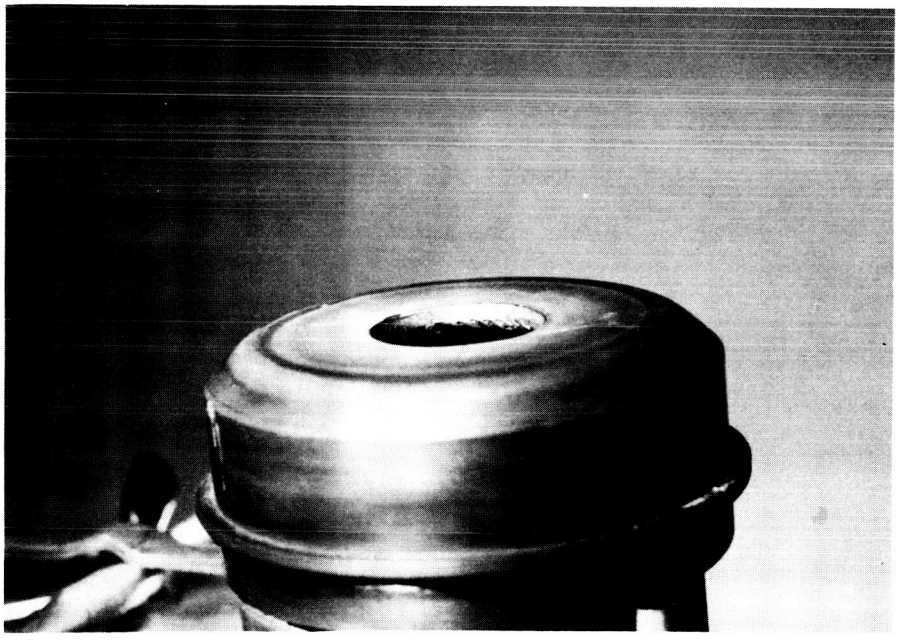

View Showing ID of Diffuser and Melted Material

Figure 6 - Anode After Test Run 4

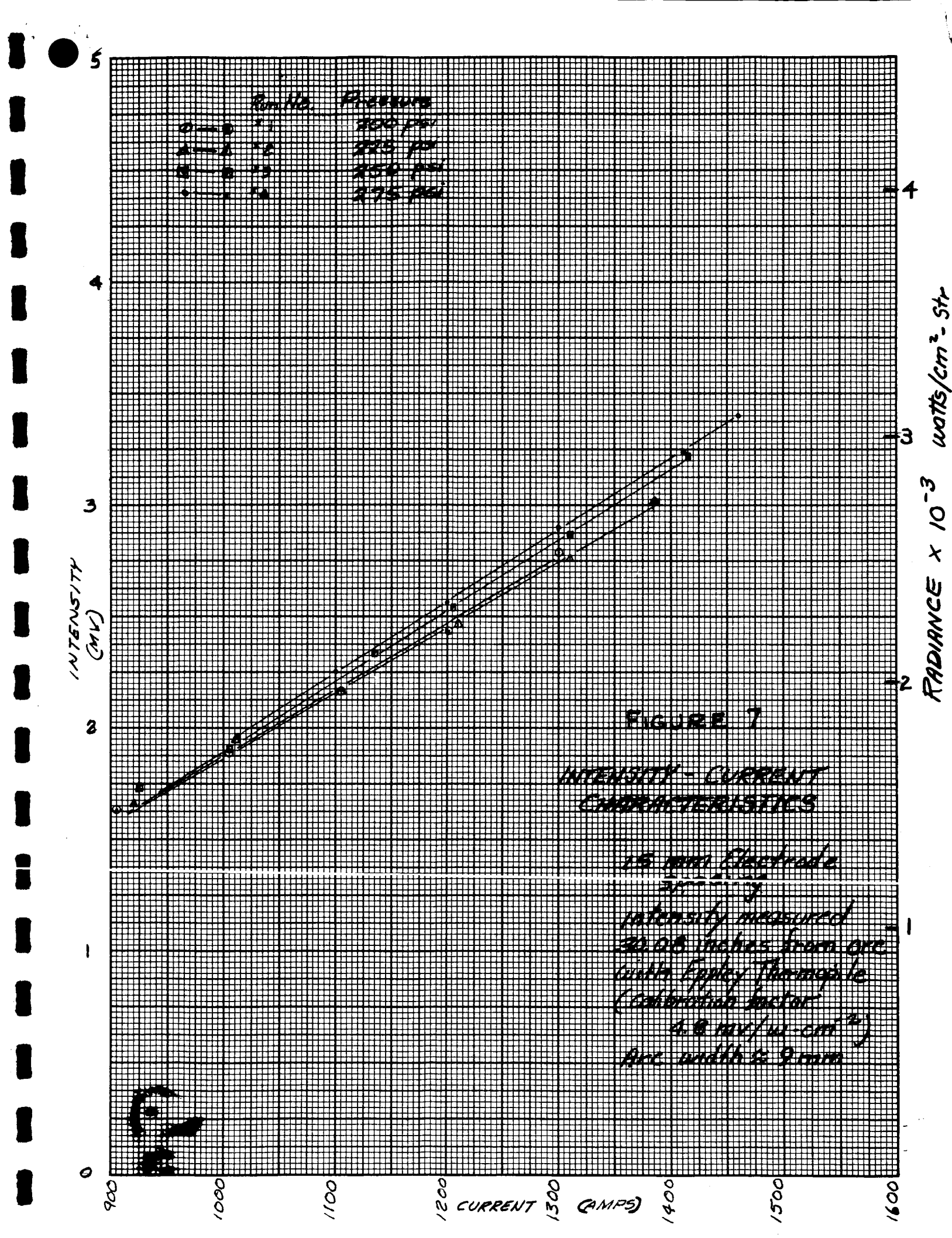

FIGURE 7

INTENSITY - CURRENT CHARACTERISTICS

25 mm Electrode

Intensity measured 30.06 inches from arc with Eppley Thermopile (Calibration factor 4.0 mv/w-cm⁻²) Arc width ≤ 2mm

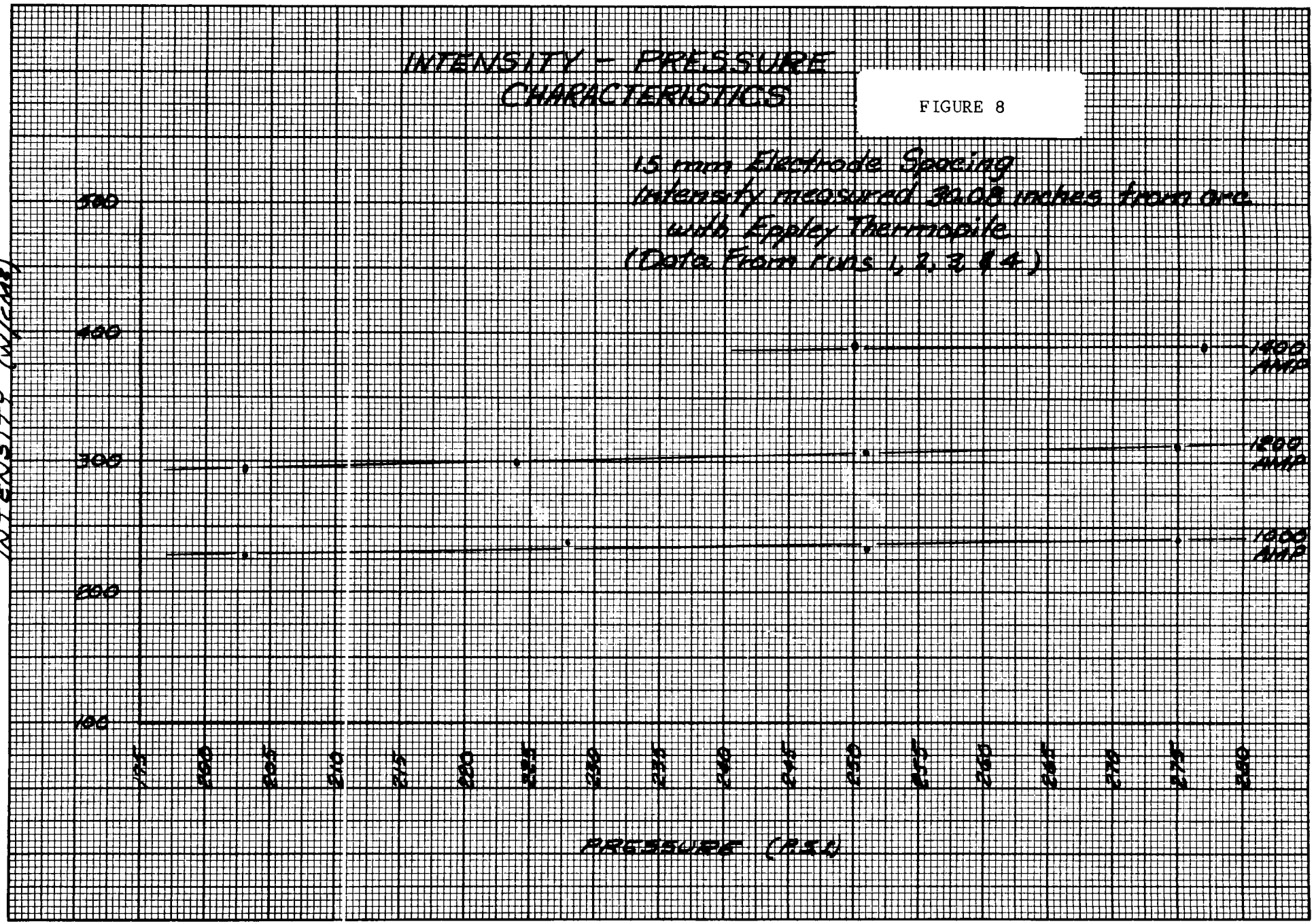
INTENSITY - PRESSURE CHARACTERISTICS
FIGURE 8
15 mm Electrode Spacing
Intensity measured 3.08 inches from arc
with Eppley Thermopile
(Data From runs 1, 2, 3 & 4.)
INTENSITY (WATTS/CM²)
500
400
300
200
100
1400 AMP
1200 AMP
1000 AMP
PRESSURE (PSIG)

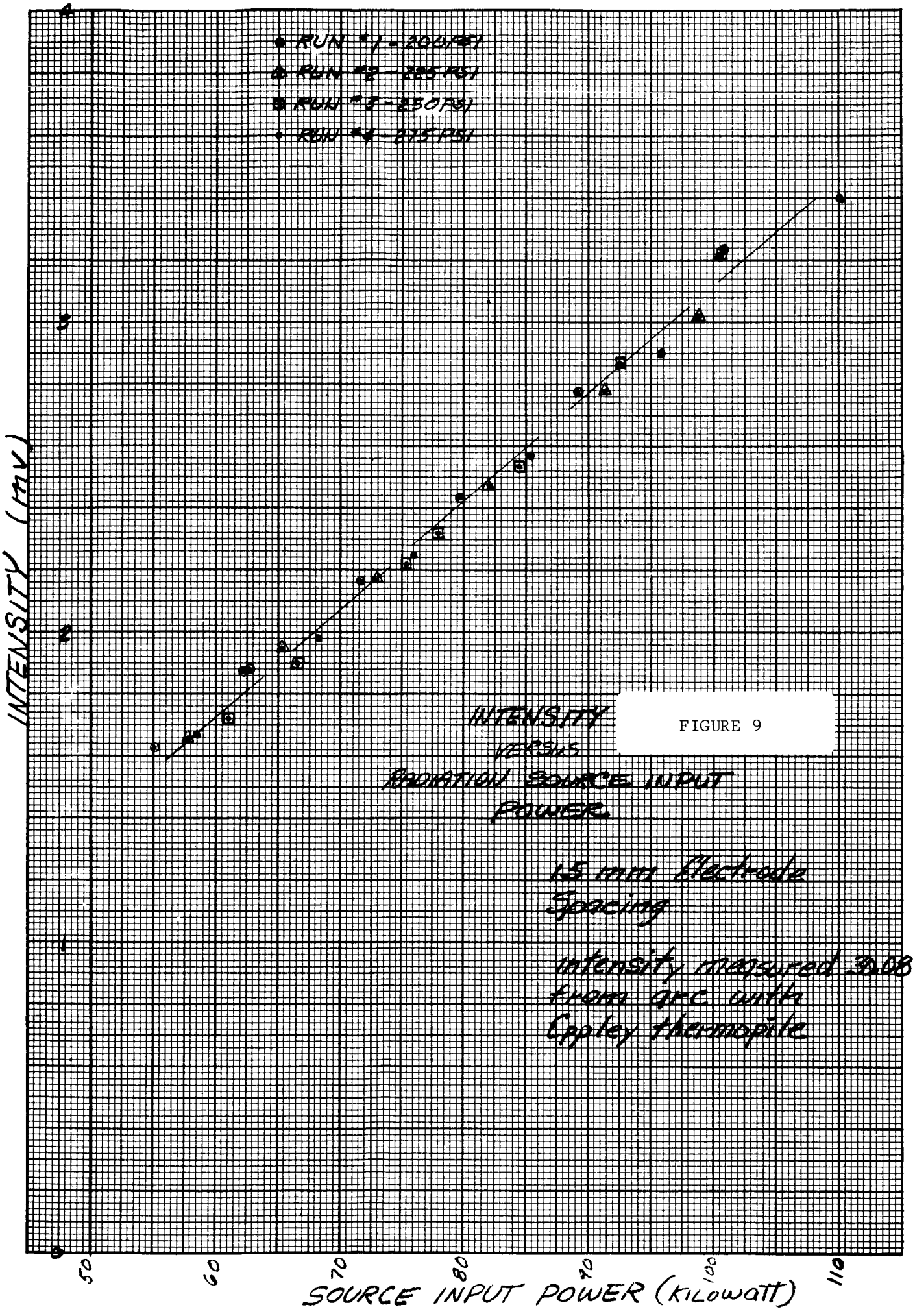

FIGURE 9

INTENSITY VERSUS RADIATION SOURCE INPUT POWER

15 mm Electrode Spacing

Intensity measured 3.08" from arc with Eppley thermopile

FIGURE 10

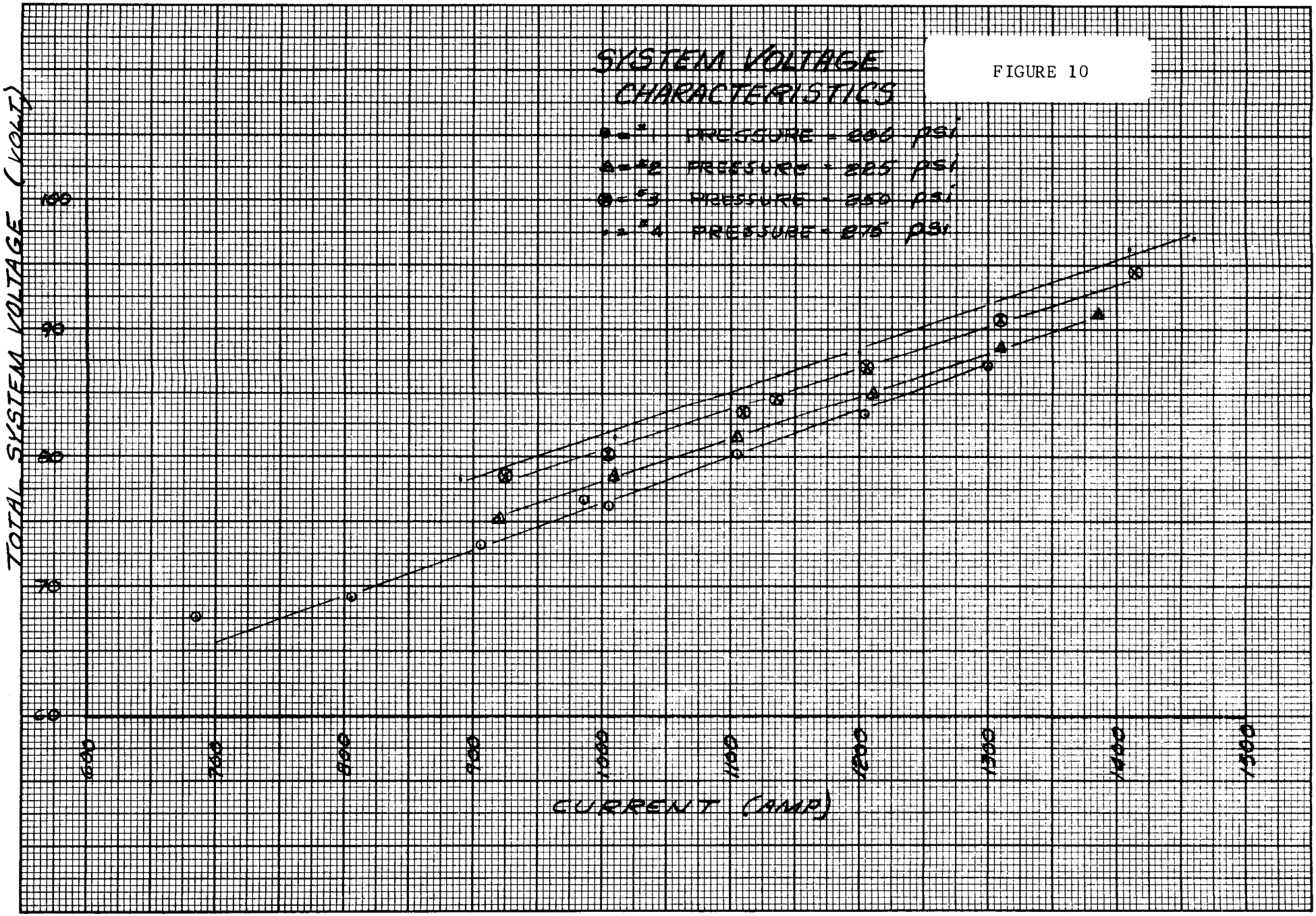
SYSTEM VOLTAGE CHARACTERISTICS
○ - #1 PRESSURE = 200 psi
△ - #2 PRESSURE = 225 psi
⊗ - #3 PRESSURE = 250 psi
□ - #4 PRESSURE = 275 psi
TOTAL SYSTEM VOLTAGE (VOLT)
100
90
80
70
60
600
700
800
900
1000
1100
1200
1300
1400
1500
CURRENT (AMP)

FIGURE 11

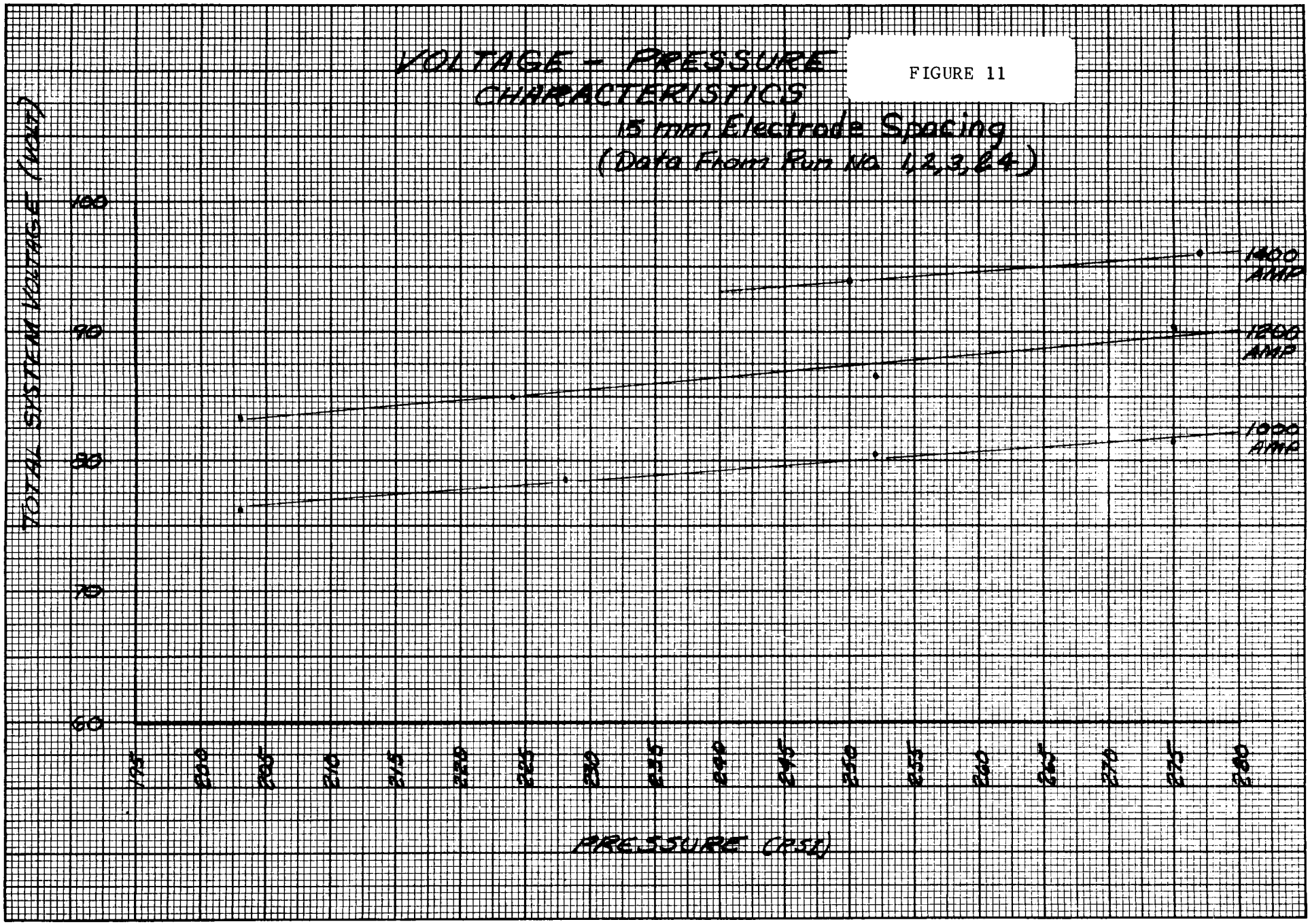
VOLTAGE - PRESSURE CHARACTERISTICS
15 mm Electrode Spacing
(Data From Run No. 1, 2, 3, & 4)
TOTAL SYSTEM IMPEDANCE (ohms)
100
90
80
70
60
1400 AMP
1200 AMP
1000 AMP
PRESSURE (PSIG)

FIGURE 12

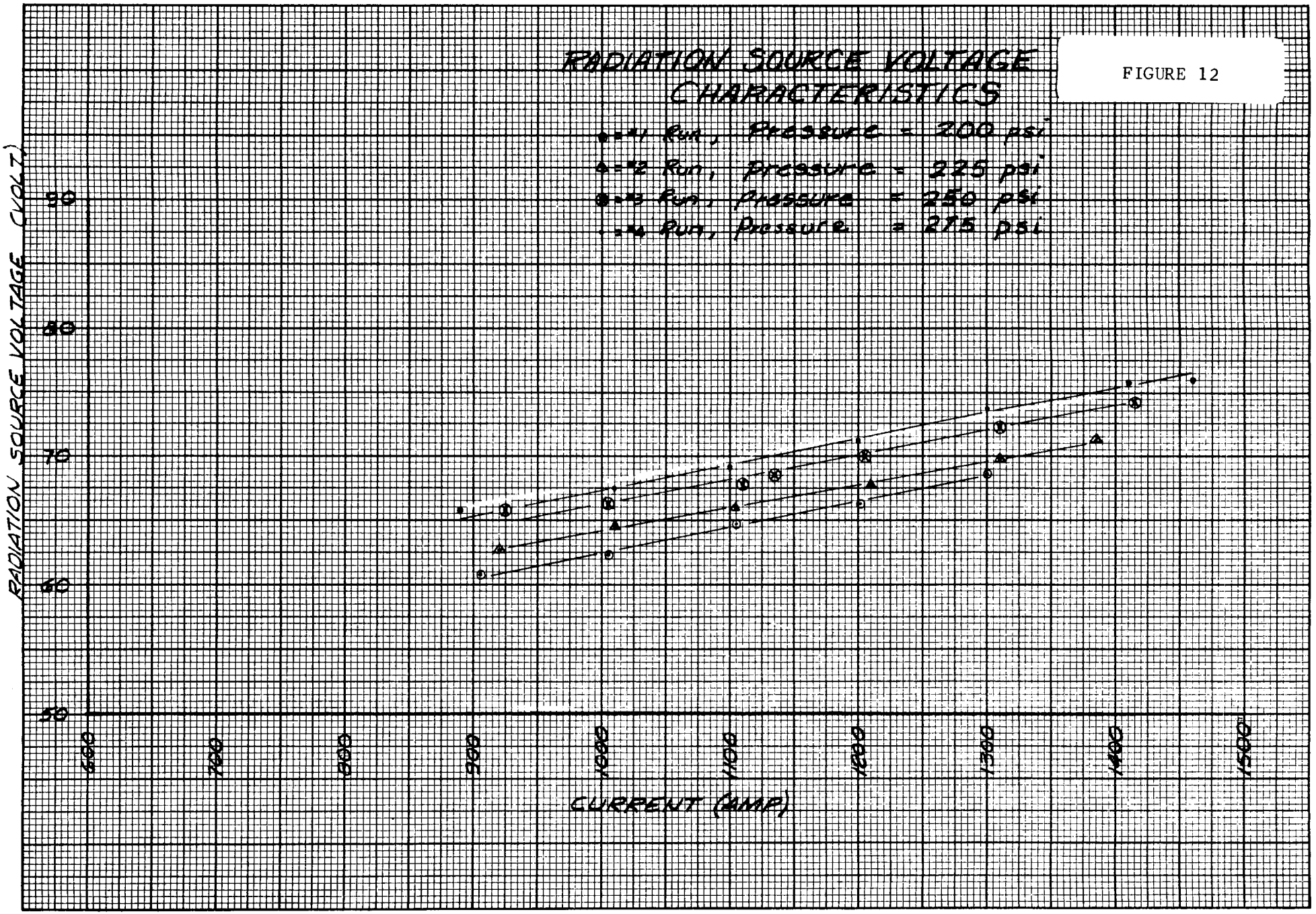
RADIATION SOURCE VOLTAGE CHARACTERISTICS
●=#1 Run, Pressure = 200 psi
▲=#2 Run, Pressure = 225 psi
⊗=#3 Run, Pressure = 250 psi
○=#4 Run, Pressure = 275 psi
RADIATION SOURCE VOLTAGE (VOLT)
90
80
70
60
50
600
700
800
900
1000
1100
1200
1300
1400
1500
CURRENT (AMP)

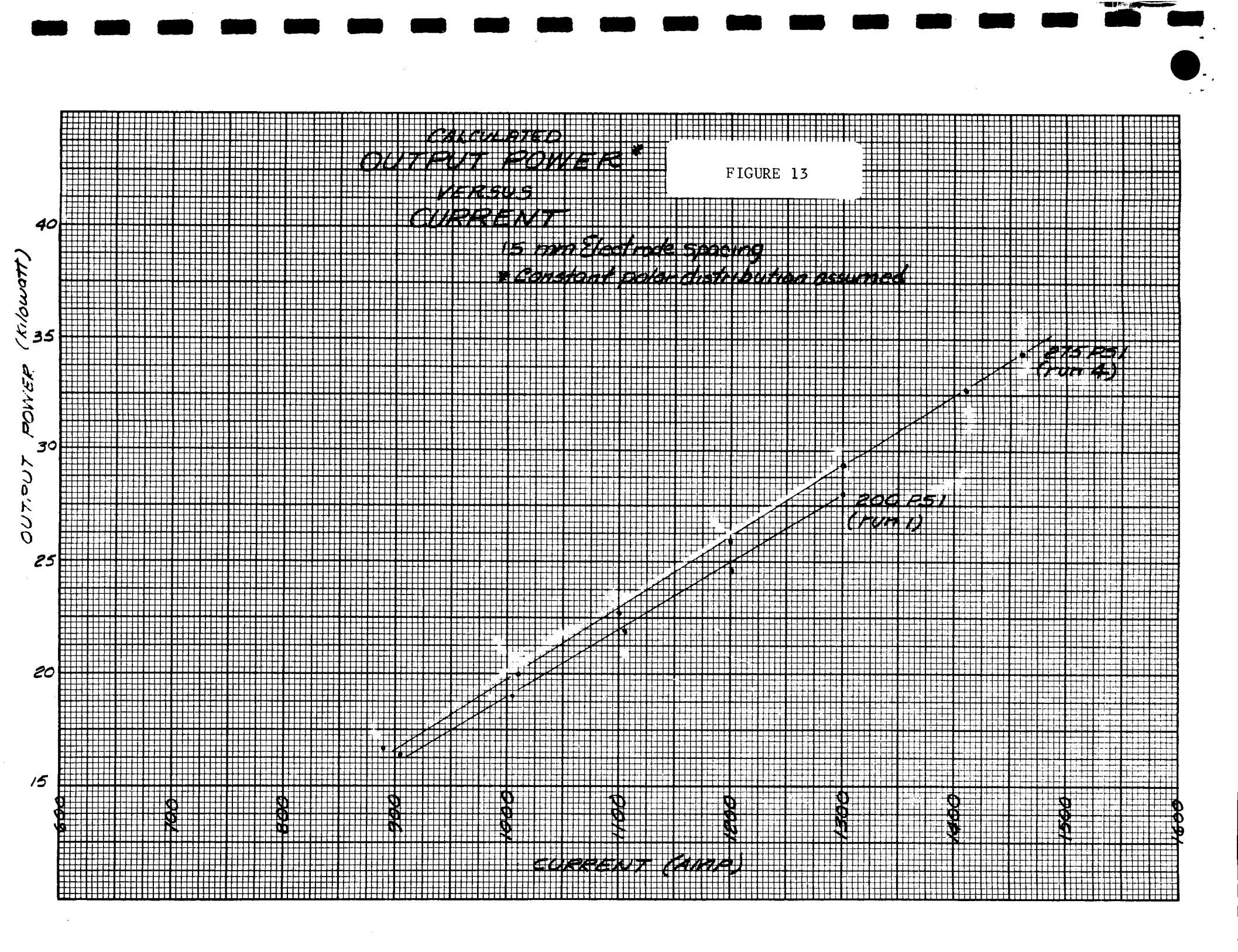
CALCULATED
OUTPUT POWER*
VERSUS
CURRENT
15 mm Electrode spacing
*Constant polar distribution assumed
FIGURE 13
OUTPUT POWER (Kilowatt)
40
35
30
25
20
15
275 PSI
(run 4)
200 PSI
(run 1)
CURRENT (AMP)

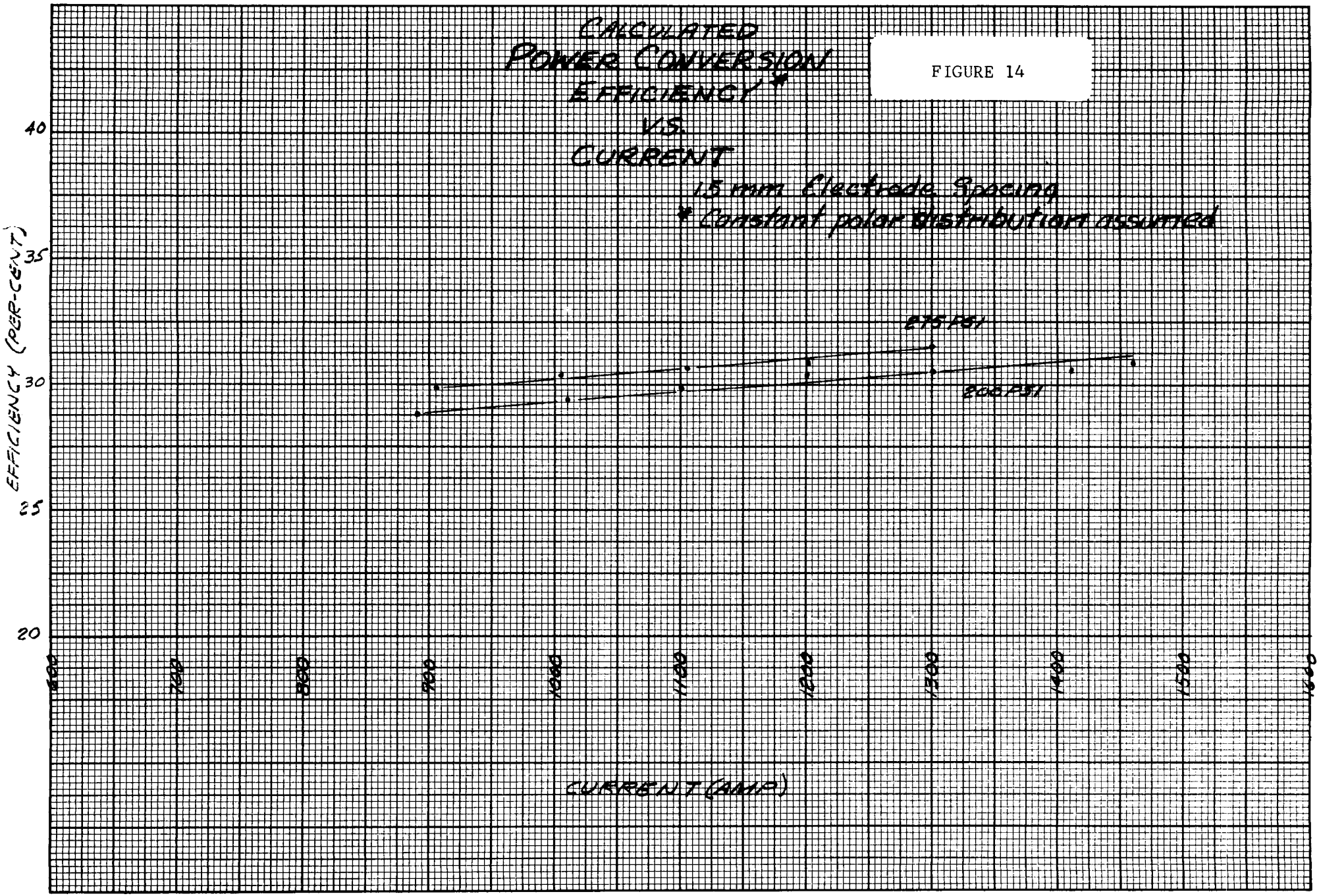
CALCULATED
POWER CONVERSION
EFFICIENCY*
VS.
CURRENT
1.5 mm Electrode Spacing
* Constant polar distribution assumed
FIGURE 14
EFFICIENCY (PER-CENT)
40
35
30
25
20
275 PSI
208 PSI
CURRENT (AMPS)

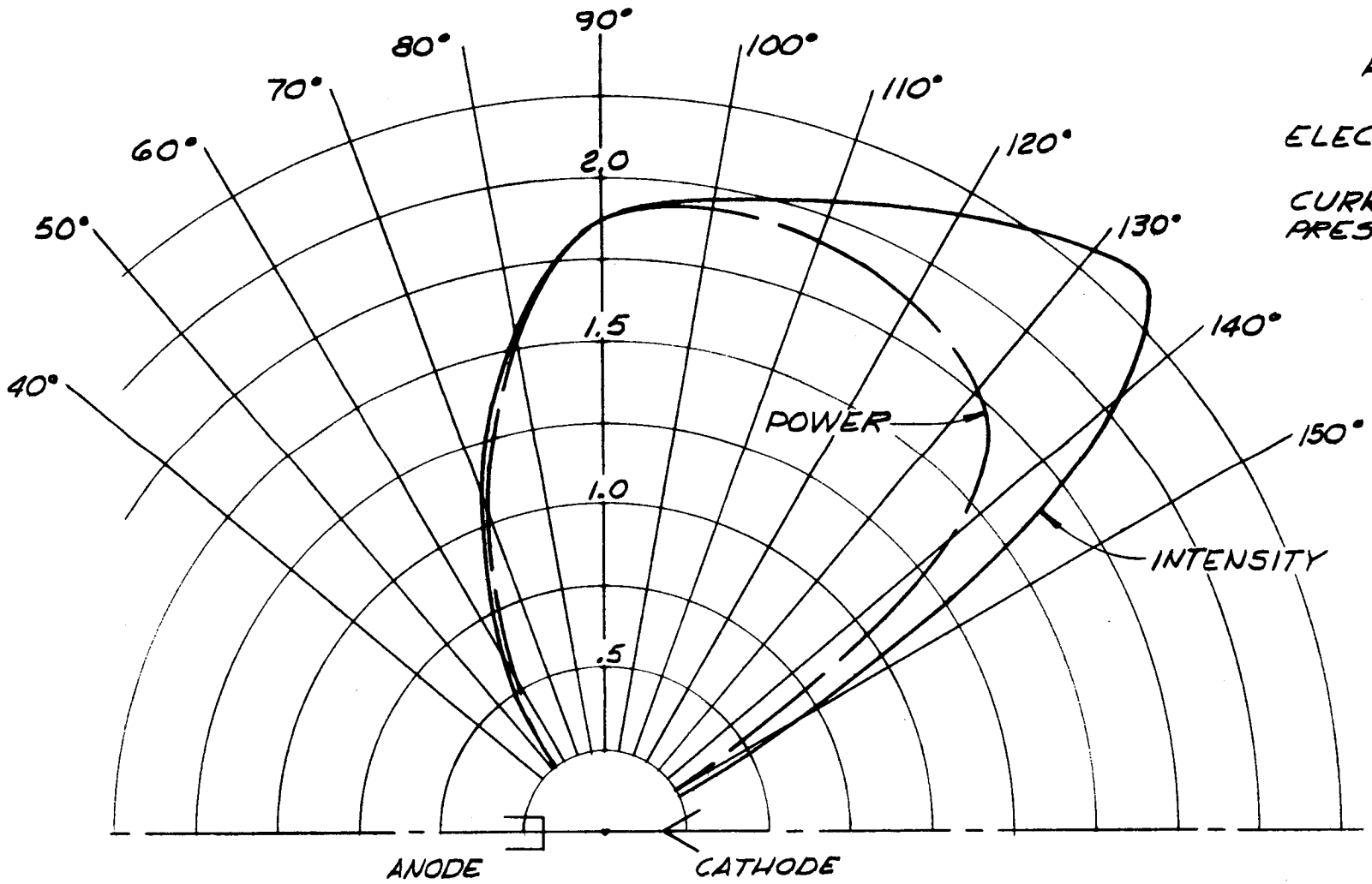

RUN No. 1.5
9-18-64
ELECTRODE SPACING
15mm
CURRENT 985 AMPS
PRESSURE 200 PSI

POLAR POWER & INTENSITY DISTRIBUTION

FIGURE 15

DEVELOPMENT MEMORANDUM NO. 272-16

SUBJECT: Radiation Source Performance During Prototype Testing (Runs 5-9)
WRITTEN BY: W. A. Geideman
DATE: October 30, 1964
JOB NUMBER: 6002-45

INTRODUCTION

After completion of the source evaluation tests which were reported in Development Memorandum No. 272-14, the source was reassembled for prototype testing. New cathode, anode and inner quartz envelope were employed. The cathode was machined to print 013881 and was one of the original cathodes manufactured by Giannini Scientific. The anode had a copper diffuser with a .650" ID. This assembly used essentially identical parts to those employed in the first series of tests.

Both quartz envelopes were cleaned prior to assembly of the radiation source and the electrode spacing was set at 15 mm. The radiation source was then mounted inside the collector as shown in Figure 1. The top photograph in Figure 1 shows the reflecting surface of the collector with the source mounted. The two copper pipes bringing the water and power to the cathode are shown in the foreground. The bottom picture in Figure 1 shows the rear mounting of the source in the collector. This view also shows the water and gas connections to the radiation source. A device was made to remove the weight of the cathode end of the radiation source from the outer quartz envelope. A portion of this device may be seen in the top picture in Figure 1. A rod was placed between the two copper pipes with a spring loading calibrated to remove the gravitational forces produced by the weight of the cathode. In addition, the water hoses were held by the clamp shown in Figure 1. This clamp removed the weight of the hoses and the copper pipes from the quartz envelope.

The purpose of these tests was to obtain data relating to the intensity in the target plane of the prototype optical system. The optical measurements and data reduction are presented in Development Memorandum 272-18.

TEST RESULTS

The first prototype test run made with the final radiation source was terminated after about two minutes of running because smoke was noticed in the test room. It was found that the water cable leading to the cathode was burning causing the smoke. The aluminum tape which was intended to protect the water cable could not withstand the high power levels. To correct this, copper leads to provide the water, in and out, to the cathode were manufactured and installed.

Test Run #5 was performed on October 7, 1964 after the modification to the cathode water lines. This test was intended to measure the target intensity. Source operating conditions were 1,000 amps at 250 psig gas pressure. The source was operated for a total of 73 minutes. The source was shut down because of a failure of the recirculator pump producing oil in the gas lines. This oil was first observed about six minutes before the test was terminated. The oil collected in the flow meters and was stopped by the filter. After the source was extinguished, some small deposits of oil were observed on the quartz envelopes. Prior to the failure of the diaphragm, the source was operating in a completely satisfactory manner.

The source was removed from the collector mounting and disassembled to clean the quartz envelopes. The oil came off easily using Ketone solvent. During the cleaning procedure, a purplish tone was noted in both the inner and outer quartz envelopes. The reason for this discoloration is believed to be solarization. The entire closed gas loop in the facility was cleaned to remove any oil. The cleaning procedure was to flush the entire loop with Keolite to dissolve any oil present. The system was then flushed with water to remove the Keolite and blown dry with air. The source parts were cleaned separately, as well as the flow meters. All the water was not removed from the lines by blowing air through them, therefore, the different sections of the loop were flushed with alcohol to remove the water and then blown dry with air. The hoses were evacuated with the vacuum pump to remove any residual vapors. The entire system was evacuated and then filled with argon and run using the recirculator pump for approximately 30 minutes with the source disconnected. No fluid was evident in the gas system during this checkout run and the source was reassembled for the next test.

The recirculator pump was repaired by replacing both diaphragms and replacing the diaphragm gaskets. Inspection of the diaphragms which were removed from the pump indicated that solid particles had been bombarding the diaphragm from the oil side and had produced dents in the diaphragm. The cause of the oil leakage appears to be a microscopic hole in one of these dents. This was reported to the representative of the pump manufacturer. An oil filter was placed in the line leading from the reservoir to the make-up pump in an effort to prevent future failures of this type.

Test Run #6 was performed on October 13, 1964. The source was operated for approximately 20 minutes. Operating conditions were the same as used in Test #5. The source was extinguished because of a phenolic smell in the R&D Lab. This smell was traced to Sid Zipser drilling phenolic in the lab and was not caused by anything relating to the test operation. The source was reignited and the arc started on the diffuser section of the anode rather than the arcing surface and the source was extinguished immediately. The cause of this failure was starting at too low a gas pressure. If the gas pressure is too low, there is insufficient vortex action to force the arc to ignite on the arcing surface. The flow rate of gas in the closed system is directly proportional to the pressure. Any arc on the diffuser itself will melt the diffuser since there is insufficient cooling to dissipate the heat produced in the anode foot of the arc. The source was removed from the collector and disassembled. Only the anode was replaced and the source was reinstalled in the collector.

Test Run #7 was performed on October 14, 1964 at the same operating conditions as employed in the previous prototype tests. This test run lasted a total of 97 minutes. The source was extinguished because of marks on the front surface of the anode diffuser. Prior to the observation of these marks, the source had been operating in a very stable manner. The source was removed from the collector for inspection. The cathode had a peculiar mushroom like surface. This surface was a small diameter eruption with a wider irregular surface at the arcing point. The diameter of the eruption at the original face of the cathode was approximately .140". Figure 2

shows two views of the cathode after the test. The marks on the front surface of the anode were traced to particles of tungsten bombarding this surface and causing small craters in the surface. The tungsten particles were still present in the anode surface and the direction of the craters was in the direction of the gas vortex. Figure 3 shows the anode from two directions. The first shows the front surface of the diffuser and the arcing surface while the second is angled to show the inside of the diffuser. The inner envelope was severely pock marked due to the impingement of small tungsten particles onto the quartz. Figure 4 shows the inner tube after the test and a closeup view of the cathode tip. A large quantity of tungsten particles were observed between the quartz envelope and the anode housing. These tungsten particles were merely resting on the O-ring seal.

On October 18, 1964, Mr. Loucks of Exotic Materials reported that the inner quartz envelope which was left with him for annealing had been annealed and the purplish discoloration of the quartz was eliminated. Thus, this discoloration which has been noticed in both the inner and outer envelopes on all test runs can be eliminated by heating the quartz. The actual temperature where the discoloration is removed should be determined experimentally.

The radiation source was reassembled on 19 October 1964, using the cathode previously employed in the source evaluation tests. The flat on the cathode was reground to remove the eroded material. The new flat on the cathode as installed in the radiation source was 0.265' diameter. The anode had a molybdenum-copper composite diffuser with an ID of .650". The electrode spacing was set at 15 mm by adjusting the cathode from the outside after the source was assembled. The source was reinstalled into the prototype system and was operated.

The first test on ignition showed a sediment on the quartz tubes and, therefore, the source was extinguished. The source was removed from the prototype system and the quartz envelopes were cleaned. It is believed that this sediment resulted from water in the gas lines which collected on the quartz envelopes and then evaporated during the purging cycle leaving dirt on the quartz. After cleaning had been completed, the source was

reassembled and reinstalled with the same setting as previously used. After this short test run of approximately a minute and a half, the electrodes were examined and were found to be in the following condition. The cathode showed that the arc had ignited on one side of the flat. The arc foot did not completely fill the flat nor was it located on the corner of the cathode. Rather, it formed a circle inside the circular flat on the cathode which small circle was approximately tangent to the larger circle. The anode showed no ill effects whatsoever except for a discoloration of the molybdenum diffuser. This discoloration was not symmetrical around the axis of the anode but rather was elliptical in shape extending out to the brazed joint on one side. This elliptical discoloration of the anode possibly can be correlated to the off center cathode location of the arc.

The source was reignited on 19 October 1964 and a successful test run of 50 minutes was obtained. This test was designated as run #8. The arc was ignited at a pressure of 45 psig and the pressure was rapidly increased to 200 lbs while maintaining a minimum current of 600 amps. The arc was then brought to the operating condition of 1,000 amps at 250 psig and maintained at this setting for the duration of the test. The total voltage drop rose slightly from the beginning of the test by approximately three volts out of 84. This voltage rise could be due to the heating of some of the components in the system.

After completion of this test run, the source was not disassembled from the prototype system as further tests were contemplated. No serious degradation of any of the parts was noted. The anode arcing surface had the characteristic bumps and craters previously observed. The diffuser suffered no degradation at all. The condition of the cathode cannot be observed while the source is mounted in the collector. No particles were observed on the quartz envelope.

Test Run #9 was made on 20 October 1964 as a variable power test to determine the intensity in the target plane at several different current levels. The arc current was varied in 100 amp steps from 900 to 1400 amps and then varied in 50 amp steps up to 1550 amps. The total duration of this test

was 25 minutes. Test run #9 was terminated because no additional significant data could be obtained. During operation at 1550 amps, the stainless steel shield which was used at the sensor in the target plane to shield the water cables for the sensor melted and fell on the floor. Because of the loss of the shield, it was necessary to close the dowser and no further target data could be obtained. The shield is shown in Figure 5 after failure. At a current level of 900 amps, a copper shield which was used for the first time in place of the stainless steel shield melted at the silver solder joint.

The gas pressure was maintained at approximately 250 psig. The parts of the radiation source did not appear to suffer any serious degradation during this test.

The anode arcing surface showed evidence of melting and possibly boiling of the copper material. The diffuser was slightly rounded but did not appear damaged. The inner quartz envelope had one spot of tungsten which was fairly large but no other occlusions were noted. The cathode had a small growth on the tip as well as some erosion.

The radiation source was disassembled from the collector at the end of this test since this was the last in the present series of prototype test runs. The radiation source was then disassembled for inspection of the electrodes. The diffuser ID was remeasured and was found to vary from .649" to .651" in different diameters. The cathode was measured to have a "hat" around the arcing tip. The diameter of this displaced material was .310" while the diameter of the original tungsten underneath this "hat" was a maximum of .280". The eruption on the surface of the cathode was measured to have an elliptical shape with a major diameter of approximately .130" and a minor diameter of approximately .100". This eruption was not centered on the axis of the cathode but was displaced slightly to one side. Figure 6 shows two different views of the cathode after disassembly. Figure 7 shows the condition of both the anode arcing surface and diffuser after this test. The inner quartz envelope had a single fairly large piece of tungsten adhering to the inner surface. This tungsten was removed easily using a slight amount of friction. After removal of the tungsten, a pit

was left in the quartz. Data on source operation, including the current, total voltage, source voltage, power and gas flow and pressure are presented in Table 1. The maximum power input to the radiation source was 126 KW. The source voltage was calculated using the calibration curves presented in Development Memorandum 272-10.

CONCLUSIONS

No problem was experienced with the outer quartz envelope during the testing. At the completion of test run 9, the radiation source had been operated for a total of 5.6 hours. The problems encountered with the radiation source have been detailed in this report and are mainly centered on the erosion of the cathode. No other parts of the radiation source have encountered difficulties. The solarization of the quartz envelopes which was encountered in this test series has not caused any apparent problems.

Point No.	Current Amps	Total Voltage Volts	Source Voltage Volts	Total Power KW	Source Power KW	Gas Pressure psig	Gas Flow Reading	Running Time min.
								377.4
9.1	900	81.4	69.1	73.3	62.2	250	49.7	382.0
9.2	1000	83.3	69.5	83.3	69.5	252	49.7	
9.3	1100	87.2	71.8	95.9	79.0	248	49.0	
9.4	1200	89.7	72.7	107.6	87.2	247	48	
9.5	1300	94.1	75.6	122.3	98.3	250	47.8	
9.6	1400	97.6	77.5	136.6	108.5	250	47.5	
9.7	1450	100.3	79.4	145.4	115.1	252	47.5	
9.8	1500	101.6	80.0	152.4	120.0	252	47.3	
9.9	1550	103.6	81.2	160.6	125.9	254	47.5	402.5
								403.1

Table 1 - Raw and Reduced Radiation Source Data for Test Run #9

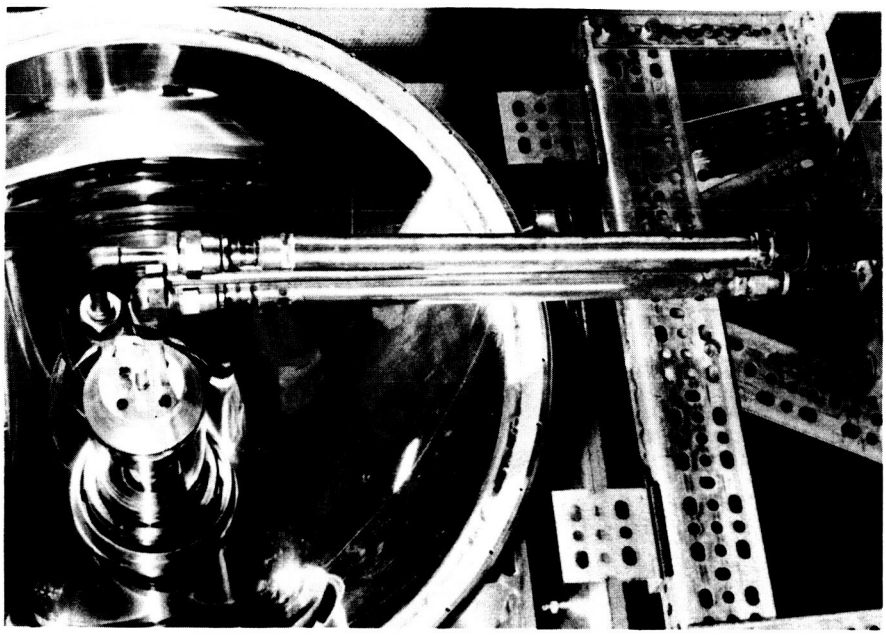

Front View

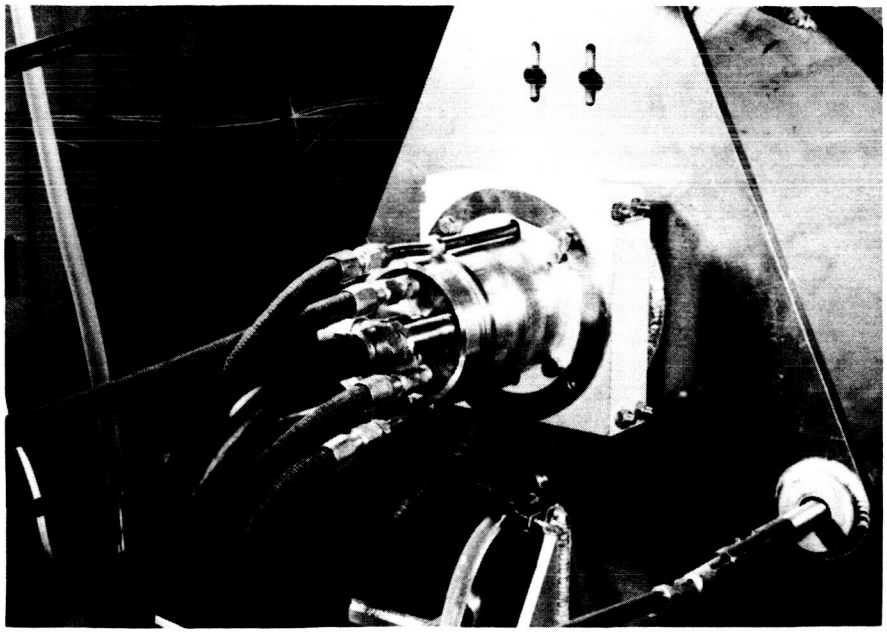

Rear Connections

Figure 1 - Radiation Source Mounted in Collector

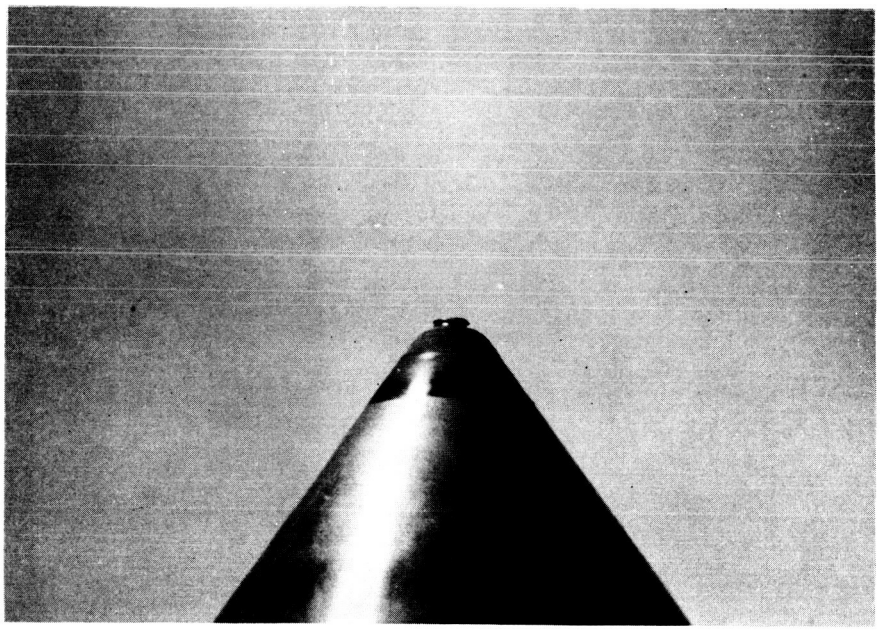

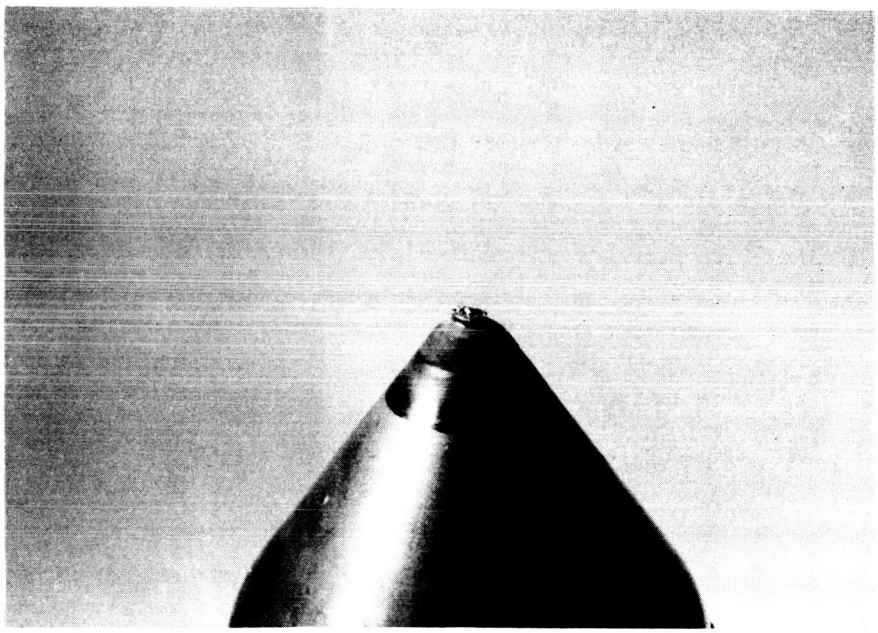

Figure 2 - Cathode Following Test Run 7

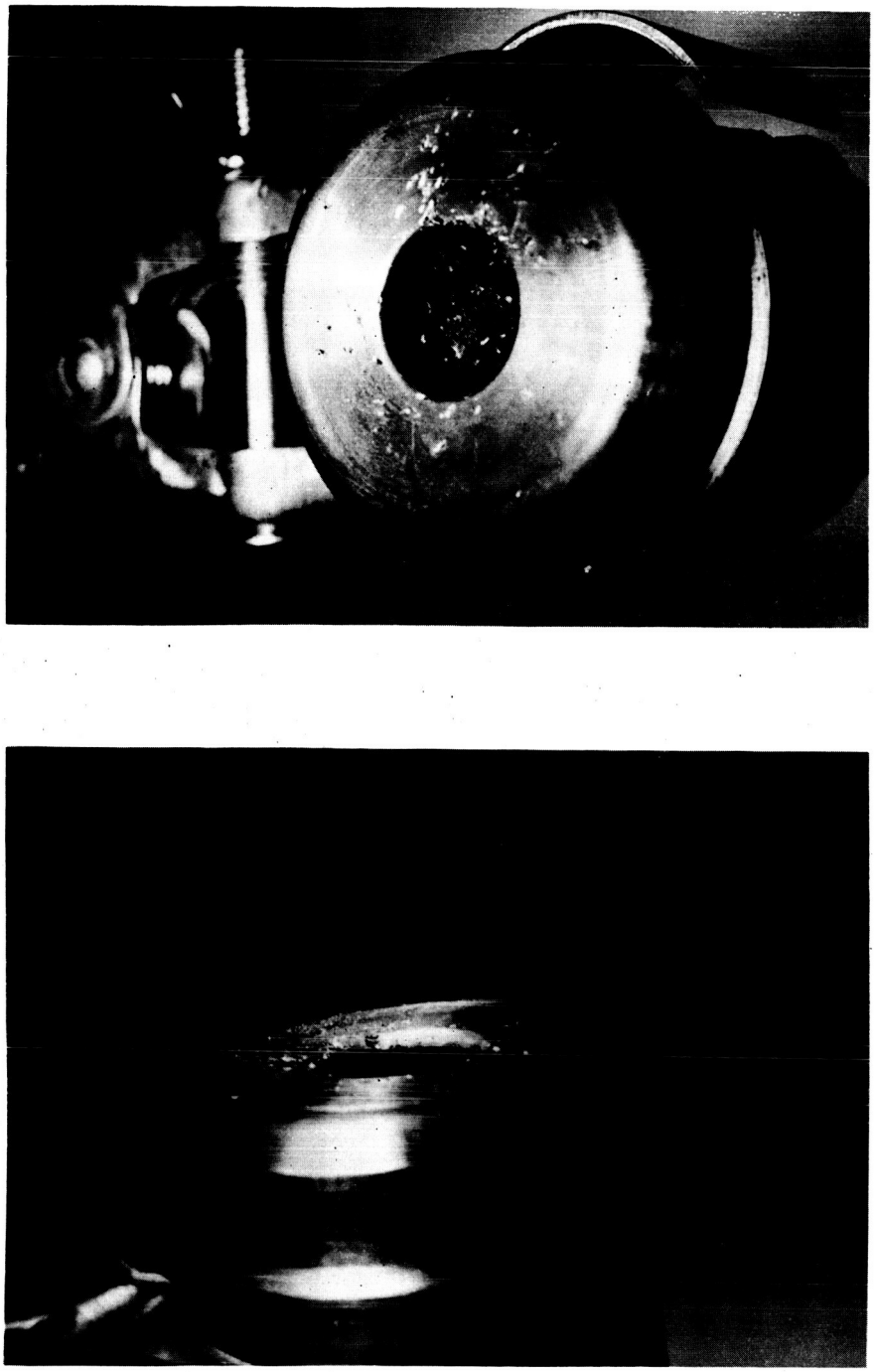

Figure 3 - Anode After Test Run 7 Showing Effects of Tungsten Bombardment

Inner Quartz Envelope Showing Pits
Left After Bombardment with Tungsten

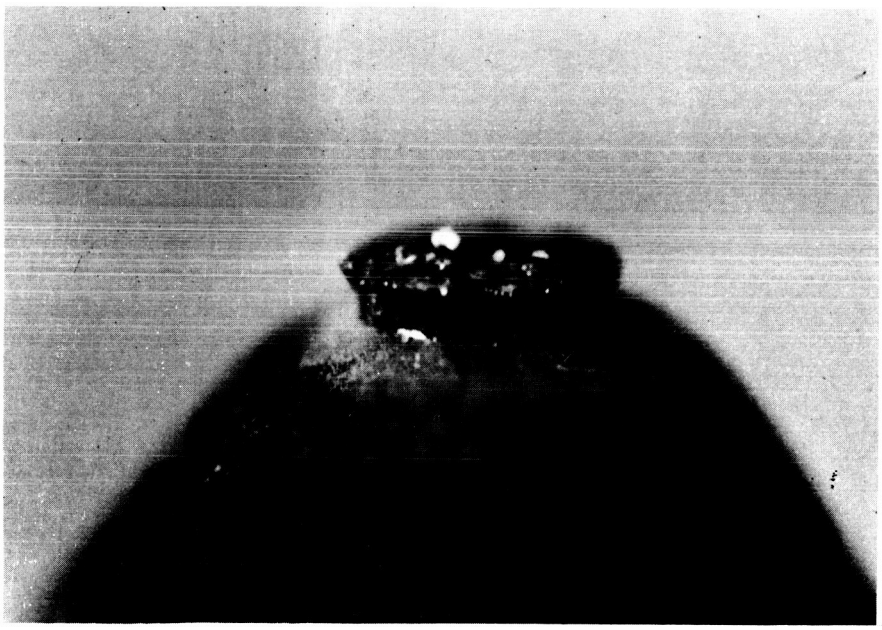

Closeup of Cathode Tip

Figure 4 - Inner Envelope and Cathode Tip After Test Run 7

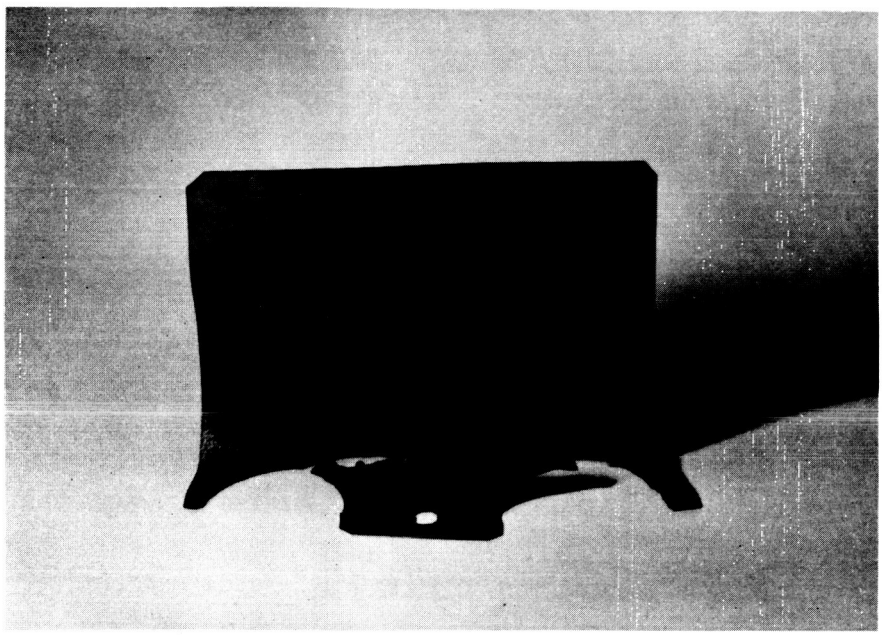

Figure 5 - Sensor Shield After Test Run 9. Gaps Caused by Melting of Stainless Steel

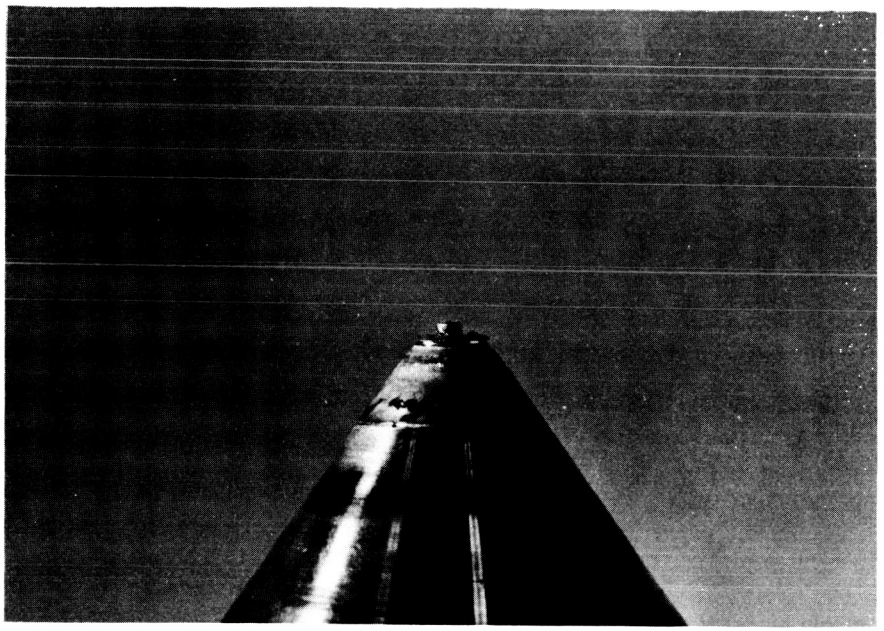

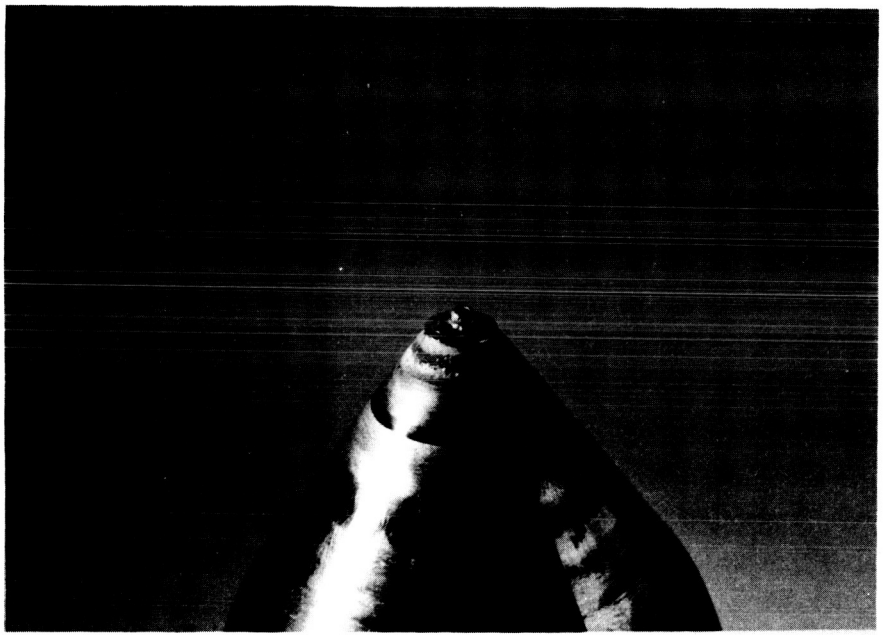

Figure 6 - Cathode After Test Run 9

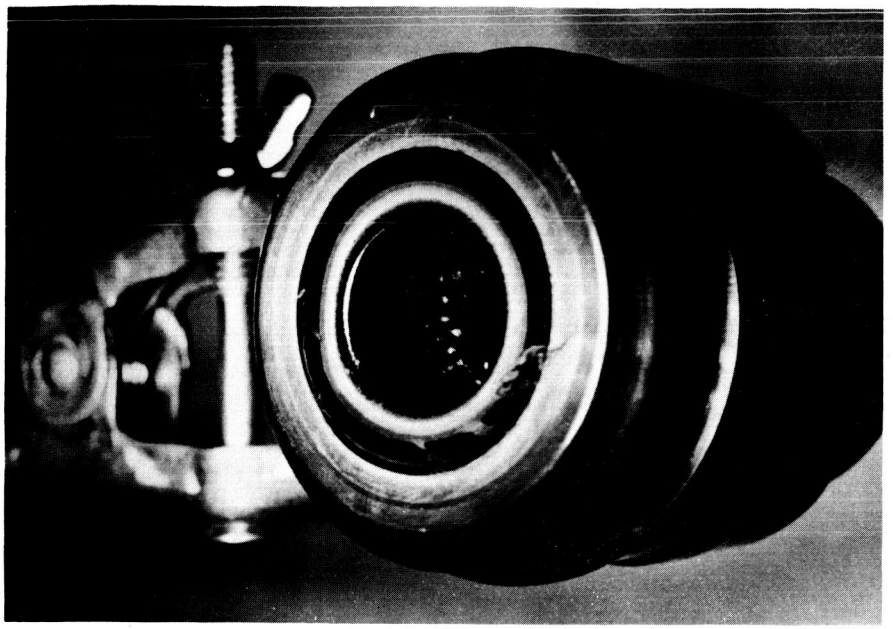

Figure 7 - Anode Following Test Run 9

SPECTROLAB

DEVELOPMENT MEMORANDUM NO. 272-17

SUBJECT: Documentation of Source Performance in Test Run 10

WRITTEN BY: W. A. Geideman
DATE: November 4, 1964
JOB NUMBER: 6002-56

INTRODUCTION

The purpose of test run 10 was to obtain a relative calibration between the NASA radiometer, the Hy-Cal calorimeter and the Eppley thermopile. The results of the sensor data are presented in Development Memorandum 272-15. This test was set up as a source evaluation test using the special mounting employed in tests 1 through 4. The anode viewer was re-positioned to enable monitoring of the anode during operation. The projection system for projecting the image of the arc at a 90° angle was also set up so that pictures of the arc could be taken. (See DM 272-14 for complete description of test setup)

The final radiation source was assembled with a new anode, cathode, and inner quartz envelope. The cathode was newly manufactured from OFHC copper and 2% thoriated tungsten. The tungsten was furnace brazed to the copper using a 65 copper-35 gold alloy. The cathode was machined to Print #013881 except that the flat on the tip of the tungsten had a final diameter of .125" instead of the .200" shown on the print. The reason for the smaller flat on the cathode was an attempt to experimentally determine the reason for cathode ablation which had occurred in the previous test. The anode had a molybdenum-copper composite diffuser with an ID of .650". Figure 1 shows both the cathode and anode prior to assembly.

TEST RESULTS

Test run #10 was performed on October 23, 1964. The source was operated for a total of 36 minutes. The source was extinguished because of an excessive amount of tungsten particles on the inner envelope. The radiation source data taken during test run number 10 is presented in

Table 1. A small projection was noted on the cathode tip during test point number 1. The projection seemed to grow larger during test points 2 and 3 and was no longer noticed during test point number 4. A flat face on the cathode was observed to begin to develop during test point number 6. During test points 8 and 9, the cathode appeared to be growing on its face. All observations of the cathode were made from the projected image of the arc which views the cathode perpendicular to its axis.

After completion of the test, the radiation source was disassembled and inspected. The cathode had eroded in an area around the tip but behind it to form a narrow projection of tungsten from the body of the cathode. The cathode after the test is shown in Figure 2. The amount of erosion can be estimated by comparing these photographs with the cathode in Figure 1. Both the anode and the inner quartz envelope suffered from impingement of tungsten particles onto their respective surfaces.

The inner envelope was coated with tungsten to the extent that it will have to be replaced to perform another test as can be seen in Figure 3. The anode, while slightly scarred on the front face of the diffuser, is not sufficiently damaged to require replacement. The anode is shown in Figure 4. Again, a measure of degradation in testing can be had by comparing Figure 4 with the anode in Figure 1. The diffuser diameter was measured following the run and was found to be .652". The arcing surface of the anode showed approximately the same appearance as noted in previous tests but the amount of molten material appeared to be smaller than previously observed. The diameter of the tip of the cathode was measured and was found to be elliptical with a .140" major diameter and a .125" minor diameter. The overall length of the cathode tip was approximately the same as before the test.

Future tests will employ the same anode and cathode in an effort to find if cathode ablation will stop at same point and also to evaluate the life of the anode.

Point No.	Current Amps	Total Voltage Volts	Source Voltage Volts	Total Power KW	Source Power KW	Gas Pressure psig	Gas Flow Reading	Running Time min.
10.1	900	80.5	68.2	72.3	61.4	250	50.0	403.1
10.2	1000	84.2	70.4	84.2	70.4	250	50.0	412
10.3	1100	88.2	72.8	97.0	80.1	248	50.2	416
10.4	1200	91.4	74.4	109.7	89.3	248	50.2	419
10.5	1300	95.5	77.0	124.2	100.1	249	48.0	423
10.6	1400	99.8	79.7	139.7	111.6	250	47.0	424
10.7	1000	84.8	71.0	84.8	71.0	250	47.0	428.4
10.8	1400	99.5	79.4	139.3	111.2	252	47.5	433.7
10.9	1500	104.7	83.1	157.1	124.7	252	47.5	437.6

Table 1 - Raw and Reduced Radiation Source Data for Test Run 10

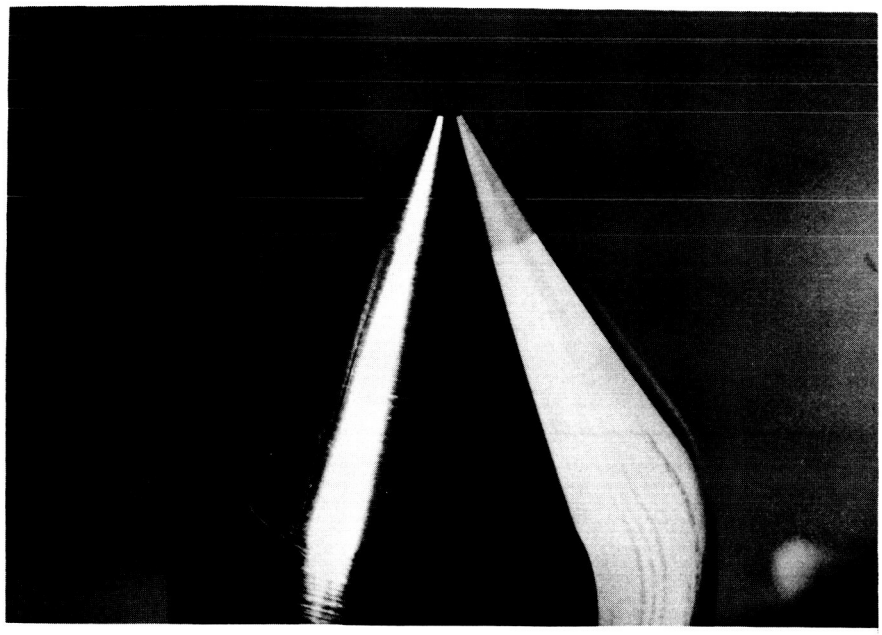

Cathode With .125" Diameter Flat

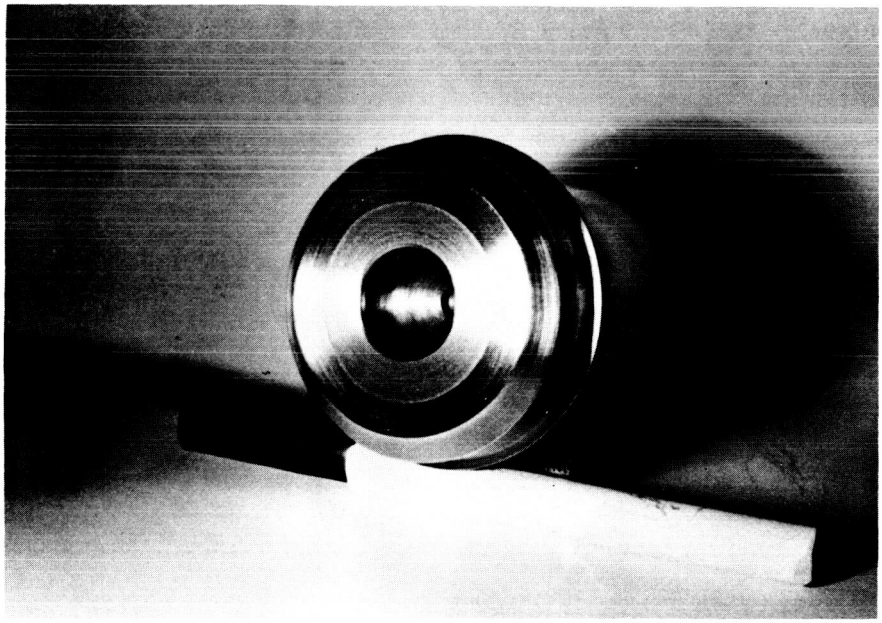

Anode with Molybdenum-Copper Composite Diffuser

Figure 1 - Electrodes Prior to Source Assembly

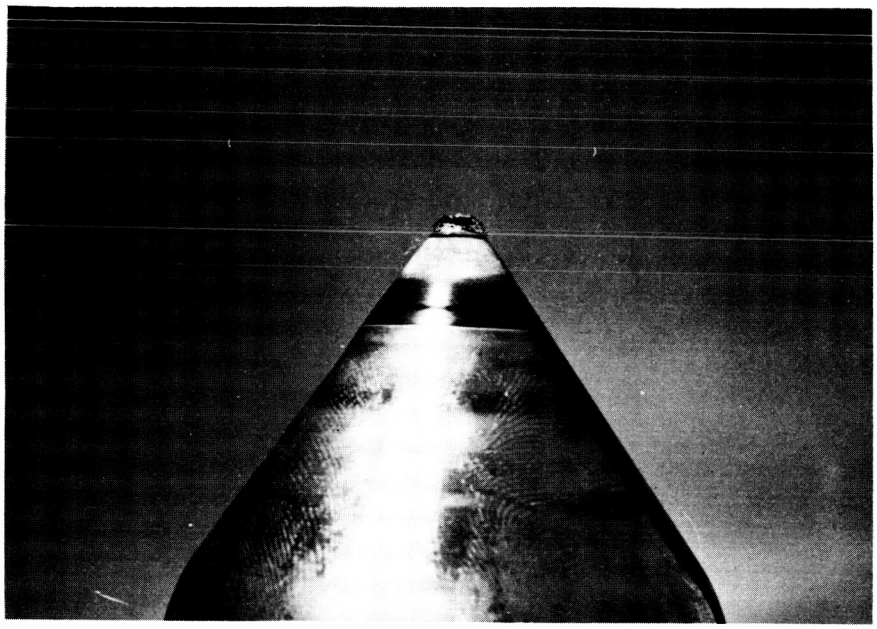

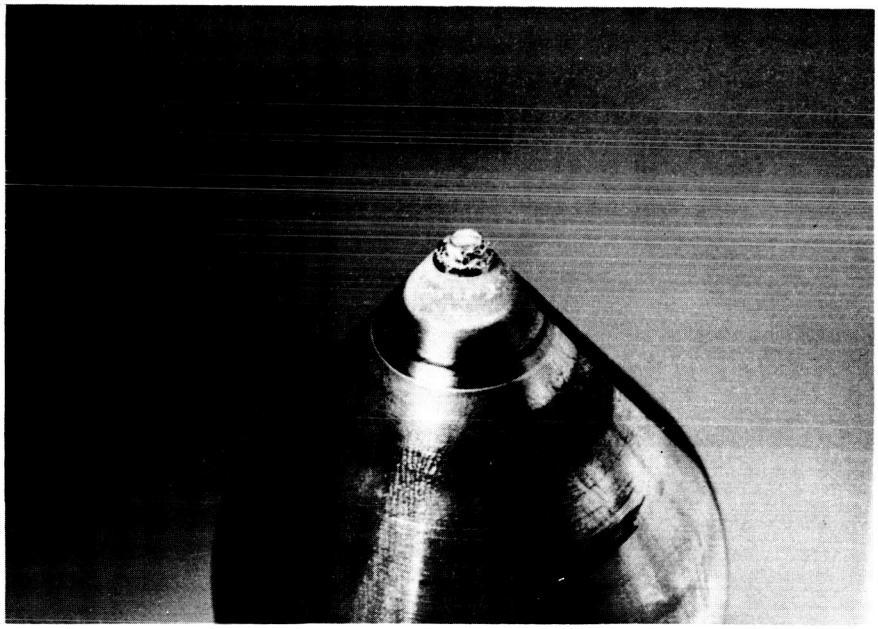

Figure 2 - Cathode After Completion of Test Run 10

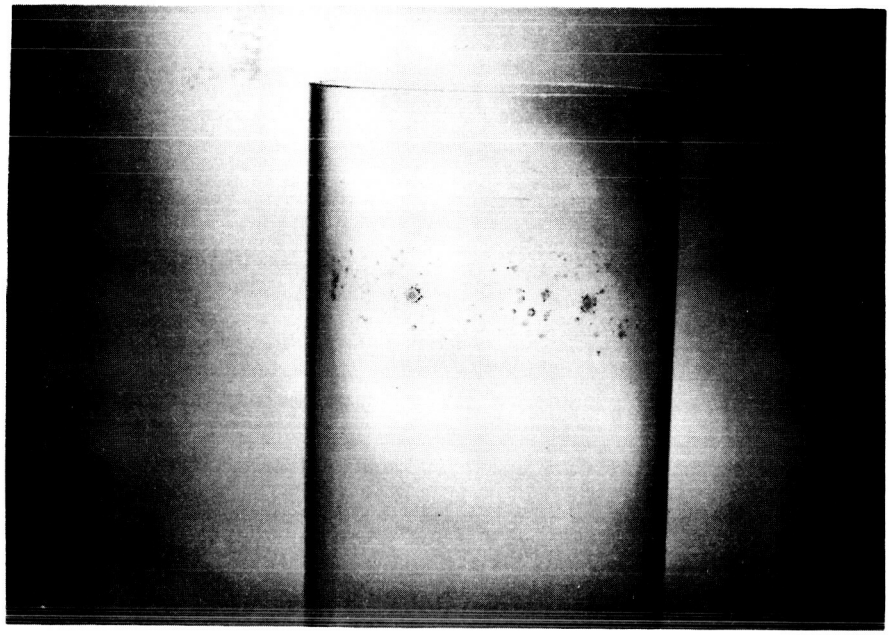

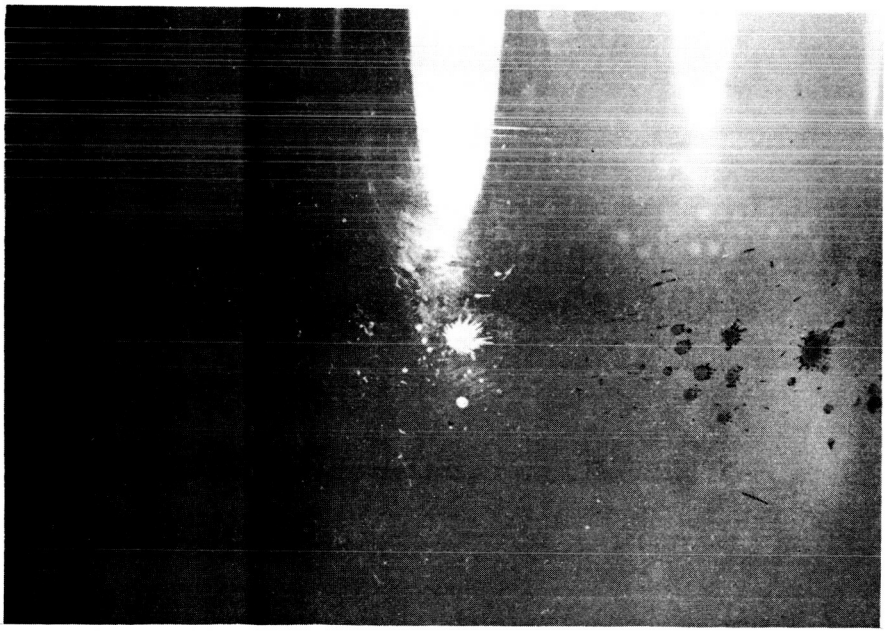

Figure 3 - Inner Quartz Envelope Showing Deposited Tungsten Particles

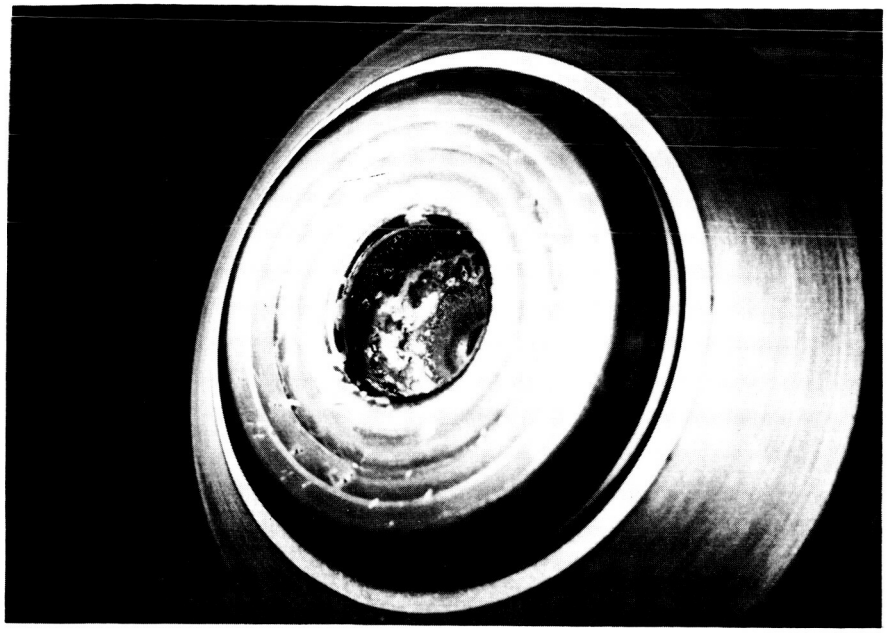

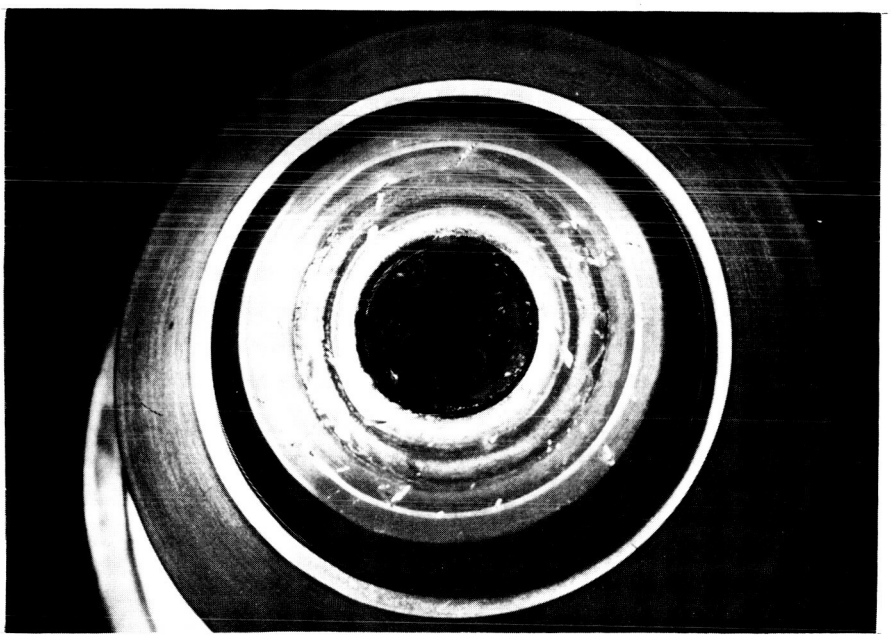

Figure 4 - Anode From Test Run 10

DEVELOPMENT MEMORANDUM NO. 272- 22

SUBJECT: Polar Distribution and Total Energy Runs 13.1, 13.2 and 13.3

WRITTEN BY: Wagner Schlesinger
DATE: November 25, 1964
JOB NUMBER: 6002-11

Runs No. 13.1, 13.2 and 13.3 were made in order to determine total output power and polar distribution of intensity and power. The runs were made under the following conditions:

RUN	AMPERES	VOLTS	GAS FLOW	GAS PRESSURE
13.1	1,000	83.5	24.5 - 25.5	245
13.2	1,200	90.3	24.5 - 25.5	250
13.3	1,400	96.3	24.5 - 25.5	249

The test setup is shown in Figure 1. An Eppley thermopile is supported on a scan arm whose horizontal axis passes through the center of the plasma arc normal to the arc axis. The thermopile sensitive surface is 30.08 inches from the arc center. The thermopile is water cooled and is protected by a water cooled shield with an opening to admit radiation. This opening is normally closed by a remotely operating occulting device so that the thermopile is shielded from radiation except during the periods of a few seconds required for each observation.

The scanning arm position is sensed and transmitted to the X-Y plotter by a precision potentiometer which is calibrated by means of a second arm carrying an indexing pin which fits into a series of precision spaced holes in the main support plate. After calibration, the scanner is remotely operated by a system of wire cables and pulleys.

Scans are made with readings at intervals from one to six degrees spaced to yield maximum information. Accurate values of the angles are determined from the potentiometer readings on the X-Y recorder.

The arc is monitored by a solar cell and strip chart recorder in order to make certain that no significant variations in output take place during any scan.

The recorder deflections for the three scans are plotted in Figure 2. These appeared so similar that they were normalized at 90° for a better comparison and replotted as shown in Figure 3. It is obvious that there is no significant variation with current and hence an average intensity plot of these points and its derived power plot are shown in Figure 4.

This average plot was not used to determine the total power output of each run. From individual plots the average intensity, expressed as mv output of the Eppley, of each five degree zone was determined. The results are tabulated Column 2 in Tables 1, 2 and 3. These values are reduced to power in watts in each zone in Column 5, and the total power and collection efficiency are also derived. The total power outputs are plotted against arc current in Figure 5.

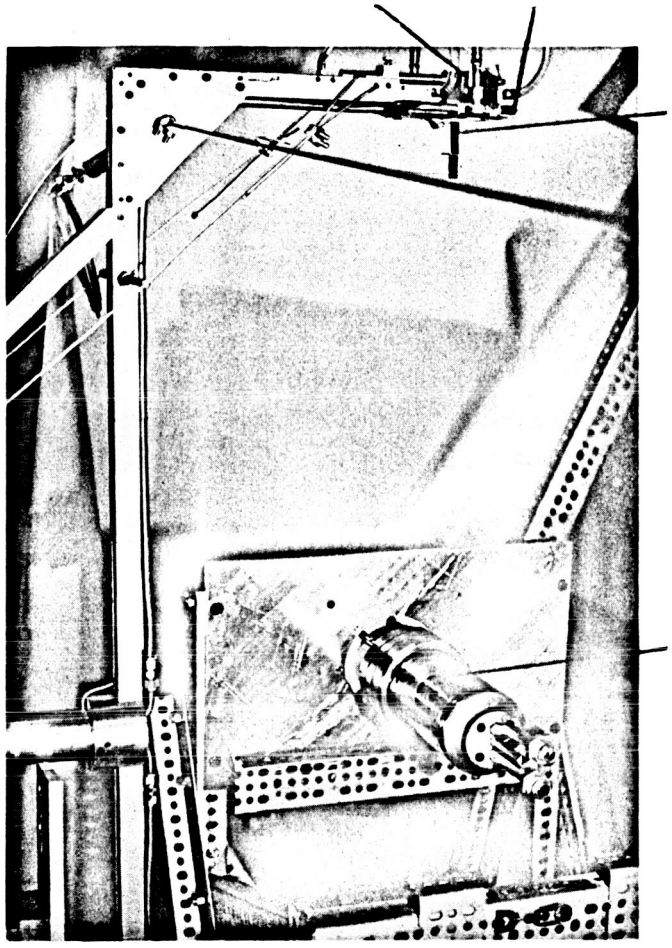
Eppley
Thermopile
Water-cooled
Shield
Occulting
Shutter
Plasma Arc
Scan
Arm
Axis

Figure 1

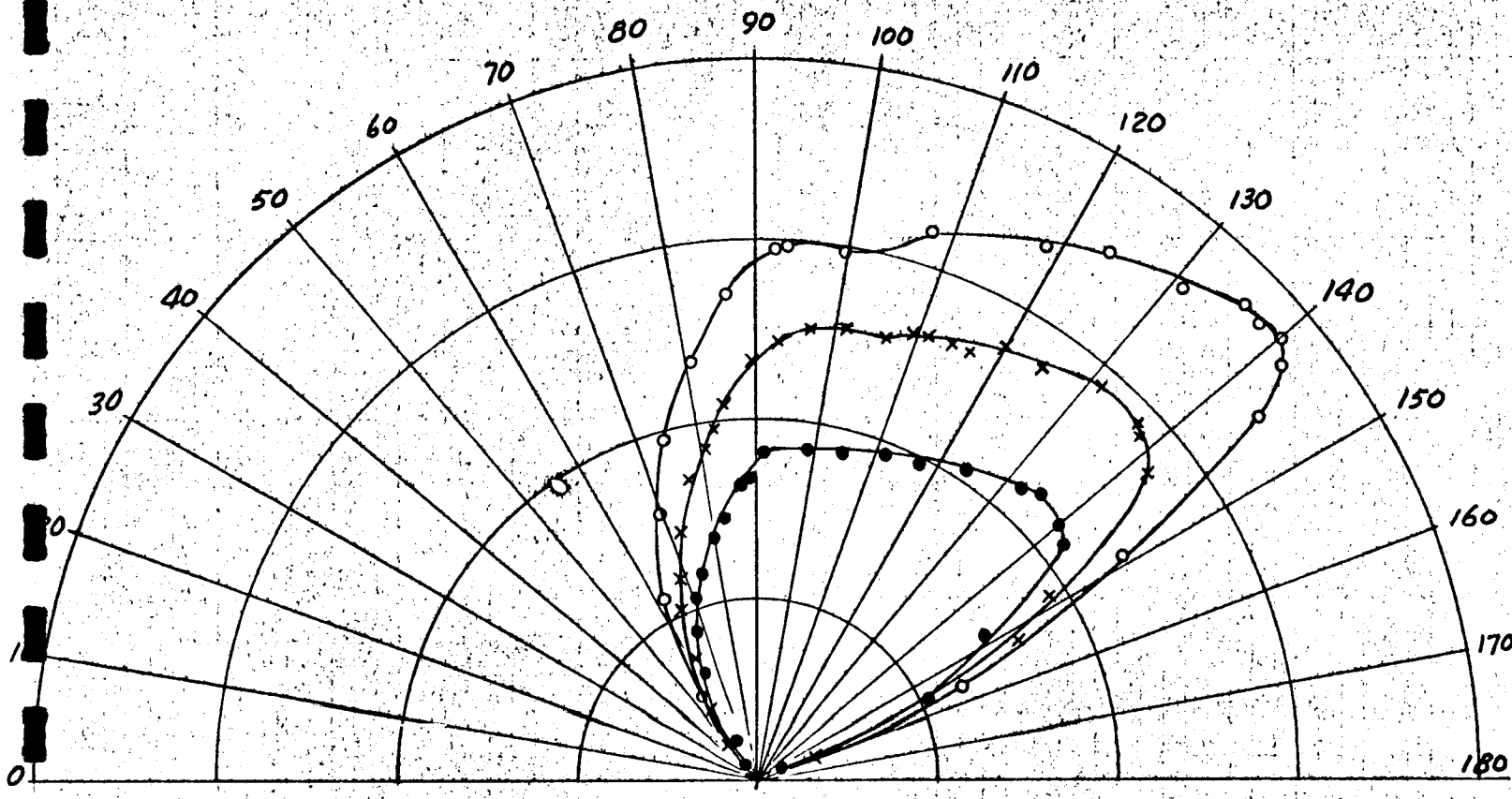

ARBITRARY UNITS

LEGEND

- • 1000 AMPS RUN 13.1
- × 1200 AMPS RUN 13.2
- ○ 1400 AMPS RUN 13.3

INTENSITY

○ RUNS 13.1, 13.2, & 13.3

FIG. 2

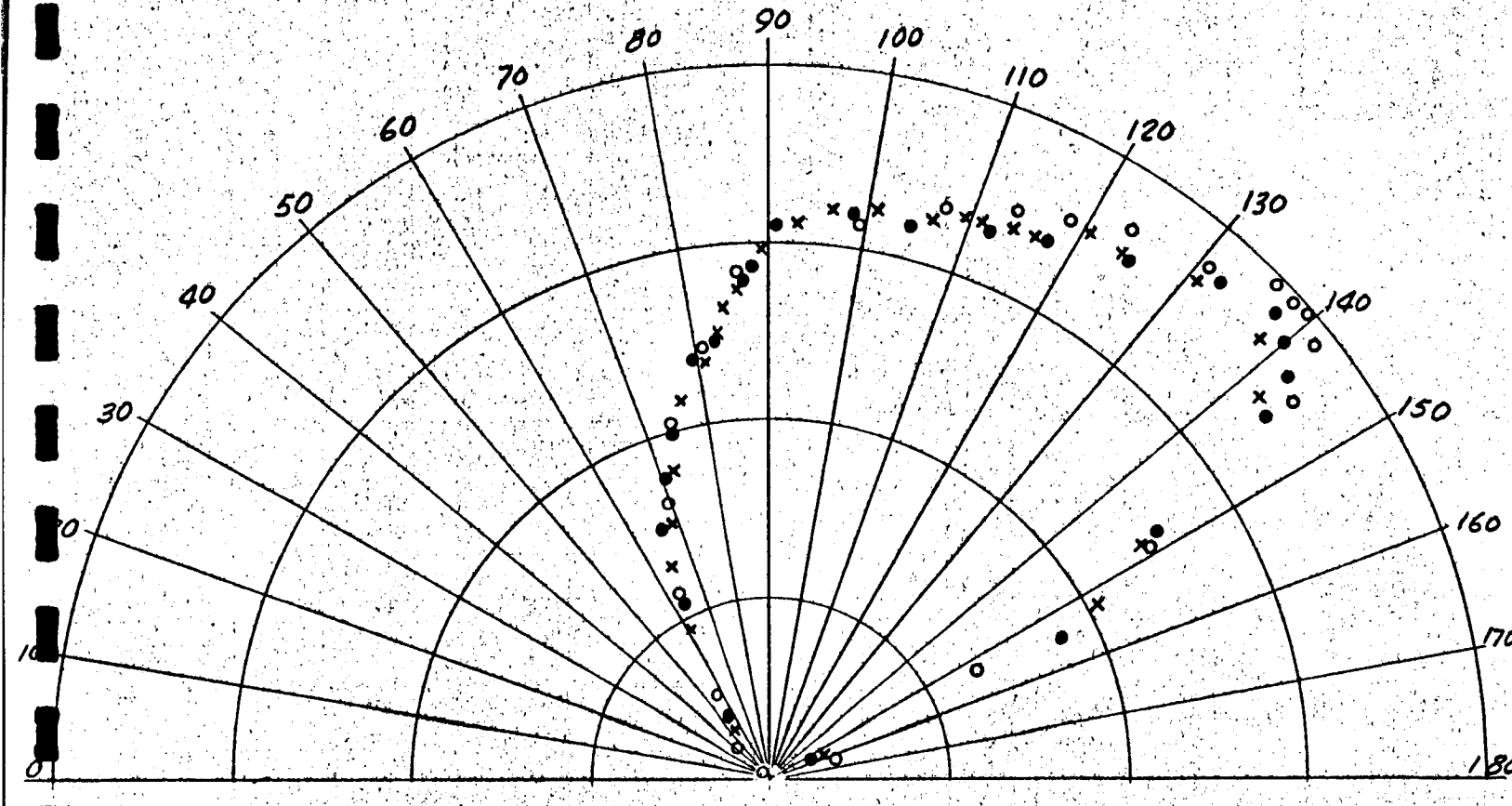

ARBITRARY UNITS

LEGEND

- • 1000 AMPS RUN 13.1
- × 1200 AMPS RUN 13.2
- o 1400 AMPS RUN 13.3

INTENSITY
NORMALIZED AT 90°
RUNS 13.1, 13.2, & 13.3

FIG 3

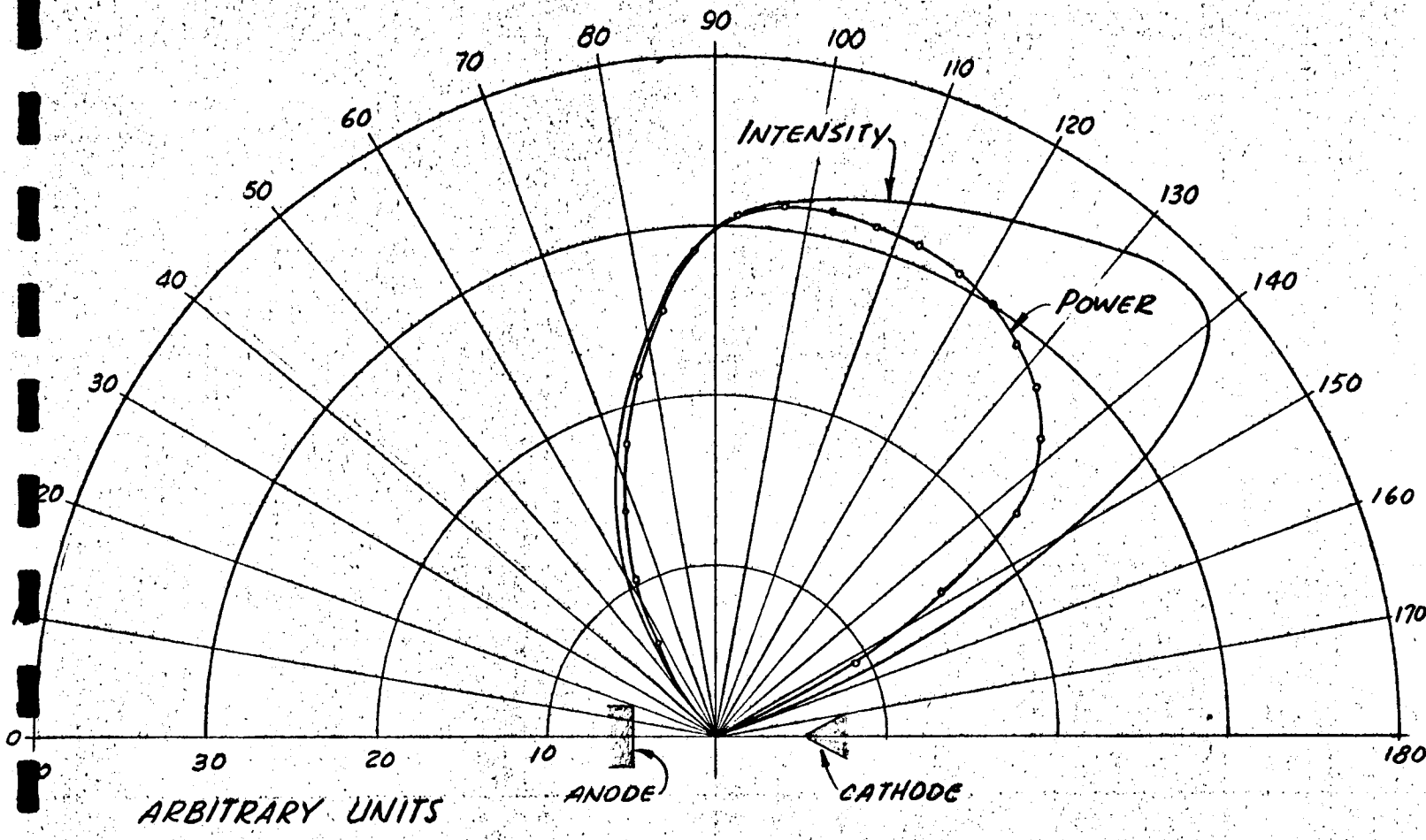

POWER & INTENSITY POLAR PLOTS
NORMALIZED AT 90°

AVERAGE CURVES OF RUNS 13.1, 13.2, & 13.3

FIG. 4

(1)	(2)	(3)	(4)	(5)	
Angular Zone	Eppley Reading mv	Zonal Constant	Zone Area cm^2	Power in Zone Watts	
45-50		.4041	2359		
50-55	.21	.4349	2539	113.9	
55-60	.32	.4623	2698	184.5	
60-65	.73	.4862	2838	442.7	
65-70	1.00	.5064	2956	631.6	
70-75	1.20	.5228	3052	782.5	
75-80	1.37	.5352	3124	914.5	
80-85	1.57	.5435	3172	1064.1	
85-90	1.71	.5476	3196	1167.8	
90-95	1.95	.5476	3196	1331.7	
95-100	1.98	.5435	3172	1342.1	
100-105	2.00	.5352	3124	1335.0	
105-110	2.03	.5228	3052	1323.8	
110-115	2.06	.5064	2956	1301.1	
115-120	2.12	.4862	2838	1285.6	
120-125	2.17	.4623	2698	1251.0	
125-130	2.24	.4349	2539	1215.2	14471.9
130-135	2.31	.4041	2359	1164.5	
135-140	2.36	.3703	2161	1089.8	
140-145	2.24	.3337	1948	932.3	
145-150	2.05	.2945	1719	753.0	
150-155	1.11	.2531	1477	350.3	
155-160	.43	.2098	1225	112.6	
			Total	20,089.6	

(1) = Zone of Polar Plot
(2) = Actual Average Eppley Reading Over Zone
(3) = Solid Angle Subtended by Zone
(4) = Zone Area cm^2 $(30.08 \times 2.54)^2$ times Zonal Constant
(5) = Zone Area Times Average Reading Divided by Eppley Constant (4.68 watts/cm^2mv)

Total Power Output = Sum of Column (5) = 20,090 watts
Total Power Collected = Sum of Column (5) up to 125° = 14,472 watts
Collection Efficiency = 72.0%

Table 1 - Reduced Data From Polar Scan (Run 13.1)

(1) Angular Zone	(2) Eppley Reading mv	(3) Zonal Constant	(4) Zone Area cm^2	(5) Power in Zone Watts	
45-50		.4041	2359		
50-55	0.30	.4349	2539	162.75	
55-60	0.60	.4623	2698	345.9	
60-65	0.90	.4862	2838	545.8	
65-70	1.42	.5064	2956	896.9	
70-75	1.60	.5228	3052	1043.4	
75-80	1.92	.5352	3124	1281.6	
80-85	2.19	.5435	3172	1484.4	
85-90	2.40	.5476	3196	1639.0	
90-95	2.60	.5476	3196	1775.5	
95-100	2.70	.5435	3172	1830.1	
100-105	2.73	.5352	3124	1822.3	
105-110	2.78	.5228	3052	1812.8	
110-115	2.85	.5064	2956	1800.1	
115-120	2.90	.4862	2838	1758.6	
120-125	2.97	.4623	2698	1712.2	
125-130	3.03	.4349	2539	1643.8	19911.4
130-135	3.10	.4041	2359	1562.7	
135-140	3.08	.3703	2161	1422.3	
140-145	2.88	.3337	1948	1198.7	
145-150	2.39	.2945	1719	877.8	
150-155	1.45	.2531	1477	457.6	
155-160	0.35	.2098	1225	91.6	
			Total	27,165.9	

(1) = Zone of Polar Plot
(2) = Actual Average Eppley Reading Over Zone
(3) = Solid Angle Subtended by Zone
(4) = Zone Area cm^2 $(30.08 \times 2.54)^2$ times Zonal Constant
(5) = Zone Area Times Average Reading Divided by Eppley Constant (4.68 watts/cm^2mv)

Total Power Output = Sum of Column (5) = 27,166 watts
Total Power Collected = Sum of Column (5) up to 125° = 19,911 watts
Collection Efficiency = 73.3%

Table 2 - Reduced Data From Polar Scan (Run 13.2)

(1) Angular Zone	(2) Eppley Reading mv	(3) Zonal Constant	(4) Zone Area cm^2	(5) Power in Zone Watts	
45-50		.4041	2359		
50-55	0.45	.4349	2539	244.1	
55-60	0.71	.4623	2698	409.3	
60-65	1.23	.4862	2838	745.9	
65-70	1.59	.5064	2956	1004.2	
70-75	1.92	.5228	3052	1252.0	
75-80	2.27	.5352	3124	1515.2	
80-85	2.64	.5435	3172	1789.4	
85-90	2.93	.5476	3196	2000.9	
90-95	3.13	.5476	3196	2137.5	
95-100	3.24	.5435	3172	2196.1	
100-105	3.32	.5352	3124	2216.1	
105-110	3.41	.5228	3052	2223.7	
110-115	3.51	.5064	2956	2216.9	
115-120	3.61	.4862	2838	2189.1	
120-125	3.71	.4623	2698	2138.8	
125-130	3.82	.4349	2539	2072.4	24360.1
130-135	3.92	.4041	2359	1976.0	
135-140	4.04	.3703	2161	1865.7	
140-145	3.99	.3337	1948	1660.1	
145-150	3.15	.2945	1719	1157.0	
150-155	1.50	.2531	1477	473.4	
155-160	0.39	.2098	1225	80.9	
			Total	33564.7	

(1) = Zone of Polar Plot
(2) = Actual Average Eppley Reading Over Zone
(3) = Solid Angle Subtended by Zone
(4) = Zone Area cm^2 $(30.08 \times 2.54)^2$ times Zonal Constant
(5) = Zone Area Times Average Reading Divided by Eppley Constant (4.68 watts/cm^2mv)

Total Power Output = Sum of Column (5) = 33,565 watts
Total Power Collected = Sum of Column (5) up to 125° = 24,360 watts
Collection Efficiency = 72.6%

Table 3 - Reduced Data From Polar Scan (Run 13.3)

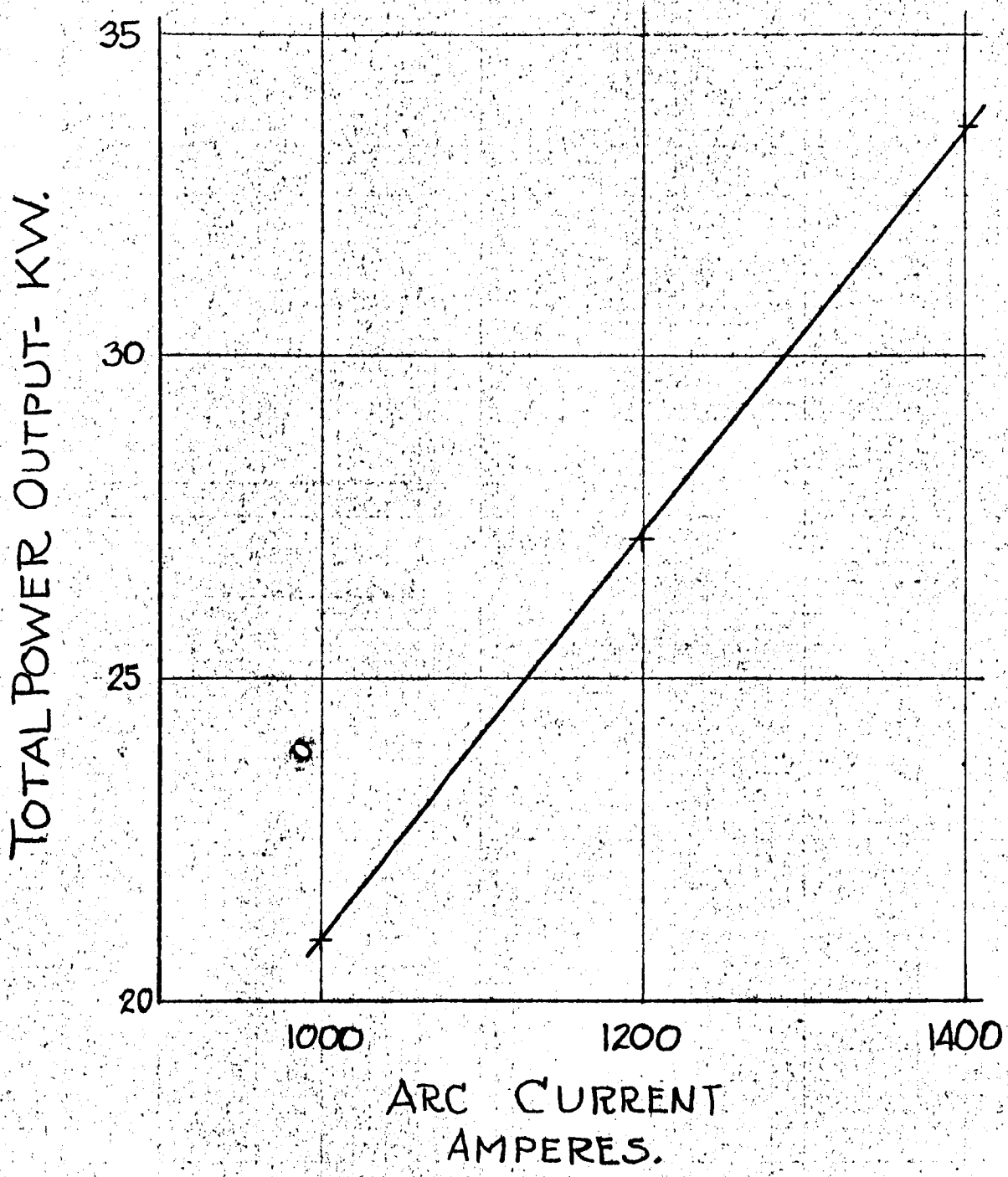
TOTAL POWER OUTPUT- KW.
35
30
25
20
1000
1200
1400
ARC CURRENT
AMPERES.

FIG. 5

DEVELOPMENT MEMORANDUM NO. 272-23

SUBJECT: Documentation of Source Performance in Test Runs 11, 12 and 13
WRITTEN BY: W. A. Geideman
DATE: December 14, 1964
JOB NUMBER: 6002-18

INTRODUCTION

The radiation source was assembled using the cathode and anode employed in Test Run Number 10 without modification. The condition of the electrodes is documented in Development Memorandum No. 272-17. The inner quartz envelope was changed since the one used in Test Run 10 had a large quantity of tungsten particles adhering to it which excessively obscured the radiation. The electrode spacing was set at 15 mm. The radiation source was installed in the special mounting employed for source evaluation tests. The installation and associated equipment in this mode of operation are described in Development Memorandum No. 272-14.

RUN NUMBER 11

Test Run Number 11 was performed on 30 October 1964. The purpose of this test was to check the relative calibration of the three sensors: Eppley thermopile #6132, the Hy-Cal calorimeter employed in Test Runs 5 through 9 (reference Development Memorandum No. 272-18) and a new Hy-Cal calorimeter with approximately one-half the sensitivity of the other one. The radiation source was ignited according to the test procedure. The first data point was taken at a current of 900 amps and a pressure of 200 psig. The recirculator pump did not operate properly because of a cavitation in head number 2. The radiation source was extinguished to check out the recirculator operation. The total duration of this short test was approximately 12 minutes. The data obtained during this run are presented in Table 1 as Point Number 11.1.

The recirculator pump was reprimed and run at approximately 200 psig gas pressure without the radiation source being ignited. Head Number 2 again cavitated after about five minutes of operation in this condition. The

cause of the cavitation was a lack of oil through the make-up pump system into the recirculator pump heads. The oil filter which had recently been installed was removed and the filter element was checked. The filter element was found to be clogged with sediment and was cleaned using Ketone and air. After the filter element was cleaned, it was replaced in the oil filter and the recirculator pump was started again. A short test run at 200 psig gas pressure indicated proper operation of the recirculator pump and the test was resumed.

The source was again ignited according to the test procedure and the operating conditions were set at 900 amps and approximately 200 psig to repeat the previous test point. Data were taken using both the Eppley and the Hy-Cal calorimeters. The current was then increased to 1,000 amps at the same pressure level and a polar intensity scan was taken. This polar intensity scan was taken at approximately the same source operating conditions as used in Test Run 1.5 where the previous polar plot was obtained. Several small pieces of the cathode ablated during this polar scan. The "flapper" on the polar scan arm stuck after completion of the polar scan and it was necessary to extinguish the radiation source in order to put the "flapper" back into operation. The duration of this test run was approximately 35 minutes.

The cause of the "flapper" sticking was a break in the cord leading to it. After this cord was repaired, the radiation source was reignited. A performance check was made at a constant pressure level of 200 psi with the current increased from 1,000 amps to 1400 amps in 100 amp increments. Data were obtained from the Eppley thermopile and the two calorimeters at each setting. After the 1400 amp data point had been obtained, the pressure was increased to approximately 250 lbs and the current reduced to 1200 amps to perform a short test as to the effects of the flow rate of argon on the radiant output of the source. These data are all presented in Table 1.

The gas flow was decreased from a meter reading of 50 to a meter reading of $46\frac{1}{2}$ and, finally, to a meter reading of 41. The Eppley thermopile was used to record the radiant intensity at each setting. Due to a fairly large amount of noise in the recorded signal from the Eppley, the data obtained in these three

tests are inconclusive although there is no indication that the intensity fell off as the flow was decreased. Rather, the data appeared to indicate an increase in radiant intensity with the decrease in flow. The duration of this third start in Test Run Number 11 was 20 minutes. The total duration of Test Run Number 11 was 67 minutes.

The radiation source was not disassembled at the completion of Test Run Number 11 since it was desired to obtain as much operation on the single set of electrodes as possible in order to evaluate their life and ablation rates. The polar plot obtained during this test run was very extensive as sufficient time was taken to assure that data were obtained at every angle of the scan arm where information was required.

TEST RUN NUMBER 12

Test Run Number 12 was performed on November 3, 1964. The purpose of this test was to check out a 1P28 photo tube and recorder which will be employed to obtain micro-radiance data on the radiation source. The radiation source was identical to that employed in Test Run Number 11. The data taken during this test are presented in Table 1. The current was varied in 200 amp increments from 1,000 to 1,400 amps at a constant gas pressure of approximately 250 psig. No intensity data were taken since the purpose of this test was merely to check out the photo tube as to its noise level and to determine if the sensitivity of the tube was proper to enable the data to be obtained at a future date.

The total duration of this test was 18 minutes, and no additional degradation of the cathode was noted. However, the screen onto which the arc was imaged had been removed for this test since this is the location of the photo tube.

TEST RUN NUMBER 13

Test Run Number 13 was performed on November 4, 1964. The purpose of this test was threefold. The first purpose was to obtain polar scans at three different current levels and at a pressure of 250 psi in order to evaluate any change in the polar intensity distribution with increasing current and pressure. The second purpose was a performance check of the radiation source at a constant

pressure level of approximately 250 lbs in order to obtain a relative calibration between the Eppley thermopile and the two Hy-Cal calorimeters. The third purpose was to obtain micro-radiance data at three different settings of the radiation source.

The radiation source was not disturbed after the completion of Test Run Number 12 and, thus, the electrodes and inner quartz envelope were identical to those employed in Test Runs 11 and 12. The raw and reduced source data for these tests are presented in Table 1.

It was necessary to repeat the sensor calibration test since the distances between the radiation source and the Hy-Cal calorimeters were not recorded in Test Run Number 11. Without accurate measurement of the distance from the arc to the sensor, no relative calibration values could be obtained. Therefore, the data obtained in Test Run Number 11 are of no value.

The first series of points were polar intensity scans at current settings of 1,000, 1,200 and 1,400 amps at a constant gas pressure of 250 psig. During this test, several particles were observed to have been ejected from the cathode. At the completion of the third polar scan, the radiation source was extinguished in order that the polar scan arm might be pinned at exactly 90° to the axis of the radiation source so that the data obtained with the Eppley thermopile would be valid in the relative calibration of the different sensors. The duration of this first part of the test was 24 minutes.

As soon as the polar scan arm had been pinned, the radiation source was reignited. A performance test was run with the current being varied in 100 amp increments from 900 to 1500 amps and with data being obtained from the three sensors. When the source was extinguished, a few small cracks were noted on the inside surface of the molybdenum diffuser of the anode. These cracks were evident in the anode viewer during the performance check and one fairly long crack was observed on the diffuser during Test Point Number 10 which was at a current level of 1500 amps. All cracks were in the radial direction. After the data had been obtained for the sensor calibration, the current was reduced to 1,000 amps and a micro-radiance distribution of the radiation source was obtained with the 1P28 photo tube.

Micro-radiance data were also obtained at a current level of 1,400 amps at a pressure of 250 psig and at a current level of 1,000 amps and a gas pressure of approximately 200 psig. During these two micro-radiance scans, several fairly large particles of tungsten were ejected from the cathode and struck the quartz envelope.

The duration of this second part of Test Run Number 13 was 63 minutes. The total duration of Test Run Number 13 was 87 minutes. At the completion of this test, the inner quartz envelope had a fairly large quantity of tungsten particles adhering to it.

The radiation source was disassembled and the electrodes and the inner quartz envelope were inspected. Figure 1 shows the anode after completion of Test Run Number 13 and a view of the inner quartz envelope used in these tests. The radial cracks in the molybdenum diffuser are quite evident in the photographs. The largest crack is located at the upper part of the picture and a fairly large crack is noticeable at the bottom in the picture. A third crack is visible in the right hand side of the picture. The quantity of tungsten particles adhering to the inner quartz envelope is quite evident from the bottom picture in Figure 1. Figure 2 shows two different views of the cathode after completion of Test Run Number 13. The erosion is fairly obvious and the cathode tip had the now familiar off-axis protrusion and overlap of the arcing surface onto the angled portion of the tungsten. The condition of the cathode at the completion of these tests may be compared with Figure 2 of Development Memorandum No. 272-17 in order to evaluate the extent of the erosion of the cathode tip during these tests.

CONCLUSIONS

The cause of the crack in the molybdenum diffuser is not evident at this time since this condition has not been observed in any of the previous test runs using the molybdenum diffuser. The ablation of the cathode does not appear to be related to the current level at which the cathode is operated since ablation occurs at current levels of 1,000 and 1,400 amps. However, there is some difference in the mode of ablation since the protrusion on the cathode tip appears

to be formed at the lower current levels while the stable operating shape at current levels in excess of 1,400 amps appears to be a flat surface. It is possible that a large amount of the ablation of the cathode tip is caused by the variations in current level which are employed in the type of tests being run at this time.

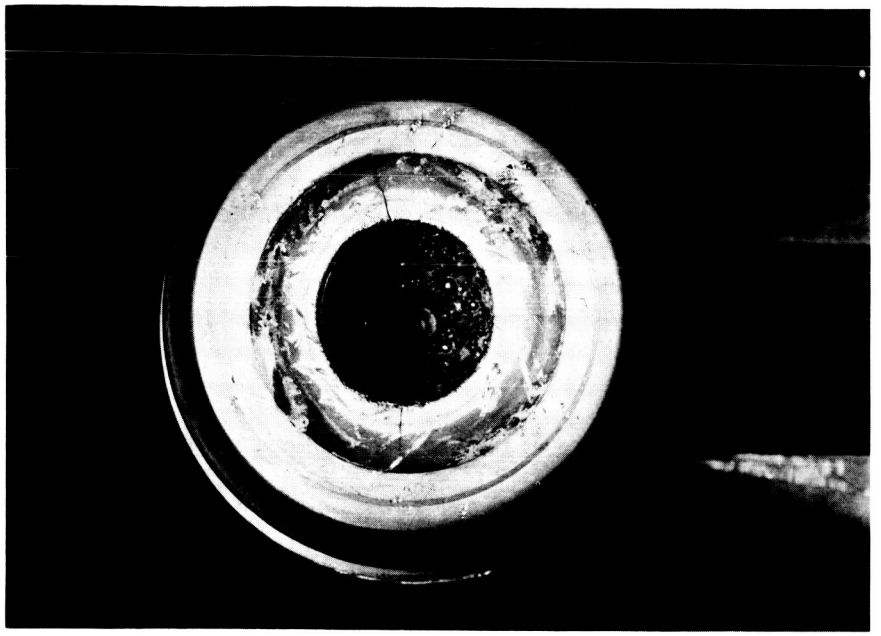

Anode Exhibiting Radial Cracks in Molybdenum Diffuser

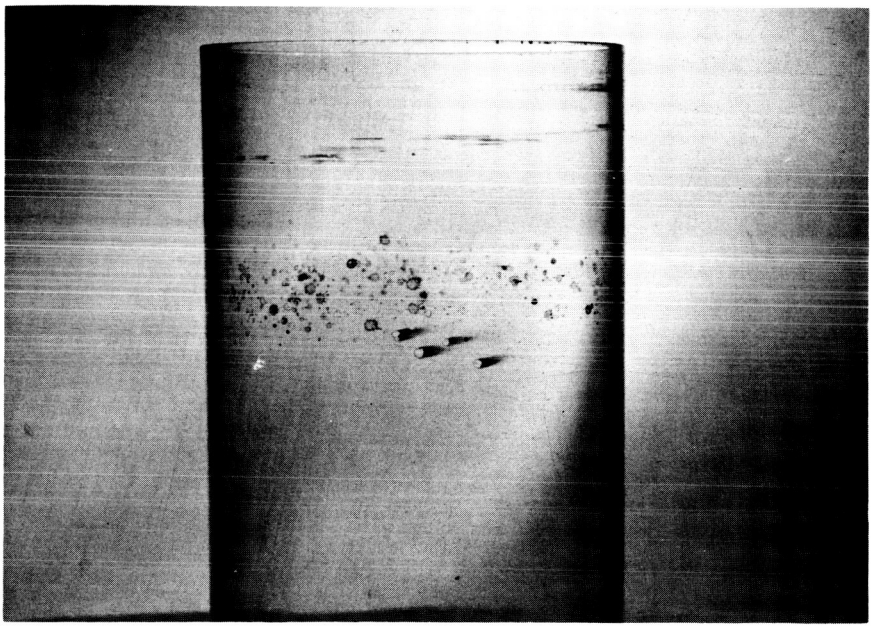

Inner Quartz Envelope Showing Deposited Tungsten Particles

Figure 1 - Condition of Anode and Inner Quartz Envelope After Completion of Test Run 13

Figure 2 - Cathode After Completion of Test Run 13

Point No.	Current Amps	Total Voltage Volts	Source Voltage Volts	Total Power KW	Source Power KW	Gas Pressure psig	Gas Flow Reading	Running Time min.
11.1	900	75.9	63.6	68.3	57.2	204	48	447.5
11.2	900	75.0	62.7	67.5	56.4	198	47	453.0
11.3	1000	78.2	64.4	78.2	64.4	198	46.5	458.0
11.4	1000	79.9	66.1	79.9	66.1	200	46.6	486.0
11.5	1100	82.7	67.3	91.0	74.0	205	47	
11.6	1200	85.9	68.9	103.1	82.7	203	47	
11.7	1300	89.3	70.7	116.1	91.9	203	47	494.0
11.8	1400	92.7	72.6	129.8	101.6	200	46.6	
11.9	1200	88.2	71.2	105.8	85.4	248	50	498.3
11.10	1200	88.4	71.4	106.1	85.7	245	46.5	
11.11	1200	89.6	72.6	107.5	87.1	245	40.2	506.8
12.1	1000	84.3	70.5	84.3	70.5	250	49.8	506.8
12.2	1200	91.3	74.3	109.6	89.2	251	50	516.3
12.3	1400	98.6	78.5	138.0	109.9	252	48	525.0
13.1	1000	83.5	69.7	83.5	69.7	245	50	525.3
13.2	1200	90.3	73.3	108.4	88.0	250	50	534.5
13.3	1400	96.3	76.2	134.8	106.7	209	50	541.3
13.4	900	81.9	69.6	73.7	62.6	248	50	549.4
13.5	1000	84.0	70.2	84.0	70.2	248	50	551.9
13.6	1100	87.1	71.7	95.8	78.9	255	50	552.9
13.7	1200	89.4	72.4	107.3	86.9	248	50	556.7
13.8	1300	92.9	74.3	120.8	96.6	248	50	557.9
13.9	1400	96.4	76.3	135.0	106.8	254	50	559.8
13.10	1500	100.2	78.6	150.3	117.9	255	50	560.8
13.11	1000	85.1	71.3	85.1	71.3	253	50	580.7
13.12	1400	96.5	76.4	135.1	107.0	255	50	592.1
13.13	1000	79.3	65.5	79.3	65.5	204	47	605.6

Table 1 - Raw and Reduced Radiation Source Data - Test Runs 11, 12 and 13

DEVELOPMENT MEMORANDUM NO. 272- 24

SUBJECT: Radiation Source Life Tests (Runs 14 Through 19 and 22)

WRITTEN BY: W. A. Geideman
DATE: December 14, 1964
JOB NUMBER: 6002-16

INTRODUCTION

Because of the uncertainty as to the exact qualification of the final radiation source in its present stage of development for the radiative heating system at NASA/Ames, it was deemed necessary to specify the life requirements of the radiation source. The operating conditions to which the radiation source will be subjected during operation in the final system at NASA/Ames were defined as a series of relatively short test runs with a maximum of five minutes duration at the rated power level. Therefore, the life test requirements on the final radiation source were specified to determine the actual life of the source when simulating the conditions to be encountered in the final system.

From the data obtained during the prototype test runs as reported in Development Memorandum 272-18, it was ascertained that the rated operating conditions of the radiation source to provide a reasonable assurance of satisfying the minimum required target power intensity are a current level of at least 1550 amps and a pressure in the radiation source of approximately 250 psig.

The radiation source was assembled using a new anode with the copper-molybdenum composite diffuser having an ID of .650", a new inner quartz envelope and the cathode shown in Figure 1. This cathode was reworked after the completion of Test Run 13 to provide the hemispherical shape shown in Figure 1. The arc gap was set at 15 mm being the distance from the closest point of the cathode to the front surface of the anode.

The radiation source was installed in the test facility using the test setup employed for source evaluation tests as described in detail in Development Memorandum 272-14. The Eppley thermopile was installed in the polar scan

arm to record the radiant intensity during operation. The polar scan arm was pinned at the 90° position relative to the arc axis. The lens system used for projecting the arc image during operation was employed, as well as the telescopic anode viewer mechanism.

TEST PROCEDURE

A test procedure for operating the radiation source during life tests was drawn up. This procedure was as follows: the source was ignited at a gas pressure of approximately 50 psig and then the gas pressure was increased to approximately 250 psig while maintaining the arc current at a minimum of 700 amps. While the gas pressure was approaching the desired setting, the bypass on the gas recirculator system was adjusted to provide a gas flow meter reading of approximately 40. After the gas flow and pressure had been set at the desired values, the current was increased fairly rapidly to the 1550 amp value. As soon as the desired test conditions had been obtained, a complete data point was recorded including an Eppley reading. After $2\frac{1}{2}$ minutes of operation at a minimum of 1550 amps, a second Eppley reading was obtained. At the completion of the five minutes of operation, a second data point was obtained along with a third Eppley reading. Since the recording of data was started at the five minute operation time, the total duration of each test at the desired conditions was guaranteed to be in excess of five minutes. The strip chart recorder measuring the output of a solar cell located in the source test area gave a secondary indication of the elapsed time of the test in addition to the primary indication used by the operator. The primary indicator was a stop watch. The arc was observed continuously through both the anode viewer and the projected arc image. The stop watch for timing the run was not started until the minimum operating conditions had been obtained.

The current level and gas pressure setting were selected on the basis of the data obtained during the prototype tests as described previously. The gas flow setting decided upon was based on the results of Test Run 13 as described in Development Memorandum 272-23.

TEST DATA

Because of the intermittent nature of the life test requirements on the final radiation source, the data are presented as several runs. The first life test series is covered in Test Runs 14 through 19. This series represents a total of seventeen complete cycles without touching the radiation source itself. Some minor modifications in the radiation source system were made between cycles in this test series. These modifications were primarily related to fixing the gas hoses at the control console to eliminate gas leaks.

Table 1 presents all the raw and reduced test data obtained during this first test series. In addition to the source operating parameters, Table 1 presents the intensity reading in millivolts as obtained from the Eppley thermopile. The cycle number is listed after the first data point for each cycle.

The first run in the life test series deviated slightly from the test procedure outlined above in that a performance check was made at various current levels from 1,000 to 1,550 amps before the five minute life test was initiated. This test is documented as Test Run 14 and was performed on November 12, 1964. When the current reached the 1,500 amp level, the tip of the cathode ablated with a resultant impingement of a large quantity of tungsten particles onto the inner envelope. This ablation included the complete hemispherical cap of the cathode leaving a flat as the arcing surface. At 1,550 amps, the cathode operated stably from this fairly large diameter flat. The arc gap was increased by a small amount due to the fairly large amount of tungsten which was ablated. The intensity listed at Test Point 14.8 is the average intensity obtained in four readings taken during the five minute life test duration. The maximum source power ever obtained with either the final radiation source or the experimental radiation source as previously tested at Giannini Scientific was the 132.6 KW obtained in Test Point 14.9.

The radiation source was extinguished after the data in Test Point 14.9 had been recorded. After approximately five minutes of down time, the source was reignited according to the test procedure. Test Runs 15 through 19 represent the additional cycles obtained during this life test series and all cycles

were performed exactly as described in the test procedure. A minimum of five minutes down time was provided after each cycle. The ablation of the cathode continued during the succeeding test cycles but at a much reduced rate as compared to the ablation encountered during Test Run 14. In the sixth cycle, the current was increased accidentally to a value of 1,600 amps. After a short time at this current level, the excessive value was noticed and the current was reduced to 1,560 amps. However, the operation of the radiation source at 1,600 amps probably produced a very slight erosion of the molybdenum ID since the voltage after this condition did not reach the values previously obtained. The total voltage drop decreased by approximately two volts as a result of this over current operation. The arc current level reached a value of 1,620 amps during the eighth test cycle. This again caused a further erosion of the diffuser, resulting in a decrease of approximately one volt in the total voltage drop. The lower voltage operation of the radiation source following the operation at excessive current levels resulted in a decrease in the radiant intensity as measured by the Eppley thermopile. These observations are apparent from a detailed study of the data presented in Table 1.

At the completion of the fifteenth cycle, the radiation source system was shut down in order to repair a gas hose leading from the console to the radiation source. The last two cycles of this test series were run on November 13, 1964. During the seventeenth and last cycle, a cloudiness was observed to form on the inner quartz envelope. This cloudiness was observed at the beginning of the test and did not appear to change during the five minutes of operation. The presence of this cloudiness on the inner quartz envelope resulted in a decision to discontinue the life tests at this point in order to evaluate its cause.

The condition of the inner quartz envelope at the completion of the life tests is shown in Figure 2. The top photograph in Figure 2 shows the entire quartz envelope. The ring on the left of the photograph is in the area immediately in front of the vortex injector holes and is believed to be contamination brought to the lamp by the gas stream. The cloudiness

which caused the test to be terminated is shown in the right center of the photograph and is also shown in an enlarged photograph in the bottom picture of Figure 2. The cloudiness was limited to only that portion of the envelope where it is evident in the photographs. The spots below the cloudiness represent the tungsten particles which impinged onto the envelope due to the ablation of the cathode tip. It is estimated that over 90% of these marks occurred during Test Run 14. It is believed that the cloudiness on the quartz was due to contamination and not to any action of the radiation source itself. In the bottom photograph of Figure 2, a portion of the cloudiness has been removed as is shown on the left side of the occluded area.

This cloudiness is not believed to be devitrification since the cloudiness occurred in only a small area of the inner envelope and did not occur in a circumferential manner. In addition, the cloudiness was not located in the region where the maximum power from the arc is transmitted through the quartz envelope. Thus, the only explanation for the occurrence of this cloudiness is contamination of some form probably carried by the argon.

Figure 3 shows two views of the cathode condition after the completion of Test Run 19. The amount of ablation of the cathode tip can be estimated by comparing these photographs with Figure 1 which shows the cathode condition prior to Test Run 14. The cathode was measured to determine the amount of ablation and the geometry following the life test series. The overall length of the cathode to the highest point of the tip (reference top photograph, Figure 3) was 3.990". The overall length to the flat portion of the tip was 3.940". The projection on the cathode tip was elliptical in shape with a major axis of .160" and a minor axis of .100". The diameter of the flat on the cathode was approximately .310". The overall length of the cathode to the highest point of the hemispherical surface when installed at the beginning of this test series was 4.080".

The condition of the anode at the completion of Test Run 19 is shown in the top photograph of Figure 4. The bottom photograph in Figure 4 shows the anode clamp ring after removal of the quartz envelope but prior to the

removal of the anode itself. The front surface of the anode diffuser contains a fairly large number of pits due to the impingement of tungsten particles during operation. The diffuser diameter was measured to be .650" after the anode had been removed. The purpose of presenting the photograph of the anode clamp ring is to indicate the large deposits of tungsten particles on the O-ring seal for the inner quartz envelope. A large majority of the tungsten particles which impinged on the inner quartz envelope during Test Run 14 were removed from the envelope by action of the gas vortex and were collected on the O-ring seal around the anode clamp ring.

Following completion of Test Run 19, the radiation source was reassembled for spectral tests. The source operation during these tests is covered in Development Memorandum 272-25. After these spectral tests had been completed, the radiation source was reassembled using the cathode as shown in Figure 2. A new anode and a new inner quartz envelope were employed. The radiation source was then installed in the test facility for a continuation of the life tests.

Test Run 22 which represents the second series of life test cycles was performed on November 18, 1964. The raw and reduced data obtained during this test are presented in Table 2. The test procedure used during Test Run 22 was identical to that described above except that the data obtained in the second test point were not recorded if they agreed essentially with the data obtained during the first data point. Thus, each point in Test Run 22 represents a cycle of the life test operation. This life test was terminated after the eighth cycle when oil was noticed in the flow meters in the control console. In addition, contamination of the inner quartz envelope similar to that shown in the left of the top photograph in Figure 2 was observed. The contamination was greater during Test Run 22 than in the previous test series.

Cathode ablation during these eight cycles was very slight and no particles adhered to the inner envelope. The cathode shape at the completion of the eighth cycle was approximately identical to that shown in Figure 3.

The reason for the reduced arc voltage and the reduced intensity readings was that the arc gap was set at 15 mm prior to the start of this test and remained at this approximate value throughout the test.

CONCLUSIONS

The reasons for termination of both life test series were related to the radiation source system, namely the recirculator pump, and were not connected with the radiation source itself. The condition of the electrodes at the completion of both test series was such that the tests could have been continued for an undetermined length of time before failure of the radiation source would have occurred. The condition of the inner quartz envelope at the completion of both test series would have been sufficient to allow an undetermined number of cycles to have been achieved if the contamination due to the presence of oil in the gas stream had not been encountered. The cleaning action of the gas vortex on the inner quartz envelope as evidenced during the first test series is encouraging in regard to the life of the radiation source.

In general, no conclusion as to the life of the radiation source itself can be obtained from either of these test series. The only useful conclusion as to the life of the radiation source is that a minimum of seventeen cycles at the conditions employed can be obtained without failure of the source.

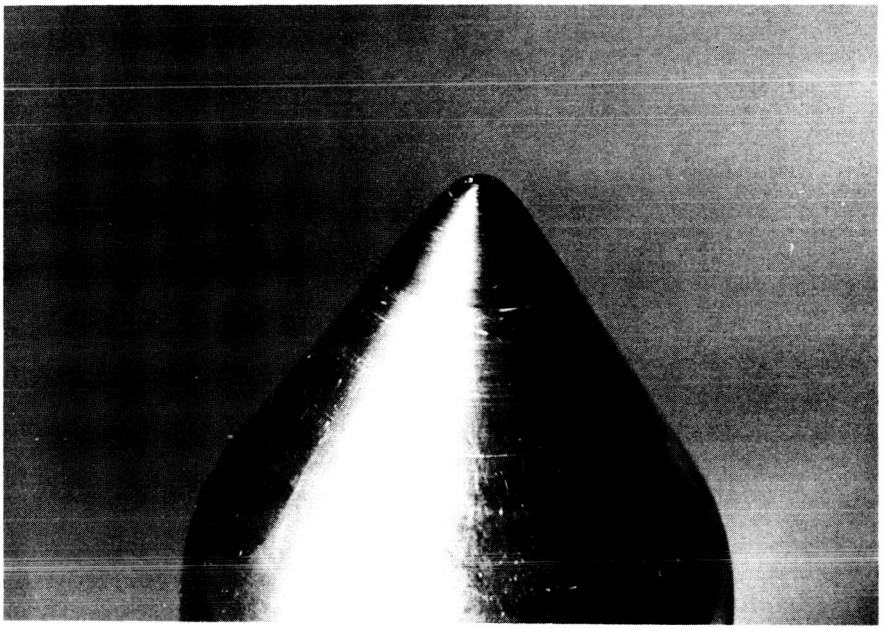

Figure 1 - Cathode Prior to Assembly

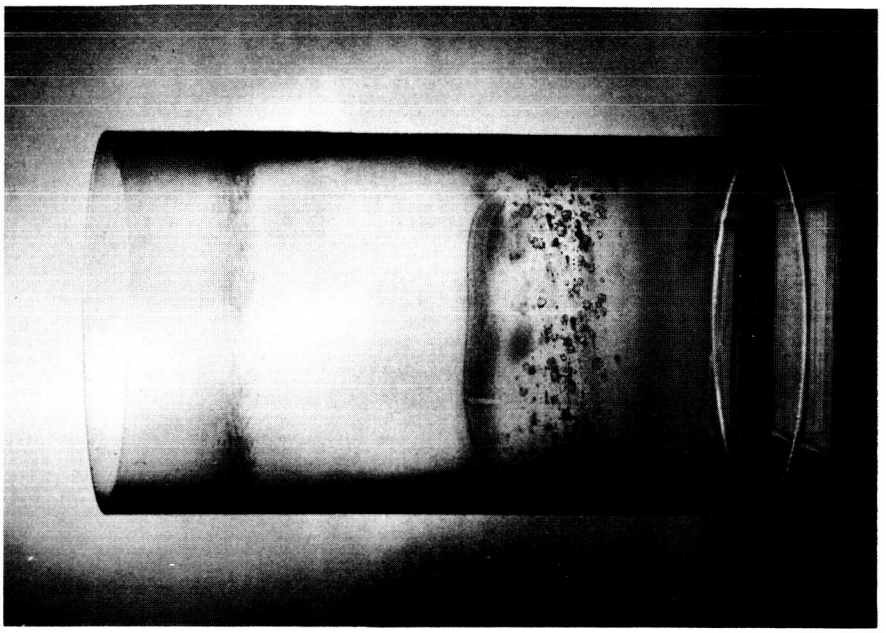

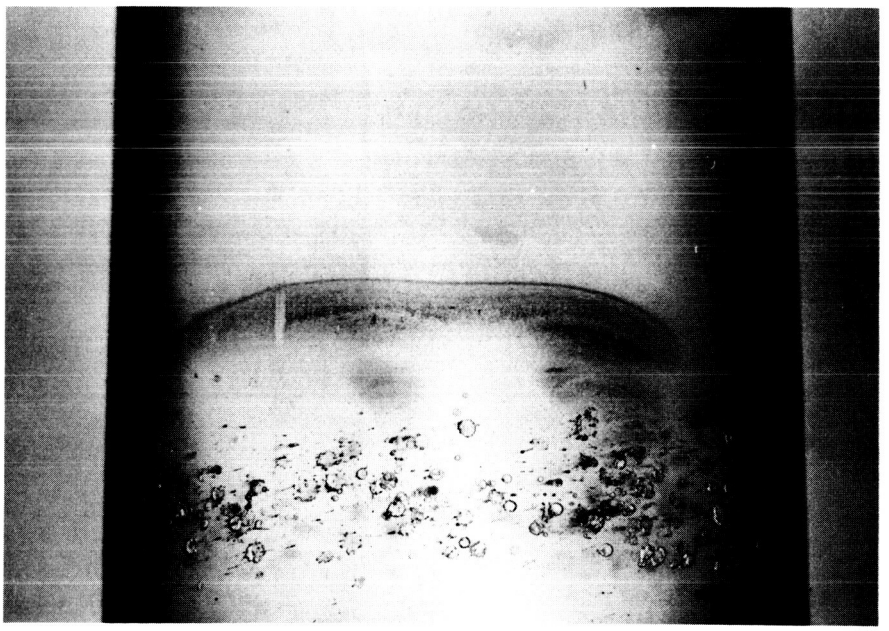

Figure 2 - Condition of the Inner Quartz Envelope After Completion of Test Run 19

Figure 3 - Condition of the Cathode After Completion of Test Run 19

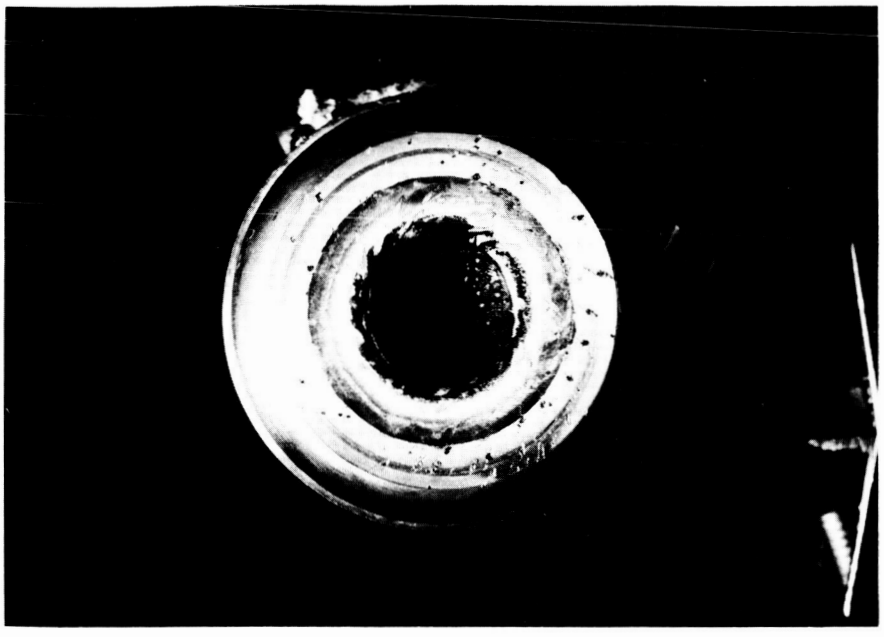

Anode After Test Run 19

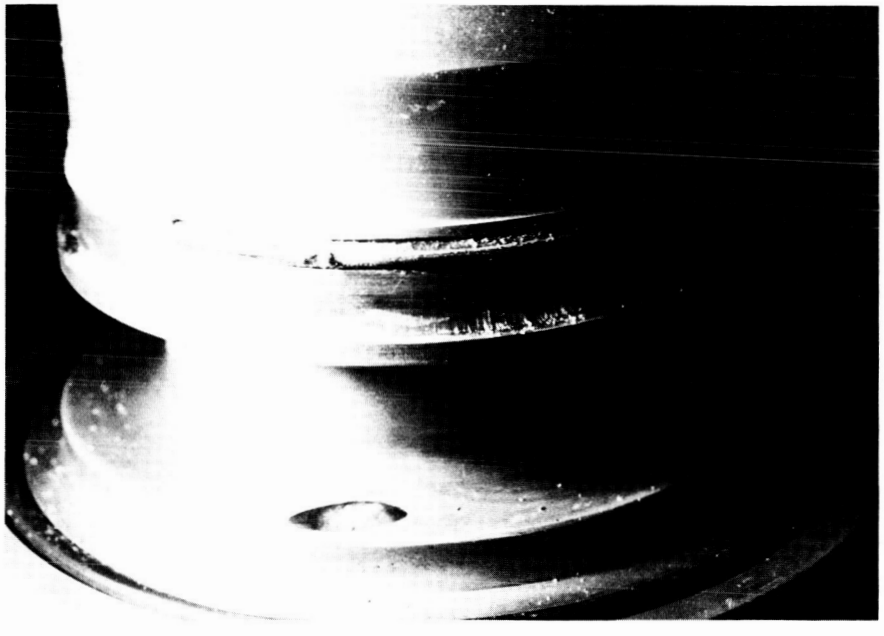

Anode Clamp Ring Showing Tungsten Particles Resting on O-Ring

Figure 4 - Condition of the Anode and Anode Clamp Ring After Completion of Test Run 19

Point No.	Current Amps	Total Voltage Volts	Source Voltage Volts	Total Power KW	Source Power KW	Gas Pressure psig	Gas Flow Reading	Running Time min.	Intensity mv.	Cycle No.
14.2	1000	80.3	66.5	80.3	66.5	245	41	642.0	1.99	
14.3	1100	84.2	68.8	92.6	75.7	243	40.5	643.4	2.34	
14.4	1200	87.1	70.1	104.5	84.1	248	40.5	644.7	2.61	
14.5	1300	91.4	72.9	118.8	94.8	248	41	645.3	3.01	
14.6	1400	95.8	75.7	134.1	106.0	250	41	645.9	3.34	
14.7	1500	99.3	77.7	149.0	116.6	253	41	647.3	3.64	
14.8	1550	103.2	80.8	160.0	125.2	255	41	648.2	3.81	1
14.9	1560	107.6	85.0	167.9	132.6	254	40.5	653.5		
15.1	1550	101.9	79.5	157.9	123.2	248	39	656.4		2
15.2	1560	101.3	78.7	158.0	122.8	252	38	662.0	3.80	
15.3	1560	102.4	79.8	159.7	124.5	250	39	667.0	3.85	3
15.4	1540	100.2	77.9	154.3	120.0	248	39	668.0	3.70	
15.5	1580	102.3	79.4	161.6	125.4	253	41	670.3	3.90	4
15.6	1560	100.7	78.1	157.1	121.8			672.4	3.75	
15.7	1560	100.6	78.0	156.9	121.7	245	39	675.9	3.75	
15.8	1560	102.6	80.0	160.1	124.8	256	42.5	677.2	3.75	5
15.9	1560	102.3	79.7	159.6	124.3	245	39	682.8	3.80	
16.1	1600	102.4	79.2	163.8	126.7	251	40.5	684.3	3.85	6
16.2	1560	100.3	77.7	156.5	121.2				3.78	
16.3	1560								3.77	
16.4	1560	100.3	77.7	156.5	121.2	248	38.5	689.5	3.78	
16.5	1560	101.4	78.8	158.2	122.9	255	42	691.3	3.75	7
16.6	1560								3.75	
16.7	1560	100.0	77.4	156.0	120.7	255	40	696.4	3.75	
16.8	1560	102.1	79.5	159.3	124.0	252	43	698.3		8
16.9	1620							699.7	3.75	
16.10	1560	99.9	77.3	155.8	120.6	255	41	703.4	3.60	
17.1	1560	99.4	76.8	155.1	119.8	252	41.5	705.8	3.74	9
17.2	1560	98.8	76.2	154.1	118.9	248	39	710.5	3.68	
17.3	1560	99.5	76.9	155.2	120.0	255	41	713.0	3.65	10
17.4	1560	98.5	75.9	153.7	118.4	248	40.5	717.7	3.61	
17.5	1560	99.3	76.7	154.9	119.7	250	40	720.3	3.65	11
17.6	1560	98.8	76.2	154.1	118.9	255	39	725.0		
17.7	1560	98.5	75.9	153.7	118.4	253	41	726.9	3.57	12

Table 1 - Raw and Reduced Radiation Source Data - Test Runs 14 through 19

Table 1 - Raw and Reduced Radiation Source Data - Test Runs 14 through 19 (Continued)

Point No.	Current Amps	Total Voltage Volts	Source Voltage Volts	Total Power KW	Source Power KW	Gas Pressure psig	Gas Flow Reading	Running Time min.	Intensity mv.	Cycle No.
17.8	1560	98.5	75.9	153.7	118.4	255	41	731.6	3.59	
17.9	1580	99.5	76.6	157.2	121.0	248	41	733.8		13
17.10	1560	98.3	75.7	153.3	118.1	248	41	738.5	3.60	
18.1	1570	99.4	76.7	156.1	120.4	255	41	740.5	3.56	14
18.2	1560	98.3	75.7	153.3	118.1	254	41	745.3	3.60	
18.3	1600	99.6	76.4	159.4	122.2	248	41	747.3	3.69	15
18.4	1560	98.6	76.0	153.8	118.6	248	41	752.1	3.61	
19.1	1600	100.0	76.8	160.0	122.9	253	43	754.2	3.61	16
19.2	1560	97.6	75.0	152.3	117.0	240	41	758.9	3.52	
19.3	1580	99.1	76.2	156.6	120.4	248	41	761.0	3.50	17
19.4	1570	98.9	76.2	155.3	119.6	252	41	765.8	3.50	

Point No.	Current Amps	Total Voltage Volts	Source Voltage Volts	Total Power KW	Source Power KW	Gas Pressure psig	Gas Flow Reading	Running Time min.	Intensity mv.	Cycle No.
22.1	1560	93.9	71.3	146.5	111.2	250	42	863.0	3.51	1
22.2	1550	93.5	71.1	144.9	110.2	248	42	873.6	3.43	2
22.3	1550	93.9	71.5	145.5	110.8	252	41.5	878.7	3.41	3
22.4	1560	93.8	71.2	146.3	111.1	252	41.7	887.7	3.38	4
22.5	1560	94.0	71.4	146.6	111.4	250	41.5	892.8	3.38	5
22.6	1560	93.4	70.8	145.7	110.4	252	42.5		3.30	6
22.7	1560	93.1	70.5	145.2	110.0	250	41.5	906.6	3.32	7
22.8	1560	93.3	70.7	145.5	110.3	252	42.9	915.3	3.30	8

Table 2 - Raw and Reduced Radiation Source Data - Test Run 22

SPECTROLAB

DEVELOPMENT MEMORANDUM NO. 272-25

SUBJECT: Documentation of Source Operation During Spectral Tests (Runs 20 and 21)
WRITTEN BY: W. A. Geideman
DATE: 14 December 1964
JOB NUMBER: 6002-60

INTRODUCTION

The radiation source was assembled using a new anode and the cathode employed in Test Run 13. The arc gap was set at 15 mm, and the source was installed in the source evaluation test setup as described in Development Memorandum 272-14.

The purpose of these tests was to obtain the spectral distribution of the radiant energy from the radiation source at three different operating conditions. The setup of the spectral instrumentation will be described in the Development Memorandum which presents the spectral data. The operating conditions chosen were 1,000 amps at 200 psig; 1,000 amps at 250 psig; and 1,400 amps at 250 psig. These conditions were chosen in order to provide an indication of any variation in spectral output of the radiation source as a function of pressure and also as a function of current.

TEST RESULTS

The raw and reduced data from the radiation source are presented in Table 1. Test Run 20 was performed on 16 November 1964. The total duration of this test was 63 minutes. Spectral data were obtained using a 1P28 detector.

Test Run 21 was performed on 17 November 1964 and lasted for a duration of 31.5 minutes. Spectral data were obtained using a lead sulphide detector.

No additional significant information concerning the operation of the radiation source was obtained during these test runs except for the spectral distribution. The spectral data will be presented in a future development memorandum.

Point No.	Current Amps	Total Voltage Volts	Source Voltage Volts	Total Power KW	Source Power KW	Gas Pressure psig	Gas Flow Reading	Running Time min.
20.1	1000	75.5	61.7	75.5	61.7	200	47	766.4
20.2	1000	78.4	64.6	78.4	64.6	250	43	794.4
20.3	1400	90.5	70.4	126.7	98.6	250	41	805.3
20.4	1400	91.5	71.4	128.1	100.0	250	41	830.2
21.1	1000	76.0	62.2	76.0	62.2	200	46.5	830.2
21.2	1000	79.5	65.7	79.5	65.7	250	41.5	841.5
21.3	1400	91.4	71.3	128.0	99.8	250	39.5	852.5
21.4	1400	91.2	71.1	127.7	99.5	248	39.5	863.2

Table 1 - Raw and Reduced Radiation Source Data - Test Runs 20 and 21

SPECTROLAB

DEVELOPMENT MEMORANDUM NO. 272-27

SUBJECT: Spectral Distribution of 150 KW Plasma Radiation Source

WRITTEN BY: Dave Guerrero
DATE: January 12, 1965
JOB NUMBER: 6002-60

INTRODUCTION

The spectral distribution of the 150 KW plasma radiation source was measured using both the 1P28 and lead sulfide quantum detectors, and the double prism monochromator. Data were obtained at three different settings of the plasma radiation source as shown in Table A. The total irradiance of the plasma source was measured with an Eppley thermopile (Serial Number 6132) at a distance of 29.725 inches from the center of the arc. The total irradiance measured at each test condition is also presented in Table A.

This memorandum presents the data reduction procedure and the actual spectral distribution curves which were obtained. A subsequent development memorandum, Number 272-28, will present details on the measurement procedure and the derivation of radiometric values.

RESULTS

The spectral distribution data were read into a Fortran program compatible with the IBM 7090 to reduce the data. Spectral curves 1, 2 and 3 are the spectral distributions plotted every 0.01μ in the interval from 0.25μ to 2.7μ. The absolute spectral irradiance in mw/cm^2-0.01μ was obtained by relating the total area under the relative spectral distribution curve with the total irradiance as measured by the Eppley thermopile. Thus, this absolute spectral irradiance constitutes what would be achieved at a distance of 29.725 inches from the center of the arc and perpendicular to the axis of the arc. Spectral Curves 4, 5 and 6 depict the spectral distribution integrated over 0.05μ bands in the same interval. The absolute spectral irradiance is given in the same units as in Spectral Curves 1, 2 and 3, in order to allow comparison of the integrated curves with the unintegrated distribution. The scales on all six curves are identical to facilitate the comparison of one run with another.

The spectral distribution curves were produced by numerical techniques for correlating the relative spectral response at different wavelengths and by normalizing the relative responses of the two detectors to produce a continuous curve over the entire spectrum from 0.25 to 2.70μ. The data reduction procedure did not include an error analysis to compensate for errors arising from the numerical manipulations. Such an error analysis, e.g. round-off, could provide greater confidence levels in the spectral distribution. The computer program and the actual data reduction as performed by the computer are available at Spectrolab if further inspection of the data or additional analyses of the data are desired.

CONCLUSIONS

The spectral distribution did not change appreciably as the pressure was increased from 200 to 250 psi at a constant current level of 1,000 amps. This is readily apparent from a close examination of Spectral Curves 1,2,4, and 5. However, the increase in current from 1000 amps to 1400 amps at a constant pressure level of 250 psi produced an appreciable change in the spectral distribution of the plasma radiation source. The ultraviolet section of the spectral region showed a much greater increase in intensity than did the infrared region. In fact, Curve 6 shows that the ultraviolet peak is higher than the infrared peak at 1400 amps. The converse is true in all curves for the operating condition of 1000 amps.

DATA REDUCTION

The factors considered in the reduction of the raw data to attain the absolute spectral irradiance were as follows:

1. Calibration of the Detectors
2. Application of the Calibration Factor to the Data
3. Numerical Integration of the Calibrated Data Over Each .05μ Wavelength Band
4. Computation of the Correction Factor to Relate the 1P28 Data with the Lead Sulfide Data
5. Normalization of the Lead Sulfide Data
6. Conversion from Relative Units to Absolute Units

Calibration of Detectors: The output of each detector was calibrated using a standard lamp which was obtained from the National Bureau of Standards as a primary calibration source. The lamp used was a QL 118 standard lamp. The spectral output of this lamp was measured with both detectors at Spectrolab, and the spectral measurements were compared with the measurement by the National Bureau of Standards on the same lamp. This comparison produced a set of calibration factors for each wavelength interval. The calibration factor was chosen to be the NBS measurement divided by the Spectrolab measurement, in order that the output of the Spectrolab detector could be multiplied by the calibration factor. Calibration factors for every .01μ in the interval of 0.25μ to 2.7μ were obtained using the computer.

Application of the Calibration Factor to the Data: The spectral measurements obtained with the 1P28 and lead sulfide detectors were calibrated by multiplying the raw data by the calibration factor as obtained above. Thus, a set of calibrated spectral data of the radiation source was obtained. This set of data is the relative response of the detector. Since a change of the gain settings in the electronics associated with the monochromator was necessary because of the different levels of output of the two detectors, an adjustment ratio was applied to the lead sulfide data in order to calibrate this lead sulfide data to the 1P28 data. The adjustment factor was merely the ratio of the gain settings.

Numerical Integration of the Calibrated Data of Each .05μ Wavelength Band: In order to obtain greater confidence in the choice of a normalizing factor to match the detector output, the calibrated data was integrated over every .05μ band in the range of interest. This resulted in 49 integrated bands. The computer was programmed in order to calculate the relative output for each band by summing the data for every .01μ over each .05μ band width. This summation was obtained by adding 1/2 of the first and the last .01μ values in the band width to the total of the four values between the ends of the band width, that is,

$$\text{Relative Output} = \sum_{N} \left[\frac{CD(.20 + .05N)}{2} + \sum_{K=.01}^{.04} CD(.20 + .05N + K) + \frac{CD(.25 + .05N)}{2} \right]$$

where CD: Corrected Data

N = 1, 2, 3, ..., 49.

Computation of the Correction Factor to Relate the 1P28 Data with the Lead Sulfide Data: The 1P28 and lead sulfide detectors overlap in the spectral region between 0.45μ and 0.70μ. For this overlapping region of the detectors, there are five band widths. Since the response of the 1P28 in the band width from 0.65 to 0.70μ is not dependable, and since the sensitivity of the lead sulfide detector in the band width of 0.45 to 0.50μ is very low, these two band widths were neglected in arriving at a calibration factor, although they were calculated by the computer. Thus, three 0.05μ band widths, where reliable data from each detector were obtained, can be compared. The ratios of the relative response of the 1P28 and lead sulfide detectors over these three band widths were calculated. The calibration factor chosen to calibrate the lead sulfide data to the same level as the 1P28 data was the median of these three ratios. The percentage deviation between the maximum and minimum of these three ratios gives an indication of the accuracy of the spectral match of the detectors.

Normalization of the Lead Sulfide (PbS) Data: The calibration factor between the two detectors, as selected by the method described above, was applied to the lead sulfide data in order to normalize the PbS data to the 1P28 data. The 1P28 data was employed up to and including the interval where the calibration factor was chosen. Every interval at longer wavelengths above the band where the calibration factor was chosen employed the lead sulfide data as normalized by multiplication by the correction factor. This correction factor was also applied to the set of spectral data obtained at each .01μ in order to normalize with respect to the 1P28 data the entire set of spectral data obtained with the lead sulfide detector.

Conversion from Relative Units to Absolute Units: The 1P28 data and the normalized lead sulfide data were summed over the entire spectral range to obtain the total relative output of the radiation source. The total relative output was then divided into the total energy as measured by the Eppley thermopile to provide a calibration factor in order to convert the relative spectral measurements to absolute spectral irradiance. This absolute spectral irradiance was then used to plot the curves as explained previously.

Constants employed in spectral measurements of 150 KW plasma radiation source are given in Table A.

Runs	Arc Current	Gas Pressure	Gain 1P28	Gain Pb-S	Ratio (4)÷(5)	Eppley Reading mw/cm^2	Ratio .45-.50
20.1-21.1	1000	200	1.72	1.76	.97727	367.52	.01943
20.2-21.2	1000	250	1.81	1.84	.98369	386.75	.01888
20.3-21.3	1400	250	3.10	3.02	1.0265	662.39	.01505

Runs	Ratio .50-.55	Ratio .55-.60	Ratio .60-.65	Ratio .65-.70	Chosen Ratio	Normalized Total Output	Energy Calibrating Factor
20.1-21.1	.01940	.01950	.01705	.01368	.01940	53.46	6.875
20.2-21.2	.01890	.01956	.01783	.01381	.01890	56.11	6.893
20.3-21.3	.01626	.02056	.01981	.01785	.01981	79.08	8.377

Table A - Constants Employed in Spectral Measurements of 150 KW Plasma Radiation Source

Spectral Distribution

of 150 KW Developmental Plasma Radiation Source

(Spectral Curve No.1)

November 1964

Run no:	20.1 - 21.1
Current:	1000 amps
Pressure:	200 PSI
Total Irradiance at 29.725 inch from center or arc	367.52 mw/cm^2

Measurement taken with 1P28 and PbS quantum detectors in conjunction with a double prism spectroradiometric instrument. Data for this curve is found in the Appendix.

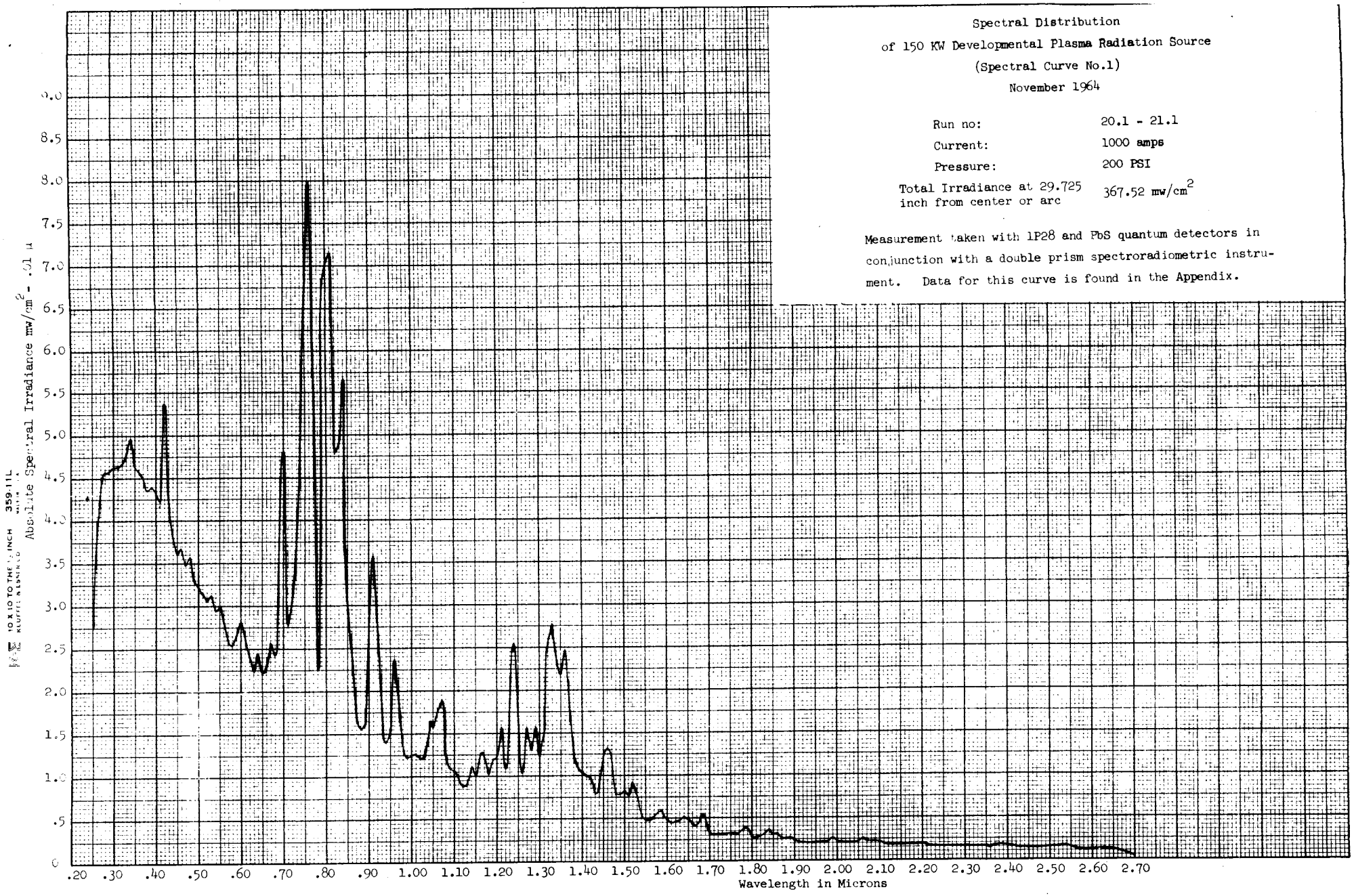

Spectral Distribution
of 150 KW Developmental Plasma Radiation Source
(Spectral Curve No.2)
November 1964

Run No:	20.2 - 21.2
Current:	1000 amps
Pressure:	250 PSI
Total Irradiance at 29.725 inch from center of arc	386.25 mw/cm^2

Measurement taken with 1P28 and PbS quantum detectors in conjunction with a double prism spectroradiometric instrument. Data for this curve is found in the Appendix.

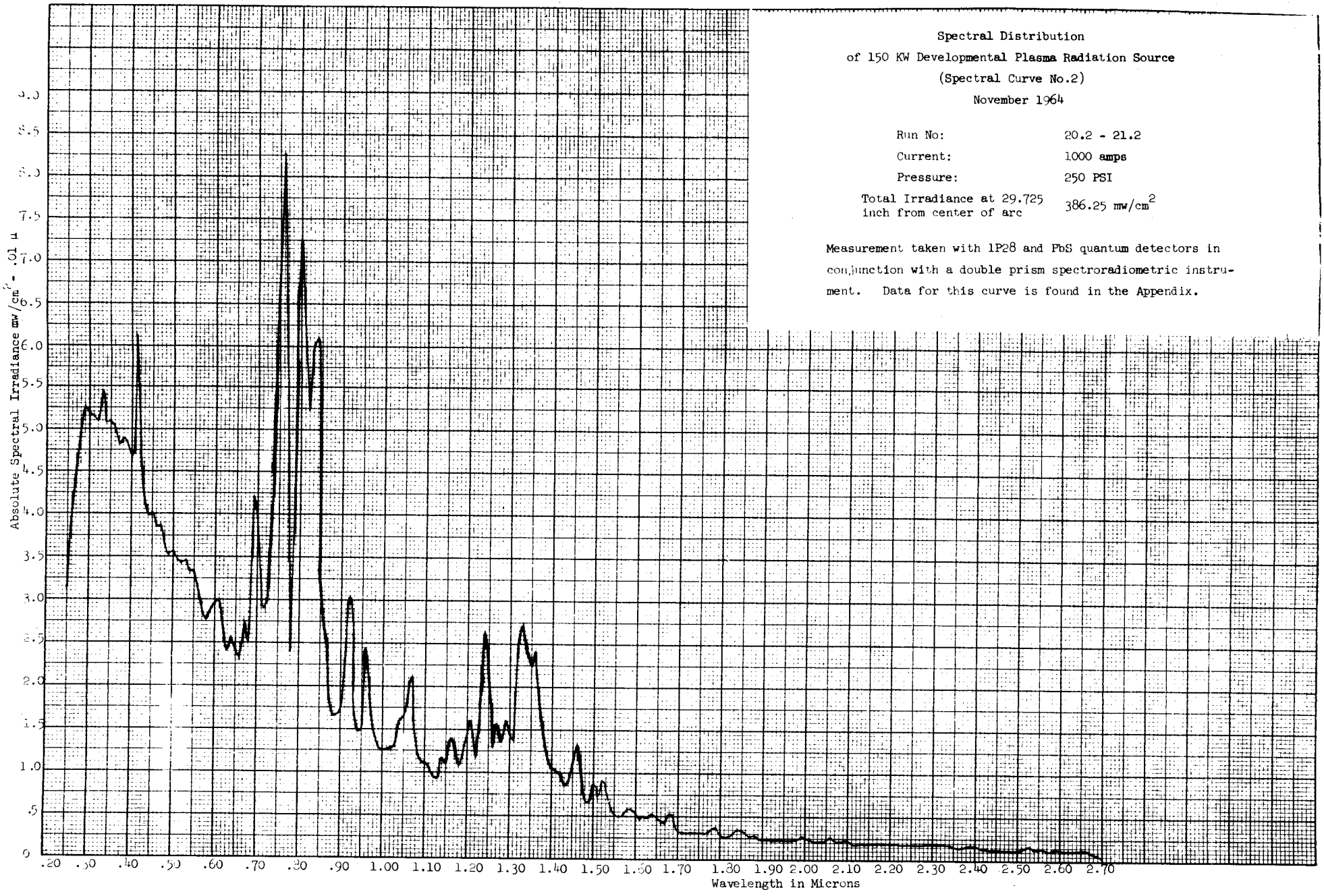

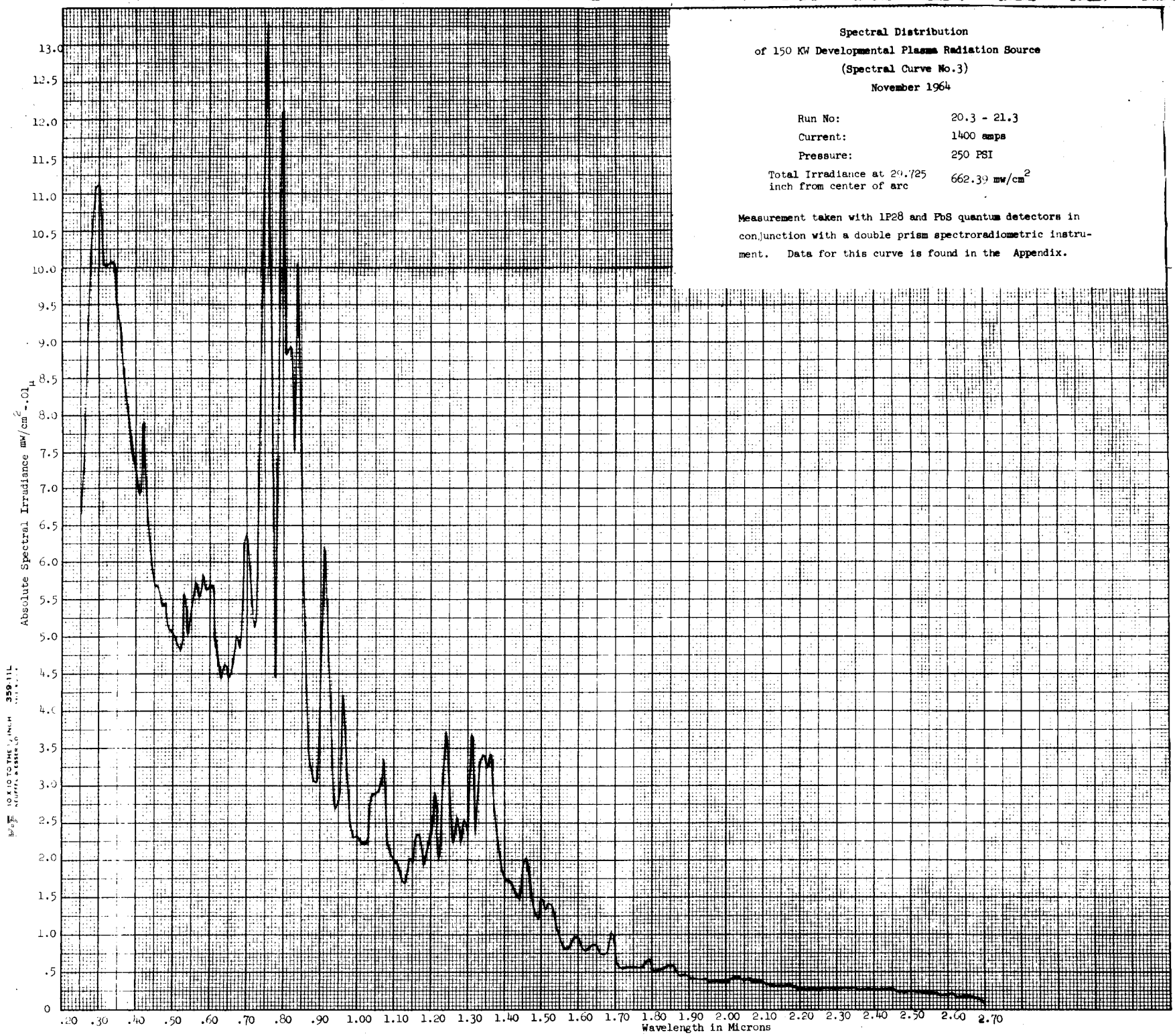
Spectral Distribution
of 150 KW Developmental Plasma Radiation Source
(Spectral Curve No.3)
November 1964
Run No: 20.3 - 21.3
Current: 1400 amps
Pressure: 250 PSI
Total Irradiance at 29.725 inch from center of arc 662.39 mw/cm2
Measurement taken with 1P28 and PbS quantum detectors in conjunction with a double prism spectroradiometric instrument. Data for this curve is found in the Appendix.
Absolute Spectral Irradiance mw/cm2-.01μ
13.0
12.5
12.0
11.5
11.0
10.5
10.0
9.5
9.0
8.5
8.0
7.5
7.0
6.5
6.0
5.5
5.0
4.5
4.0
3.5
3.0
2.5
2.0
1.5
1.0
.5
0
.20 .30 .40 .50 .60 .70 .80 .90 1.00 1.10 1.20 1.30 1.40 1.50 1.60 1.70 1.80 1.90 2.00 2.10 2.20 2.30 2.40 2.50 2.60 2.70
Wavelength in Microns

Spectral Distribution
of 150 KW Developmental Plasma Radiation Source
(Spectral Curve No.4)
November 1964

Run no:	20.1 - 21.1
Current:	1000 amps
Pressure:	200 PSI
Total Irradiance at 29.725 inch from center of arc	367.52 mw/cm^2

Measurement taken with 1P28 and PbS quantum detectors in conjunction with a double prism spectroradiometric instrument. Data for this curve is found in the Appendix.

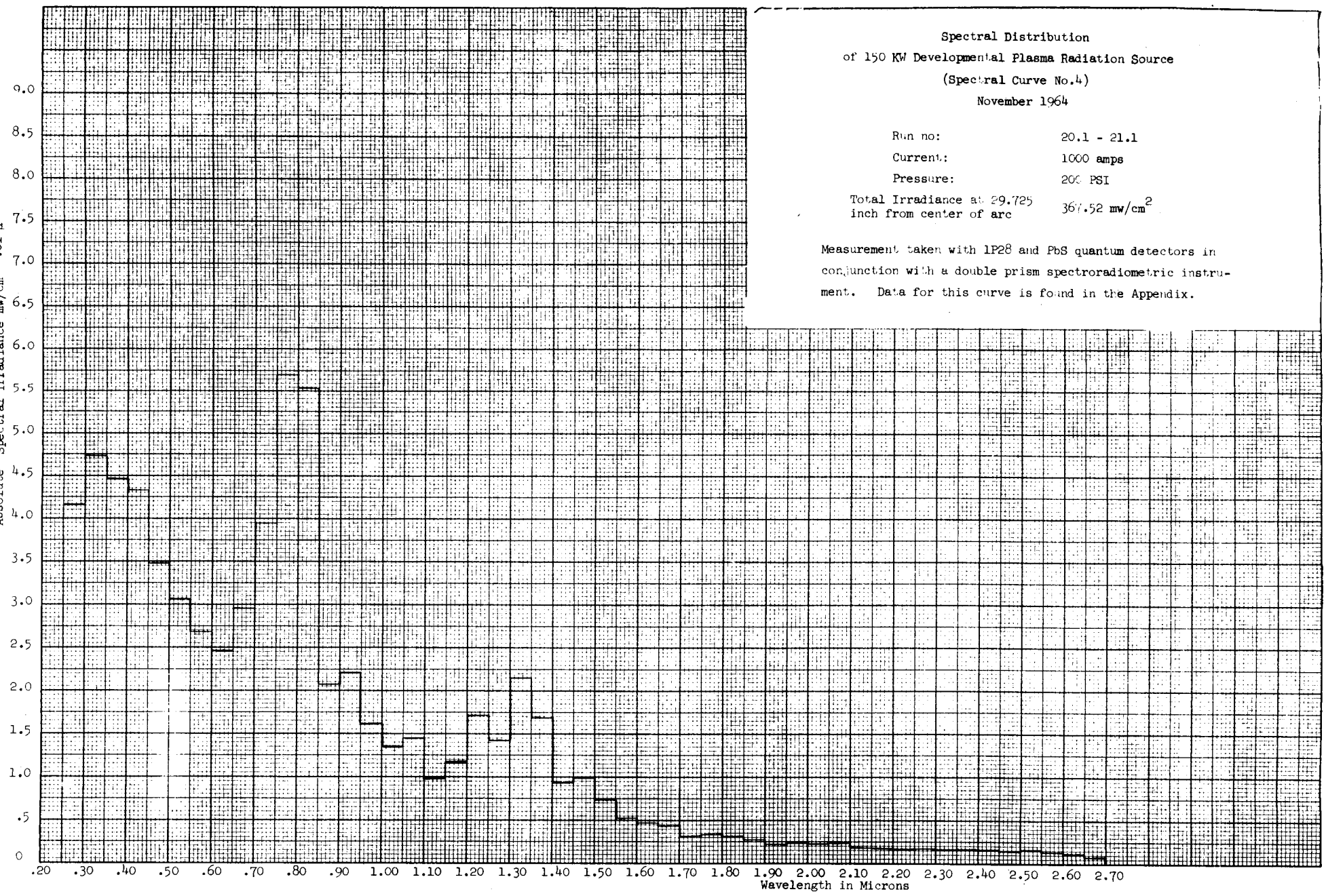

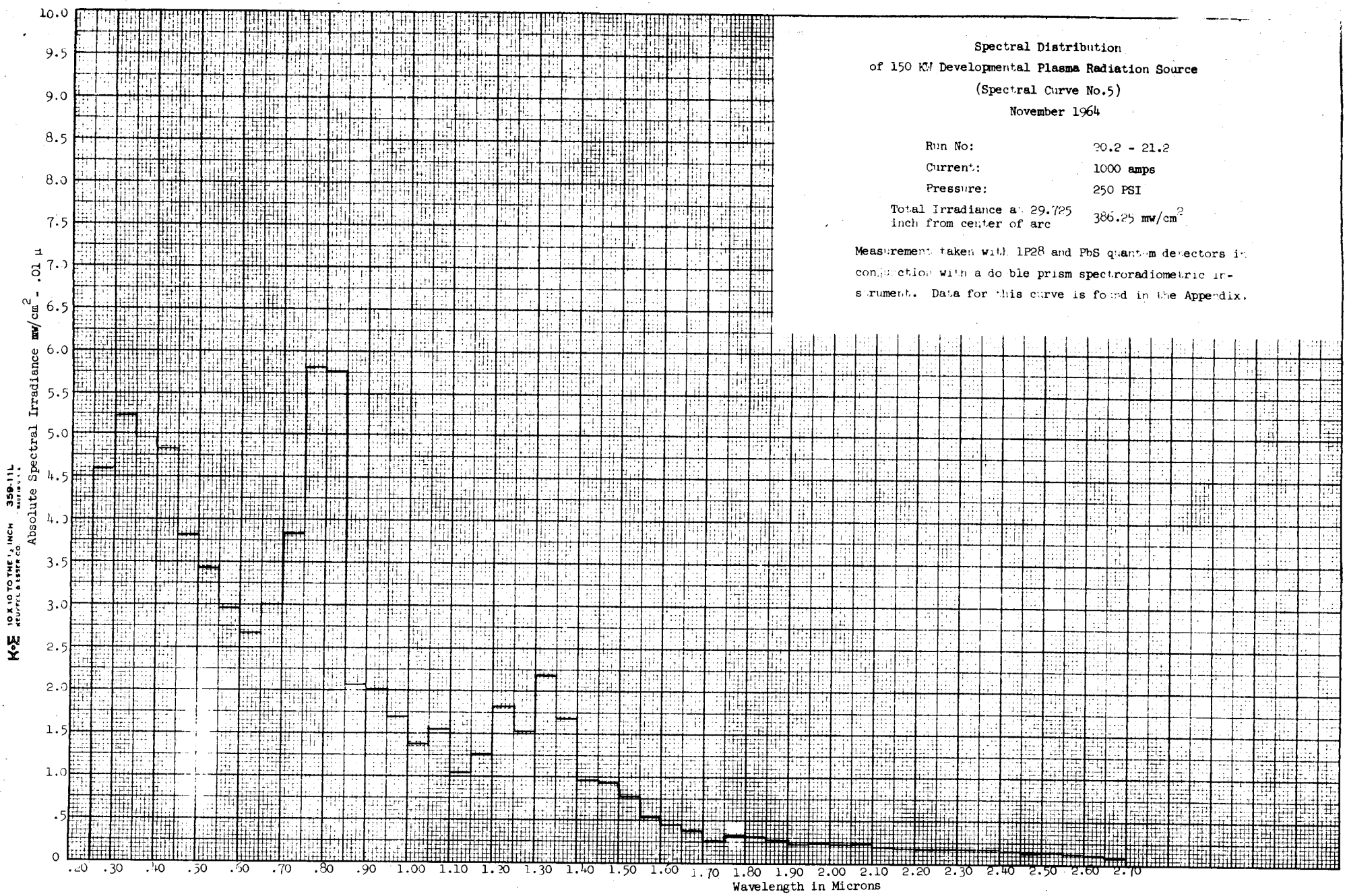
Spectral Distribution
of 150 KW Developmental Plasma Radiation Source
(Spectral Curve No.5)
November 1964
Run No: 20.2 - 21.2
Current: 1000 amps
Pressure: 250 PSI
Total Irradiance at 29.725 inch from center of arc 386.25 mw/cm2
Measurement taken with 1P28 and PbS quantum detectors in conjunction with a double prism spectroradiometric instrument. Data for this curve is found in the Appendix.
Absolute Spectral Irradiance mw/cm2 - .01 μ
10.0
9.5
9.0
8.5
8.0
7.5
7.0
6.5
6.0
5.5
5.0
4.5
4.0
3.5
3.0
2.5
2.0
1.5
1.0
.5
0
.20 .30 .40 .50 .60 .70 .80 .90 1.00 1.10 1.20 1.30 1.40 1.50 1.60 1.70 1.80 1.90 2.00 2.10 2.20 2.30 2.40 2.50 2.60 2.70
Wavelength in Microns

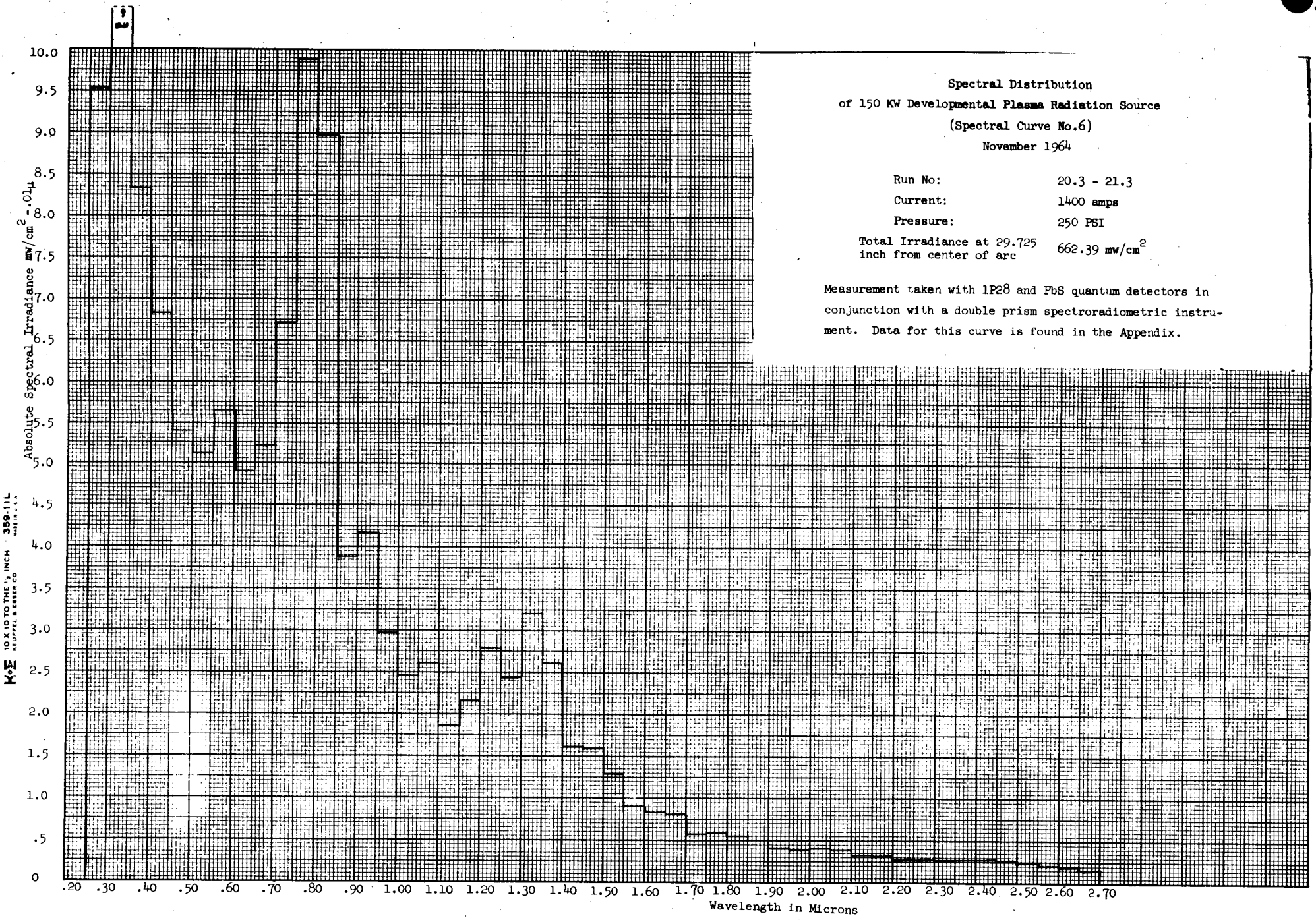

Spectral Distribution
of 150 KW Developmental Plasma Radiation Source
(Spectral Curve No.6)
November 1964

Run No:	20.3 - 21.3
Current:	1400 amps
Pressure:	250 PSI
Total Irradiance at 29.725 inch from center of arc	662.39 mw/cm²

Measurement taken with 1P28 and PbS quantum detectors in conjunction with a double prism spectroradiometric instrument. Data for this curve is found in the Appendix.

SPECTROLAB

DEVELOPMENT MEMORANDUM NO. 272-28

SUBJECT: Spectral Distribution of 150 KW Vortex Stabilized Argon Plasma Arc Source
WRITTEN BY: Henry Lee
DATE: 3 February 1965
JOB NUMBER: 6002-60

INTRODUCTION

Spectral irradiance from an argon arc was measured on a tangential plane to the radiation flux which was normal to the cathode-anode axis at the center of the arc. Assuming symmetrical flux distribution about the axis, a thermopile was mounted on the Y axis to determine the total incident energy while the relative spectral distribution was measured with a radiometer system mounted on the X axis as shown in Figure 1.

These measurements were made to establish the dependence of the arc spectrum on the two parameters of the arc operation. The two parameters are the input current, I, and the pressure of argon, P, in the arc source. In order to measure the effect of these parameters on the arc spectrum, three measurements were made as designated below. The spectral irradiance is given in Development Memorandum No. 272-27. Source operating data are presented in Development Memorandum No. 272-25.

RUN NO.	PRESSURE PSI	CURRENT AMPS
20.1 - 21.1	200	1000
20.2 - 21.2	250	1000
20.3 - 21.3	250	1400

INSTRUMENTATION

Perkin-Elmer Model 350 double prism monochromator was used with the wavelength shaft driven by a constant speed motor. The wavelength range of the monochromator is from 0.20μ to 2.80μ. The wavelength accuracy of the monochromator was checked against an Osram low pressure mercury arc lamp and is within the tolerance specification. The stray radiation at 0.25μ was checked to be less than 0.02%.

To cover the wavelength range from 0.21μ to 2.7μ, two detectors were used. A 20 mm x 5 mm Eastman Kodak Ektron PbS cell was employed in the wavelength range from 0.45μ to 2.70μ. In the wavelength range of 0.21μ to 0.7μ, an RCA 7102 photomultiplier was utilized. The two detectors are overlapping in the 0.45μ to 0.70μ range.

The incoming flux was chopped at 13 c.p.s. and the detected signal was amplified by a Perkin-Elmer Model 107 synchronous demodulator to be displayed on a Moseley Model 680 strip chart recorder.

A plain aluminum mirror was used to reflect the incoming flux toward the entrance slit of the monochromator from the argon arc and the standard lamp. The setup of the radiometer system is shown in Figure 2.

An Eppley single junction constantan-manganin thermopile bearing the serial number 6132 was used to measure the absolute energy. The thermopile was mounted 29.725" away from the origin on the Y axis as shown in Figure 1 and was exposed to the beam for a short period at the end of each spectral measurement to obtain the total incident energy reading. The calibration factor of 4.68 mv $w^{-1}cm^{2}$ was used for the thermopile (See Development Memorandum 272-13). During the period of spectral measurements, the intensity fluctuations of the arc were monitored by a P/N silicon solar cell and the reading was recorded on a strip chart recorder.

METHOD OF MEASUREMENT

The relative spectral irradiance at the measurement plane was determined by comparing the spectral measurement readings of the arc to those of a standard source. A 200 watt NBS QL 118 quartz iodine lamp was used as the standard (See Table 1 for the "Standard Spectral Irradiance"). Between the standard and arc measurement, all the parameters of the radiometer system were kept under identical conditions to be able to make a direct comparison of the two measurements.

The slit width of the monochromator was set at 0.1 mm which gives resolution bandwidths of 0.8 Å at 0.25μ, 61 Å at 1.30μ and 33.5 Å at 2.70μ. The resolution bandwidth vs wavelength is given in Figure 3.

The absolute spectral irradiance at the measurement plane was obtained by normalizing the area under the relative spectral distribution curve to the total incident energy measured with the thermopile. Two assumptions were made in obtaining absolute spectral irradiance by this method.

1. Since the thermopile was located 29.725" from the source on the Y axis and the relative spectral distribution was measured at 45.0" from the source on the X axis, it was assumed that the relative spectral distribution at 29.725" and at 45.0" on the X axis was the same.

2. It was assumed that most of the argon arc source radiation was in the wavelength band from 0.25μ to 2.70μ.

ERRORS AND COMMENTS

The maximum uncertainty of the standard spectral irradiance is estimated to be 8% in the ultraviolet and 3% in the visible and infrared. The repeatability of the radiometer system is estimated to be 3%. During the measurement, the stability of the arc source was monitored and the result shows an uncertainty of 6%.

The root mean square error of the measurement is estimated to be about 7% in the visible and infrared and about 10% in the ultraviolet.

Since narrow resolution bandwidth was employed in the measurement, the original data displayed on the strip chart shows many fine spectral lines with a few angstrom bandwidth. However, such a fine structure of spectrum cannot be shown in the reduced data because the data reduction was performed at a discrete wavelength point in a 100 Å interval.

The spectral irradiance of the plasma source was reduced in the wavelength range from 2.70μ to 0.25μ; however, the ultraviolet continum was detected down to 0.21μ. The spectral irradiance below 0.25μ can be reduced by extrapolating the spectral irradiance of a standard lamp below 0.25μ.

Figure 1

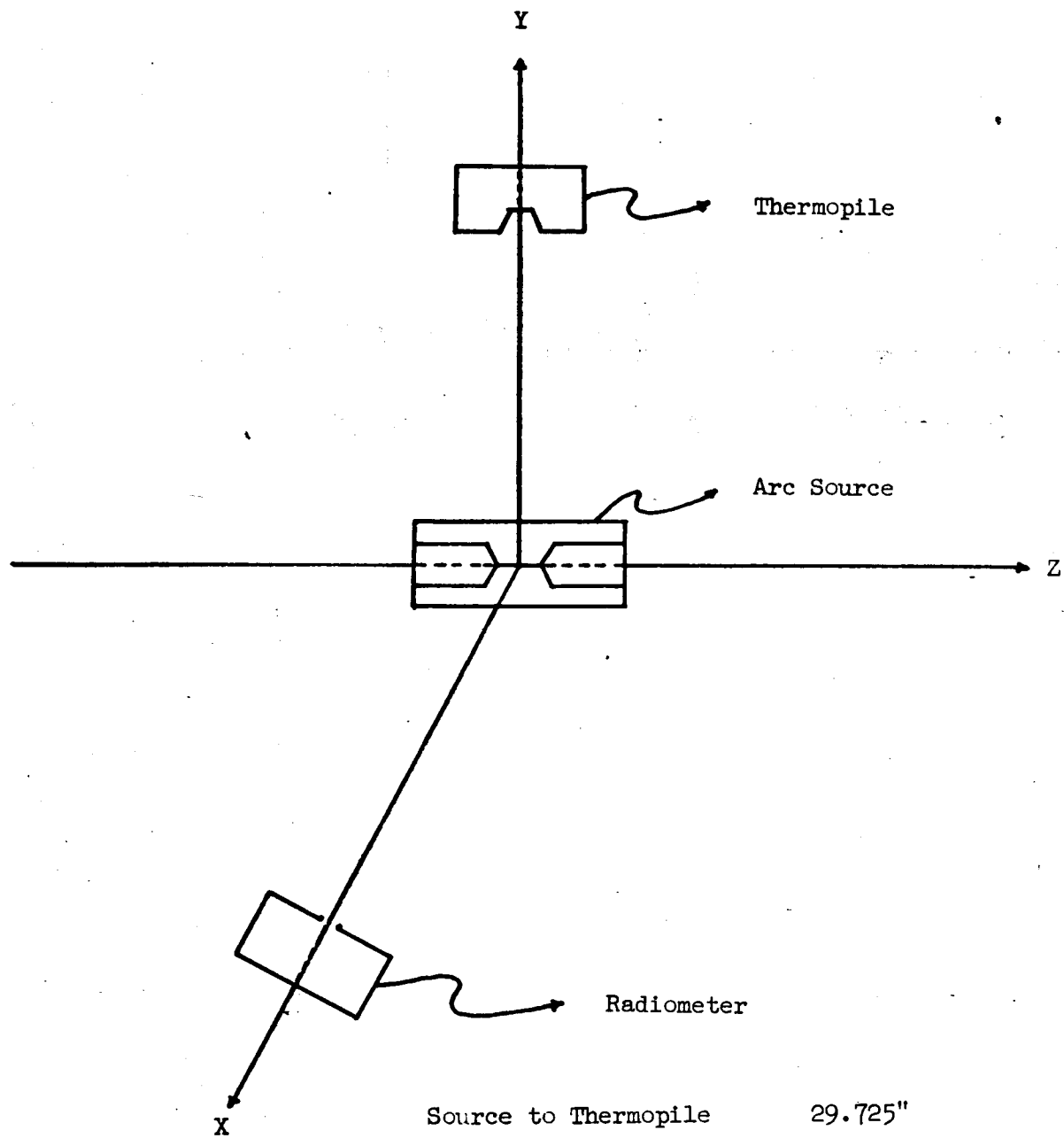

Source to Thermopile	29.725"
Source to Radiometer	45.0"

Figure 2 - Block Diagram of Radiometer Setup

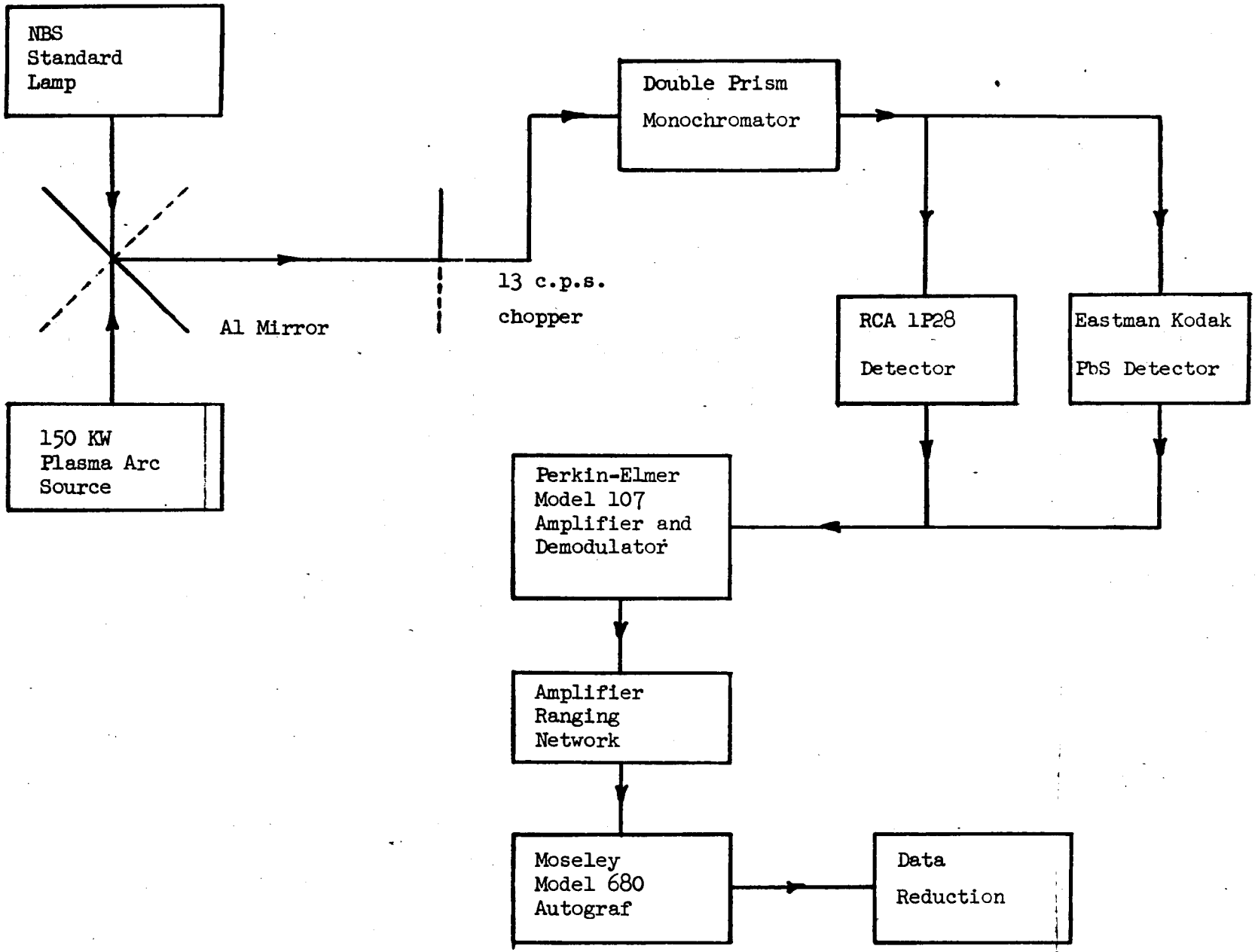

Figure 3 - Double Prism Monochromator Resolution vs Wavelength
(For Slit Width of 0.1 mm)

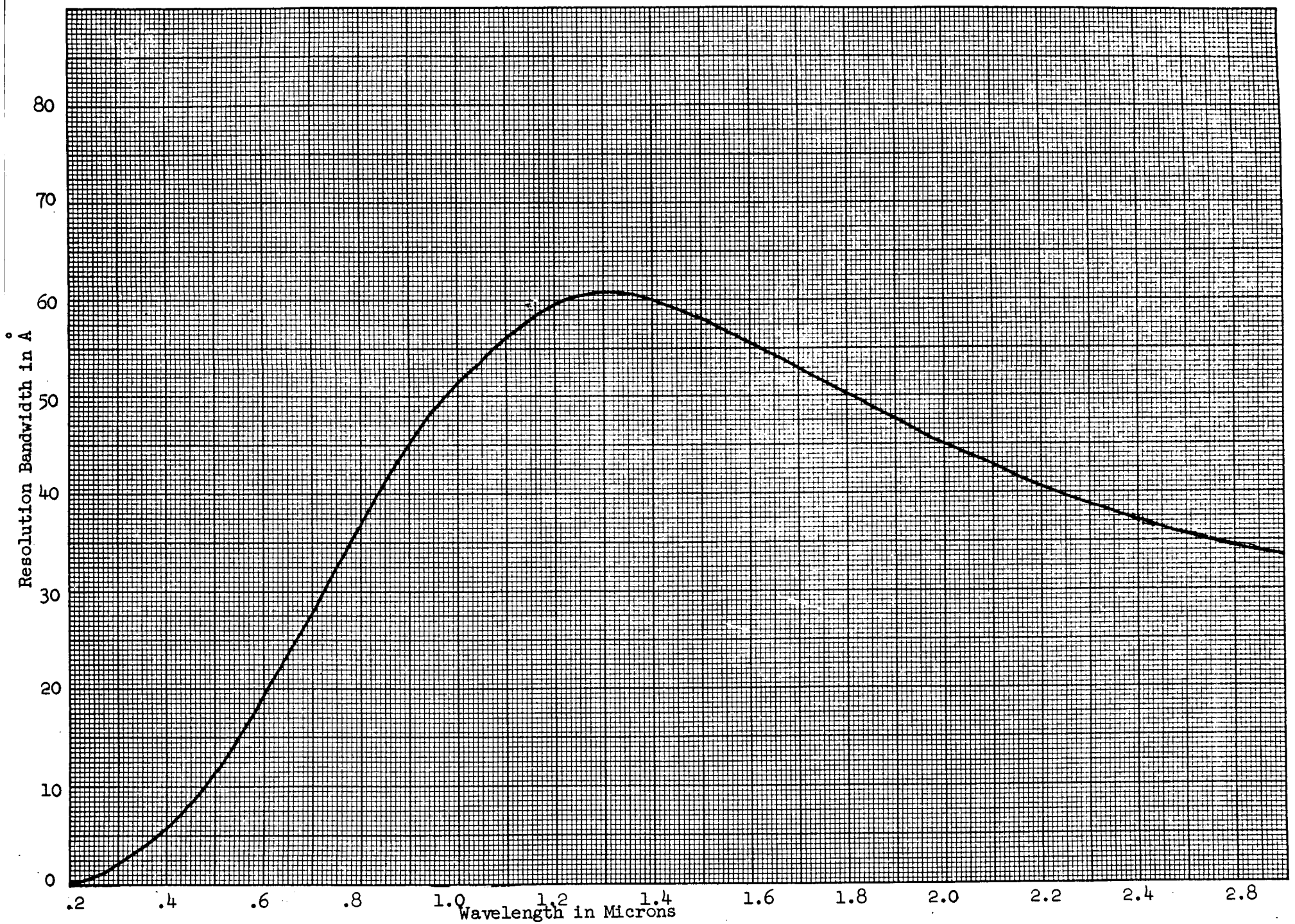

TABLE I

SPECTRAL IRRADIANCE OF N.B.S. QL-118 STANDARD LAMP

λ (in μ)	H_λ ($\mu w/cm^2$ -10 A)	λ (in μ)	H_λ $\mu w/cm^2$-10Å	λ (in μ)	H_λ $\mu w/cm^2$-10Å	λ (in μ)	H_λ $\mu w/cm^2$-10Å
* .25	.0045	.58	3.45	.91	6.80	1.25	5.40
* .26	.0082	.59	3.64	.92	6.80	1.26	5.34
* .27	.0140	* .60	3.91	.93	6.80	1.27	5.29
* .28	.0225	.61	4.06	.94	6.78	1.28	5.23
* .29	.0342	.62	4.23	.95	6.75	1.29	5.16
* .30	.0498	.63	4.40	.96	6.73	* 1.30	5.10
.31	.0710	.64	4.60	.97	6.71	1.35	4.80
* .32	.0967	* .65	4.82	.98	6.70	* 1.40	4.52
.33	.135	.66	5.00	.99	6.67	1.45	4.30
.34	.180	.67	5.16	* 1.00	6.64	* 1.50	4.08
* .35	.223	.68	5.30	1.01	6.60	1.55	3.80
.36	.280	.69	5.42	1.02	6.57	* 1.60	3.55
* .37	.349	* .70	5.60	1.03	6.51	1.65	3.33
.38	.420	.71	5.68	1.04	6.45	* 1.70	3.09
.39	.510	.72	5.80	1.05	6.40	1.75	2.89
* .40	.610	.73	5.90	1.06	6.38	* 1.80	2.68
.41	.720	.74	6.02	1.07	6.35	1.85	2.50
.42	.860	* .75	6.18	1.08	6.28	* 1.90	2.32
.43	.960	.76	6.22	1.09	6.23	1.95	2.17
.44	1.10	.77	6.30	* 1.10	6.21	* 2.00	2.01
* .45	1.21	.78	6.38	1.11	6.18	2.05	1.89
.46	1.40	.79	6.45	1.12	6.12	* 2.10	1.76
.47	1.53	* .80	6.53	1.13	6.04	2.15	1.64
.48	1.70	.81	6.60	1.14	6.00	* 2.20	1.53
.49	1.84	.82	6.65	1.15	5.98	2.25	1.44
* .50	2.03	.83	6.70	1.16	5.91	* 2.30	1.37
.51	2.17	.84	6.75	1.17	5.85	2.35	1.28
.52	2.33	.85	6.80	1.18	5.79	* 2.40	1.23
.53	2.60	.86	6.80	1.19	5.73	2.45	1.18
.54	2.70	.87	6.80	* 1.20	5.66	* 2.50	1.13
* .55	2.96	.88	6.80	1.21	5.61	2.55	1.10
.56	3.10	.89	6.80	1.22	5.56	* 2.60	1.06
.57	3.27	* .90	6.80	1.23	5.51	2.65	1.03
				1.24	5.45	2.70	1.01

* N.B.S. Original Data.
All other data is interpolated.

SPECTROLAB

DEVELOPMENT MEMORANDUM NO. 272-29

SUBJECT: Micro-radiance Distribution in Final Radiation Source

WRITTEN BY: Wagner Schlesinger WS
DATE: January 18, 1965
JOB NUMBER: 6002-16

Three runs were made under the following conditions.

RUN NO.	AMPS	SYSTEM VOLTS	SOURCE VOLTS	GAS PSI	GAS CFM
13-11	1000	79.3	65.5	204	23.5
13-12	1400	96.5	82.5	255	23.5
13-13	1000	85.1	71.3	253	23.5

A one inch diameter plano-convex quartz lens with focal length of approximately 13 inches was used to project a magnified image of the source. The lens was approximately 14 inches from the source axis and the image was 152 inches from the lens. The magnification was determined by measuring the projected silhouette image of the electrodes produced in the scanning plane when a spotlight illuminated the electrodes from behind.

The interelectrode spacing in the image was 159.5 mm and the actual spacing was 15 mm, giving a magnification of 10.63.

The scanner was the same device as that previously described in Development Memorandum No. 272-18, except that the Hy-Cal sensor was replaced by a 1P28 photomultiplier tube used as a photo cell without multiplication. The cell was inside a metal box with a one-eighth inch opening for the entrance of radiation. Between the opening and the tube were four quartz diffusers, each with one fine ground surface.

The 1P28 tube, a 90-volt battery and the Y input of a Mosley 6S X-Y recorder were connected in series. The X input of the recorder was connected to the potentiometer on the horizontal rail of the scanner.

Twenty-two horizontal scans spaced one-fourth inch apart vertically were made for each run. These scans were parallel to the source axis. The total time required for each set of 22 scans was approximately 10 minutes. A solar cell connected to a Mosley strip chart recorder was used to monitor the source in order to be sure that no significant variations in output took place during the scans.

From the intensity scans, micro-radiance plots were derived and these are shown in Figures 1, 2 and 3. The arbitrary values given on the contours are equal for all three plots. The size of the arc and the general character of the distribution appear to be nearly unaffected by changes in current or gas pressure. The radiance from the apparently solid portion of the anode is due to two factors. Part of it is simply a highlight, a reflection of the arc on the rounded shoulder of the anode. The remainder results from the fact that the lens has a relatively large diameter and hence can receive a significant amount of radiation from inside the anode opening.

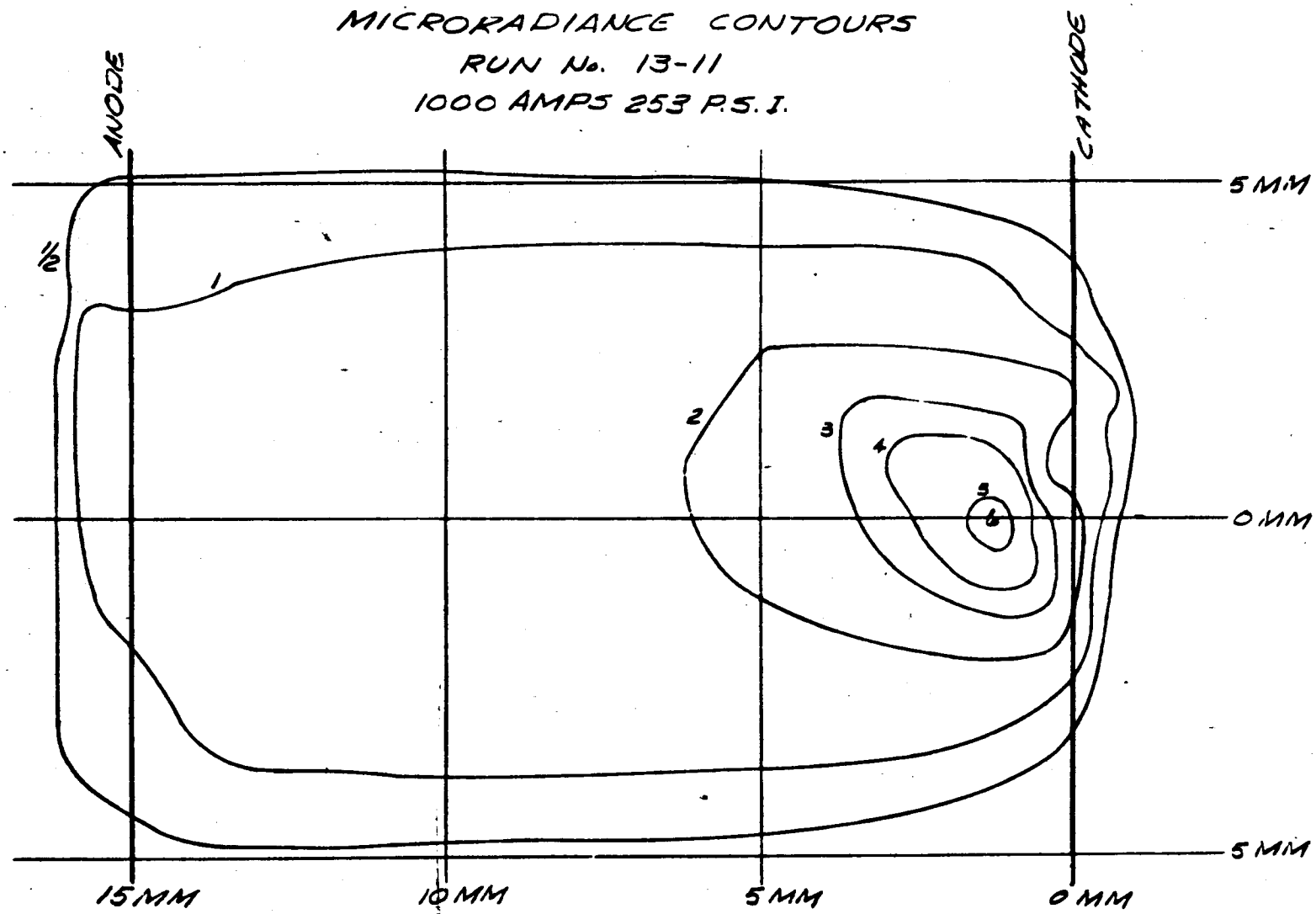
MICRORADIANCE CONTOURS
RUN No. 13-11
1000 AMPS 253 P.S.I.
ANODE
CATHODE
5 MM
0 MM
5 MM
½
1
2
3
4
5
6
15 MM
10 MM
5 MM
0 MM

FIGURE 1

MICRORADIANCE CONTOURS
RUN No. 13-12
1400 AMPS. 255 P.S.I.

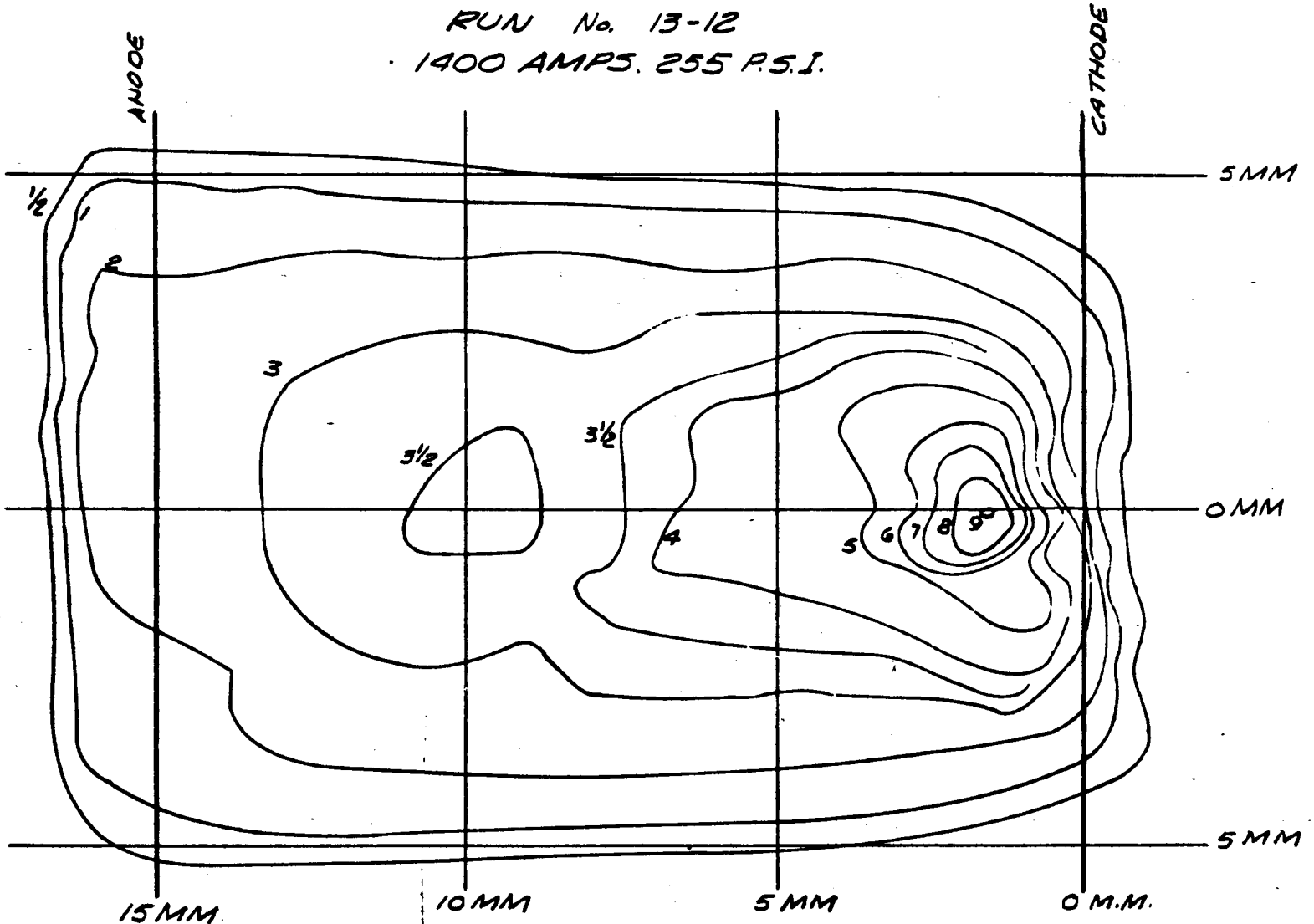

FIGURE 2

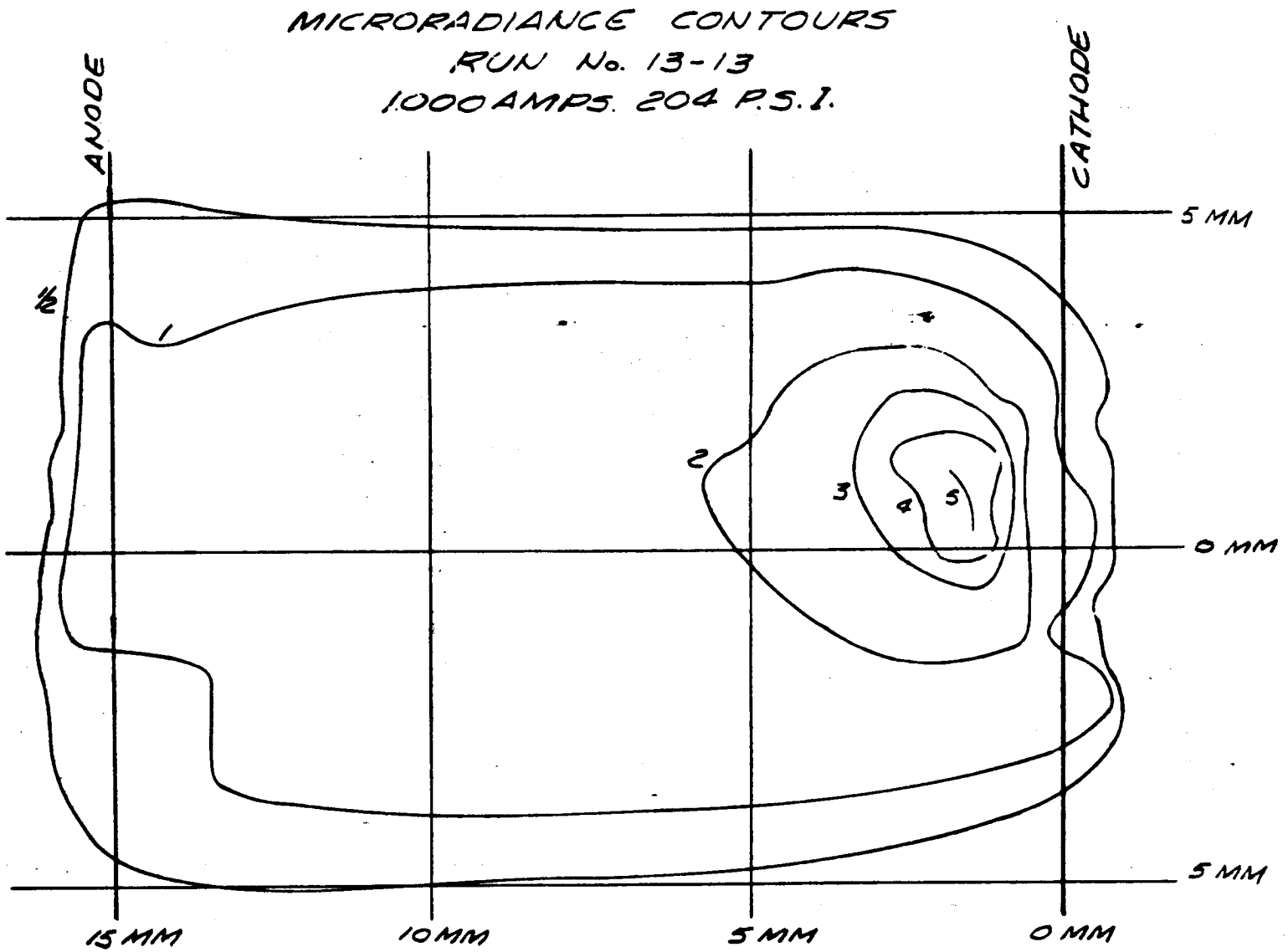
MICRORADIANCE CONTOURS
RUN No. 13-13
1.000 AMPS. 204 P.S.I.
ANODE
CATHODE
5 MM
0 MM
5 MM
½
1
2
3
4
5
15 MM
10 MM
5 MM
0 MM

FIGURE 3

SPECTROLAB

DEVELOPMENT MEMORANDUM NO. 272-30

SUBJECT: Source Documentation - Runs 23 through 30

WRITTEN BY: W. A. Geideman and Mike Onufrechuk
DATE: 27 January 1965
JOB NUMBER: 6002-45

INTRODUCTION

Following the completion of Test Run 22, the gas system in the prototype setup was dismantled and cleaned thoroughly to remove the oil which was present in the gas lines. New diaphragms and diaphragm gaskets were installed in the recirculator system. The cause of the recirculator pump failure was a fatigue type fracture of the diaphragm. The fracture occurred along the ID of the diaphragm gasket and was caused by the gaskets being undersized. The cleaning procedure was identical to that described in Development Memorandum No. 272-8. A more complete discussion of the cause of the recirculator failure was presented in a letter from W. A. Geideman to Peter Prentiss of G. D. Pribble Company, dated 4 January 1965.

The prototype optical system was reinstalled in the test facility for additional prototype tests. The test setup was identical to that described in Development Memorandum No. 272-16. The radiation source was thoroughly cleaned and reinstalled. The cathode used for the previous life tests was employed without any modification. The diameter of the arcing surface of the cathode tip was approximately .350". A new anode and a new inner quartz envelope were installed. The spacing between the cathode tip and anode face was set at 15 mm.

TEST RESULTS

Test Run 23 was performed on December 17, 1964. This test encompassed five data points. The first three points were performed to obtain transmission data on the water cell. Points 1 and 3 were runs made without the water cell in place to compare target intensity data with Point Number 2 which was performed with the water cell in place. The target intensity was measured using the Hy-Cal calorimeter #2 for all three test points. During Run 23-2, the temperature of the outlet water from the water cell rose a total of 13°F

at a flow rate of 1 gpm and a water inlet pressure of 12 psi. A water swirl was visible in the cell under high intensity conditions. The water swirl could possibly be caused by air bubbles or differential temperature conditions causing different water densities. The exact reason for this water swirl is undetermined and needs additional confirmation.

A projection plane scan was performed during Run 23.1 to double check the symmetrical distribution of energy in order to confirm alignment of the optical system. The operating conditions for Runs 23-1, 23-2 and 23-3 were essentially identical in order to provide information on the transmission of the water cell.

Test Run 23-4 was a projection plane scan at various heights in the projection plane for comparison with previous projection plane scans made in the first prototype test series (Runs 5 through 9). Test Run 23-5 was a complete target scan in order to provide comparison with the data obtained in Test Runs 8 and 9. All points during this run were made at a current level of approximately 1550 amps with a gas pressure of 250 psig. The raw and reduced source data are presented in Table 1 for all tests covered in this memorandum.

The total elapsed operating time at current levels in excess of 1550 amps was 66.7 minutes during Run 23. The total number of starts in this run was five. On the first start, a small amount of tungsten was ablated from the cathode and deposited on the inner envelope. Subsequent running and the additional starts did not indicate any further degradation of either the anode or cathode. Ablation of the cathode tip was much less than had been previously encountered indicating a stable cathode tip configuration.

At the completion of Run 23, the console was modified to incorporate the argon filling system which was previously located on the instrument board at the opposite side of the R&D Lab from the console. This modification was made to enable operation of the radiation source by only one man in order to reduce the number of people necessary to perform tests.

The optical configuration was modified in order to allow an intensity distribution at the field lens plane to be obtained. The folding mirror was rotated to change the reflection angle of the collected radiation. The scanner was aligned in the field lens plane with the refocused beam in order to scan the intensity. The folding mirror was aligned with the scanner using the boresight telescope. A dual transite backstop was mounted behind the sensor in order to protect the door and walls of the room from radiation.

The readout instrumentation was connected and calibrated with the sensor. A preliminary test run was performed at a current level of 1550 amps in order to check out the new setup. After 150 seconds of operation, the lamp was extinguished due to ignition of the transite backstop.

The beam douser was removed from its position in the optical train and was mounted as a backstop for the radiation. The plane of the douser was mounted perpendicular to the incident energy. The dual transite backstop was placed behind the douser in order to shield the stray radiation. The water cooling system for the douser was retained as in the previous tests with the water being in series with the projection lens and calorimeter backstop. The water flow under these conditions was 1.3 gpm at 18 psi.

Test Run 24 was performed with this setup. The outlet water temperature from the douser was monitored during this test and a temperature rise of 47°F was observed. The outlet water temperature came to an equilibrium at an operating condition of 1560 amps.

The total duration of Test Run 24 was 10.2 minutes. After 10 minutes of operation, the Mosley Autograph Plotter began operating erratically in its X axis movement and the radiation source was extinguished. After the radiation source had been extinguished, the setup was examined and a significant bulge in the surface of the douser along with a discoloration of the special 4,000° black paint on the douser was observed. The probable cause of this bulge in the douser was boiling of the water stream behind the area of maximum heat input causing poor heat conduction to the water and consequent heating of the 0.062" stainless steel sheet producing the bulge.

The douser was removed from the series water hookup and connected directly to the water manifold and drain. The water flow was increased to 3 gpm at 28 psi inlet pressure. The douser was also rotated approximately 45° so that the incident energy would not strike the wall surface of the douser directly but at a 45° angle. The transite backstop was moved in order to protect the walls from the reflected radiation from the douser surface.

Test Run 25 was performed on December 28, 1964 to repeat the field lens intensity scan. The complete set of data of the intensity distribution at the field lens plane was obtained from this test run. The total duration of this test was 22.2 minutes at a current level of 1560 amps. In addition to the field lens scan, the focus of the radiation source inside the collector was checked by monitoring the peak intensity while the collector focus was adjusted. The optimum position of the collector was found to be that which was previously set during the alignment procedure.

Examination of the radiation source at the completion of Test Run 25 indicated that very little ablation of the cathode had occurred during these last tests. No problems were encountered with the radiation source during the extended periods of operation at current levels of 1550 amps.

After completion of the intensity scan at the field lens plane, the folding mirror was returned to its original position and the scanner was mounted in the projection plane. Test Run 26 was a short run performed to check the realignment of the optical system. A projection plane scan was made and the distribution of energy indicated the alignment to be correct. The total operating time at 1560 amps in Test Run 26 was 5.5 minutes.

Test Run 27 was performed on December 30, 1964 with the water cell and uniformity filter in place. The uniformity filter was deposited on the outside surface of down stream plate of the cell. The complete target plane intensity distribution was obtained during this test.

After 22.3 minutes of operation of the radiation source at a current level of 1560 amps, an emergency shutdown of the radiation source was performed. The

cause of this shutdown was a failure of the gas exhaust hose at the radiation source. The gas hose came loose from the high pressure fitting. Thus, the cause of the failure was not a rupture of the gas hose but was traceable to improper assembly of the hose with the ferrule of the fitting.

The gas hose ruptured while the source was operating at 1550 amps causing a rapid reduction in the gas pressure inside the source and a probable increase in the arc current level. The source was extinguished about three seconds after the rupture occurred. The source was examined closely and no severe damage was evident although the molybdenum diffuser had several radial cracks from the inside diameter. The radiation source was removed from the mounting in order to perform a more detailed examination of the condition of the electrodes.

Figure 1 is a photograph of the anode after completion of Test Run 27. Four radial cracks in the molybdenum diffuser are evident in the photograph. Three of these cracks are fairly wide while the fourth is a hairline crack. The ID of the anode was measured and was found to be approximately 0.650" indicating very little, if any, erosion of the inside surface of the molybdenum. Figure 2 shows the cathode tip after completion of Test Run 27. The condition of the arcing surface of the cathode tip is quite different from the condition encountered previously. The arcing surface had a concave contour with a small spot located slightly off-axis as indicated in the photograph. The condition of this spot was such as to indicate a rapid solidification of molten tungsten due to the emergency shutdown. Apparently, the stable operating shape for the cathode tip is a wide concave surface. This shape is correct for operating at a current level of 1550 amps but may not be adequate for operation at lower current levels. Figure 3 is a photograph of the inner quartz envelope at the completion of Test Run 27. Although some ablation of the cathode is evident from the spots on the surface of the tube, the number of these spots is significantly less than previously encountered for comparable operating time.

The radiation source was reassembled using the same anode and cathode and a new inner quartz envelope. The outer quartz envelope was cleaned. The copper

portion of the cathode was polished to remove a deposition of what appeared to be finely divided copper particles. It is possible that this copper powder was deposited on the cathode during the system purging operation. When a vacuum is pulled on the source, the gas flow direction through the source itself is reversed and some finely divided copper, which is probably deposited in the heat exchanger in the source during operation can be removed by action of the gas flow and deposited on the cathode. It is not likely that this copper powder came through the gas system in the normal direction since in that case the copper would be deposited on the inner quartz envelope and not on the cathode due to the operation of the vortex injectors. In order to avoid this deposition and also to prove out the above reasoning, subsequent purging of the radiation source will be performed simply by pressurizing the source to a level of 250 psi and then dumping the argon out of the system. This will maintain the gas flow in the same direction at all times.

Run Number 28 was performed on January 4, 1965 in order to obtain a spectral distribution in the target plane. This test was performed at a current level of 1400 amps and the spectral response was measured with the 1P28 detector. Test Point 1 was performed with the water cell and uniformity filter in place while Test Point 2 was run with the water cell removed. The response of the detector during Test Point 2 of this run was abnormally low indicating a malfunction in the recording instrumentation. A subsequent investigation revealed that the magnesium carbonate reflecting block used with the double prism monochromator had severe multiple surface fractures due to the intensity level of the radiation resulting in a poor reflection to the detector. Thus, the results of Run 28.2 must be discarded. The total operating time at 1400 amps during Test Run 28 was 19 minutes.

Run Number 29 was performed on January 5, 1965 as a continuation of the spectral intensity measurements in the target plane. Point 1 was a repeat of Run 28.1 using the 1P28 detector with the water cell and uniformity filter in place. After 13.2 minutes of operation, the source was extinguished because the magnesium carbonate block fractured again. The block was replaced and the run duplicated as Run 29.2. Point 3 was identical to the previous two points

except the water cell and uniformity filter were removed. Points 4 and 5 in Run 29 were taken with the water cell and uniformity filter in place. Point 4 employed the 1P28 detector while Point 5 employed the lead sulfide detector. The total operating time during Test Run 29 was 54.6 minutes at a current level of 1400 amps.

Upon completion of Test Run 29, oil was again noticed in the gas flow meters. Only a very small amount of oil was evident and the filter in the console was checked and was found to be not saturated with oil as yet. To continue the spectral tests in order to avoid repetition of the long setup time required for the spectral instrumentation, it was decided to operate the radiation source with an open loop gas system bypassing the recirculator pump and associated equipment. Accordingly, the argon supply line was connected directly to the console after the components inside the console were cleaned. The filter element was replaced to avoid contaminating the argon by the oil contained in this element. The argon was exhausted through the blower in the roof of the test site.

Test Run 30 was performed on January 6, 1965 as a continuation of the spectral response tests. Point 1 was a measurement of the spectral distribution using the lead sulfide detector without the filter and water cell in place. This test point essentially completed the determination of the spectral intensity distribution in the target plane of the prototype system. Test Points 2 and 3 of Run 30 were performed with the Hy-Cal #2 sensor mounted in the projection plane in order to obtain a correlation between the spectral data and other intensity readings at the projection plane. Test Point 3 was performed with the water cell and uniformity filter in place. The total elapsed time during Run 30 was 11.8 minutes at a current level of 1400 amps.

At the completion of Test Run 30, the recirculator system was dismantled for cleaning and replacement of the diaphragms. Inspection of the diaphragms indicated that the cause of failure was the same as the last failure; namely, fatigue cracking of the diaphragm due to undersized diaphragm gaskets. In order to avoid future failure of the diaphragms in the same manner, it

was decided to manufacture soft aluminum gaskets for the diaphragms at Spectrolab rather than purchase these from the pump manufacturer. In order to accomplish this, a sketch showing the proper dimensions of the gaskets was made. This sketch increased the inside diameter of the gasket 1/8 of an inch over the inside diameter of the gasket flange in order to assure that the gasket would remain on the flange and would not overlap the head. In addition, the OD of the gasket was increased above the manufacturer's recommendations in order that the OD of the gasket would match the diameter of the diaphragm. New diaphragms and the new gaskets were installed in the recirculator pump and the system was operated without the source in the loop for a short time to make sure that all contamination had been removed from the gas system.

During this latest series of prototype tests, the aluminum surface on the collector mirror had degraded due to the effects of condensation of moisture on the aluminum. The collector was removed from the optical system and the aluminum coating was removed. The collector was then realuminized to provide a good reflecting surface.

At the completion of Test Run 30, the source was disassembled and the components were inspected. A contamination of the inside diameter of the outer envelope was noticed on this inspection. It was necessary to use Barnesite to remove the contamination. The circular Kel-F seal which sits against the inside flange of the outer envelope was found to be cracked and severely distorted. A new Kel-F seal has been manufactured for use with the radiation source. This cracking and discoloration of the Kel-F will be kept in mind in the final design of the radiation source. The condition of the electrodes at the completion of Test Run 30 was essentially identical to that shown in Figures 1 and 2 indicating that no degradation had been encountered in the last three test runs. The anode cracks did not grow in any fashion in these last three tests indicating that the radial cracking of the diffuser is not a cause for replacement of the anode during source operation.

CONCLUSIONS

1. The optimum shape of the cathode tip for operation at a current level of 1550 amps appears to be a flat of approximately .350" diameter with a slight concavity to the surface.

2. The total operating time of the radiation source in Runs 23 through 30 was 213.3 minutes with 127.9 minutes being performed at a current level in excess of 1550 amps. This entire test series was performed using the same electrodes. The inner quartz envelope was changed once for the spectral tests merely as a precaution against spurious radiation and not because of any requirement of the radiation source or optical system.

3. The failure of the argon gas line indicates that a great deal of care must be taken in the manufacture of the high pressure gas hoses for the final radiative heating system.

4. The failures encountered with the recirculator pump should be alleviated by the use of the proper size gaskets.

Point No.	Current Amps	Total Voltage Volts	Source Voltage Volts	Total Power KW	Source Power KW	Gas Pressure psig	Gas Flow Reading	Running Time Min.
23.1	1540	92.7	70.7	142.8	108.9	250	46.5	924.2
23.2	1540	93.7	71.7	144.3	110.4	250	44.5	932.4
23.3	1540	93.9	71.9	144.6	110.7	252	42.5	946.4
23.4	1550	93.1	71.0	144.3	110.1	250	45.0	961.9
23.5	1550	92.5	70.4	143.4	109.1	250	44.5	1000.0
24.1	1560	94.1	71.8	146.8	112.0	250	41.0	1022.5
25.1	1560	94.5	72.2	147.4	112.6	250	43.0	1045.9
26.1	1560	94.4	72.1	147.3	112.5	260	45.0	1053.1
27.1	1560	95.4	73.1	148.8	114.0	250	43.0	1077.0
28.1	1400	89.6	69.7	125.4	97.6	248	41.0	1093.0
28.2	1400	88.9	69.0	124.5	96.6	250	45.0	1106.0
29.1	1400	88.5	68.6	123.9	96.0	248	43.0	1107.8
29.2	1400	88.8	68.9	124.3	96.5	248	43.0	1130.8
29.3	1400	89.7	69.8	125.6	97.7	248	41.0	1143.0
29.4	1400	88.7	68.8	124.2	96.3	250	43.0	1156.3
29.5	1400	85.5	65.6	119.7	91.8	250	43.0	1165.7
30.1	1400	87.9	68.0	123.1	95.2	248	45.0	1166.7
30.2	1400	88.0	68.1	123.2	95.3	250	44.0	1176.6
30.3	1400	88.0	68.1	123.2	95.3	252	45.0	1181.6

Table 1 - Raw and Reduced Source Data for Test Runs 23-30

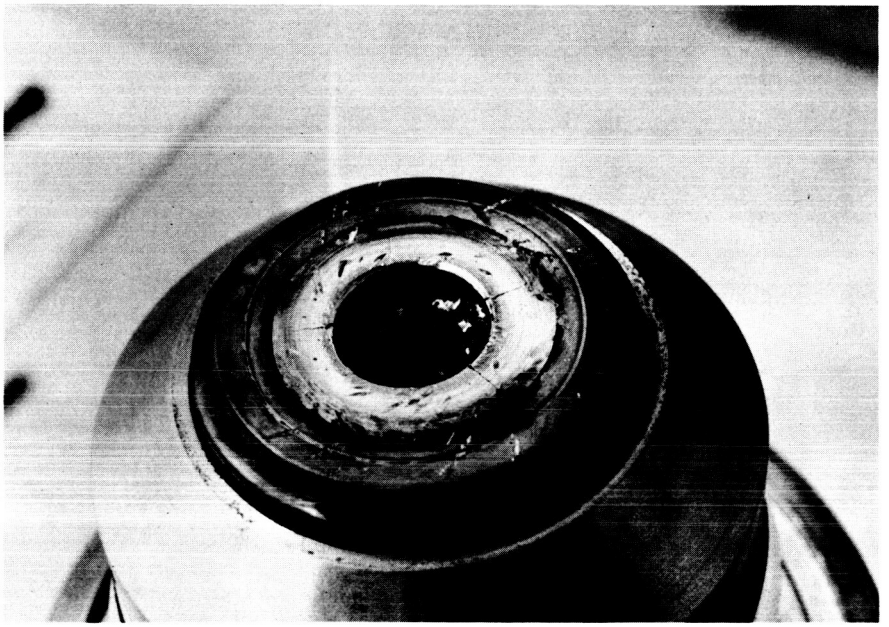

Figure 1 - Anode at the Completion of Test Run 27

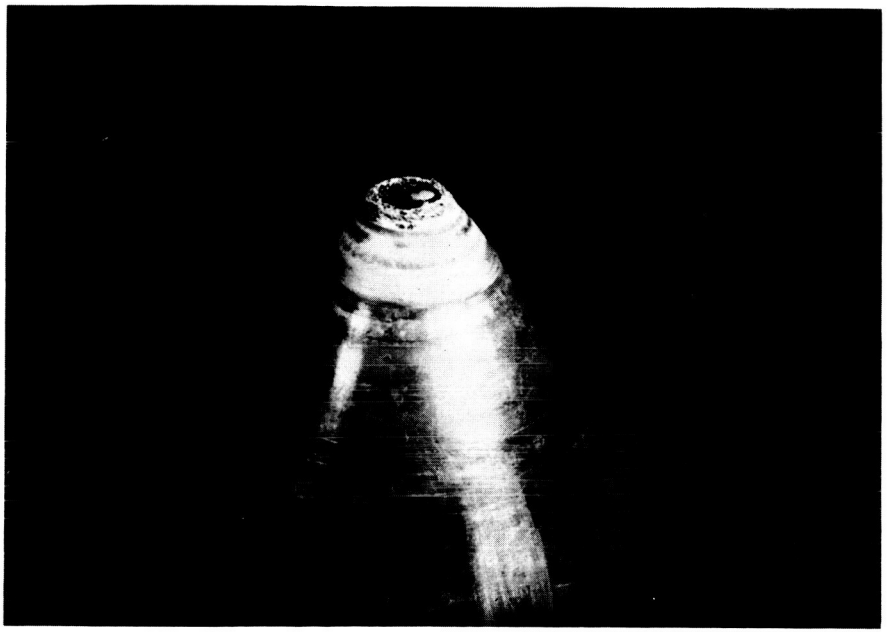

Figure 2 - Cathode at the Completion of Test Run 27

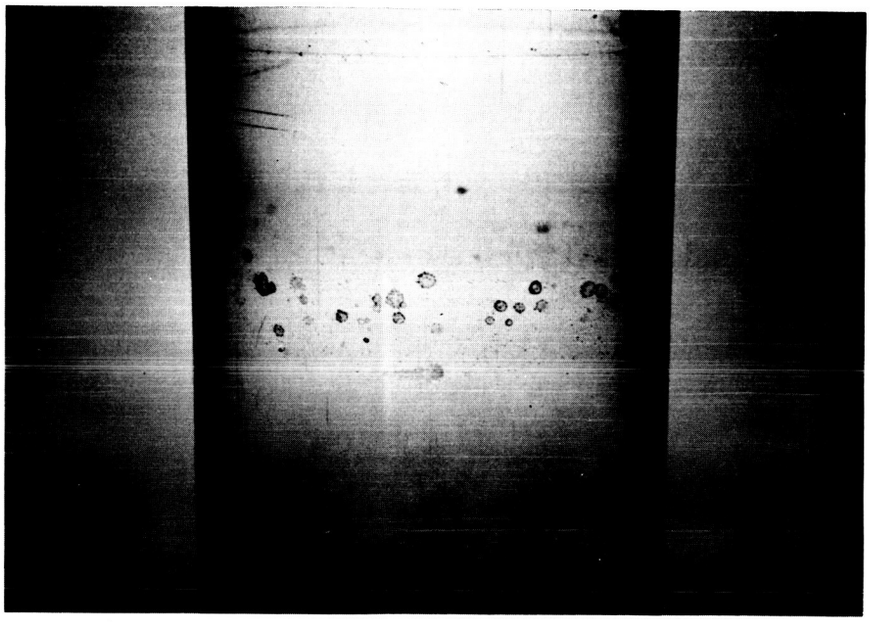

Figure 3 - Inner Quartz Envelope at the Completion of Test Run 27

SPECTROLAB

DEVELOPMENT MEMORANDUM NO. 272-34

SUBJECT: Recalibration of Prototype DC Electrical System

WRITTEN BY: W. A. Geideman
DATE: 9 February 1965
JOB NUMBER: 6002-54

INTRODUCTION

The DC electrical system was calibrated previously as reported in Development Memorandum No. 272-10. Since the time this calibration was made, a water-cooled cable was changed in the setup. Therefore, it was decided to recalibrate the DC system since this voltage calibration is important in the calculation of source power during any test run and, therefore, plays an important roll in the calibration of system efficiency.

The test setup was identical to that employed in the previous calibration test as reported in Development Memorandum No. 272-10. The voltage across the starter coil was not measured this time since only the total electrical system voltage drop enters into the calculation.

RESULTS

The voltage drop across both the cables and the starter coil as measured by the digital voltmeter is plotted vs the current in Figure 1. For the recalibration, data were obtained as shown by the circles on the curve. The values at 1500, 1550, and 1600 amps were repeated to obtain the highest accuracy. The value shown on the curve is the average voltage drop at these current settings.

The recalibration indicates a slightly reduced voltage drop in the system over that previously obtained.

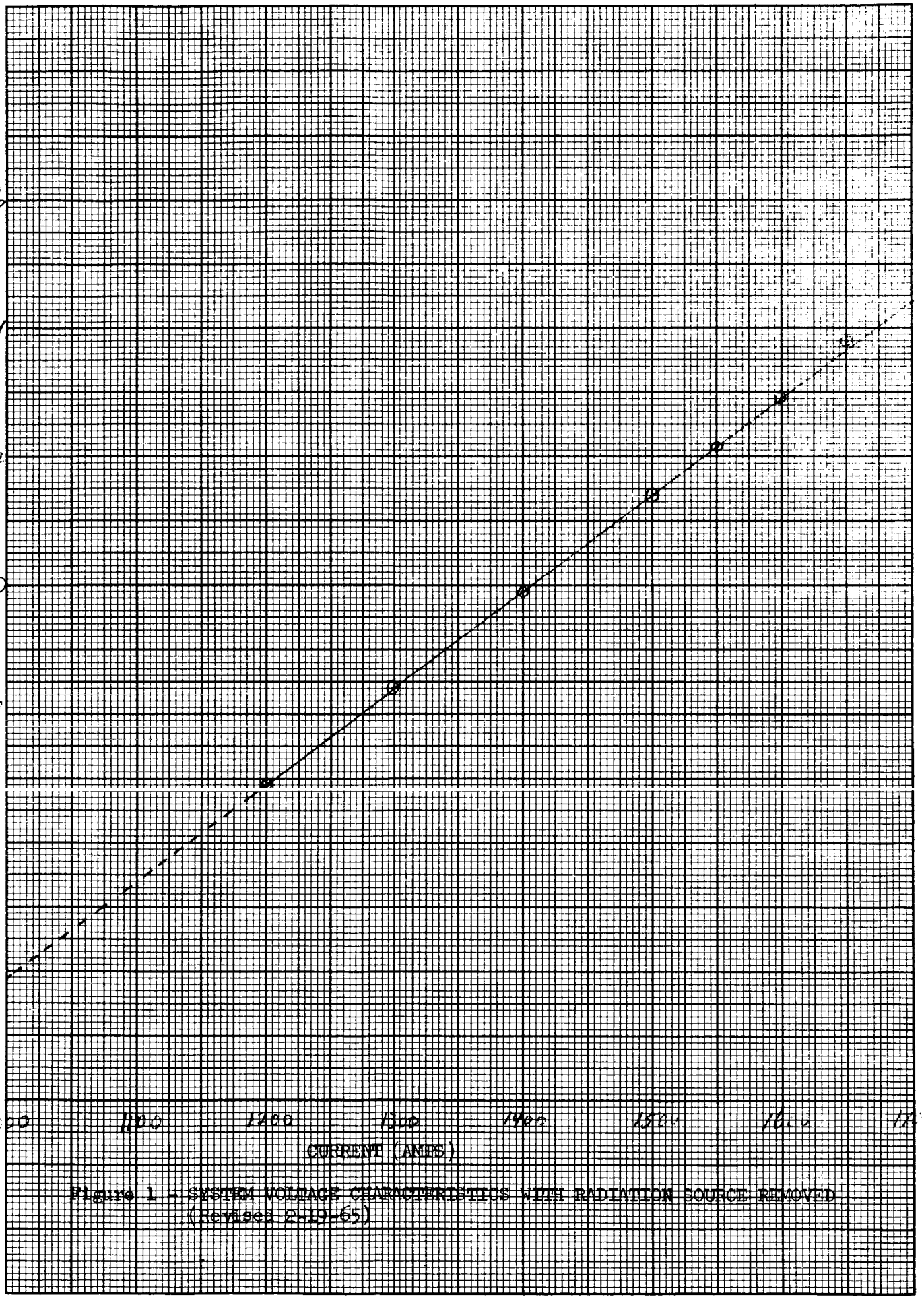

Figure 1 - SYSTEM VOLTAGE CHARACTERISTICS WITH RADIATION SOURCE REMOVED
(Revised 2-19-65)

SPECTROLAB

DEVELOPMENT MEMORANDUM NO. 272-36

SUBJECT: Documentation of Source Performance in Test Runs 33, 34 and 35
WRITTEN BY: Michael Onufrechuk
DATE: 19 February 1965
JOB NUMBER: 6002-54

INTRODUCTION

The collector was reinstalled in the facility and pressure tested for leaks following realuminizing. The source was reassembled using a new anode, the previous quartz envelope and the previous cathode. The anode was marked as Anode 1 in order to provide an identifying number system to evaluate anode replacement and modification. The anode had a .650" diffuser diameter and the gap was set at 15 mm. The source was reassembled in the standard manner with the quartz envelopes being cleaned and all parts being visually inspected including O-ring seals.

A temperature monitoring system was incorporated into the water leading from the holders of the optical elements and was also incorporated into the surfaces of these holders. This temperature monitoring system used thermocouples and a pyrotest to read the temperatures using a multiple switch. Before installation of the radiation source, the collector alignment was rechecked both with and without water flowing to determine whether the additional weight of water contributed any distortion. The amount of distortion was negligible. Following this, the optical alignment was rechecked. After the source was installed in the system, the entire system was pressure checked with both water and gas and a pin hole leak was observed in the source cap causing water to drip on the freshly aluminized collector. The source was disassembled and the source cap was resoldered to repair the leak.

A cardboard shroud was fabricated for the collector in order to enclose the open end of the collector when the system was nonoperational. A 75 watt lamp was used to provide a heated atmosphere inside this shroud in order to prevent deterioration of the aluminized surface of the collector due to moisture condensation.

TEST RESULTS

Test Run 33 was performed on January 20, 1965. The purpose of this test run was to check the alignment of the collector with the source operating. The collector was moved in all directions possible with the remote alignment provisions and the source was focused. Alignment was checked by observing the location of the peak of the detector output in the projection plane. The total duration of this run was 99.4 minutes at an operational current of 1550 amps. The raw and reduced data on the radiation source for Runs 33, 34 and 35 are presented in Table I. A visual inspection of the radiation source at the conclusion of this test indicated no change in appearance of the electrodes or quartz envelopes.

Test Run 34 was performed on January 21, 1965. This was a short run of 14.8 minutes in order to recalibrate the Hy-Cal #2 detector. After completion of the run, no appreciable change in source appearance was observed.

Test Run 35 was performed on January 22, 1965. The purpose of this run was a calibration of the Hy-Cal #1 detector with the calorimeter surface unsooted and newly sooted to determine the variation of the sensitivity of the detector between these two states. On the second start of Run 35, the arc struck on the diffuser surface causing the test to be aborted.

ANALYSIS OF SOURCE FAILURE

On the second start of Run 35, a failure of the anode occurred. The radiation source was being ignited according to normal procedures and the normal precautions according to the test procedure were observed. Two observers watching the arc and radiation source simultaneously observed the arcing to the diffuser surface. The observer looking through the arc viewer noticed the inner quartz tube to be slowly revolving after flow and pressure of the argon gas was increased. The arc was extinguished immediately.

The source was removed from the collector and was disassembled for examination. The molybdenum diffuser was ruined due to the attachment of the anode foot point of the arc to it. It was also noticed on disassembly that the inner quartz envelope slid very easily off the sealing O-rings. Both O-rings

Point No.	Current Amps	Total Voltage Volts	Source Voltage Volts	Total Power K.W.	Source Power K.W.	Gas Pressure PSIG	Gas Flow Reading	E.T.I. Reading	Running Time Min.
33.1	1550	93.1	72.0	144.3	111.6	250	45	1186	99.4
33.2	1560	93.7	72.6	145.1	112.5	250	42	1231	
33.3	1550	93.5	72.4	144.9	112.2	250	43	1292	
33.4	1550	93.5	72.4	144.9	112.2	250	43	1298	
34	1550	93.1	72.0	144.3	111.6	250	43	1314	14.8
35.1	1550	94.3	73.2	146.1	113.4	250	46	1333	17.5

Table I - Raw and Reduced Radiation Source Data - Test Runs 33, 34 and 35

were examined and were found to have a flattened cross section such that their OD's were insufficient to provide a seal for the inner quartz envelope. The leaking of gas past the O-rings disrupted the vortex flow pattern of the gas in the arc chamber, thus causing the arc to strike on the diffuser surface rather than going through the diffuser to the normal arcing surface.

The procedures being employed in the operation of the radiation source were examined after this failure. The previous procedure on shutdown was to turn off the recirculator pump immediately after extinction of the radiation source. Thus, the gas would not flow in the radiation source to provide convective cooling of the quartz envelope during the period immediately following arc extinction. In light of this failure, the procedure was changed to have the recirculator pump run for at least five minutes after arc extinction in order to cool the inner quartz envelope and, therefore, protect the O-ring seals from deterioration due to excessive temperature.

SPECTROLAB

DEVELOPMENT MEMORANDUM NO. 272- 37

SUBJECT: Source Documentation in Test Runs 36 through 39, Including $2\frac{1}{2}$ Hour Continuous Run
WRITTEN BY: Michael Onufrechuk
DATE: 22 February 1965
JOB NUMBER: 6002-54

INTRODUCTION

Following the anode failure as reported in Development Memorandum No. 272-36, the radiation source was reassembled. A new anode designated Number 2 was employed and the O-ring sealing the inner quartz envelope was replaced. The same inner quartz envelope, as well as the same cathode as used in the previous tests were employed. The cathode tip measured .365" across the flat and the gap was set at 15 mm on reassembly. The inner and outer quartz envelopes were cleaned prior to reassembly.

TEST RESULTS

Test Run Number 36 was performed on January 25, 1965. The purpose of this test was to calibrate the Hy-Cal #2 sensor both in the unsooted and sooted condition. The raw and reduced source data for all the test runs covered in this development memorandum are presented in Table I. Test Point Number 1 of Run 36, in addition to calibrating the sensor in the unsooted condition, also was performed to check the collector alignment to peak the intensity. Test Point Number 2 produced an absolute intensity scan in the target plane with a newly sooted detector.

During Test Point Number 1 of Run 36, the flow rate of the argon gas was reduced to determine its effect on the output intensity. As the flow rate was decreased from the 45 scfm reading of the previous tests to the 32 scfm reading employed in this test, the arc voltage was observed to increase at constant current producing a consequent increase in the target intensity. The arc voltage during these two test points was approximately six volts higher than had previously been recorded. The cause of this voltage increase with decreasing flow rate of argon is undetermined at the present. The current and gas pressure were maintained at a constant level while the flow was decreased.

Test Run Number 37 was performed on January 26, 1965. This test was a repeat of Test Run Number 23.5 being a target plane scan. The purpose of this test was to evaluate the relative target intensity with the difference in flow rate at the same current and gas pressure. The target plane scan was obtained by positioning the detector $2\frac{1}{2}$" above the mechanical optical axis and then scanning horizontally across the target plane in increments of 1/4" along the vertical axis. A total of twenty such scans were made during this test. Observations of the peak intensity indicated a nonsymmetrical distribution of energy about the horizontal axis of the target plane. The possible cause of this nonsymmetry could be caused by reflected radiation from the detector shield adding to the signal received by the detector.

While this run was being performed, gas pressure data were obtained at five different locations in the argon system in order to evaluate various pressure drops in the system to provide inputs to the design of the final radiative heating system.

Test Run Number 38 was performed on January 27, 1965. The purpose of this test was to evaluate the influence of the heat shield on the detector relative to the output intensity reported by the detector. A series of exploratory scans of the target plane indicated that radiation from the heat shield or reflection from the heat shield onto the detector were negligible. This test run was extended as a check on the operational life of the radiation source to a continuous operating time at current levels in excess of 1550 amps of 145.4 minutes. The current was increased several times to a level of 1600 amps without any indication of degradation of the radiation source. During the long duration run, the edge intensities in the target plane were read out without making complete scans. Part of the purpose of this life test was to ascertain if any component of the radiation source was critical with time in order to provide inputs for the source modifications for the final radiative heating system design which were being performed concurrently.

At the conclusion of this test run, visual inspection of the source in the collector was made. This inspection showed heat discoloration of the cathode and some degradation of the O-ring seals. The source was not removed from the collector.

Test Run Number 39 was initiated on January 28, 1965. The purpose of this test was to calibrate the NASA slug calorimeter. Visual examination of the source at the completion of Run 39 indicated a deformed inner quartz envelope.

The source was removed from the collector assembly for disassembly and examination and analysis of the component parts. The inner quartz envelope, which was purchased from General Electric Company, was partially devitrified and showed some plastic deformation as shown in Figure 1. The top photograph gives an indication of the area of maximum devitrification and also shows the tungsten particles which impacted onto the quartz envelope from the cathode. The bottom photograph in Figure 1 shows the area of maximum plastic deformation of the quartz. Neither the devitrification nor the plastic deformation was symmetrical around the circumference of the inner quartz tube indicating an uneven heating of the quartz.

The O-rings which seal the inner quartz envelope were seriously degraded during these tests. Figure 2 shows a close-up of the deformed O-ring on the inner quartz envelope. In addition, the Kel-F gasket which joins the inner flange of the outer quartz envelope to the steel spacer ring melted and deformed seriously during these tests. The top photograph in Figure 3 shows the steel spacer with the remnants of the Kel-F gasket visible. The bottom photograph in Figure 3 shows the outer quartz envelope before removal of the spacer indicating some "Christmas tree" type growths on the outer quartz envelope from the region of the Kel-F gasket.

The three items which showed severe deformation during these tests were degraded primarily from the extended periods of operation at maximum current levels. The failure of the O-ring seals and the plastic deformation of the inner quartz envelope were expected. The failure of the Kel-F gasket was the first of its kind which has been encountered with the radiation source. The reasons for the failure of this gasket are believed to be thermal in nature and are presently being investigated.

The condition of the cathode at the completion of Run 39 is shown in Figure 4. The arcing tip has an essentially concave surface with a small protrusion in the center of the crater. The condition of the anode is shown in Figure 5. The anode suffered very little from the long duration test runs. The marks on the surface of the diffuser are similar to those observed previously and are a result of tungsten ablation from the cathode tip. The cathode assembly exhibited a greater discoloration of the copper than previously. The outer envelope showed no damage whatsoever.

The contribution of the decreased flow rate of gas to the thermal degradation of the O-rings and quartz envelope is questionable. Further tests will be required in order to determine whether this thermal degradation could be decreased for the same operating time if higher flow rates of argon were employed.

Point No.	Current Amps	Total Voltage Volts	Source Voltage Volts	Total Power K.W.	Source Power K.W.	Gas Pressure PSIG	Gas Flow Reading	E.T.I. Reading	Running Time Min.
36.1	1550	100.9	79.8	156.3	123.6	250	32	1336	
36.2	1550	98.9	77.8	153.2	120.5	250	32	1372	38.2
37	1550	99.1	78.0	153.6	120.9	250	32	1408	34.1
38	1550	100.6	79.5	155.9	123.2	250	32	1558	145.4
39	1550	99.2	78.1	153.7	121.0	250	32	1617	60.5

Table I - Raw and Reduced Radiation Source Data - Test Runs 36, 37, 38 and 39

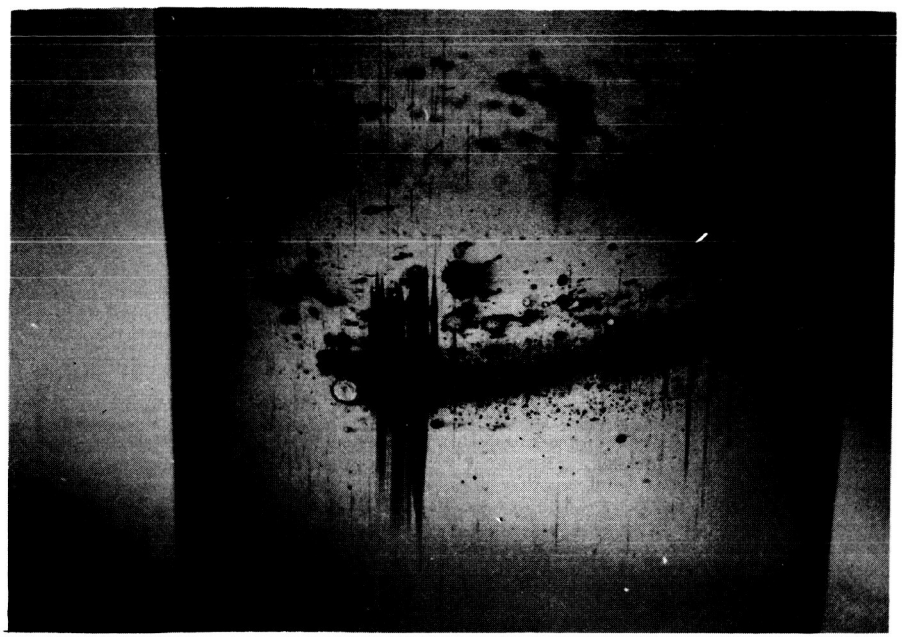

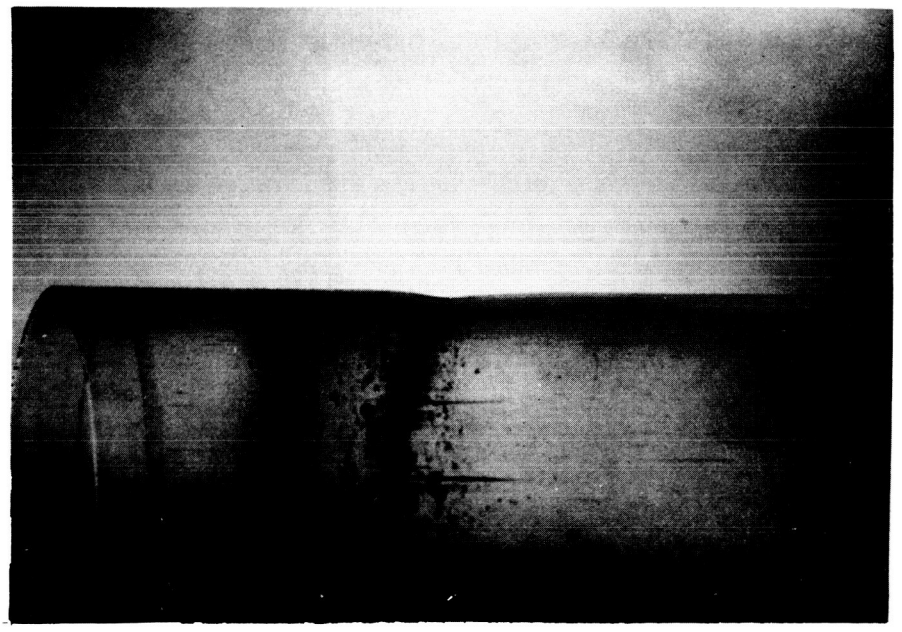

Figure 1 - Condition of the Inner Quartz Envelope at the Completion of Test Run Number 39

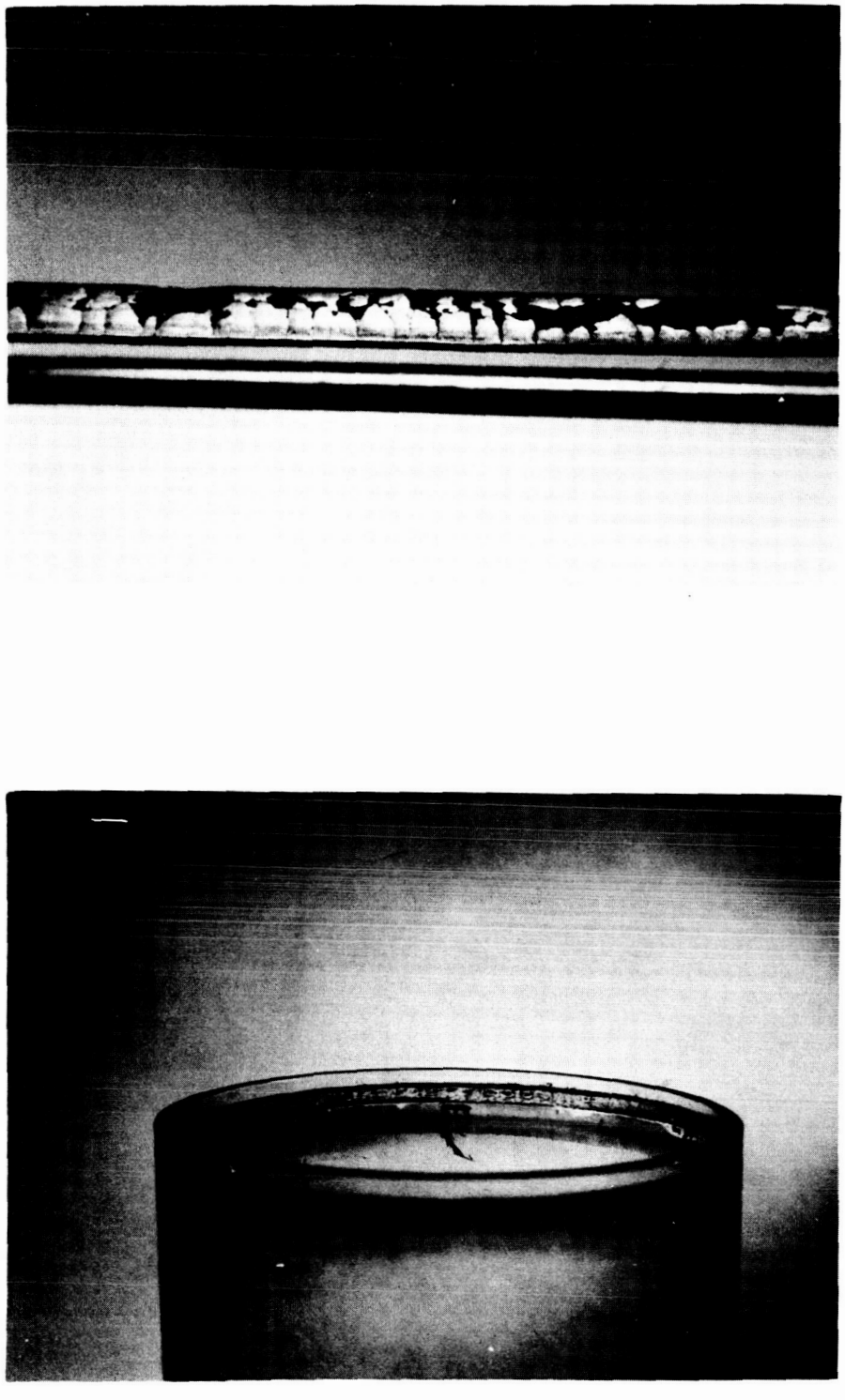

Figure 2 - Degradation of O-Ring Seal on Inner Quartz Envelope

DM 272-37

Figure 3 - Degradation of Kel-F Gaskets After Test Run 39

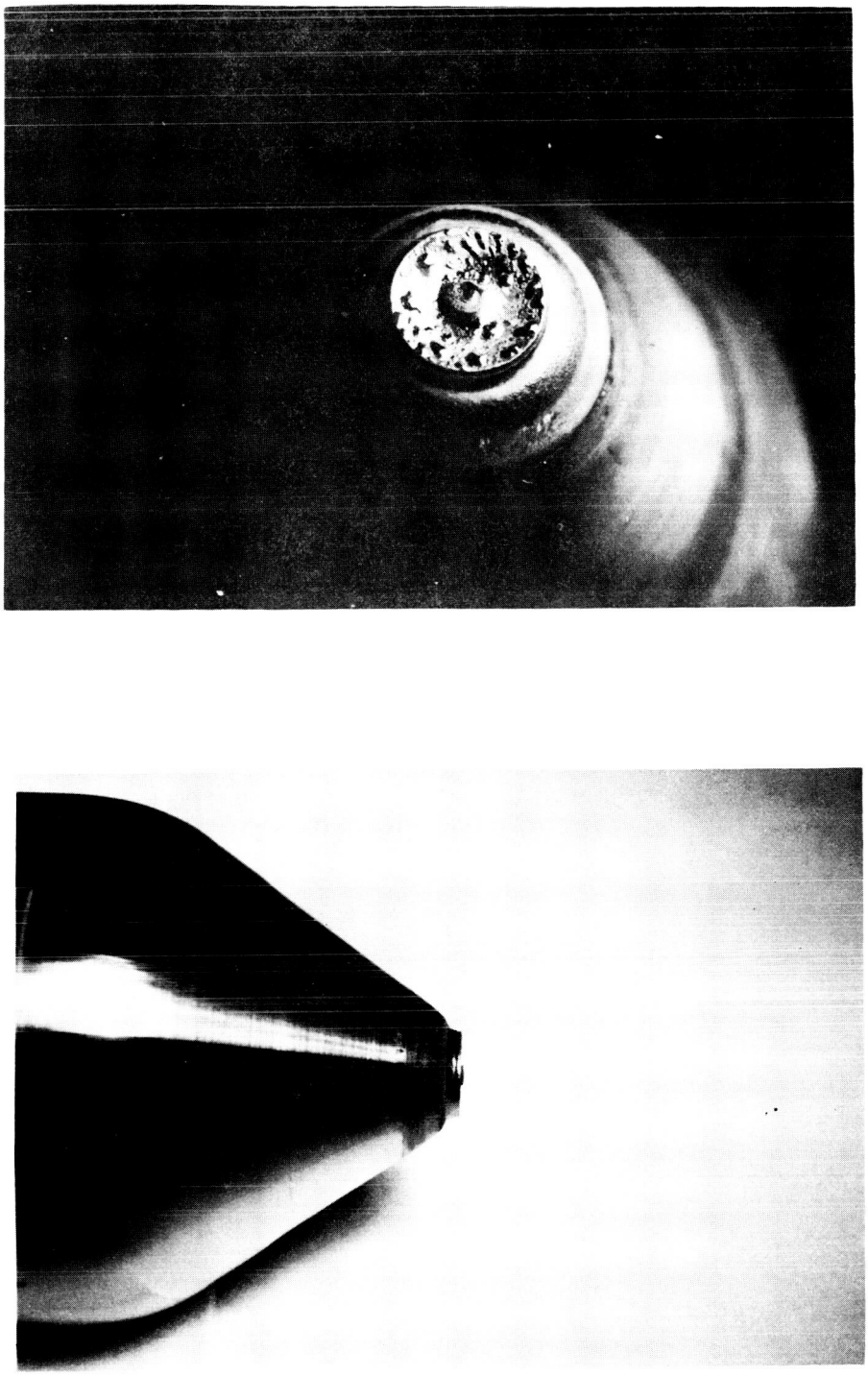

Figure 4 - Condition of Cathode After Test Run 39

Figure 5 - Condition of the Anode After Test Run 39

SPECTROLAB

DEVELOPMENT MEMORANDUM NO. 272- 38

SUBJECT: Documentation of Source Performance in Runs 40 and 41, Including Failure of Outer Envelope
WRITTEN BY: Michael Onufrechuk
DATE: 23 February 1965
JOB NUMBER: 6002-54

INTRODUCTION

After completion of the evaluation of source failure after Run 39, the radiation source was reassembled. The outer envelope was cleaned with Barnesite to remove all remnants of the Kel-F seal and also some surface discoloration of the quartz. An Amersil inner envelope was substituted for the General Electric inner envelope in order to evaluate the difference between the two materials on the target intensity. All O-ring seals were replaced and a new Kel-F gasket was installed. The new gasket was .062" thick.

A new anode assembly designated Number 3 was installed. The diameter of the diffuser was .650". The cathode which was used for previous tests was re-installed and the diameter of the arcing tip was measured to be .390". The radiation source was assembled with an arc gap of 15.5 mm.

While the source was being repaired, the alignment of the prototype optical system was rechecked. The alignment lamp fixture was modified to accept a short filament lamp. A recheck of the system alignment using the telescopic viewing apparatus was made to determine the accuracy of the alignment which was made with the final radiation source operating. Deviations no greater than 1 mm were observed in either the horizontal or vertical alignment of the center point of the target. The collector alignment relative to the optical bench was checked using the alignment lamp and aperture disk and was found to be optimum. A remote control device was incorporated into the collector assembly in order to allow the collector to be moved vertically under operating conditions in order to effectively peak and focus the collector in the target plane.

TEST RESULTS

Test Run Number 40 was performed on February 2, 1965. The purpose of this test was to adjust the collector in the vertical direction in order to peak the detector and determine the vertical center of the beam. The raw and reduced source data from both test runs covered in this development memorandum are presented in Table I. The Hy-Cal #2 detector was employed having been freshly sooted with camphor. In Test Point Number 2 of Run 40, the focusing adjustment of the collector was also adjusted in order to further peak the detector.

Test Run Number 41 was performed on February 3, 1965. The purpose of this test was to obtain intensity data around a 2" radius from the center point of the target plane. The Hy-Cal #2 detector freshly sooted was used in this test.

After 25 minutes of operation in Test Run 41, the source was extinguished due to the appearance of contaminants on the inner quartz envelope. The contamination was traced to the presence of oil in the argon system. The recirculator pump was disassembled and it was discovered that both diaphragms had ruptured permitting oil to enter the argon system.

The argon gas system was dismantled and cleaned with Ketone as had been performed previously. While the system was being cleaned, an investigation was undertaken to determine if anything could be done to increase the life of the recirculator diaphragms. The failure of the diaphragms this time was of a fatigue fracture along the mating surface with the diaphragm gaskets. This failure was identical to the last one. The failure cannot be attributed to undersized gaskets since a gap of 1/16" radius was provided between the edge of the gasket lip on the heads of the recirculator pump and the ID of the gasket itself. The apparent reason for failure is the basic design of the recirculator pump in that the diaphragm is experiencing a stress level which exceeds its endurance limit. A quick examination of the fatigue strength of the diaphragm taking into account various materials and the effect of the diaphragm thickness was made. This study indicated that the Type 316 stainless steel which was utilized by Lapp was as good as any available material for this application. However, analysis showed that the tangential stress at the fixed edge of the diaphragm, where fracture occured, is inversely proportional to thickness for this application

when diaphragm displacement is constant. Therefore, new diaphragms of .010" thick stainless steel (as compared to the .018" thick material previously used) were fabricated.

In order to protect the thin diaphragms from failure due to contaminants in the oil stream, a new oil filter was purchased and incorporated in the reservoir. This new filter was larger than the one previously employed in order to allow a greater flow of oil to prevent cavitation of the pump due to clogging of the filter element. At the same time, new apparatus to enable easier priming of the recirculator pump was incorporated into the facility.

The source was removed from the collector and was disassembled for cleaning. On disassembly, the O-ring sealing the inner quartz envelope revealed some degradation indicating a high heat exposure. The .062" thick Kel-F seal had plasticized and flowed onto the outer envelope. Both inner and outer quartz envelopes did not show any damage. The outer envelope was cleaned with Barnesite and water and prepared for reassembly. The inner quartz envelope was also cleaned and reinstalled. The cathode arcing tip was measured and was found to be .410" in diameter. The ID of the anode diffuser was measured and was found to have increased to .665-.670" diameter. The lamp was reassembled using these components and the gap was set at 15.5 mm.

Before installation of the lamp into the facility, the recirculator system was checked by bypassing the source and running the recirculator pump for approximately one hour in order to evaluate the decontamination of the system. The source was then reinstalled in the facility.

During the previous test series, difficulties had been experienced with the starter in that it was difficult to ignite the arc at the same conditions where ignition was satisfactorily obtained on previous tests. Therefore, the starter was removed and checked. The bank of capacitors was replaced and the primary transformer was reinsulated because of an existing short. Following this, the starter was reinstalled in the test site.

FAILURE OF OUTER QUARTZ ENVELOPE

On February 9, 1965 in accordance with the established test procedure, a static gas pressure test of the reassembled source at 250 psi was performed. As soon as the gas pressure reached the value of 250 psig, the outer quartz envelope exploded. The immediate post explosion examination indicated that the outer quartz envelope had fractured at the outer flange near the anode assembly and that the tube and cathode end of the source had been propelled outward essentially along the axis of the radiation source. Figure 1 is a photograph showing the portions of the radiation source which remained intact in the collector after the failure occurred. It is noteworthy that the inner quartz envelope was not damaged in any form by this failure as is quite evident from Figure 1. The fracture of the outer quartz envelope was not smooth, as can be seen from the jagged points of quartz remaining under the anode quartz retainer ring.

The cathode end of the radiation source, as best as can be reconstructed, probably moved outward from the anode in an axial direction until further movement was hindered by the water cables whereupon the cathode section moved in an arc downwards until the force produced by the momentum of the cathode structure caused the solder joint between the tubes and fittings which were attached to the water hoses to fracture, thus releasing the cathode assembly from the restraining water tubes. The cathode assembly and the remaining portion of the outer quartz envelope then impacted against the cement floor. This impact caused the remainder of the quartz envelope to shatter. Figure 2 is a photograph of the floor of the test site after failure of the envelope and shows the location of the cathode assembly as well as the fragments of quartz.

Before any of the parts of the radiation source were removed, the entire failure was documented photographically. All components were photographed on the bench prior to and during disassembly. A close-up of the cathode assembly is shown in the top photograph of Figure 3 while the view of the anode assembly after removal of the quartz retaining ring is shown in the bottom photograph of Figure 3.

Further evidence of the above description of the mode of failure of the outer quartz envelope was obtained by observing the damage done to the collector by this explosion. Only slight superficial damage of the collector surface was encountered. The collector was pressurized with water and no punctures were observed. A complete analysis of the effects of this explosion on the collector is presented in Development Memorandum No. 272-35. No other components of the optical system were damaged since they all had protective covers on them at the time of the failure.

Since the source envelope failed during static testing and since tests of this identical nature had been performed many times in the past, an investigation was undertaken to determine the probable cause of failure of the quartz envelope. The source had been assembled in the same manner as previous assemblies and by the same personnel. Nothing different was done in the assembly and cleaning procedure. Two theories were proposed to explain the failure. The first involved a build up of residual stresses in the outer quartz envelope due to operation. The second involved a local increase in pressure at the point of failure due possibly to imperfections in the Kel-F gasket.

The possibility of the build up of residual stress in the outer quartz envelope was investigated by contacting several manufacturers of quartz to ascertain if they could shed any light on the problem. All information obtained, except for one reference, indicates that fatigue due to pressure loading and unloading of the quartz could not have built up residual stresses in the material. The one exception was a reference supplied by the General Electric quartz salesman which indicated that the strength of glass decreases with flexing. The General Electric salesman also indicated that he was familiar with some applications at Rocketdyne whereby General Electric quartz had declined in tensile strength under rapid loading and unloading of pressure stresses. These data were for a flat piece of quartz of unknown quality. The Amersil factory was contacted by telephone and they disclaimed any knowledge of quartz developing internal stresses under mechanical loading. They did indicate, however, that it was possible to build up stresses in the quartz due to uneven circumferential cooling of the material causing residual thermal stresses to build up.

The forces are transferred to the outer flange of the quartz envelope by the stainless steel quartz retaining ring. In order to avoid a metal to quartz contact, a Kel-F gasket is employed between these two parts in order to transfer the forces. Since it is possible to develop imperfections in this Kel-F gasket, it is possible that the stress could have been concentrated in a local area, thus increasing the loading on the quartz envelope beyond the tensile strength of the material.

Upon disassembly of the radiation source, it was ascertained that the Kel-F seal between the retaining cap and the quartz surface had, indeed, been deformed. During reassembly of the radiation source, the Kel-F seal was inverted such that the surface which had previously been adjacent to the stainless steel cap was now located on the quartz surface. Figure 4 shows photographic close-ups of the sealing surface of the stainless steel cap and also the surface of the Kel-F gasket. It is obvious from these photographs that the sealing surface on the stainless steel part has a quantity of tool marks and that these had been transferred to the Kel-F gasket during previous operation. The Kel-F was serrated and could possibly have increased the stresses in the quartz tube by localizing the forces. This gasket had been inverted previously without these drastic results indicating that this could not have been the sole cause of the failure. The one variation between this test and previous reassemblies was the length of time which the source had been operated before the gasket was inverted. Thus, it is possible that the deformation of the Kel-F as observed after the failure was greater than had previously been encountered due to the effects of the long duration test run previously reported. The pressurization of the source in a fairly rapid manner as was employed before the failure did not allow the Kel-F gasket to flow and eliminate the imperfections in its surface.

It is possible that the present design of the radiation source produces uneven cooling of the outer quartz envelope since the argon gas is admitted to the annulus between the two quartz envelopes at only two points. Thus, the cold argon impinging on the outer quartz envelope in two locations could have produced uneven circumferential cooling of the quartz especially during the long life test

run. Previous calculations had indicated that an operating time of approximately one hour was required in order to bring the temperature of the quartz envelopes to an equilibrium value. The present theory for failure of the quartz envelope is a combination of residual thermal stresses in the envelope along with an increased localized pressure loading due to the serrations in the Kel-F gasket.

In order to avoid future failure of the quartz envelope, several steps are being taken to revise testing procedures and also several inputs are being made to the redesign of the radiation source for the final system. Pressurization of the source after reassembly will be performed in a manner to allow the Kel-F gasket to flow and thus reduce localized pressure loading on the envelope. Thus, the source will be pressurized statically at 100 psi for five minutes, then increased to 150 psi for five minutes and finally to 200 psi for 30 minutes. The quartz will not be pressurized to 250 lbs in a static load until after the gaskets have been seated.

The radiation source will not be operated continuously at current levels of 1550 amps or higher for periods longer than 30 minutes in order to avoid elevated temperatures in the outer envelope. The flow rate of argon will be increased in order to increase the cooling of the quartz. After each disassembly of the radiation source, the outer quartz envelope will be checked with crossed polaroids in order to ascertain if any residual stresses are present in the material. This will be done as a precaution against build up of stresses from uneven thermal cooling and will also give an indication if the theory on the cause of failure of this first quartz envelope is correct.

The anode housing in the final radiation source will be redesigned to incorporate a number of gas entry holes in place of the two holes in the present design. This should avoid any question of uneven thermal cooling of the outer quartz envelope. The sealing surface of the quartz retaining ring will be changed to call out a polished finish in order to eliminate the serrations and minimize the deformation of the Kel-F gasket. In addition, tolerances have been placed on the thickness of the material used to manufacture the Kel-F gaskets.

Point No.	Current Amps	Total Voltage Volts	Source Voltage Volts	Total Power K.W.	Source Power K.W.	Gas Pressure PSIG	Gas Flow Reading	E.T.I. Reading	Running Time Min.
40.1	1550	106.9	85.8	165.6	132.9	250	32	1623	
40.2	1550	106.9	85.8	165.6	132.9	250	32	1651	28.2
41	1550	107.2	86.1	166.1	133.4	250	31	1694.7	15.0

Table I - Raw and Reduced Radiation Source Data - Test Runs 40 and 41

Figure 1 - Radiation Source Parts Remaining in Collector After Failure of Outer Envelope

Figure 2 - Location of Cathode Assembly and Quartz Fragments in Test Site after Outer Envelope Failure

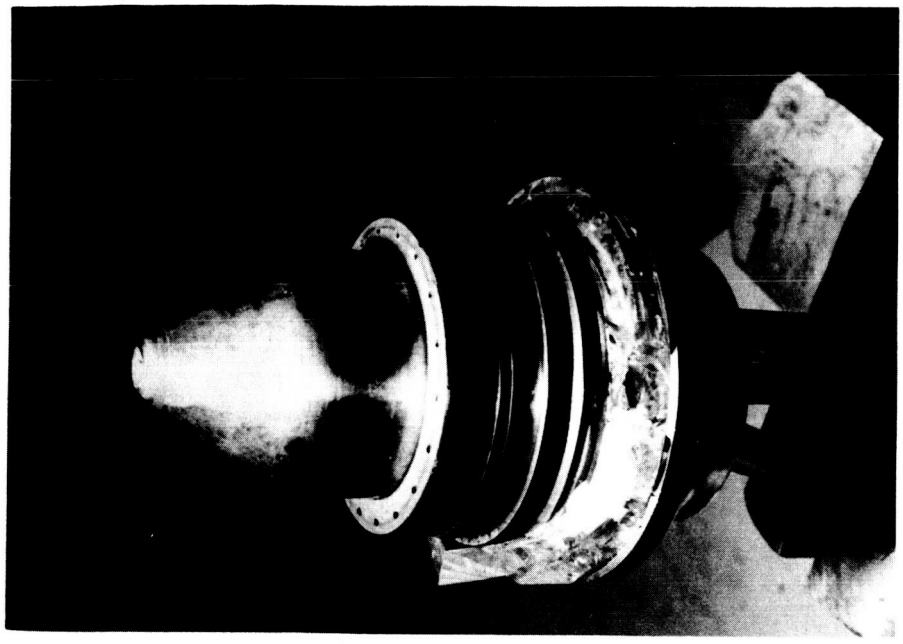

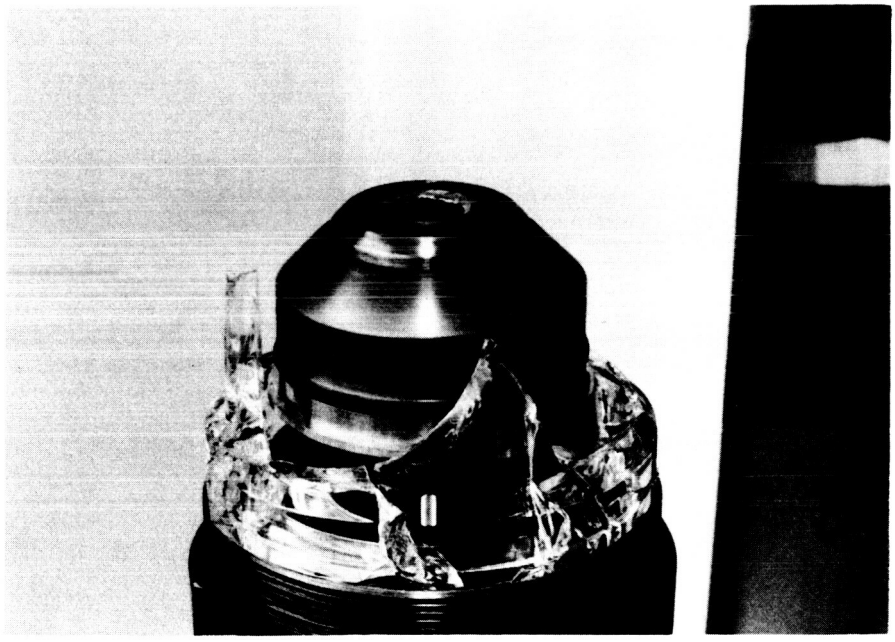

Figure 3 - Close-ups of Cathode and Anode Assembly After Outer Quartz Failure Showing Remnants of Outer Envelope

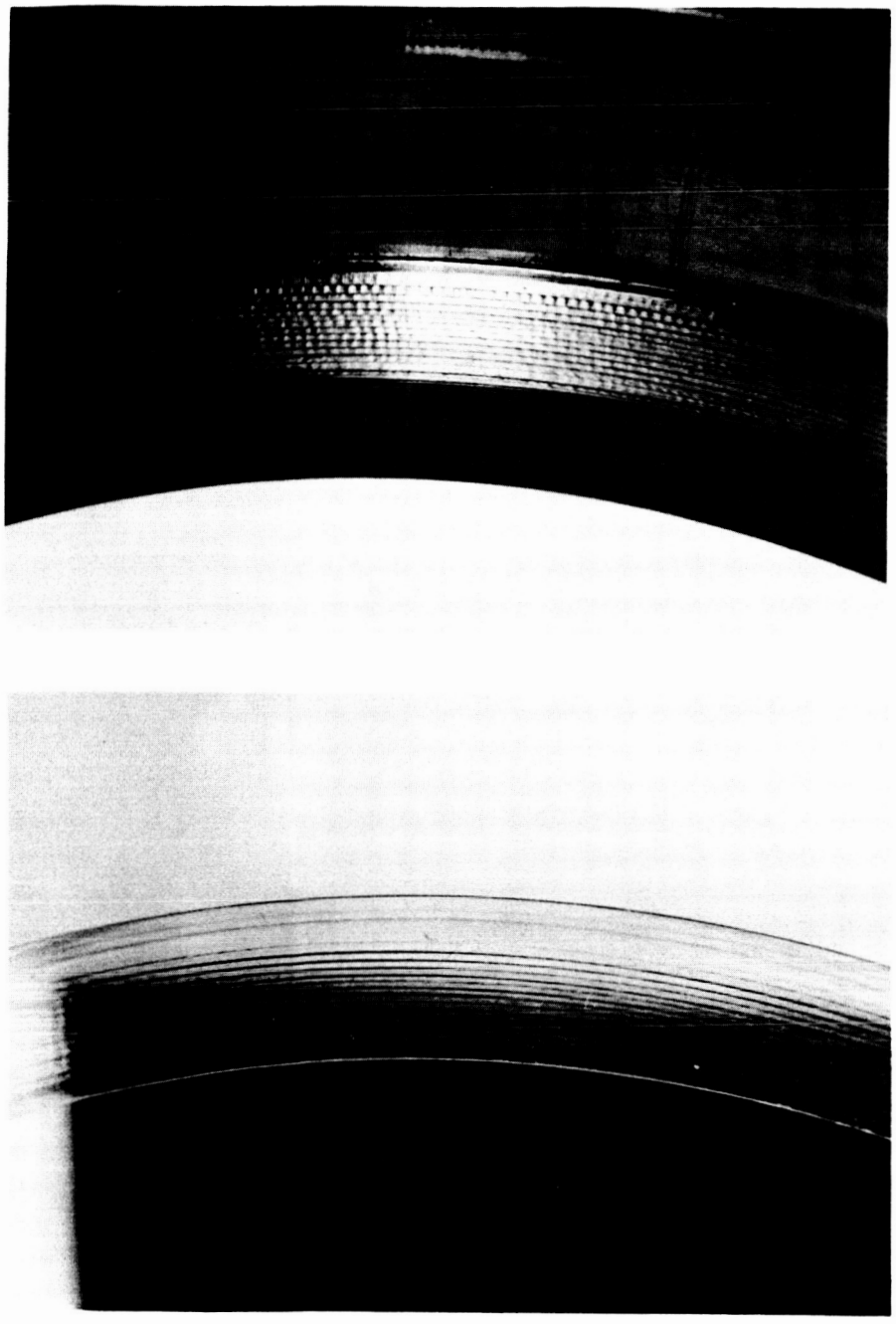

Figure 4 - Close-ups of Steel Retaining Ring and Kel-F Gasket Showing Serrations

SPECTROLAB

DEVELOPMENT MEMORANDUM NO. 272-43

SUBJECT: Source Documentation - Test Runs 42 through 49

WRITTEN BY: Mike Onufrechuk
DATE: 25 March 1965
JOB NUMBER: 6002-54

INTRODUCTION

Following the source outer envelope failure, as described in the previous memorandum, No 272-38, all source components were bench inspected, repaired as necessary, and modified as required for compatibility to the new outer quartz envelope. At this time, a new anode, described as Number 4, was installed to replace anode #3. The inner envelope was replaced with another Amersil tube. The same nonmodified cathode was reinstalled. At present, the diameter of the arcing surface of the tungsten tip is .410 in diameter. The anode-cathode gap was set at 15.5 mm. The programmed static pressure test as described in the previous memorandum, No. 272-38, was incorporated into the pre-starting test procedure culminating in a pressure of 200 psig for 30 minutes.

TEST RESULTS

Test Run #42, performed on February 16, 1965, was initiated as a "run-in" for the new anode while, simultaneously, scans were made for comparison with previous runs at similar parameters for data to determine the possible introduction of system aberrations due to the previous source failure. The scans indicated a misalignment resulting in noncoincident optical axes. It was determined that the collector system was physically shifted approximately 1/8". The source was then removed and the alignment devices were substituted. This run was of 22.4 minutes duration at an operating current of 1550 amps with Hy-Cal #2, sooted, as the detector in a target plane scan. The raw and reduced data are presented in Table 1 for all tests covered in this memorandum.

Test Run Series #43 was initiated on February 18, 1965 upon completion of alignment when the system was in a nonoperative condition. Run #43-1 was

an operational collector alignment with a detector peaking series of scans. Run #43-2 was a 2" radius edge intensity scan in the target plane. Operational current for both runs was 1550 amps. The detector was the Hy-Cal #2, sooted, and the runs were 20 and 21 minutes with 10 minute cooling periods between runs.

Runs #44-1 through 44-4 began on February 19, 1965 with a collector alignment by activating the collector vertically by remote control. Run #44-2 was a detector peak through multiple collector manipulations. Run #44-3 was a repeat 2" radial edge intensity scan in a target plane. The detector, Hy-Cal #2, sooted, was now removed from the scanner and the NASA slug calorimeter substituted. Run #44-4 was now made for a 2" radial edge intensity plot in the target plane. Total elapsed operational time was 73.1 minutes at 1550 amps with 10 minute cooling periods between 20 minute runs.

Run #45-1 was performed on February 19, 1965 and was a comparison recheck of Run #44-4, a target plane plot. Run #45-2, a repeat of Run #45-1, was necessary due to an improper setting of the Moseley readout making #45-1 invalid and requiring fresh data. Both runs lasted 20 minutes each with additional 10 minute cooling intervals between runs at an operational current of 1550 amps. Upon completion of this run, a small pin hole water leak was noticed in a solder joint in the source cap necessitating source disassembly. Total elapsed operational time between assemblies was 176.5 minutes.

Prior to disassembly during bench inspection, the inner envelope O.D. and the outer envelope I.D. indicated what appeared to be a local contamination of unusual color and configuration justifying a careful clinical analytical documentation of these phenomena.

Upon disassembly, it was found for the first time that both Kel-F gaskets had formed optical bonds at the outer envelope interfaces, thereby compounding maintenance complications. The outer envelope ID showed soot deposition which indicated strong influence of the argon flow force. Figure 1 illustrates this. This is not unusual. Each time a new anode assembly is utilized, an abnormal amount of soot contamination is filtered in the system. Part of this finely

decomposed soot forms on the envelopes. This may be due to "ageing" by copper boiling in the fresh anode. The inner quartz envelope was free of soot and showed the most minimal tungsten deposition to date. However, there evidenced a narrow gray colored film, translucently occlusive, being about 1/8" in width and 2-3/4" in length, diagonally positioned in respect to the longitudinal axis of the envelope near the middle on the OD. Figure 2 illustrates this. The outer envelope also exhibited a similar phenomenon on its ID with the exception that the apparent occlusions were simuous and represented half a sine wave. Figure 3 illustrates this. Obviously, they were not "match" marks nor were they adjacent. Cleaning with water and Barnesite removed the soot stains but not the translucent occlusions. However, when the quartz was wet, the translucence became practically invisible. One hypothesis for this occlusion is the possible introduction of foreign matter during hose disconnects to the source. This bypasses all filters in the recirculator system.

The anode, Number 4, showed extraordinary cleanliness for this series of runs. Figure 4 illustrates this. These runs were very stable. The anode diffuser increased in diameter from .650 to .665". The cathode indicates a stability has been reached regarding tungsten ablation and tip configuration as a result of operational parameters. It remains at a .410 diameter and has not changed radically. Figure 5 illustrates this. Since increasing the argon flow to the original amount, the O-ring seals show no signs of heat degradation or malformations and are still functional per design. The cap leak was repaired and the source components fitted with fresh O-rings prior to reassembly.

The source was reassembled with the same anode and cathode and with the same 15.5 mm spacing. The inner tube was replaced with another Amersil envelope. Prior to assembly, the outer envelope was inspected under a stereo microscope at 30X at the questionable shaded area. Inputs and analysis were solicited from competent individuals resulting in diverse opinions as to causes or origins. A question arose as to whether the envelope should be re-polished at the original manufacturer's or simply reinstalled and made operational. Consequently, the source was not polished, was reassembled, reinstalled, and statically pressure tested in the accepted procedure at 200 psig for 30 minutes. The quartz held.

Runs #46-1 and #46-2, performed on March 3, 1965 were initiated as a fresh assembly "run-in" combined with a collector focus check and realignment using the sooted Hy-Cal #2 as a peaked detector resulting in two successful runs of 20 minutes each at the operational current of 1550 amps in a target plane scan.

Runs 47a, b, c, d, initiated on March 3, 1965, were of 31 minutes duration and were made to record various voltage readings under different argon flow rates at fixed amperage of 1550 and fixed pressure of 250 psig.

Run #48 was made on March 4, 1965, was of 20 minutes duration and was a modification of Run #46-1 for an edge intensity scan in the target plane at 2" radially. The Hy-Cal #2 served as the detector.

Runs 49a, b, c, d, were also performed on March 4, 1965 and were of 20 minutes duration and a repeat of Runs 47a, b, c, d, as a comparative check. The exception was the range setting on the Moseley 6-S readout which was changed from 2 mv/in. to 1 mv/in. to clarify data analysis. At present, the source showed minimal ablation of the cathode with minimal anode and inner envelope splattering. This is illustrated in Figure 6.

CONCLUSIONS

1. Each new assembly shall be statically pressure tested with a gradual increase of pressure in increments of 50, 100, 150 psig at 5 minute intervals, culminating at 200 psig for 30 minutes to permit gradual seating of the Kel-F gaskets to minimize quartz envelope strain.

2. Maximum argon flow rates shall be maintained to minimize O-ring seal degradation or malformation due to excessive operational heat parameters.

3. Care shall be exercised in the prevention of introducing foreign matter into the gas system during line disconnects at the source.

4. The latest series of runs - Numbers 42 to 49 which were of 287.5 minutes duration with the new quartz envelope at 250 psig, should validate the envelope design configuration.

Point No.	Current Amps	Total Voltage Volts	Source Voltage Volts	Total Power KW	Source Power KW	Gas Pressure PSIG	Gas Flow Reading	E.T.I. Reading	Running Time Min.
42	1550	103.5	81.4	160.4	126.1	250	44.0	1717.2	22.4
43-1	1550	103.3	81.2	160.1	125.8	250	44.0	1738.6	20.0
43-2	1550	102.2	80.1	158.4	124.1	250	44.0	1761.1	21.0
44-1	1550	102.2	80.1	158.4	124.1	250	44.0	1784.3	21.0
44-2	1550	101.3	79.2	157.0	121.7	250	44.0	1805.4	21.1
44-3	1550	101.2	79.1	156.8	121.6	250	44.0	1817.2	10.0
44-4	1550	100.8	78.7	156.2	120.9	250	44.0	1838.1	21.0
45-1	1550	101.1	79.0	156.7	121.4	250	44.0	1857.4	20.0
45-2	1550	100.8	78.7	156.2	120.9	250	44.0	1876.9	20.0
46-1	1550	101.3	79.2	157.0	121.7	250	44.0	1897.2	20.0
46-2	1550	100.5	78.4	155.7	120.5	250	44.0	1917.5	20.0
47-A	1550	99.3	77.2	153.9	118.5	250	44.0		
47-B	1550	101.7	79.6	157.6	122.3	250	38.0		
47-C	1550	105.4	83.3	163.3	129.1	250	32.0		
47-D	1550	99.4	77.3	154.0	118.7	250	44.0	1948.7	31.0
48	1550	99.3	77.2	153.9	118.5	250	44.0	1968.2	20.0
49-A	1550	98.7	76.6	152.9	117.7	250	44.0		
49-B	1550	101.4	79.3	157.1	121.9	250	38.0		
49-C	1550	104.4	82.3	161.8	127.5	250	32.0		
49-D	1550	98.7	76.6	152.9	117.7	250	44.0	1990.1	20.0

Table 1 - Raw and Reduced Source Data - Test Runs 42 Through 49

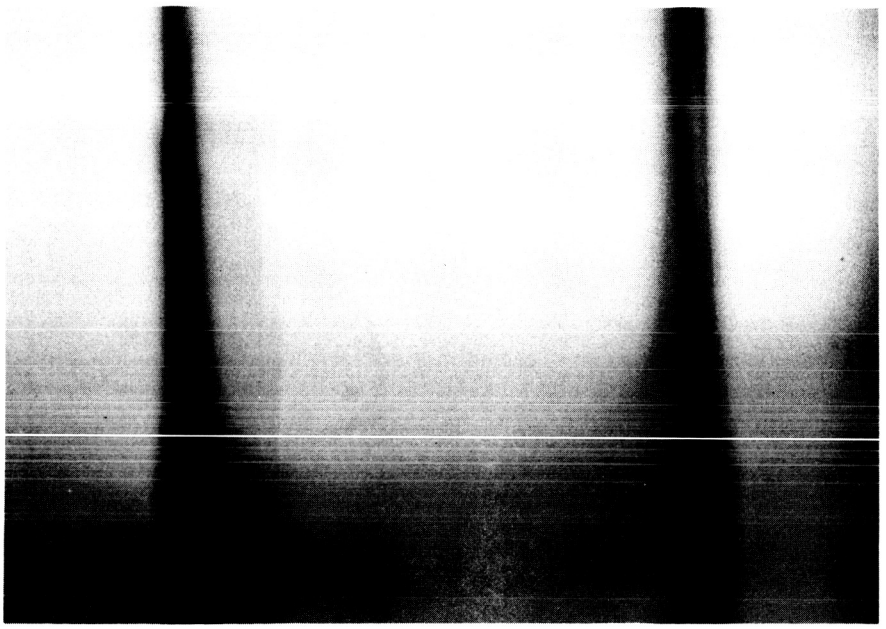

Figure 1 - Outer Quartz Envelope at the Completion of Test Run 45

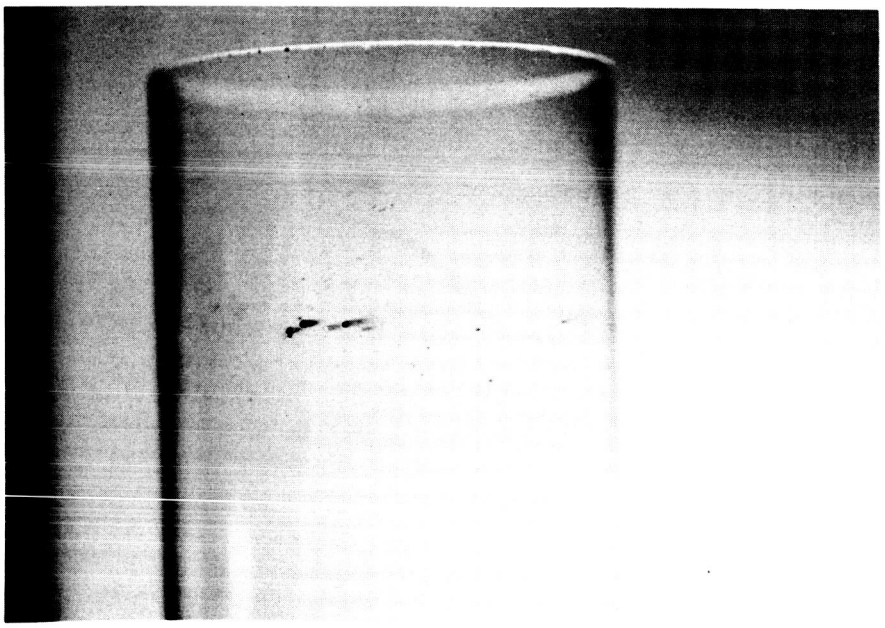

Figure 2 - Inner Quartz Envelope at the Completion of Test Run 45

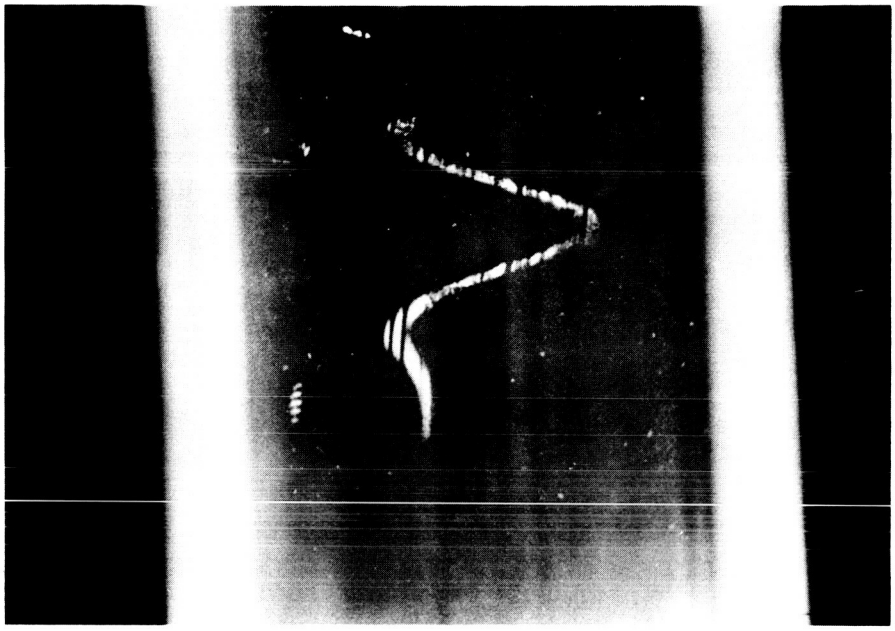

Figure 3 - Outer Quartz Envelope at the Completion of Test Run 45

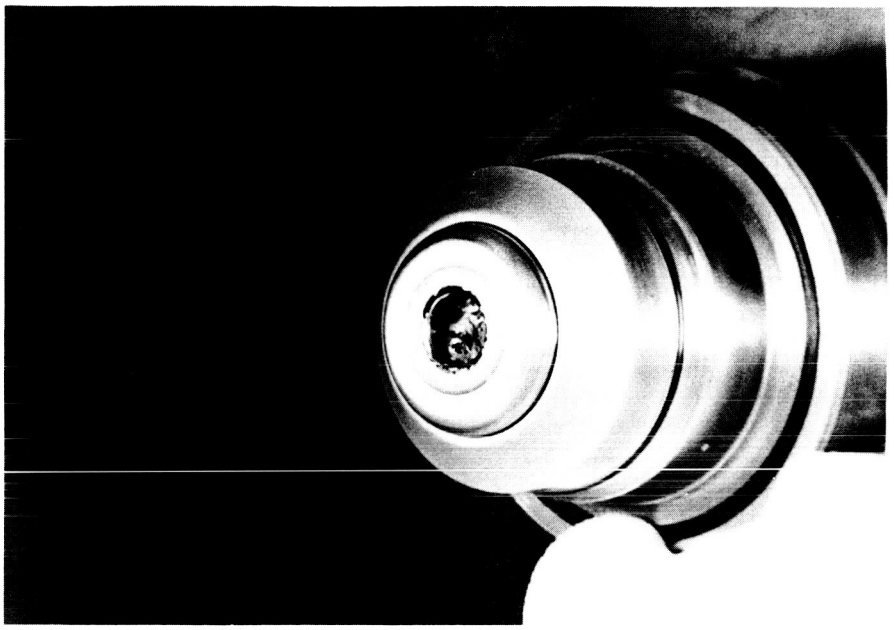

Figure 4 - Anode Assembly #4 at the Completion of Test Run 45

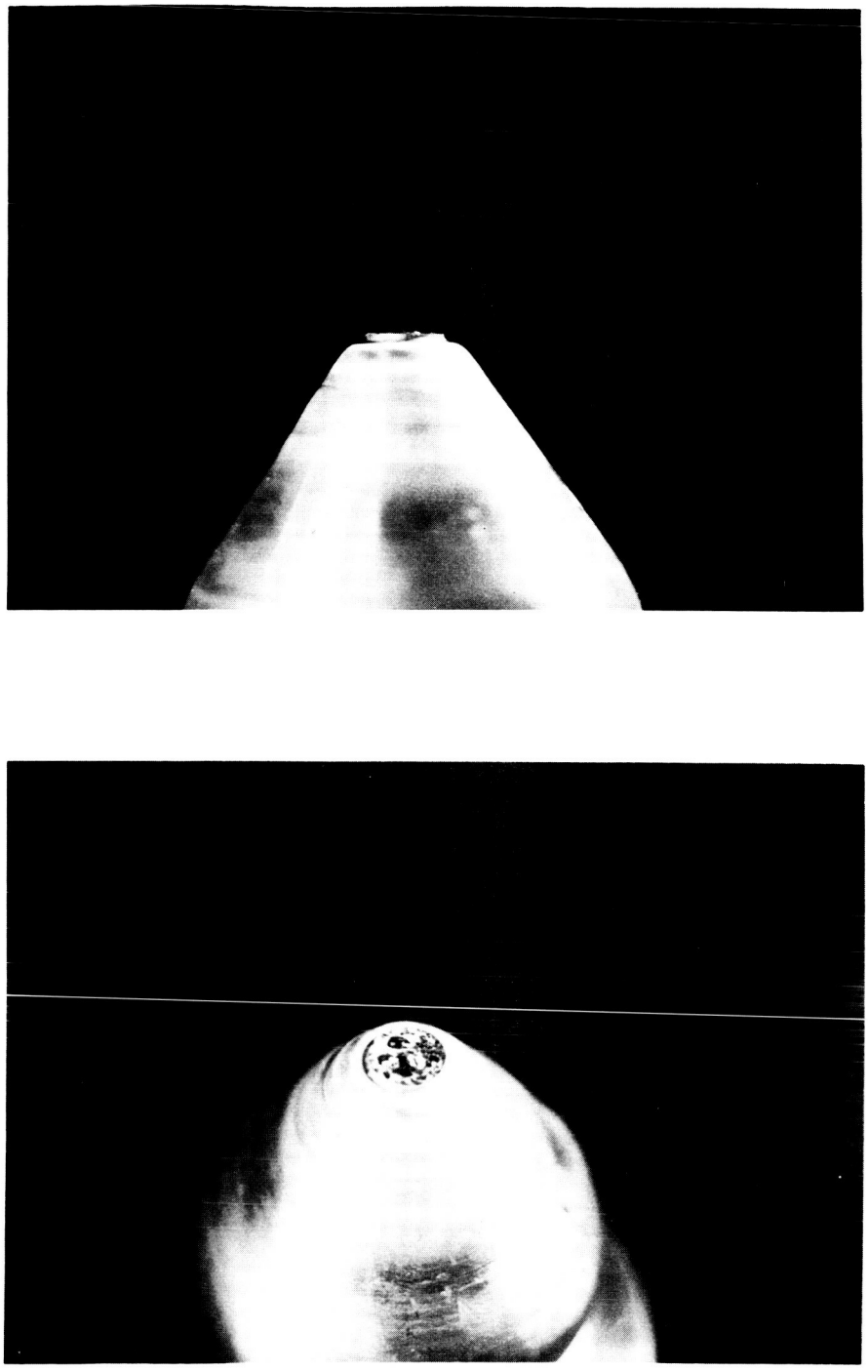

Figure 5 - Cathode at the Completion of Test Run 45

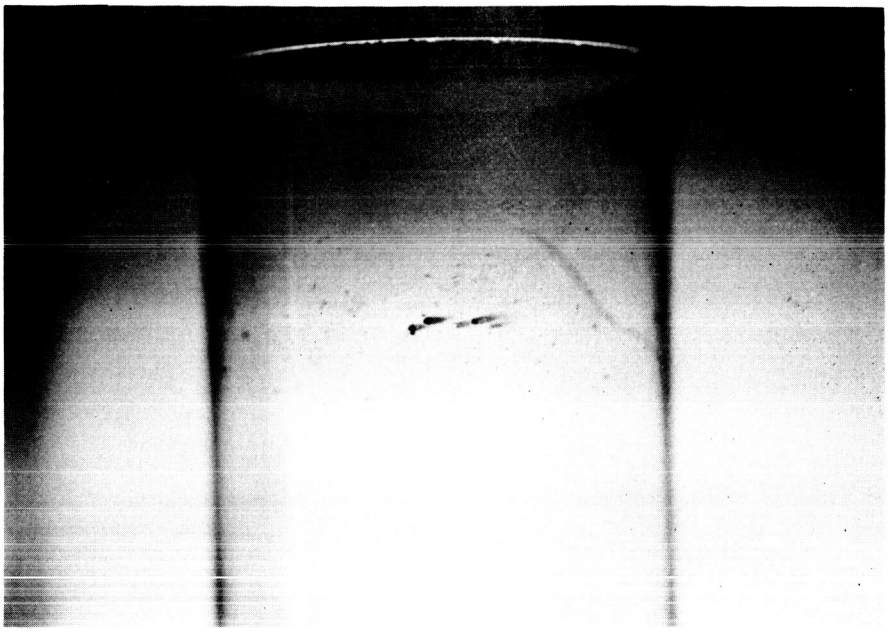

Figure 6 - Inner Quartz Envelope at the Completion of Test Run 45

SPECTROLAB

DEVELOPMENT MEMORANDUM NO. 272-48

SUBJECT : Micro-radiance Plot Calibration

WRITTEN BY: Wagner Schlesinger WS
DATE : 29 June 1965
JOB NUMBER: 6002-54

Run Number 72 was made on May 27, 1965 in order to obtain data so that absolute values could be substituted for the relative values on the micro-radiance contours plotted on Figures 1, 2 and 3 of Development Memorandum No. 272-29.

Procedure

The run was made under the following conditions:

1550 amperes
104.7 volts
250 psi gas pressure
44 cfm gas flow

A GE 101 quartz lens was used as shown below to form a projected image of the plasma arc.

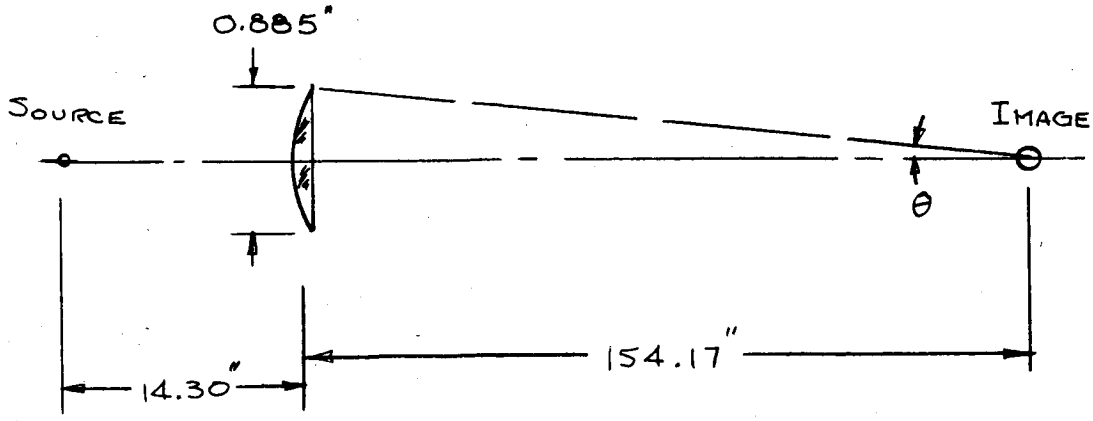

The image was explored with an Eppley thermopile to find the point of maximum intensity. The thermopile output, amplified by a Beckman Fitgo DC amplifier, was recorded on the Y axis of a Moseley 6S X-Y recorder. A maximum displacement of 7.00 inches was obtained at 1 mv per inch and an amplification of 10X.

Data Reduction

The calibration constant of the Eppley thermopile (No. 6132) is 4.68 mv/watt/cm^2.

$$7.00/(10 \times 4.68) = 0.1496 \text{ watts/cm}^2 \text{ in the image}$$

The radiometric equation formula

$$E = \pi kB \sin^2 \theta$$

can be used to determine the micro-radiance of the arc.

where E = irradiance on sensor receiver area
B = radiance of that portion of the arc viewed by the sensor
k = transmission of lens
θ = half angle subtended at image by lens

Since θ is small, less than 10 minutes, $\sin\theta = \tan\theta$

$$\begin{aligned} \text{Sin } \theta &= 0.4425/154.17 \\ &= 0.002807 \\ \text{Sin}^2\theta &= 0.000008238 \end{aligned}$$

The reflection loss of the lens can be calculated using Fresnel's formula and an index of refraction of 1.46.

$$\text{reflectivity} = r = (1-n/1+n)^2 = (1-1.46/1+1.46)^2$$

$$= 0.2116/6.052 = 0.035$$

k = transmission of 2 surfaces

$$= (1-0.035)^2 = (0.965)^2$$

$$= 0.93$$

Since the lens is very thin, it is assumed that there is no absorption loss.

$$\text{hence } E = B_\pi\ (0.93)(0.000008238)$$

$$B = E/0.00002407$$

$$= 41547E$$

$$= 41547 \times 0.1496$$

$$= 6215 \text{ watts/cm}^2\text{/steradian}$$

The diameter of the sensor element in the Eppley thermopile is 0.125 inch. The magnification of the image is 154.17/14.30 = 10.78. Hence, the diameter of the element of the arc viewed by the sensor is 0.125/10.75 = 0.01160 inch or 0.30 mm. A circle of this diameter is drawn on the micro-radiance plot shown in Figure 1. This plot is reproduced from Development Memorandum No. 272-29.

The original micro-radiance plot shown in Figure 1, resulting from Run 13-12, was made at a magnification of 10.63. The element of the arc viewed by the sensor was 0.125/10.63 = 0.01176 inch. This is less than 0.0002 inch larger than the element viewed during Run Number 72. It is not necessary to make any correction for this very small difference.

Micro-radiance plots of the arc operating at 1000 and 1400 amperes are presented in Development Memorandum No. 272-29. Comparison of these plots

shows no significant differences in the contour shapes. It therefore appears reasonable to use the 1400 ampere plot to serve as a pattern for the micro-radiance of the arc operating at 1550 amperes.

The peak relative radiance value shown on Figure 1 is 9.0. This represents the absolute value of 6215 watts/cm^2/steradian derived above. Hence, absolute radiance values for the contours of Figure 1 can be obtained by multiplying the contour values by 6215/9 = 690.6 watts/cm^2/steradian.

MICRORADIANCE CONTOURS
RUN No. 13-12
1400 AMPS. 255 P.S.I.

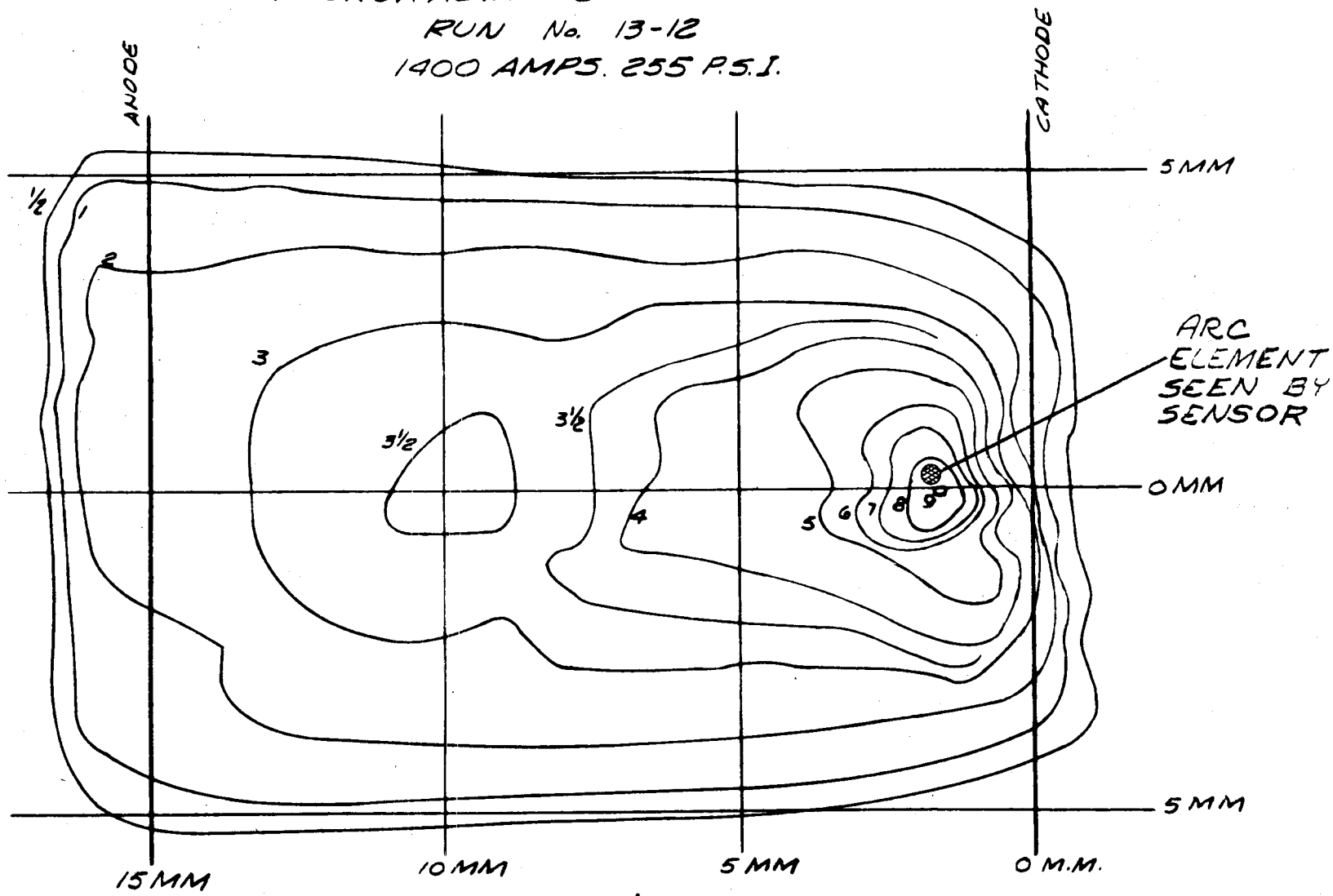

FIGURE 1

ABSOLUTE VALUES
≅ CONTOUR NUMBER × 691

SPECTROLAB

DEVELOPMENT MEMORANDUM NO. 272-52

SUBJECT : Recirculator Evaluation ///

WRITTEN BY: Mike Onufrechuk
DATE : 13 August 1965
JOB NUMBER: 6002-34

Operational life utilizing recommended factory manufactured gaskets and diaphragms proved to be inadequate. Although proper installation and assembly directives were adhered to, diaphragm ruptures occurred at inconsistent periods, with an intermittently accumulated time of 10 operational hours between shut-downs being about average.

Several operational functions of the compressor were improved upon by Spectrolab personnel, thereby increasing pump reliability. These modifications are described in Development Memorandums 272-8 and 272-11. However, further improvements were required.

Original factory equipment relative to gaskets was improved upon. Specifically, the originals were stamped, consequently warped, and out of round. Both the ID and OD were heavily burred, making for a poor installation resulting in an abrupt circumferential pressure point at the diaphragm interface. Most important, the radial distances of both the ID and OD were insufficient to properly interface over the serrated sealing areas of both the compressor head plate and the clamp ring. Consequently, Spectrolab fabricated new gaskets of a soft .025" thick aluminum sheet resulting in a flat, concentric, deburred component. The radial dimensions were increased resulting in a more compatible interface. The OD was held at 16.150" and the ID at 16.000". A combination of new gaskets and factory diaphragms resulted in a run of 19.5 hours before shutdown due to diaphragm fatigue failure.

The cause of failure was circumferential ruptures of the diaphragms adjacent to the gasket seal interface resulting in oil in the product side. A rough stress analysis on the diaphragms was made which indicated thinner diaphragm material would provide increased life. A thickness of .010" for the 316 stainless steel material was selected. The original thickness was .018" of the same material.

These diaphragms were fabricated by Spectrolab. The OD of these diaphragms corresponded exactly to the compressor headplate and clamp ring OD's to assure concentric installation both manually and visually, thereby minimizing nonuniform pressure points at the gasket-diaphragm, head-ring interface. Originally, a manufactured product "RUBBAWELD" was used as a flexible adhesive to adhere the gaskets to the head plates and clamp rings for concentric component installation. Ordinary stationery rubber cement has proven most satisfactory.

Immediately following installation of the modified components, a careful operations log was kept recording every running minute under various operational parameters. Initiated February 2, 1965, it terminated May 27, 1965, with a total elapsed time of 24.1 hours.

Prior to shipment to NASA, the recirculator heads were dismantled for the purpose of modification evaluation and diaphragm longevity analysis. The area of the diaphragm-gasket interface visibly indicated no evidence of crystallization or work hardened loss of flexibility. The "offset" of the diaphragm at the gasket interface caused by operational pressures on the oil side appeared to be identical to the offset of the thicker factory installed diaphragm. From the limited test results, it appears the thinner diaphragms will have a significantly longer life.

SPECTROLAB

DEVELOPMENT MEMORANDUM NO. 272-61

SUBJECT : Heat Transfer in the Cathode

WRITTEN BY: Kurt Muller
DATE : 16 November 1965
JOB NUMBER: 6002-21

INTRODUCTION

The heat input to the cathode primarily results from the impact of positive ions. Other sources are ohmic heating and radiation from the arc. If the melting temperature of the cathode material is considered the limiting factor, a minimum cross section is required to conduct a given heat rate from the tip in the axial direction toward the cooling passage. A violation of this fact, that is, when the cathode is too pointed, will result in melting of the tip until the required bluntness is established. Molten material in the arc chamber will gradually deposit on the envelope which is detrimental to the source operation. A simplified equation has been derived to establish the bluntness required to avoid melting of the cathode tip. Although a number of influences are disregarded, the test results are in fair agreement with the predicted data.

ASSUMPTIONS

Calorimetric measurements indicated that about 3% of the total source power was dissipated in the cathode. Assuming that a lamina perpendicular to the cathode axis is at a uniform temperature, the linear heat conduction is expressed by

$$\frac{dq}{dx} = - k A \frac{d^2T}{dx^2}$$

The term dq/dx is zero since any heat exchange with the environment is disregarded.

Using the notation as indicated in Figure 1, the cross section of the cathode is calculated

$$A = \pi y^2$$

The cathode contour is governed by

$$y = mx + y_o$$

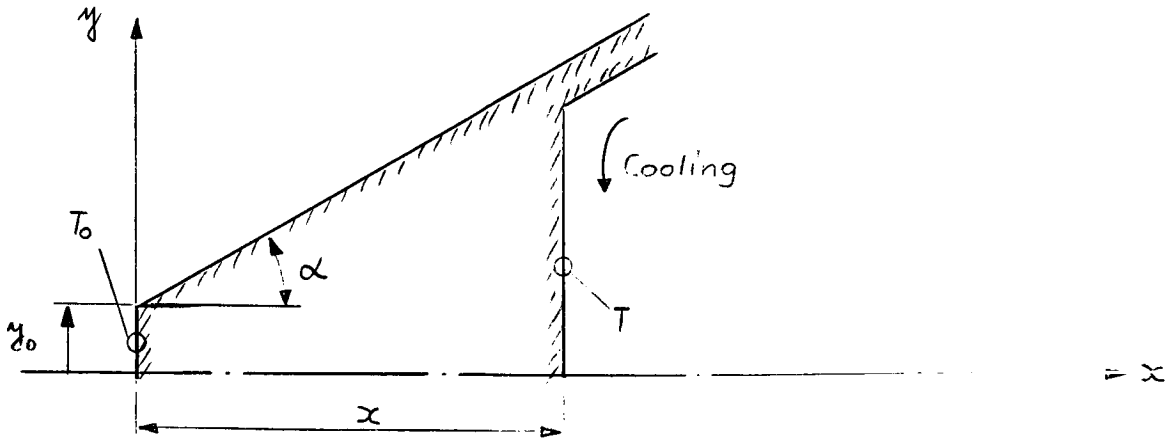

Figure 1 - Geometry of the Cathode Tip

From the first equation

$$q = - k A \frac{dT}{dx}$$

resolved for dT, and A substituted by its equivalent gives

$$dT = - \frac{q}{\pi k} \frac{dx}{y^2}$$

or

$$dT = - \frac{q}{\pi k} \frac{dx}{(mx+y_o)^2}$$

integrated $$T = \frac{q}{\pi k m} \quad \frac{1}{mx + y_o} + C$$

Boundary condition: at $x = 0 \rightarrow T = T_o$

Thus $$C = T_o - \frac{q}{\pi k m} \frac{1}{y_o}$$

Finally, the temperature becomes

$$\underline{\underline{T_o - T = \frac{q}{\pi km} \left[\frac{1}{y_o} - \frac{1}{mx + y_o} \right]}}$$

T_o represents the melting temperature of the material

T indicates the temperature at the location x on the rear end of the cathode tip near the cooling passage

The equation above resolved for the tip radius y_o yields

$$y_o = \frac{- mx \pm \sqrt{(mx)^2 + 4G}}{2}$$

The negative root of the quadratic equation is to be ignored since y_o cannot be negative according to our definition.

The letter G includes all constants as follows:

$$G = \frac{qx}{(T_o - T)\pi k}$$

NUMERICAL EXAMPLE

The 60 KW prototype source dissipates approximately 3% or 1.8 KW of the input power in the cathode. The bluntness y_o is to be established such that melting of the tungsten tip does not occur.

DATA:

q	=	1800 watt	input power
k	=	1.46 watt/cm °C	thermal conductivity
x	=	1.4 cm	length
α	=	30°	divergent half angle
T_o	=	3400 °C	melting temperature
T	=	100 °C	cathode rear end temperature

There was evidence that little nucleate boiling occurred in the cathode cooling passage, thus the rear end temperature of the cathode was assumed as 100°C.

$$m = \tan 30° = 0.577$$

$$G = \frac{1800 \times 1.4}{3300 \times 3.14 \times 1.46} = 0.166 \text{ cm}^2$$

$$y_o = \frac{-0.805 + \sqrt{0.65 + 0.664}}{2} = 0.16 \text{ cm}$$

$$y_o = 1.6 \text{ mm}$$

CONCLUSIONS

The analysis shows that the design of the cathode tip deserves special attention in order to avoid excessive melting. Although a pointed cathode is desirable from the viewpoint of starting and constriction of the arc, a blunt tip is recommended if the source is operated for any length of time.

Tests with the 60 KW prototype source utilizing a blunt cathode with a tip diameter of 1/8" as calculated above, indicated that no excessive melting takes place.

SPECTROLAB

DEVELOPMENT MEMORANDUM NO. 272-62

SUBJECT : Total Reflection in the Plasma Radiation Source

WRITTEN BY: Kurt Muller
DATE : 16 November 1965
JOB NUMBER: 6002-21

INTRODUCTION

Total reflection in the quartz envelope is to be avoided because the internally trapped energy is converted into heat and endangers the tube as well as the O-ring seals on both ends.

In the following sections a short investigation is made to establish the percentage of the energy falling in the region of total reflection.

METHOD OF ANALYSIS

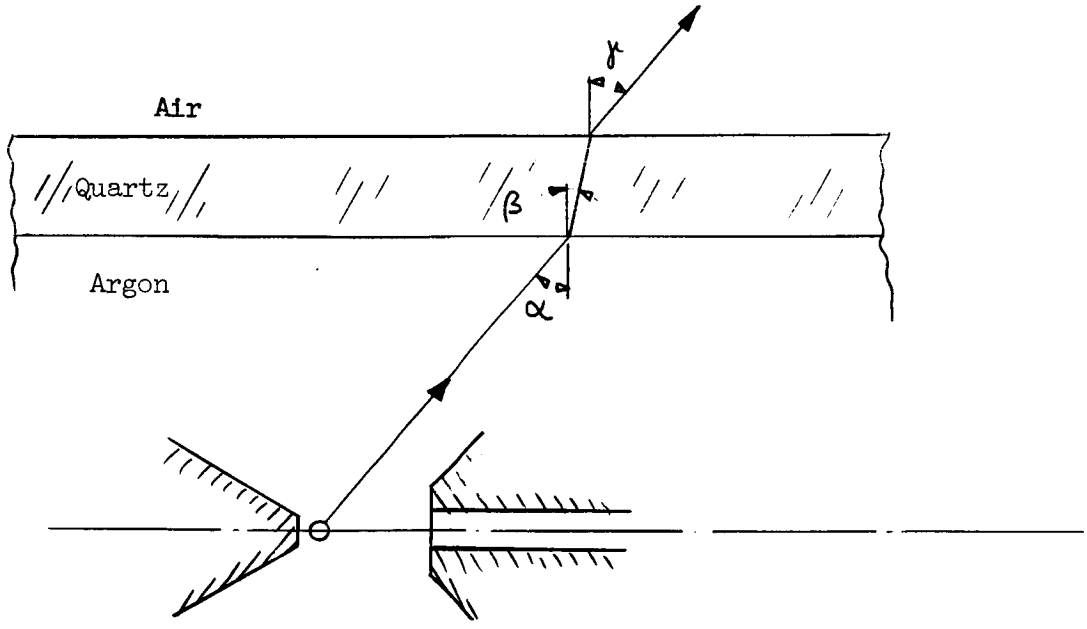

Figure 1 - Propagation of a Light Ray

A light wave propagates in three media, namely, from argon (21 atm) through clear fused silica and then into air (1 atm) as shown in Figure 1.

According to Snellius' law of refraction

$$\frac{\text{Sin}\alpha}{\text{Sin}\beta} = \frac{n_Q}{n_{Ar}}$$

and

$$\frac{\text{Sin}\beta}{\text{Sin}\gamma} = \frac{n_{Air}}{n_Q}$$

n_Q, n_{Ar}, n_{Air} denote the coefficients of refraction for quartz, argon and air respectively.

The combination of the two equations leads to

$$\frac{\text{Sin}\alpha}{\text{Sin}\gamma} = \frac{n_{Air}}{n_{Ar}}$$

Total reflection occurs when $\gamma \geq 90°$, that is, the Sine of the angle γ becomes unit, hence,

$$(\text{Sin}\ \alpha)_{crit} = \frac{n_{Air}}{n_{Ar}}$$

The index of refraction for air at atmospheric condition is

$$n_{Air} = 1.000292$$

The index of refraction of argon at elevated pressures and temperatures is given by

$$n_t - 1 = \frac{n_o - 1}{1 + at} \quad \frac{P}{760}$$

n_t = index of refraction at the temperature t °C

n_o = index of refraction at atmospheric conditions p = 760 mmHg, T=0°C

a = thermal coefficient of expansion for gas a = 1/273 $°C^{-1}$

P = gas pressure mm Hg absolute

n_o = 1.000281 (Argon at 0°C, 760 mm Hg)

Taking an average temperature of t = 500°C and a gas pressure of 21 atm, the index of refraction n_t becomes

$$n_t = 1 + \frac{1.000281 - 1}{1 + \frac{500}{273}} \quad \frac{21 \times 760}{760}$$

$$n_t = 1.002084$$

The critical angle α for total reflection is calculated as

$$\alpha_{crit} = \text{arc Sin } \frac{1.000292}{1.002084} = \text{Arc Sin } 0.99821$$

$$\alpha_{crit} = 86° \ 34' \ 17''$$

CONCLUSIONS

The geometry of the arc chamber allows a variation of α between the limits

$$-70° \leq \alpha \leq +70°$$

Hence, total reflection cannot occur. However, it is conceivable that the critical angle could be approached by beams reflected from the electrodes. Inspection of the 60 KW prototype source did not reveal any such cases.

Literature: 1) American Institute of Physics Handbook, McGraw-Hill

2) Handbook of Chemistry and Physics, The Chemical Rubber Publishing Company

3) Optik und Atomphysik, Springer Verlag

SPECTROLAB

DEVELOPMENT MEMORANDUM NO. 272-63

SUBJECT : Radial Heat Flux and Thermal Stresses in a Sleeve

WRITTEN BY: Kurt Muller
DATE : 19 November 1965
JOB NUMBER: 6002-21

INTRODUCTION

The design of a bore type anode requires knowledge of the optimum geometry with regard to cooling and thermal stresses. The bore type anode consists essentially of a sleeve where the heat input takes place on the inside. The heat is then conducted in the radial direction toward the outside and finally transferred to the coolant. For a given inside diameter of the sleeve, a thicker wall exhibits a greater thermal resistance, but the consequent larger outside surface results in a greater heat transfer rate. Thus, for optimum heat transfer there is definite optimum wall thickness.

Furthermore, the radial temperature differential in a sleeve imposes thermal stresses. The maximum allowable temperature differential between the inside and outside of the sleeve such that cracking does not occur is of great interest.

These two problems of optimizing the anode geometry from the viewpoint of cooling and stress limitations are discussed in the following sections.

HEAT TRANSFER THROUGH THE WALL OF A SLEEVE

Nomenclature

T = temperature
ℓ = length
r = radius
k = thermal conductivity
h = heat transfer coefficient
q = heat transfer rate
R = radii ratio

Subscript 1 = inner wall of sleeve
2 = outer wall of sleeve
C = cooling medium

The following consideration is based on the assumption that the heat transfer rate to the cooling medium is a constant.

Disregarding axial heat flow, the heat conducted in the radial direction through the wall of a sleeve is expressed by

$$q = 2\pi\ell k \frac{T_1 - T_2}{\ell n\, r_2/r_1} \qquad (1)$$

The heat transferred from the outside surface to the cooling medium is

$$q = 2\pi r_2 \ell h (T_2 - T_C) \qquad (2)$$

The same amount of heat which is conducted through the wall is dissipated on the cooling side, hence, the heat flux q in eq. (1) and (2) assumes the same value.

Equation (1) resolved for T_1 gives

$$T_1 = \frac{q}{2\pi k \ell} \ell n \frac{r_2}{r_1} + T_2 \qquad (3)$$

From eq. (2) follows

$$T_2 = \frac{q}{2\pi r_2 \ell h} + T_C \qquad (4)$$

The combination of eqs. (3) and (4) yields

$$T_1 = \frac{q}{2\pi\ell k} \left[\ell n \frac{r_2}{r_1} + \frac{k}{r_2 h} \right] + T_C \qquad (5)$$

Substituting R for the ratio r_2/r_1, eq. (5) becomes

$$T_1 = \frac{q}{2\pi \ell k}\left[\ell n\, R + \frac{k}{R\, r_1\, h}\right] + T_C \qquad (6)$$

Eq. (6) expresses the inside temperature T_1 as a function of R. The derivative of T_1 with respect to R equated to zero leads to the optimum r_2 for a given r_1

$$\frac{dT_1}{dR} = \frac{q}{2\pi \ell k}\left[\frac{1}{R} - \frac{k}{r_1\, h}\;\frac{1}{R^2}\right] \qquad (7)$$

$$\frac{1}{R} - \frac{k}{r_1 h}\;\frac{1}{R^2} = 0 \qquad (8)$$

The first solution R = 0 has no physical meaning because $r_1 \neq 0$ and $r_2 > r_1$.

The second solution gives

$$\underline{\underline{R_{opt} = \frac{k}{r_1\, h}}} \qquad (9)$$

For a given heat flux the optimum radii ratio for the lowest inside temperature of the sleeve is directly proportional to the thermal conductivity and indirectly proportional to the heat transfer coefficient.

Figure 1 shows the correlation between R, r_1 and h for copper and tungsten. The heat transfer coefficient for nucleate and film boiling is as much as 6000 BTU/hr sqft °F.

THERMAL STRESSES IN A SLEEVE

Thermal stresses in a thin wall cylinder are controlled by the following equations:

$$\sigma_1 = \frac{E}{1 - \nu}\,\lambda\,\frac{T_1 - T_2}{4}\left[1 + \frac{2}{1 + r_1/r_2}\right] \qquad (10)$$ Stresses on the inside

$$\sigma_2 = - \frac{E}{1 - \nu} \lambda \frac{T_1 - T_2}{4} \left[1 + \frac{2}{1 + r_2/r_1} \right] \quad \text{(11) Stresses on the outside}$$

where:

E = Modules of elasticity

ν = Poisson's ratio

λ = Thermal expansion

R = Radii ratio

For radial heat flux, the inside of the sleeve, being at a higher temperature than the outside, is under compression and the outside under tension.

The yield strength of sintered tungsten in compression is 120,000 psi at 20°C. The yield strength of sintered tungsten in tension is 80,000 psi at 20°C.

The ratio of compression and tensile strength follows from eqs. (10) and (11).

$$\left| \frac{\sigma_1}{\sigma_2} \right| = \frac{1 + 3R}{R+3} \qquad (12)$$

Eq. 12 indicates that the ratio of the compression and tensile strength increases with increasing R.

The ratio of the maximum allowable compression and tensile strength of a material is generally greater than unity. This ratio is referred to as "S" and it is a material constant.

The value of "R" determines whether for a given "S" the tensile strength or the compression strength limit of the material is reached first if the maximum allowable temperature differential is the subject of investigation.

There is a distinct value of R leading to the concurrent stress limits on the inside and on the outside of the sleeve. This value of "R" which is called "R^*" may be derived as follows:

$$S = \frac{1 + 3R^*}{R^* + 3} \qquad R^* = \frac{3S - 1}{3 - S}$$

Thus, we arrive at the following conclusion:

$R > \frac{3S - 1}{3 - S}$ the compression on the inside of the sleeve is the limit

$R < \frac{3S - 1}{3 - S}$ the tension on the outside of the sleeve is the limit

$R = \frac{3S - 1}{3 - S}$ the limits of compression and tension on the inside and outside respectively are approached simultaneously

The maximum allowable tensile strength of tungsten decreases considerably with increased temperature. The average temperature of the sleeve is assumed to be 1600°C which corresponds to a tensile strength of 20,000 psi. The compression strength of tungsten as a function of temperature is not available to date, hence it is assumed that the ratio of compression and tensile strength at ambient temperature also holds true at elevated temperatures. This assumption is highly artificial, nevertheless, it was used to perform the following calculations.

$$S = \frac{120,000}{80,000} = 1.5$$

$$R^* = \frac{3 \times 1.5 - 1}{3 - 1.5} = 2.33$$

For anode applications, the radii ratio R does not exceed 2. Therefore, we only have to be concerned with the tensile strength on the periphery of the sleeve, that is

$$|\sigma_2| = \frac{E}{1 - \nu} \lambda \frac{T_1 - T_2}{4} \left[1 + \frac{2}{1 + R} \right]$$

σ_2 = 20,000 psi max. yield strength in tension at 1600°C

E = 34×10^6 psi at 1600°C

ν = 0.284

T_1 = 6100°F melting temperature of tungsten

λ = 3.7×10^{-6} °F^{-1} at 1600°C

$k = 62$ BTU/hr ft °F

Figure 2 indicates the maximum allowable temperature differential through the cylinder wall in terms of stresses as a function of the radii ratio, and Figure 3 presents the heat rate transferred through the wall under those conditions.

CONCLUSIONS

For the anode employed in the 60 KW prototype source a tungsten insert was used having the following dimensions.

r_1 = 0.250" inside radius

r_2 = 0.375" outside radius

ℓ = 1.0" length of heat input

The radii ratio is calculated as

$$R = r_2/r_1 = 1.5$$

Figure 2 indicates a maximum allowable temperature differential of 254° F at R = 1.5. Figure 3 shows the corresponding heat conducted through the wall $q/\ell = 20 \times 10^3$ BTU/hr inch.

The length of the sleeve at which the heat input takes place is approximately 1". Thus the total amount of heat conducted through the sleeve such that cracking does not occur is 20×10^3 BTU/hr.

The dissipated energy in the anode of a radiation source is about 60% of the input power, that is, for the 60 KW prototype source 36 KW or 123×10^3 BTU/hr.

The investigation shows clearly that the geometry of the tungsten insert was not compatible with the heat loading present. The thermal stresses could only be reduced by a segmented tungsten insert supported by a copper shroud.

Furthermore, the geometry was not optimized from the viewpoint of the lowest inside temperature. For r_1 = 0.250" and R = 1.5 the heat transfer coefficient (h) was 2000 BTU/hr sq ft°F according to Figure 1. Since a higher value of h could be assumed a thinner wall would have been required.

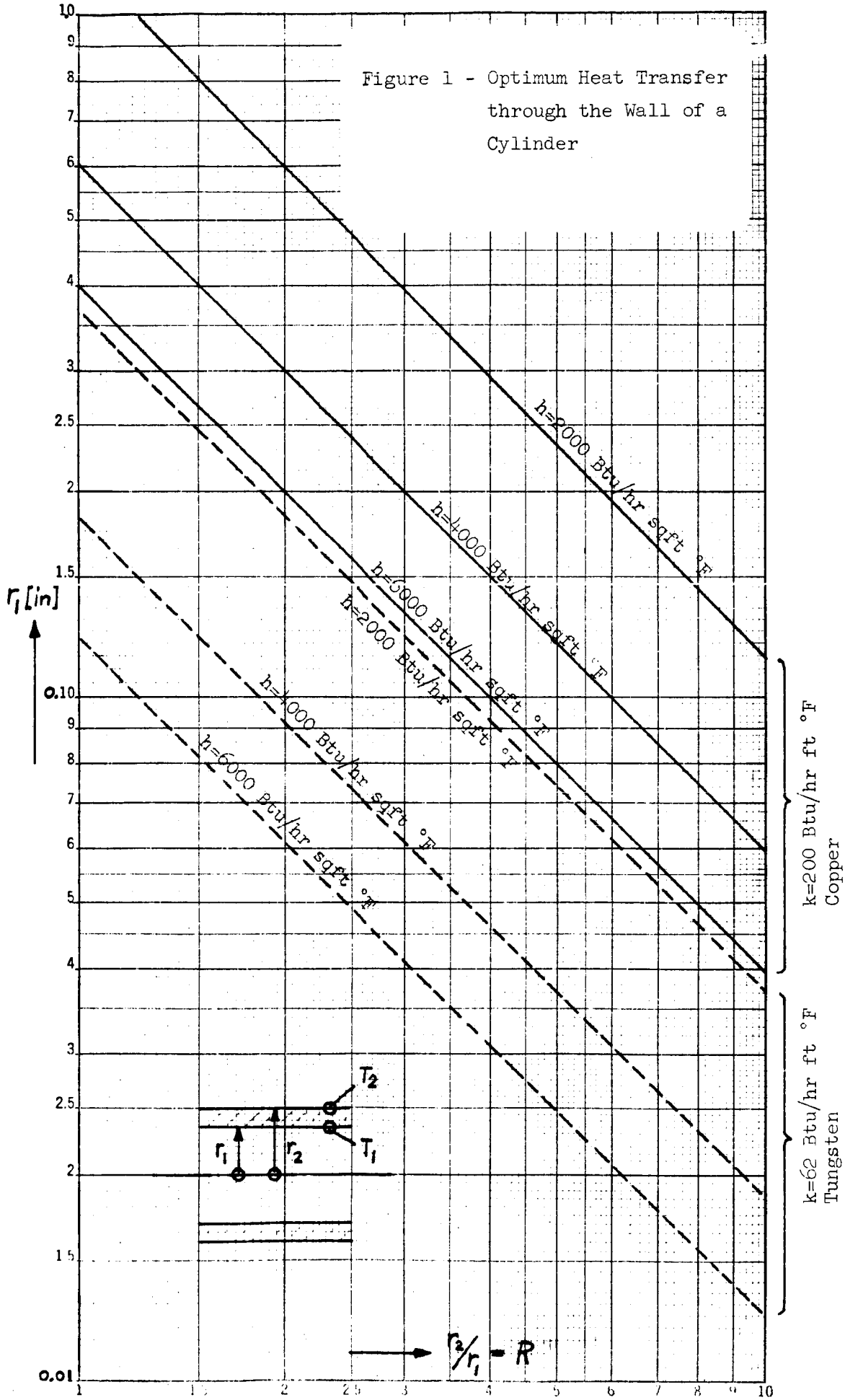
Figure 1 - Optimum Heat Transfer through the Wall of a Cylinder
h=2000 Btu/hr sqft °F
h=4000 Btu/hr sqft °F
h=5000 Btu/hr sqft °F
h=2000 Btu/hr sqft °F
h=4000 Btu/hr sqft °F
h=6000 Btu/hr sqft °F
r_1 [in]
$r_2/r_1 = R$
T_2
T_1
r_1
r_2
k=200 Btu/hr ft °F
Copper
k=62 Btu/hr ft °F
Tungsten